University of Strathclyde

Strathclyde Institute of Pharmacy and Biomedical Sciences

Regulation of the Autophagy Pro-Survival Mechanism by ULK1

By Leon E. Williamson

A thesis presented in fulfilment of the requirements for the degree of
Doctor of Philosophy
2017

This thesis is the result of the author‘s original research. It has been composed by the author and has not been previously submitted for examination which has led to the award of a degree.

Signed:

Date:

Acknowledgements

First and foremost, I would like to thank my supervisor Dr Edmond Chan for giving me the opportunity to undertake a PhD in his lab. I am extremely grateful for his constant help and support throughout my project and his willingness to share knowledge when needed. Without this my thesis would not have been possible and I wish you all the best for the future.

I would also like to thank Prof Robin Plevin and Dr Andy Paul for their help and advice, not only from our weekly Cell Biology group meetings, but also throughout my undergraduate degree and entire time spent at Strathclyde Uni.

I have made a lot of good friends during my PhD project and want to give a special mention to my gym buddy Qadyr 'Mike Chan' Mohtar. Also to Martin Werno (MFW) for all the good times and for all the Munros we have bagged together - we will climb the last 90% percent at some point…..

Big thanks to the entire 4th floor who helped keep me sane during all the emotional highs and lows of being a PhD student. There is not enough space to name you all but you know who you are!

I would also like to thank my family whose help and understanding over the final few months has been greatly appreciated.

Last but not least, I would like to thank my fiancé Rachael who has been with me from the start to the very end of this long journey. Your love and support has kept me going, especially over the last few months.

Publications

Gallagher, L.E., **Williamson, L.E**., Chan, E.Y (2016) Advances in Autophagy Regulatory Mechanisms. *Cells*. (5)2: 24.

Watson, D.G., Tonelli, F., Osaimi, M., **Williamson, L.E**., Chan, E.Y., Gorshkova, I., Berdyshev, E., Bittman, R., Pyne, N.J and Pyne, S (2013) The roles of sphingosine kinase 1 and 2 in regulating the Warburg effect in prostate cancer cells. *Cell Signal.* 25: 1011-1017.

McAlpine, F., **Williamson, L.E**., Tooze, S. A., Chan, E.Y (2013) Regulation of nutrient-sensitive autophagy by uncoordinated 51-like kinases 1 and 2. *Autophagy*. 9: 361-373.

Tonelli, F., Alossaimi, M., **Williamson, L. E**., Tate, R.J., Watson, D.G., Chan, E.Y., Bittman, R., Pyne, N.J and Pyne, S (2013) The sphingosine kinase inhibitor 2-(p-hyroxyanilino)-4-(p-chlorophenyl) thiazole reduces androgen receptor expression via an oxidative stress-dependent mechanism. *Br J Pharmacol*. 168: 1497-1505.

Abbreviations

4E-BP1	eIF4E-binding protein 1
-AA	Amino Acid Starvation
ACC	Acetyl-CoA Carboxylase
AMBRA-1	Autophagy and beclin-1 regulator 1
AMP	Adenosine Monophosphate
AMPK	5' AMP-Activated Protein Kinase
ARP2/3	Actin-related protein 2/3
Atg	Autophagy related gene
ATP	Adenosine triphosphate
Bak	Bcl-2 Homologous Antagonist/Killer
Bax	Bcl-2 like protein 4
CaMKK-β	Ca^{2+}/CaM-Dependent Protein Kinase Kinase β
CBP	Calmodulin binding protein
CDD	Conserved domain database
CMA	Chaperone mediated autophagy
CO-IP	Co-immunoprecipitation
COPII	Coat protein complex
CTD	C-terminal domain
CVT	Cytoplasm to vacuole
DEPTOR	DEP domain containing MTOR interacting protein
DFBS	Dialysed foetal bovine serum
DFCP1	Double FVYE containing protein-1
DKO	Double knockout
DMEM	Dulbecco's Modified Eagle's Medium
DPBS	Dulbecco's Phosphate Buffered Saline
DUF3543	Domain of unknown function 3543
EAT	Early autophagy targeting/tethering

EGO	Exit from rapamycin induced growth
ER	Endoplasmic Reticulum
ERES	ER exit sites
ERGIC	ER-golgi-intermediate compartment
Erlin-2	Endoplasmic reticulum lipid raft associated protein 2
FAK	Focal adhesion kinase
FIP200	FAK family kinase- Interacting Protein of 200kDA
FKBP12	FK506-binding protein 12kDa
FLCN	Folliculin
FNIP2	Folliculin interacting protein 2
FM	Full Media
FRB	FKB12-rapamycin binding
FUNDC1	FUN14 domain containing 1
GABARAP	γ-aminobutyric acid receptor associated protein
GAP	GTPase activating protein
GD3	Acidic glycophospholipid
GDP	Guanosine diphosphate
GEF	Guanine exchange factor
GFP	Green fluorescent protein
GSK3	Glycogen-synthase kinase 3
GTP	Guanosine triphosphate
HDAC6	Histone deacetylase-6
HEK293A	Human embryonic kidney cells 293A
HOPS	Homotypic fusion and vacuole protein sorting
Hsc70	Heat shock conjugate protein 70kDa
IM	Isolation membrane
IMAT	Isolation membrane-associated tubular structures
I-TASSER	Iterative threading assembly refinement
KO	Knock-out

LAMP-2A	Lysosomal associated membrane protein 2A
LC3	Microtubule-associated proteins 1A/1B light chain 3
LIR	LC3-interaction region
LKB1	Liver kinase B1
MAM	Mitochondrial associated ER-membrane
MAP1-LC3	microtubule associated protein 1 light chain 3
MAPK	Mitogen Activated Protein Kinase
MATG13	Mammalian homologue of yeast ATG13
MEF	Mouse Embryonic Fibroblast
MIM	MIT interacting motifs
MIT	Microtubule Interacting and Trafficking Molecule Domain
mRFP	Monomeric red fluorescent protein
mRNA	Messenger ribonucleic acid
MSA	Multiple sequence alignment
MTOC	Microtubule organising centre
MTOR	Mechanistic target of rapamycin
MTORC1/2	Mechanistic target of rapamycin Complex 1/2
p62	Sequestosome-1
p7056K	p70 ribosomal protein S6 kinase
pACC	Phosphorylated acetyl-coA carboxylase
pAMPK	Phosphorylated AMP-Activated Protein Kinase
PAS	Pre-autophagosomal structure
PE	Phosphatidylethanolamine
PI3P	Phosphatidylinositol-3-phosphate
PI3K	Phosphatidylinositol-3-kinase
PI5P	Phosphatidylinositol-5-phosphate
PP2A	Protein phosphatase 2A
PRAS40	Proline rich Akt substrate of 40kDa
pS6	S6 ribosomal protein

Rag	RAS-related GTP-binding protein
RAPTOR	Regulatory associated protein of TOR
RICTOR	Rapamycin-insensitive companion of MTOR
ROS	Reactive oxygen species
RSA	Relative solvent accessibility
SBP	Streptavidin binding peptide
SERCA	Sarco/endoplasmic reticulum Ca^{2+} -ATPase
SNARE	Soluble N-ethylmaleimide-sensitive fusion attachment protein receptor
STRAD	STE20-related adaptor
Stx17	Syntaxin17
TOR	Target of rapamycin
TRAF6	Tumor necrosis receptor-associated factor 6
TSC2	Tuberous Sclerosis Complex 2
TX-100	Triton X-100
Ub	Ubiquitin
ULK1/2	Uncoordinated-51-like kinase 1/2
UPP	Ubiquitin-proteasomal pathway
UVRAG	UV radiation resistance associated gene
V-ATPase	Vacuolar Type H^+ ATPase
VAMP-3	Vesicle-associated membrane protein 3
Vps34	Vacuolar Sorting Protein 34
WHAMM	WAS protein homolog associated with actin, golgi membranes and microtubules
WIPI-1/2	WD Repeat Domain, Phosphoinositide Interacting 1/2

Abstract

Autophagy (from Greek to mean self-eating) is a highly conserved pro-survival pathway found in almost every type of eukaryotic cell. Autophagy occurs constitutively but also serves as an important stress induced cellular response in multiple contexts. Dysfunction of the autophagic pathway is strongly associated with numerous human pathologies such as cancer and neurodegeneration driving the need for better overall understanding of the fundamental mechanisms. The Uncoordinated 51-like kinases (ULK1/2) are essential autophagy regulators that function in complex with several additional regulatory proteins. ULK complexes are critically positioned early during the signalling pathway controlling autophagosome biogenesis, receiving and integrating information from the upstream nutrient sensors mechanistic target of rapamycin (MTOR) and AMP-activated protein kinase (AMPK). Specific roles for ULK1 as compared to its related, but less understood family member, ULK2, were unclear. However, this issue needed to be resolved to better understand how to target this kinase pathway to block autophagy.

Therefore, within this thesis, it has been investigated ULK1 and ULK2 might differentially regulate autophagic activation was investigated. Findings within this thesis support functional redundancy between ULK1 and ULK2 for nutrient-dependent initiation of autophagy. In addition, these data have indicated unexpectedly that glucose starvation fails to induce canonical autophagy as observed in amino acid withdrawal, therefore highlighting the differential autophagy responses that arise following amino acid-dependent MTOR vs. glucose-dependent AMPK signalling events. Finally, this thesis aimed to understand regions of ULK1 that were

critical for autophagy function, focussing on C-terminal (early autophagy tethering "EAT") domain. The findings indicate that small helical sub-regions of the EAT are sufficient to mediate binding to its accessory protein Atg13 and also for binding to membranes. However, more complete regions of the EAT are needed for ULK1 function in cells. Data also suggests that ULK1 interacts with specialized membrane micro-domains known as lipid rafts.

Overall, these combined approaches offered definitive evidence for ULK1/ULK2 functional redundancy *in vivo*, evidence of distinct MTOR and AMPK nutrient sensing pathways for autophagy; and lastly, further definition of distinct regions within the ULK1/2 EAT regulatory domain. These basic findings further support the development of novel inhibitors that could provide similar effects to modulate autophagy in applied settings.

Contents

List of Tables and Figures

Chapter 1- Introduction

Chapter 2- Materials and Methods

Chapter 3- Regulation of Nutrient-Sensitive Autophagy by ULK1/2

Chapter 4-Role of the ULK1 EAT Domain for Autophagic Membrane Formation.

Chapter 1: Introduction

1.0 Introduction to Autophagy

In order for organisms to maintain cellular homeostasis and adapt to changes in their environment, a precise dynamic balance must co-exist between their biosynthetic and degradation pathways. Within mammalian cells, there are two main degradative pathways: the ubiquitin-proteasomal and autophagic-lysosomal pathways.

The ubiquitin-proteasomal pathway (UPP) involves the tagging of abnormally folded or short-lived proteins by ubiquitin (Ub) as a signal for breakdown via proteolysis. Briefly, the UPP is an ATP dependent process that involves three key classes of enzymes (Ub activating enzymes (E1), Ub conjugating enzymes (E2) and Ub ligases (E3)) that are all required to transfer poly-ubiquitin polymers onto substrate proteins. This polyubiquitin-protein complex is then recognised by the 26S proteasome. The Ub-tagged protein is thought to be unravelled to reveal the protein primary sequence which is then transferred into the inner cylindrical core of the proteasome where it is digested and the products (amino acids) are released into the cytoplasm. This process is essential for protein degradation and signalling homeostasis, but it is not the main interest of this thesis and is reviewed extensively elsewhere (Lecker et al., 2006) (Lilienbaum, 2013)

The autophagic-lysosomal pathway is the primary focus of this thesis. The term autophagy, was originally derived from Greek “auto” meaning self and “phagy” representing eating, therefore, translates to “self-eating”. This expression was first introduced by the biochemist Christian de Duve, in 1963, who later was awarded the Nobel Prize in 1973 for his work involving lysosomes (De Duve, 1963). Autophagy

involves bulk sequestering of long-lived proteins, abnormal protein aggregates and excess/damaged organelles, within double membranes vesicles known as autophagosomes. These vesicles subsequently fuse with endosomes and/or lysosomes where the contents are eventually degraded and recycled back into the cytoplasm. When autophagy was first discovered, it was hard to believe why a cell would digest its own cellular contents; however, over recent decades, there has been a myriad of evidence recognising that autophagy enables cells to survive various stresses such as nutrient deprivation and organelle toxicity (Meijer and Codogno, 2004). Dysfunction of the autophagic pathway is strongly associated with numerous human pathological processes including cancer, neurodegenerative diseases, diabetes, cardiac disease and also microbial infection (Ravikumar et al., 2010, Jiang and Mizushima, 2014).

1.1 Types of Autophagy

To date, there have been three main types of autophagy that have been described in higher eukaryotes; microautophagy, chaperone-mediated autophagy (CMA) and macroautophagy. All three processes are unique in regard to their mechanisms of action and also in the site of material sequestration.

1.1.1 Microautophagy

Since the discovery of microautophagy over four decades ago, relatively less progress has been made into the elucidation of the role, regulation and physiological relevance of this process in mammalian cells. This is primarily a direct result of the lack of viable techniques for dissecting the pathway. In fact, the majority of our understanding of micro-autophagy has arisen from investigation of *Saccharomyces cerevisiae* using electron microscopy (Uttenweiler and Mayer, 2008).

Microautophagy involves whole cytosolic regions being directly engulfed by the lysosome. This process is constitutively active, however, can be rapidly upregulated during nitrogen starvation or rapamycin treatment (Krick et al., 2009). There are distinct stages to microautophagy, the first of which involves the direct invagination of the lysosome membrane leading to the formation of autophagic tubes (Figure 1). Along these autophagic tubes, lateral sorting of proteins and lipids occurs leading to the development of an autophagic vesicle (Muller et al., 2000). The growth and expansion of this vesicle is mediated by two ubiquitin like conjugation systems involving Atg8 and Atg12, which are discussed in more detail in the macroautophagy section. The final step is the scission and release of the vesicle into the lysosomal lumen which is subsequently followed by degradation by vacuolar hydrolases (Figure 1). Microautophagy in yeast is known to be regulated by two signalling complexes; the target of rapamycin (TOR) and also the exit from rapamycin-induced growth arrest (EGO complex) comprised of Ego1, Gtr2 and Ego3 (Dubouloz et al., 2005).

There is still much to be revealed regarding the role and importance of microautophagy. However, there is evidence that this process may be essential in regulating membrane homeostasis by compensating for the huge membrane influx from macroautophagy (Muller et al., 2000). In addition, microautophagy may be involved in reducing organellar size and also in aiding cell survival during nitrogen starvation in yeast (Mijaljica et al., 2007).

1.1.2. Chaperone-mediated autophagy

Chaperone-mediated autophagy (CMA) is distinct from micro- and macroautophagy by the fact that this pathway targets only specific cytosolic proteins. By contrast,

organelles are not used as cargo. In addition, CMA target cytosolic proteins are not surrounded by any type of segregating membrane (Figure 1).

Briefly, the CMA pathway involves the targeting of proteins from the cytosol directly into the lysosome where they are degraded as they cross the lysosomal membrane (Chiang and Dice, 1988). One key feature of CMA is that all targeted proteins contain a pentapeptide recognition motif, with a sequence similar to Lys-Phe-Glu-Arg-Gln (KFERQ) which allows for specific degradation of excess or damaged proteins without degrading entire regions of cytoplasm (Chiang and Dice, 1988). This motif is recognised by molecular chaperones including heat shock cognate protein MW 70kDa (hsc70). Hsc70 forms a complex with the target protein aiding recognition and binding to the lysosome surface (Chiang et al., 1989). On the surface of the lysosome, the chaperone-substrate protein complex binds to the cytosolic tail of the lysosomal associated membrane protein 2A (LAMP-2A) (Cuervo and Dice, 2000). This LAMP-2A receptor protein resides as a monomer but upon substrate binding, forms a multimeric complex that is required for translocation into the lysosomal lumen. Finally, for the substrate to cross the lysosome membrane, protein unfolding must occur and is dependent on the presence of the lysosomal chaperone hsc70 (lys-hsc70) in addition to ATP and $MgCl_2$ (Figure 1). The expression of the LAMP-2A receptor is believed to be the rate limiting step for the translocation process. Overall, CMA has been proposed as a critical process that contributes to cellular homeostasis by modulating enzymatic metabolic processes and transcription factors (Kaushik and Cuervo, 2012).

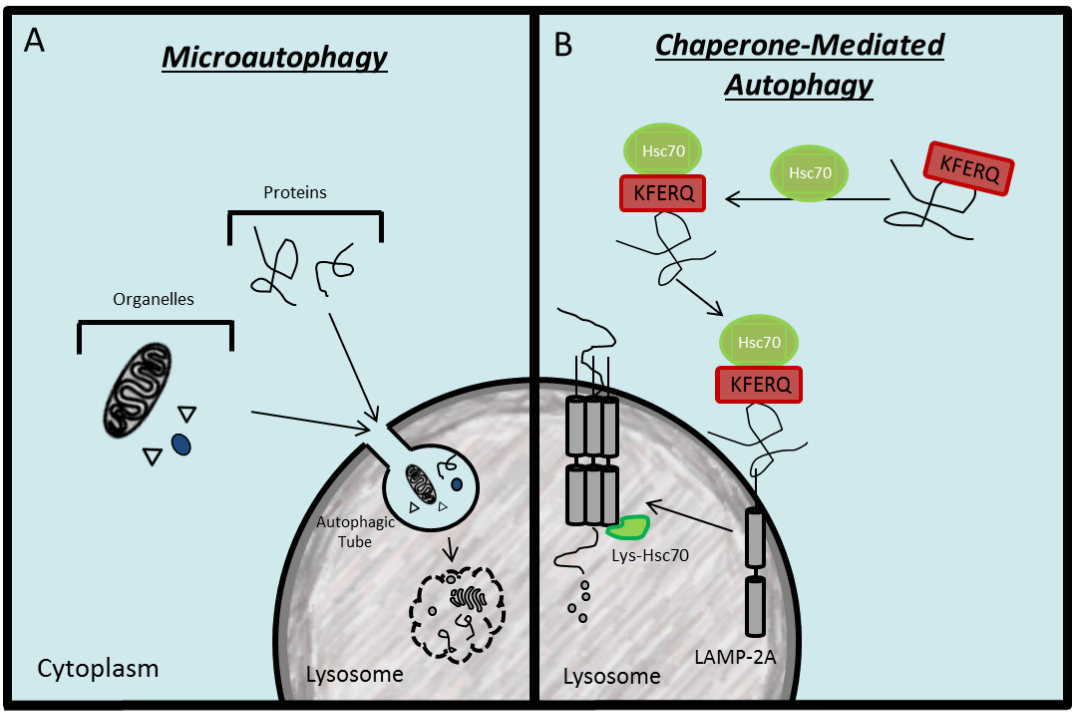

Figure 1. **Mammalian micro-autophagy and chaperone-mediated autophagy (CMA) pathways.** (A) Microautophagy involves the direct invagination of the lysosomal membrane to form autophagic tubes. Along these unique elongations of membrane, autophagic vesicles are formed. Subsequently these vesicles bud off into the lysosomal lumen where the vesicle and contents are degraded. (B) Chaperone-mediated autophagy. Proteins containing the KFERQ motif are recognised by molecular chaperones such as Hsc70 which mediates their targetting to the lysosome surface. This chaperone-substrate complex binds to the LAMP-2A receptor. Once bound the LAMP-2A forms a mutimeric complex. Next the substrate is unfolded by lys-Hsc70, a process requiring to ATP and MgCl2, and translocates accross the lysosome membrane where it is degraded and recycled.

1.1.3 Macroautophagy

Overall, across all the cell systems, the most extensively studied form of autophagy is macroautophagy, hereafter, referred to simply as autophagy. Originally, autophagy was believed to be a completely non-selective bulk degradation process. Further subtypes have since been found that are selective in their cargo sequestration (e.g. peroxisomes (pexophagy) (Sakai, Oku et al. 2006) and mitochondria (mitophagy) (Kim et al., 2007). In addition to this, the cytoplasm-to-vacuole (Cvt) pathway is another type of autophagy-related membrane trafficking found only in yeast (Bryant and Stevens, 1998). Cvt is the only autophagy-related biosynthetic pathway and is responsible for the delivery of aminopeptidase-I and α-mannosidase to the vacuole (Klionsky et al., 1992) (Hutchins and Klionsky, 2001).

Despite these selective subtypes of autophagy, the work carried out in this thesis primarily investigates the regulation of the nutrient-sensitive (non-selective bulk degradation) facet of this essential cellular degradation/recycling pathway.

Autophagy in mammalian cells proceeds through a number of different stages as displayed in figure 2. The first of these, is the initiation stage, where the isolation membrane (phagophore) is formed. Next, is the elongation step where the isolation membrane elongates to form a double membrane vesicle (autophagosome), subsequently, a newly formed autophagosome undergoes maturation and fusion with an endosome and/or lysosome. Completion of autophagy involves the degradation of the vesicle contents by lysosomal hydrolases and recycling of nutrients back into the cell cytoplasm (Yang and Klionsky, 2010a);

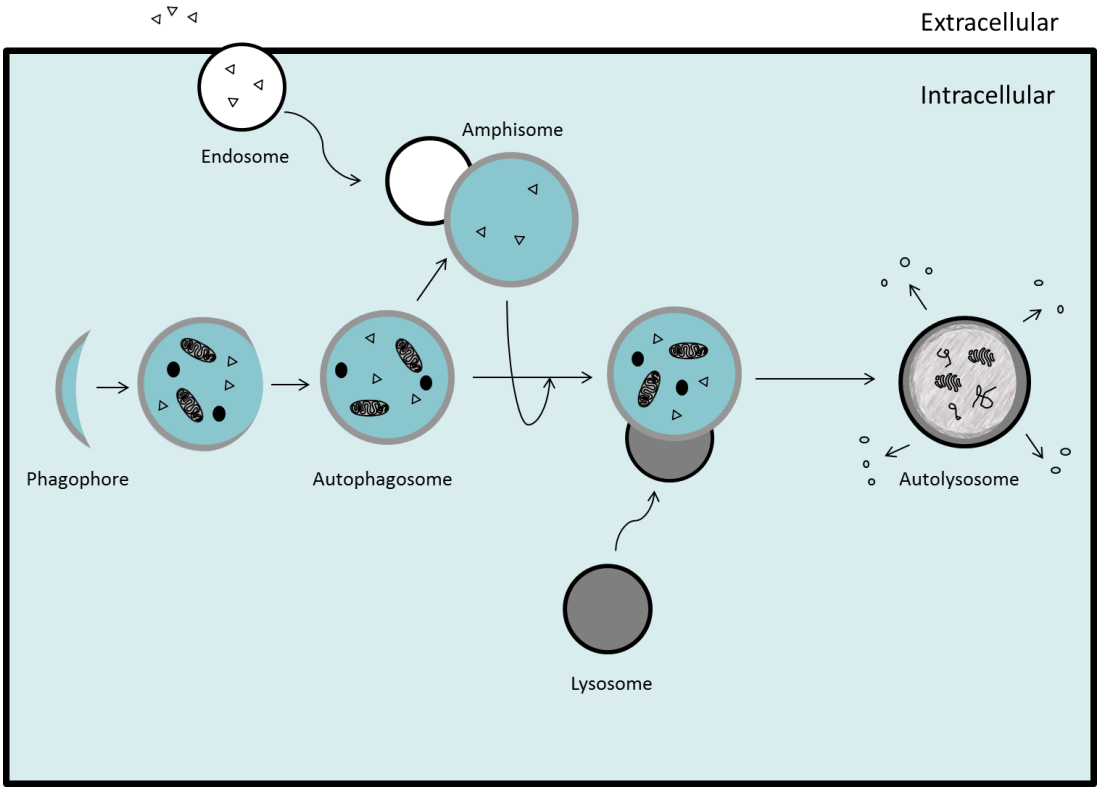

Figure 2: **Schematic diagram of Mammalian Autophagy.** Autophagy commences with the formation of the phagophore/isolation membrane. Several core autophagy proteins are essential for this step as well as for the elongation of the membrane to generate a double membrane vesicle, called the autophagosome. This autophagosome completely engulfs sections of the cytoplasm containing proteins and organelles, transporting them to the lysosome. Once fused with the lysosome (autolysosome) the intracellular contents are degraded by action of lysosomal hydrolases and the products are finally recycled back into the cytoplasm.

1.2 The Physiological and Pathological roles of autophagy.

While my interest in this thesis is the biochemistry of autophagy signalling, it is important to first briefly summarise a case for the importance of autophagy research in biology. The normal and essential physiological role of autophagy in maintaining cellular homeostasis and promoting cell survival is now widely acknowledged (Levine and Kroemer, 2009). In the general consensus, during periods of nutrient deprivation, autophagy is upregulated to degrade excess intracellular proteins and organelles, generating energy or metabolic building blocks during periods of nutrient scarcity. This process is crucial for overall mammalian survival and this importance is exemplified by the study showing that mice with Atg5 (a key autophagy related protein) knockout (KO), die within 1 day after birth during the post-maternal starvation period (Kuma et al., 2004). Recently the lethality of Atg5 null neonates has been linked to neuronal dysfunction in addition to a suckling defect. Restoration of Atg5 expression specifically in neurons can rescue lethality (Yoshii et al., 2016).

Mice with conditional KO of the essential Atg7 protein in the haematopoietic system developed severe anaemia (Mortensen et al., 2010). In addition, $Atg7^{-/-}$ erythroid cells were associated with a reduced lifespan and increased cell death due to an altered membrane potential (Mortensen et al., 2010). To understand this phenotype, recall that increased abnormal/damaged mitochondria is a known contributor to oxidative stress via increases in reactive oxygen species (ROS). Oxidative stress has been shown to reduce the life-span of haematopoietic stem cells (Ito et al., 2006). As autophagy (mitophagy) is now accepted to be key for maintaining proper healthy mitochondrial content, this role of autophagy is thereby the likely critical mechanism for promoting haematopoietic stem cell maintenance and survival.

Despite the widely appreciated pro-survival function for autophagy in maintaining homeostasis, there is also a substantial body of evidence supporting roles in mediating Type II cell death (autophagic cell death). Type II autophagic cell death can be distinguished from the well-known Type I apoptotic death by the presence of addition autophagic structures and in some cases can also be caspase independent (Schweichel and Merker, 1973, Baehrecke, 2005). The role of autophagy in mediating cellular death remains controversial to this day due to the larger base of evidence linking autophagy to cell survival. However, the evidence for autophagy in driving cell death can be also compelling.

Originally, autophagic cell death was conceived based on multiple observations that dying cells also showed high-scale autophagic vacuole formation within the cytoplasm (Liu and Levine, 2015). However, this correlation alone was recognized to be only limited evidence for a bona fide causal relationship between autophagy and cell death. In fact, induction of autophagy was proposed to be merely an incomplete attempt to maintain homeostasis as a 'last ditch' attempt to survive. This attempt was ultimately not enough, progressing inevitably to cell death. However, since initial findings, further studies have been carried out providing stronger evidence of a direct relationship between the autophagic machinery and programmed cell death in certain contexts. For example, *Dictyostelium discoideum* has provided a robust cell model for examining the link between autophagy and cell death due to the absence of apoptotic machinery in this amoeboid species. During starvation, these cells form multicellular aggregates in which a sphere of spores are supported by a cellular stalk. These stalk cells typically undergo programmed cell death which can be suppressed

by mutation of key autophagy related gene, *Atg1* (Kosta et al., 2004). Thus, loss of Atg1-dependent autophagy blocked programmed cell death.

As additional evidence, cells that are incapable of undergoing apoptosis due to caspase inhibition or KO of pro-apoptotic proteins can be channeled towards autophagic cell death. For example, cells with KO in pro-apoptotic proteins Bax/Bak or overepxression of Bcl-2/Bcl-XL (anti-apoptotic proteins) drive autophagic cell death (Shimizu et al., 2004). Conversely, reducing the expression of Atg7 or Beclin-1 (two essential autophagy proteins) by siRNA in mouse fibroblasts almost completely abolished cell death progression (Yu et al., 2004). Therefore, it is clear that autophagy can help promote some forms of programmed cell death in mammalian and more distantly related cells.

More recently, a new form of autophagy-dependent cell death has been identified which has been termed “autosis” (Liu et al., 2013). Autosis is regulated by Na^+/K^+ATPase and can be induced by starvation, hypoxic ischemia and autophagy-inducing peptides (e.g. Tat-Beclin-1). This novel form of autophagic cell death in early stages is characterised by an initial dilation and fragmentation of the ER coupled with nuclear membrane convolution. This is subsequently followed by the disappearance of the ER and focal swelling of the perinuclear space (Liu and Levine, 2015). It is unclear, at this stage, what further cell death machinery is utilised to mediate this process. However, this pathway does not appear to involve the canonical apoptosis and necrosis machinery. As yet, it remains to be determined if autosis is a merely subdivision of autophagic cell death or if this might in fact be the primary route by which autophagic cell death occurs.

Mirroring the examples of autophagy as a key player in normal physiology, disruption of normal autophagy is also acknowledged to underpin a wide range of pathophysiology. The role of autophagy in cancer serves as one prime example, as this area has been particularly well studied, further highlighting a complex duality in which autophagy plays both tumour suppressive and tumour promoting roles, depending on context (Brech et al., 2009) (White, 2015). Based on this, the consensus in the field is that autophagy has double edged roles which need to be carefully dissected when considering strategies to target the pathway for anti-cancer therapy. Originally autophagy was described with tumour suppressive roles, based on initial reports that the *Beclin-1* gene is monoallelically deleted in a large percentage and range of cancers including prostate (Gao et al., 1995), breast (Saito et al., 1993) and ovarian (Russell et al., 1990). The other prominent model is that autophagy contributes to tumour suppression via its inhibition of oxidative stress and p62 accumulation (White, 2012). In the current understanding, it is accepted that cellular homeostasis in normal non-malignant cells likely contributes to normal housekeeping that counteracts chronic levels of stress encountered during normal physiology. Loss of autophagy function leads to an accumulation of cellular and nuclear genetic damage that then contribute to early stages of oncogenic transformation.

On the other side of the autophagy double edged sword, it is conceptually more straightforward to appreciate how autophagy function could be hijacked to promote tumour cell survival, growth and cancer progression. It has been widely reported that cancer cells rely heavily on autophagy due to increased metabolic requirements associated with the unregulated cellular proliferation frequently observed with cancer. The niche microenvironment of cancer cells deep within tumours is commonly

nutrient deprived, as well as hypoxic, due to an inadequate supply from blood vessels (Degenhardt et al., 2006). In addition, certain Ras-driven cancers have specifically been described as being autophagy addicted to maintain a sufficient pool of metabolic intermediates to sustain cancer cell growth and thus tumorigenesis (Guo et al., 2011) (Yang et al., 2011). Eileen Whites group has also suggested that established tumours have a greater dependency on autophagy for their proliferation and survival in comparison to newly developed tumours or even normal tissues (Karsli-Uzunbas et al., 2014). This group established a genetically engineered mouse model of Atg7 conditional deletion to examine acute autophagy ablation in non-small cell lung cancer. Results demonstrated that acute autophagy ablation blocked mTOR and MAP Kinase signalling, promoted cell death and also led to the increased development of oncoytomas (benign tumours) (Karsli-Uzunbas et al., 2014).

A wide range of evidence has also indicated that autophagy becomes activated following stress of cancer cells following chemo- or radio-therapy. Thereby, inhibition of autophagy has been proposed as a strategy to increase the efficacy of therapeutics by sensitising the cancer cells. The potential for targeting autophagy in cancer has been long recognised and explored, although mechanistic models are still rapidly evolving (Mathew et al., 2007) (Rabinowitz and White, 2010) (Kimmelman, 2011) (White, 2015).

Another key set of autophagy pathophysiology evidence that will be summarised concerns roles for suppressing neurodegeneration. Autophagy is involved in a wide range of disorders including Parkinson's, Alzheimer's and Huntington disease. Although each disorder displays unique mechanistic aspects, a common observation in multiple late-stage neurodegenerative diseases is the accumulation of misfolded

and aggregated proteins in addition to mitochondrial dysfunction. Autophagy has become an attractive target for the therapeutic treatment of these neurodegenerative disorders through the degradation of these abnormally folded proteins. It has been shown that autophagic activity is adversely affected in post mortem tissue in many neurodegenerative diseases (Menzies et al., 2015). From an alternative line of evidence, it was shown that blocking autophagy by conditional KO of autophagy genes Atg5 and Atg7 in mice is sufficient to induce neuronal damage and neurodegenerative phenotypes (Komatsu et al., 2006) (Hara et al., 2006). Therefore strategies that aim to upregulate autophagy to protect neuronal cells against neurodegeneration are promising to a medical viewpoint and the development of novel drugs and therapies. The recent findings between autophagy and neurodegeneration are well reviewed (Nixon, 2013) (Vidal et al., 2014) (Frake et al., 2015).

1.3 Molecular Control of Autophagy

While the morphological features of autophagy have been documented for over half a century, our molecular understanding of this process has only significantly progressed in recent decades. The first major advance was the identification of the **A**u**t**opha**g**y (Atg) genes from mutational screens in yeast such as *Saccharomyces cerevisiae* (Tsukada and Ohsumi, 1993) (Matsuura et al., 1997). Generally, the majority of these initial Atg genes have now been further explored for their orthologs in mammalian cells, indicating generally high levels of mechanistic conservation (Meijer et al., 2007). To date, over 40 Atg proteins have been discovered in yeast that are essential for different forms of core or specialised autophagy (Ravikumar et al., 2010).

Within the primary non-selective autophagic pathway, there is a subset of core Atg proteins which are vital for initiation and completion of autophagosome formation. (Xie and Klionsky, 2007) (Mizushima et al., 2011). The core molecular machinery can be split into four main functional modules: (1) Atg1/Unc-51-like kinase 1 (ULK1) complex, (2) Class III phosphatidylinositol 3-kinase (PI3K) complex, (3) Two ubiquitin-like conjugation systems involving Atg8, Atg12 (and associated protein Atg16) and finally; (4) The transmembrane protein Atg9 (Yang and Klionsky, 2010b).

The focus of this thesis is the ULK1 complex. Indeed, the ULK1 signalling kinase which has been identified as the most upstream regulator of nutrient-dependent autophagy near or at the pinnacle of the hierarchical cascade (Itakura and Mizushima, 2010), and this model has remained consistent in light of other newer data. ULK1 functions as part of a multimeric complex including mammalian Atg13, focal adhesion kinase (FAK) family interacting protein of 200kDa (FIP200) and Atg101. Generally, the ULK1 complex becomes activated upon nutrient depletion to trigger further downstream signalling for autophagy initiation. Next, I will summarise the stages of autophagosome formation, which introduces how ULK1 function controls the other main autophagy regulatory modules (with emphasis on its relationship to the class III PI3K complex). Further details regarding the role of ULK1 signalling in mammalian cells and its role in autophagy initiation is the primary focus of this thesis and will be discussed in further detail in subsequent sections.

1.4 Process of Mammalian Autophagy

1.4.1 Isolation membrane Initiation / Nucleation

Once nutrient starvation signals are received, the biogenesis of the phagophore (also known as the isolation membrane (IM)), can be considered the first step of

mammalian autophagy membrane trafficking. The site at which IM is formed, to date, remains a controversial question reflecting the unique aspects for this rapid formation of a new organelle (Lamb et al., 2013). In yeast, the IM is generated at a single perivacuolar compartment known as the pre-autophagosomal structure (PAS) (Reggiori and Klionsky, 2013).

In mammalian cells, IM formation had become more complex and dynamic, with tens of multiple IM sites present at any given point during the early initiation phase. However, the preponderance of evidence has now led to a general consensus that the primary localisation of the IM in most cells under typical conditions lies on or in close association with the endoplasmic reticulum (ER). Indeed, the role for the ER for autophagy was noted a number of years ago when it was proposed morphologically that the ribosome free region of the rough ER is the most likely origin of the IM double membrane (Dunn, 1990). More recently, the morphological details were further confirmed using 3D electron tomography identifying a direct interaction between the IM and the ER (Yla-Anttila et al., 2009).

Another key advance was the finding that IM form at distinct ER membrane domains that are associated with the protein DFCP-1 (double FYVE containing protein -1) (Axe et al., 2008). In response to amino acid starvation, DFCP-1 was identified for its translocation onto phosphatidylinositol 3-phosphate (PI3P) enriched membrane regions which were subsequently termed omegasomes, simply due to their Ω-shaped morphology. The omegasome would be proposed to mark a prime site for IM formation on the ER and was observed to distinctly co-localise with key downstream core molecular machinery proteins LC3 and Atg5 (Axe et al., 2008). However, the

functional role of DFCP-1 during autophagy remains unclear, since loss of this protein has no appreciable inhibition on autophagy.

Since initial findings, multiple studies have further investigated the morphological relationship between the ER-omegasome-IM. Utilising electron tomography, it has demonstrated that the ER can form narrow membrane extensions, directly extending to the IM and these interconnections associate with both the inner and outer surface, thus leading to the formulation of the ER cradle model for the IM (Hayashi-Nishino et al., 2009) (Yla-Anttila et al., 2009). More recently, one report utilised an Atg3-deficient mouse embryonic fibroblast (MEF) system to generate incomplete autophagosomes (as Atg3 is important for IM expansion) resulting in an accumulation of omegasome and IM hybrid structures (Uemura et al., 2014). Using electron microscopy, the authors found that the majority of DFCP-1 localised to regions close to the edge of the IM, and interestingly, on tubular membrane structures. Importantly, these clusters of tubular membrane, which they termed IM-associated tubular structures (IMAT), required function of the ULK1 complex (FIP200, specifically) for formation. However, IMAT were still observed when further downstream Atg proteins such as Atg5 and Atg7 were disrupted, suggesting that IMAT represent the earliest stages of IM formation driven by ULK1. Additionally, these data suggest that numerous tubular structures project from a subdomain of the ER forming the omegasome of DFCP-1 associated sites. During the closure step of IM formation, these tubular elements have been proposed to further undergo homotypic fusion or can fuse with additional IM membrane (Uemura et al., 2014).

In conjunction with this data, another set of studies have established that autophagosome IM formation is closely associated with ER–mitochondria contact

sites (Hamasaki et al., 2013). For example, using subcellular fractionation, it was shown that endogenous Atg14L (a member of the Beclin 1-Vps34-PI3K complex) co-fractionated with the mitochondrial-associated ER membrane (MAM) fraction during autophagy induced by nutrient starvation. However, in nutrient-rich conditions, where autophagy is inhibited, Atg14L was not detected in the MAM. In addition to this, disruption of the ER-mitochondrial contact site was sufficient to block Atg14L localisation onto punctate membrane sites (puncta formation). Furthermore, several other autophagy related proteins including Atg5 and DFCP-1 were also present in the MAM biochemical fraction upon starvation. Another approach utilising live-cell imaging indicated that Atg5, a marker for the forming IM, co-associated closely with ER and mitochondrial markers. Interestingly, Atg5-positive IM were mostly associated with ER markers but interaction with the mitochondria was much more transient. These observations lead to a theory suggesting that the ER acts as the predominant scaffold membrane structure for stable IM assembly site with more dynamic interactions with mitochondria.

Overall, the ER-mitochondria contact sites may represent the core pathway in the formation of the isolation membrane. However, it is necessary to recognize the vast array of other evidence suggesting additional contributions and intracellular membrane sources/sites. These further mechanisms include elements of *de novo* membrane synthesis and incorporation of membranes donated from other membranes such as Golgi, plasma membrane and endosomes (early/late) (Tooze, 2013). Overall, it seems that there may be a primary route for IM formation that functions in combination with other pathways depending on more individual cellular contexts.

As mentioned previously, one key component for driving IM nucleation is function of the class III phosphatidylinositol 3-kinase (PI3K) Vps34. Importantly, this PI3K complex is now appreciated to receive signals immediately downstream from the ULK1 complex (Di Bartolomeo et al., 2010) (Russell et al., 2013) (Egan et al., 2015). To introduce this PI3K complex, it can be noted that this key autophagy signalling module contains Vps34, p150 (Vps15), Beclin-1 (Atg 6) and Atg14L. Within this core complex, the Beclin-1 subunit is vital for the catalytic activity of Vps34 and IM nucleation via its network of interacting proteins (He and Levine, 2010). In the consensus model, Beclin-1 can also form a complex with the anti-apoptotic Bcl-2 proteins through its BH3 domain (Liang et al., 1998) (Erlich et al., 2007), thus competitively interfering with Beclin-1/Vps34 interaction. Upon autophagy stimulation, Beclin-1 is released from Bcl-2 and becomes available to interact with Vps34. Once active, Class III Vps34 phosphorylates phosphoinositol to produce enriched sites containing the active PI3P lipid which drive IM and autophagosome assembly.

The key role for PI3P has been long established, for example, the inhibition of Vps34 by 3-methyladenine or wortmannin inhibits autophagy, while, on the other hand, exogenous addition of PI3P, stimulates autophagic activity (Petiot et al., 2000). Once PI3P is generated, specific lipid binding effectors containing PX or FYVE domains are recruited to the forming autophagosome (Obara and Ohsumi, 2011). In yeast, these include Atg18 and PpAtg24 (Burman and Ktistakis, 2010).

As discussed above, PI3P binding is the basis of DFCP-1 recruitment to omegasomes. In mammalian cells, a key functional PI3P binding effector was recently identified as the WIPI-2 family member of the WIPI family. (Dooley et al., 2014). Recruitment of WIPI-2 then helps drive further assembly of factors via interactions with Atg12-Atg5-

Atg16L complex (Dooley et al., 2014). These all lend evidence to the initiation model in which the action of PI3P is fundamental for autophagic IM assembly.

The function of the Vps34 complex is critically dependent on each of its subunits. Atg14L has been proposed to play an important role for the recruitment of the PI3K complex to the IM assembly site (Matsunaga et al., 2009). For example, reduction of Atg14L function leads to the inhibition of LC3 and Atg16L1 puncta formation and subsequent inhibition of autophagy (Matsunaga et al., 2009). As mentioned above, ATG14L is observed translocating to ER-mitochondrial contacts specifically upon autophagy induction. More recently it has been shown that ULK1 interacts with and phosphorylates Atg14 during starvation conditions and MTORC1 inhibition (Park et al., 2016).

From within the core complex, Beclin-1 can associate with several other co-factors that can further modulate (either increase or decrease) autophagic activity. Examples include, UV radiation resistance-associated gene (UVRAG), Bax-interacting factor 1 (Bif-1) and as mentioned above, Bcl-2 (Liang et al., 2006) (Takahashi et al., 2007) (Liang et al., 1998). UVRAG can stimulate autophagy by competing for binding to Beclin-1 with Atg14 (Itakura et al., 2008) (Matsunaga et al., 2009). UVRAG can also bind to Bif-1 which is suggested to have the ability to bind to membranes and alter curvature driven by its N-BAR domain (Itoh and De Camilli, 2006).

On the other hand, as mentioned above, binding to Bcl-2 negatively suppresses autophagy by sequestering Beclin-1 away from the main Vps34 complex. In terms of regulation, phosphorylation of Bcl-2 by c-Jun N-terminal kinase 1 and also death associated protein kinase has been reported to drive disassociation of Bcl-2 and Beclin-1 during starvation induced autophagy (Wei et al., 2008) (Patkar et al., 2012).

The early steps of IM formation have also been shown to involve membrane vesicles containing the transmembrane protein Atg9. The interrelationship between early IM formation, Atg9 and ULK1 function has been established by several lines of evidence. Membrane vesicles containing Atg9 have been proposed to cycle between endosomal and Golgi-associated pools, likely deriving bilayer material from each of these sources along the dynamic cycle (Young et al., 2006). The ability of Atg9 to properly traffic depends on the ULK1 complex and this regulatory link is conserved from yeast (Chan et al., 2009) (Papinski et al., 2014). ULK1$^{-/-}$ MEF displayed defective Atg9 localisation in nutrient rich conditions (Mack et al., 2012). Yeast Atg1 directly phosphorylates Atg9 and this modification is essential for the proper recruitment of downstream autophagy factors Atg8 and WIPI-1 (Papinski et al., 2014). In mammalian cells it is evident that Atg9 and ULK1 can interact during autophagy induction on membrane assembly sites (Orsi et al., 2012) (Puri et al., 2013) . Recent evidence directly indicates Atg9 vesicles contribute to the earliest stage ULK1 positive structures (Karanasios et al., 2016). This study could further demonstrate that Atg13 (part of ULK1 complex) is found on specialised compartments that associates with small Atg9 vesicles and ER-Golgi-intermediate compartment (ERGIC) membranes. This interaction was independent of PI3P, thereby suggesting Atg9 and ERGIC associated membranes contribute to the earliest ULK1-dependent stages of IM formation before activating Vps34 to drive subsequent stages. This mechanism appears to be conserved from yeast. It has been recently been shown that an Atg1-Atg13 subcomplex helps tether and recruit Atg9 vesicles in an Atg17-dependent manner during autophagosome formation in *Saccharomyces cerevisiae* (Rao et al., 2016) .

1.4.2 Isolation membrane Elongation / Expansion

Although IM initiation may originate from ER and mitochondria, the elongation stage appears to involve several converging membrane contributions. Recent evidence has indicated a role, in particular, for the ER exit site (ERES) during IM elongation (Zoppino et al., 2010) (Graef et al., 2013). The function of ERES is to direct protein sorting into coat protein complex (COPII) vesicles for further trafficking towards the ERGIC and following, to the Golgi (Brandizzi and Barlowe, 2013). The existence of functional crosstalk between ERES and the autophagy pathway has been demonstrated as the number of DFCP-1 positive omegasomes is strongly reduced in cells where COPII vesicle production is abrogated (Ge et al., 2013).

Several possible theories have been proposed that include the ERES acting as a scaffold for autophagosome biogenesis. In this regard, the distinction between ER-mitochondria contact sites vs ERES serving as the initial IM cradle scaffold may be difficult to definitively discern as these may be intermixed and dynamic membrane populations. Secondly, the ERES could provide membranes via COPII vesicles to drive elongation of the emerging IM (Sanchez-Wandelmer et al., 2015). Interestingly, the ERGIC has also been implicated in promoting LC3 lipidation-dependent IM elongation. The ERGIC is required for autophagosome formation and the lipidation of LC3 (Shpilka et al., 2011). The ERGIC has also been further shown using cell-free systems to particularly contain potent LC3-lipidation activity (Ge et al., 2013). It has been proposed that starvation induces the translocation of the membrane protein SEC12 (key for COPII assembly) from the ER to the ERGIC. This translocation, in combination to PI3K activation, allows COPII vesicles to act as a basis for providing LC3 lipidation enzymatic activity and further membranes to drive elongation (Ge et al., 2014).

Elongation of the autophagic membrane supports the recruitment of further autophagic proteins that allow for the sequestration (in some cases specific) of cytoplasmic cargo for degradation. Two inter-dependent ubiquitin-like conjugation systems are critically involved in this stage. One of these systems involves Atg12. The second system involves Atg8, of which comprises a large family of proteins in mammalian cells (Shpilka et al., 2011). To date, the best characterised mammalian Atg8 member is microtubule-associated protein 1 light chain 3 (MAP1-LC3), which is commonly referred to simply as LC3.

The Atg8-Atg12 system has been widely studied as an intricate post translational signalling mechanism that is unique to autophagy and highly conserved from yeast to mammals. In the first reaction, Atg12 is activated by Atg7 (E1-like reaction) to form an Atg12-Atg7 intermediate. Atg12 is then transferred to Atg10 (E2-like reaction) and subsequently Atg12 is covalently bound to Atg5 by an isopeptide bond (Mizushima et al., 1998). In mammalian cells, this Atg12-Atg5 complex is further conjugated to Atg16L1 to form tetrameric complexes of 800kDa (Mizushima et al., 2003). Interestingly, this Atg12-Atg5-Atg16L1 oligomeric complex is found constitutively within the cytoplasm independent of autophagy induction.

The second conjugation system begins with the cleavage of the Atg8 protein (e.g. LC3) at its C-terminal by a cysteine protease, Atg4, leading to the formation of cytosolic (inactive) LC3-I. LC3-I is then conjugated to phosphatidylethanolamine (PE) via similar reactions to the Atg5-Atg12 system. This includes activation of Atg8/LC3 by Atg7 (E1-like reaction), transfer to Atg3 (E2-like reaction), and then conjugation of LC3 to PE to form activated LC3-II (LC3-PE). Unlike the Atg12 complex, the formation of LC3-II from LC3-I occurs primarily as a highly regulated event following autophagy induction. As

such, generation of LC3-II biochemically and via imaging has become the most commonly used robust marker to date for autophagy activity (Kabeya et al., 2000). LC3 on the autophagosome membrane then becomes the anchor for other cargo adaptor proteins such as p62 and NBR1. The interaction between these adaptors and LC3 occurs through an LC3 interacting region (LIR) motif (Stolz et al., 2014).

It must be noted however that LC3 also plays a key non-canonical autophagic role in a process called LC3-assisted phagocytosis (LAP). Following engagement of certain receptors, e.g. TLR1/2, TLR2/6, and TLR4, LAP recruits LC3 molecules to single membrane phagosome membranes (Sanjuan et al., 2007). This is believed to serve several important functions including delivery of the phagosome cargo to pathogen recognition receptors and by acting as a facilitator enhancing peptide presentation. However the LAP is also important to promoting the maturation/fusion of single membrane phagosomes to the lysosome and LC3-II is essential for this to occur (Martinez et al., 2015).

In contrast to roles during early IM formation, as already discussed, Atg9 was originally recognised for coordinating IM elongation (Karanasios et al., 2016). Vesicles containing Atg9 have been established to dynamically cycle from the Golgi and endosomes, which could then donate membranes during IM initiation and further throughout the expansion phase (Young et al., 2006) (Orsi et al., 2012). An additional study has shown that Atg9 vesicles are generated from the plasma membrane to transport towards the recycling endosome via clathrin mediated endocytosis (Puri et al., 2013). Interestingly, Atg16L1 positive vesicles were also localised to the same recycling compartment. Furthermore, the study showed that nutrient starvation increases the fusion between Atg9-positive early endosomes and Atg16L1-positive

endosomes in a process that is dependent on the SNARE protein VAMP3. Together, the studies suggest that Atg9 vesicles, dynamically cycling between a number of membranes, can serve as a major transport route of the bilayer to sustain autophagy IM expansion. Following the elongation phase, the next stage is the closure of the autophagosome. However the mechanisms behind this are a poorly understood step. LC3 appears to be critical as overexpression of mutant Atg4 results in defective autophagosome completion (Fujita et al., 2008).

It has been shown that upon formation of the autophagosome, LC3-II found on the outer membrane becomes deconjugated from PE by the action of Atg4 and this pool of LC3 is recycled back into the cytosol (Kirisako et al., 2000). In addition to this the Atg12-Atg5-Atg16L complex also disassociates from the surface of the autophagosome (Matsushita et al., 2007).

1.4.3 Autophagosome Transport / Fusion / Maturation

Completed autophagosomes are trafficked to lysosomes in a process that is structured around the cytoskeleton. Microtubules and microfilaments have both been implicated in autophagosome trafficking and lysosome fusion. In contrast, intermediate filaments (IF) are associated with autophagy, but more for autophagy inhibition through the formation of the Beclin-1/14-3-3/Vimentin complex (Wang et al., 2012). Autophagosome trafficking is not associated with IF.

Microtubules, one of the three major components of the cytoskeleton, are tubular and highly dynamic structures. In terms of autophagosome translocation, dynein and kinesin motor protein families interact and bind to microtubules to further autophagosomal trafficking and fusion. For over twenty years, it has been known that blocking microtubule polymerisation with drugs such as nocodazole and vinblastine

can slow the fusion of autophagosomes with lysosomes (Webb et al., 2004) (Fass et al., 2006). Using live-cell imaging, it was observed that mature autophasosomes move bi-directionally along microtubules in a dynein-dependent fashion towards lysosomes which are found in high abundance around the microtubule organising centre (MTOC) (Jahreiss et al., 2008). This dynein dependency has been confirmed by others (Kimura et al., 2008).

A recent report also shows roles for microfilaments and actin comet tails (branched actin filaments) for generation of forces required to traffic autophagosomes (Kast and Dominguez, 2015). Actin comet tails, generated by the ARP2/3 (actin-related protein 2/3) complex were already understood to direct movement of endosomes and lysosomes (Taunton et al., 2000). Following on from this, it was shown that WHAMM (WAS protein homolog associated with actin, Golgi membranes and microtubules), which interacts with the branch stabilising protein cortactin, also associates with the ARP2/3 complex leading to actin comet tail formation on autophagosomes during nutrient sensitive autophagy.

Histone deacetylase-6 (HDAC6) is an example of a microtubule-dependent factor that has been associated with selective autophagy and the removal of mitochondria and protein aggregates (Lee et al., 2010b). Interestingly, the HDAC6 mechanism also involves recruitment of cortactin and F-actin remodelling. Deficiency of HDAC6 resulted in abrogation of autophagosome maturation and accumulation of protein aggregates. Thus, HDAC6 might be a convergence point linking autophagosome transport to both the microtubule and actin cytoskeletons. WHAMM and HDAC6 appear to be complementary actin-based mechanisms that both contribute during autophagosome transport and maturation steps, speculatively for both non-selective

vs selective forms of autophagy. The actin motor protein myosin VI has also been linked to autophagosome maturation via control of membranes containing the ESCRT-0 component Tom1 to the autophagosome (Tumbarello et al., 2012). Altogether the findings indicate that formed autophagosomes have a number of motor dependent mechanisms for transport to the lysosome, relying on a combination of microtubule and actin cytoskeletons. This diverse set of pathways seems evolutionarily sensible given the diverse potential origins for autophagosomes amongst the different cellular contexts. Once the autophagosome arrives near the vicinity of the lysosome, components of the canonical intracellular membrane remodelling machinery direct autophagosome/lysosome fusion. Membrane fusion typically requires the input of three types of proteins: Rab proteins; membrane tethering factors; and SNAREs. Examples of the most prominent pathways for each category are briefly summarised, below.

Multiple studies have shown that the late endosome Rab7 GTPase plays a particularly important role in autophagosome/lysosome fusion. For example, down regulation of Rab7 inhibits the autophagosome/lysosome fusion in cardiomyocytes (Su et al., 2011). Furthermore, inhibition of the SERCA Ca^{2+} pump, by thapsigargin, abrogated Rab7 recruitment to autophagosomes, blocking downstream fusion (Ganley et al., 2011). For membrane tethering, the homotypic fusion and vacuole protein sorting (HOPS) complex may be a predominant regulator. The HOPS complex has recently been demonstrated to translocate and interact with Syntaxin17 (Stx17) on the autophagosomal membrane (Jiang et al., 2014). This interaction was essential for autophagosome/lysosome fusion as knockdown of HOPS complex components VPS33A or VPS39 results in the accumulation of Stx17 and LC3 positive

autophagosomes (Jiang et al., 2014). More recently the pleckstrin homology domain containing protein family member 1 (PLEKHM1) was shown to directly associate with this HOPS complex, however interestingly also contains a LC3-interacting region (LIR) that regulates autophagosome binding (McEwan et al., 2015). Further work investigating the HOPS complex is required however as other studies have shown that depletion of another complex component VPS16 in mice does not affect autophagic flux (Ganley et al., 2011).

SNARE proteins are well understood to be the main drivers for membrane fusion. SNARE membrane proteins form a four-helix bundle comprised of a single R-SNARE subunit and three Q-SNARE subunits, which together effectively drive close interaction and fusion between two bilayers (i.e the autophagosome and lysosome). To date, several candidate SNAREs have been identified for mammalian autophagosome fusion, including R-SNARE (Vamp3, Vamp7 and Vamp8) whilst the Q-SNARE (Vti1B) has also been identified in this context (Fader et al., 2009) (Furuta et al., 2010). More recently, the Q-SNARE Stx17 (mentioned above for interaction with HOPS) has been identified to be an autophagosomal-specific SNARE protein essential for autophagosome-lysosome fusion (Itakura et al., 2012b). This study found that Stx17 is recruited to completed autophagosomes and further interacts with SNAP-29 and the endosomal/lysosomal SNARE, Vamp8. In fact, knockdown of Stx17 and SNAP-29 both led to autophagosome accumulation. In agreement, these essential SNAREs were also required for a proper autophagosome fusion in *Drosophila melanogaster* (Takats et al., 2013). Thus, although the itinerary of an autophagosome encounters several key membrane fusions, the specific machinery involved in remodelling in the

bilayers have already been substantially described, although it seems likely other regulatory factors have not yet been identified.

In addition to the Rab7, tethering complexes and SNARE proteins, several other interesting mechanisms have recently been shown to be critical for autophagosome/lysosome fusion.

It has long been recognised that autophagosome fusion and maturation requires fully functional lysosomal activity. Inhibition of vacuolar ATPase (v-ATPase) by bafilomycin A_1 blocks pumping of H^+ into the lysosome and inhibits the activity of lysosomal enzymes through abnormal increases in lumen pH (Yoshimori et al., 1991). After longer times of treatment, bafilomycin also inhibits fusion of the autophagosome and lysosome (Jahreiss et al., 2008). Until recently, it was an accepted dogma that inhibition of v-ATPase at the lysosome explained poor levels of lysosomal fusion. However, a recent study has suggested an alternative model that involves bafilomycin targeting SERCA Ca^{2+} pumps on the ER (Mauvezin et al., 2015). In this model, disruption of the ER Ca^{2+} gradient has been proposed to cause leakage of Ca^{2+} into the cytosol which ultimately inhibits autophagosome-lysosome fusion, although further mechanistic details are unknown. Nonetheless, this work suggests that autophagosome-lysosome fusion is unexpectedly independent of lysosomal pH and further implicates the SERCA pump as a key regulator for autophagic fusion, as highlighted by other data mentioned above using SERCA-inhibitor thapsigargin (Ganley et al., 2011).

Another recent study is also important to mention due to insights on roles of different Atg8 family members at early vs. late stages of autophagy trafficking. LC3 and the related Atg8-member GABARAP (γ-aminobutyric acid receptor-associated protein)

had been earlier recognised to have distinct functions in autophagy by mediating autophagosome biogenesis and maturation respectively (Weidberg et al., 2010). Further mechanistic details on the unique role of GABARAP have been revealed. It was shown that GABARAP was critical to recruit a palmitoylated form of the lipid kinase, PI4K IIα (Barylko et al., 2009) (Lu et al., 2012), from a Golgi-resident pool to the autophagosome (Wang et al., 2015a). PI4K IIα activity subsequently leads to an increased production of phosphatidyinositol-4-phosphate (PI4P) on the autophagosome, which speculatively could form a stable platform for formation of specific GABARAP complexes required for autophagosome-lysosome fusion. This step was critical and robust as depletion of PI4K IIα inhibited lysosomal acidification and subsequent autophagosome/lysosome fusion. This study is important as it further highlights how different Atg8 members (LC3 and GABARAP) and different signalling lipids (PI3P vs PI4P) can direct distinct stages of autophagy traffic.

Above, the four major phases of autophagosome formation have been outlined, through to fusion with the lysosome. Following this, the final step of *bona fide* autophagy degradative flux results in the degradation of the mixed contents by lysosomal acidic hydrolases. The resulting macromolecules of amino acids and lipids are generally acknowledged to be recycled back into the cytoplasm by the action of membrane permeases, although this end stage event has not shown as much molecular dissection as its preceding steps. On this note, studies over recent years have re-focussed attention to the lysosome as a primary centre for cellular amino acid sensing, this is further discussed later in this introduction, thus linking late stage autophagy with upstream signalling networks.

1.5 Mechanistic target of rapamycin (MTOR)

The work of this thesis studies the role of ULK1 complex during autophagy initiation. As such, it is essential to understand the details of nutrient-sensitive signalling that directly regulate ULK1. Current literature is consistent with Mechanistic Target of Rapamycin (MTOR) as the key regulator of acute nutrient sensitive autophagy signalling, via activation of the ULK1 pathway.

MTOR is a large 289kDa multidomain protein which is classified into the Class I phosphatidylinositol 3-kinase (PI3K) like protein kinase (PIKK) superfamily (Harris and Lawrence, 2003). This atypical serine-threonine kinase family is involved in a variety of anabolic cell processes such as cell growth/proliferation, cell cycle progression, migration, protein transcription and translation (Fingar et al., 2004) (Zhou and Huang, 2011) (Wang and Proud, 2006). Activation of MTOR is widely appreciated to promote protein translation and cell growth through phosphorylation of a number of critical substrates, of which the best characterised are p70 S6 kinase and eIF4E- binding protein 1 (4E-BP1). Simultaneously, MTOR serves to coordinate opposing pathways by suppressing the pro-catabolic autophagy pathway via the ULK1 and Vps34 complexes under conditions of high nutrient availability (Kim and Guan, 2015). In addition, MTOR activation can further inhibit autophagic protein transcription by preventing the translocation of transcription factor EB (TFEB) to the nucleus through sequestration in the cytoplasm (Pena-Llopis et al., 2011) (Martina et al., 2012).

Interestingly, homozygous $MTOR^{-/-}$ mice have severe development issues which lead to embryonic lethality emphasising the importance of MTOR (Gangloff et al., 2004). MTOR functions within two distinct multimeric complexes: MTOR complex 1 and complex 2 (MTORC1 and MTORC2) (Sabatini, 2006), and nutrient-dependent

regulation of cell growth and autophagy are primarily directed by MTORC1. MTORC1 is composed of a core module of MTOR, regulatory associated protein of TOR (Raptor), mammalian lethal with SEC13 protein 8 (mLST8) and DEP domain containing MTOR-interacting protein (DEPTOR) (Laplante and Sabatini, 2012). MTORC1 can further be regulated by proline-rich Akt/PKB substrate of 40 kDa (PRAS40), Tti1 and Tel2 (Vander Haar et al., 2007) (Kaizuka et al., 2010). The Raptor subunit is important for recognition and phosphorylation of MTORC1 substrates whilst PRAS40 and DEPTOR suppress MTOR kinase activity. This complex has been found to be highly sensitive to nutrients and also to the drug, rapamycin (Chen et al., 1995). Rapamycin forms a complex with the FK506-binding protein 12kDa (FKBP12) intracellular receptor. The rapamycin-FKBP12 complex subsequently interacts with the FKB12-rapamycin binding (FRB) domain in MTOR, thus interfering with the MTOR - Raptor interaction, robustly suppressing MTORC1 signalling (Chen et al., 1995).

The MTORC2 on the other hand contains MTOR, rapamycin-insensitive companion of TOR (Rictor), mammalian stress-activated protein kinase interacting protein 1 (mSin1), mLST8, DEPTOR and protein observed with Rictor (PROTOR) (Laplante and Sabatini, 2012). Reports indicate that only MTORC1, not MTORC2, interacts with the ULK1 complex (Hosokawa et al., 2009, Jung et al., 2009). MTORC2 is primarily understood to regulate cell survival and proliferation through its activation of Akt (reviewed in (Manning and Cantley, 2007)). However MTORC2 has also been linked to actin-cytoskeletal organisation (Jacinto et al., 2004).

1.5.1 Regulation of MTORC1

MTORC1 can integrate signals from several nutrient, growth factor and energy sensing pathways. Currently the most well defined signalling mechanism of activation

is through growth factor signalling. During times of high nutrient availability growth factors such as insulin bind to their corresponding receptor tyrosine kinase (RTK) to induce a signalling cascade. This leads to the activation of the class I phosphoinositide 3-kinase (class I PI3K) (Myers et al., 1992). This subsequently catalyses the conversion of the plasma membrane bound $PI(4,5)P_2$ to form $PI(3,4,5)P_3$ (Stephens et al., 1993). The PI3K reaction can be antagonised by the phosphatase PTEN (Maehama and Dixon, 1998).

Next $PI(3,4,5)P_3$ interacts with pleckstrin homology domain containing proteins such as Akt recruiting this protein to the plasma membrane where it is activated via phosphorylation by PDK1 and MTORC2 (Sarbassov et al., 2005). Akt also plays a key role in modulating the tuberous sclerosis complex (TSC1/2). TSC1 and TSC2 form a heterodimeric complex that acts as a Rheb specific GTPase activating protein (GAP). Activated Akt then phosphorylates and negatively regulates the TSC2 (which leads to the activation of the small G-protein Ras homolog enriched in brain (Rheb) activating MTORC1 at the lysosome (Inoki et al., 2002) (Menon et al., 2014). Rheb has been reported to interact with MTORC1 independently of GDP/GTP binding state however MTORC1 activity is only increased by GTP-Rheb (Long et al., 2005). Akt additionally phosphorylates the MTORC1 component PRAS40 to increase MTOR kinase activity (Sancak et al., 2007) (Wiza et al., 2012).

1.5.2 Regulation of MTORC1 by Amino Acids

The correlation between amino acid availability and protein synthesis has been characterised in different contexts for decades. Autophagy activation occurs upon MTORC1 inactivation (when amino acids are scarce). Thus, understanding of autophagy regulation is fundamentally linked to MTORC1 mechanisms. In recent

years, huge advancements have been made in regard to the molecular details of MTORC1 regulation via a lysosomal-localised signalling pathway. In the current model, basal resting conditions lends to inactive MTORC1 predominately localised within the cell cytoplasm. However, during nutrient (amino acids and/or energy) rich conditions, MTORC1 is recruited to the lysosome surface where it becomes fully active and subsequently functions to stimulate downstream protein synthesis pathways (Sancak et al., 2010). In particular, Arginine (Arg), Glutamine (Gln) and Leucine (Leu) have consistently been reported to be the most potent amino acids in respect of the activation of MTORC1 (Jewell et al., 2015).

1.5.3 Activation of MTORC1 by lysosomal amino acid sensing

The association of MTORC1 with the lysosome membrane promotes its activation by promoting interactions with the small GTPase Ras homolog enriched in brain (Rheb) via its Raptor and mLST8 subunits (Long et al., 2005) (Tee et al., 2005). Interaction with Rheb is absolutely required for maximal MTORC1 kinase activation (Sancak et al., 2007). Activity of Rheb, in turn, is primarily under robust regulation downstream of growth factor signalling which switches on Rheb via the PI3K dependent activation of Akt and spatial regulation of tuberous sclerosis complex (TSC) complex (Reviewed in (Huang and Manning, 2009) (Dibble and Cantley, 2015).

If bringing MTORC1 to the lysosome is the critical event, how is this regulated? The mechanism for MTORC1 subcellular localisation by amino acids is now widely appreciated to be driven by the concerted action of the Rag GTPase family (Kim et al., 2008) (Sancak et al., 2008). Within mammalian cells there are 4 Rag members (Rag A, Rag B, Rag C and Rag D). Rag A/B are functionally interchangeable, as are Rag C/D. These proteins form heterodimers with Rag A (or B) interacting with Rag C (or D). In

amino-acid rich conditions, these heterodimers are converted to their active conformation with Rag A/B being GTP loaded, while Rag C/D remains in its GDP bound form (Sancak et al., 2008). In contrast, during amino acid starvation, RagA/B GDP-Rag C/D remain constitutively associated. Interestingly, unlike other GTPases, Rags are unable to undergo lipid modification to mediate their targeting to membranes. Instead, Rag GTPases require the Ragulator complex to promote its tethering to the lysosomal surface (Zoncu et al., 2011) (Bar-Peled et al., 2012). The Ragulator complex consists of 5 subunits which include: p18 (LAMTOR1/C11orf59); p14 (LAMTOR2/ROBLD3); MP1 (LAMTOR3/MAPKSP1); LAMTOR4 (C7orf59); and LAMTOR5 (HBXIP) (Sancak et al., 2010). Additionally, the Ragulator can further act as a guanine nucleotide exchange factor (GEF), promoting active GTP-bound Rag A/B in a v-ATPase-dependent manner. Therefore, a wide range of data support the model where the Ragulator and Rag heterodimers act as a docking site for MTORC1 at the lysosome (Sancak et al., 2008).

Via the Ragulator and Rags, the lysosome serves an amino acid sensing docking station for MTORC1. Understanding of lysosomal amino acid sensing has dramatically expanded in recent years due to the further elucidation of specific components of the signalling machinery or specific amino acid receptors driven by proteomic approaches. Interestingly, the v-ATPase lysosomal proton pump forms multiple interactions with different Ragulator subunits and has been established to be crucial for transmitting or sensing of amino acids from inside the lysosomal lumen, termed as an inside-out mechanism (Zoncu et al., 2011). In addition, the lysosomal amino acid transporter family member, SLC38A9.1, has also been shown to interact with the Ragulator complex and Rag GTP complex by multiple groups (Wang et al., 2015b)

(Jung et al., 2015) (Rebsamen et al., 2015). Mechanistically, further studies were able to outline roles for SLC38A9.1 as predominately a lysosome lumen Arg-specific sensor. For example, CRISPR mediated gene deletion of SLC38A9.1 blocked MTORC1 activation predominantly following Arg treatment (Wang et al., 2015b). Currently, the relative contribution levels between the V-ATPase and SLC38A9.1 pathways remain unclear. For example, inhibition of V-ATPase only partially diminished the stimulatory effects from SLC38A9.1 overexpression (Jung et al., 2015). Therefore the V-ATPase and SLC38A9.1 may represent interconnected amino acid sensing pathways that both converge on the Ragulator, but yet retain some functional independence.

1.5.4 Regulation of Rag GTP loading

It is now better established that amino acid availability controls the GDP/GTP state of the Rag GTPases. However, this general form of regulation is understood to be dependent on a wide range of upstream factors. As discussed above, the Ragulator complex has already been introduced for its role in directing localisation of the Rags to the lysosome and for acting as GEF driving GTP loading and activation of Rag A/B (Sancak et al., 2010). This mechanism cooperates and integrates with other proposed pathways. For example, the folliculin (FLCN)-folliculin interacting protein 1/2 (FNIP1/2) complex that has been proposed to serve as a GTPase activating protein (GAP) for Rag C/D (Tsun et al., 2013) (Petit et al., 2013). In addition, the leucyl-tRNA synthetase has recently been suggested as a leucine sensor by acting as a leucine-dependent GAP for Rag D (Han et al., 2012). This finding has been demonstrated in parallel studies in Gtr1 yeast cells (Bonfils et al., 2012). In contrast, the SH3 domain-binding protein 4 (SH3BP4) has been described as an overall negative regulator of the Rag GTPase complex (by acting on both Rag B and Rag C) during nutrient starvation,

thereby preventing the translocation of the MTORC1 to the lysosome and promoting autophagy (Kim et al., 2012).

Rag proteins also receive critical negative regulation from the GTPase-activating protein activity towards Rags (GATOR) complex. This complex is made up of two further subcomplexes; GATOR1 and GATOR2 (Bar-Peled et al., 2013). Recent work has indicated that Sestrin-2 can act as a cytosolic Leu sensors (Wolfson et al., 2016). In the absence of Leu, Sestrin-2 can directly interact with GATOR2 to supress its activity. This subsequently leads to the activation of GATOR1 which acts as a GAP for Rag A/B suppressing of MTORC1 signalling (Bar-Peled et al., 2013) (Chantranupong et al., 2014).

A newly identified protein, cellular arginine sensor for MTORC1 (CASTOR1) can function in parallel with SLC38A9.1, to regulate MTORC1 activity (Chantranupong et al., 2016). Mechanistically CASTOR1 forms a dimeric heterocomplex with CASTOR2, upon formation this interacts with GATOR2 negatively regulating MTORC1 activity. Only Arg can disrupt these interactions and the structural basis of the CASTOR1/Arg interact has been described in detail.

Although the Rag/Ragulator complexes are likely the predominant pathway for activation of MTORC1 by amino acids, further work has outlined other pathways that are Rag-independent that also contribute to amino acid signalling. One of these pathways involves the Golgi-regulatory GTPase protein Arf1. This pathway occurs independently of Rag A and Rag B and can be induced by Gln but not Leu or Arg (Jewell et al., 2015). A second alternative pathway links the Rab1A GTPase to MTORC1 activation. Interestingly, the interaction between Rab1A and MTORC1 occurred at Golgi membranes and was co-dependent on Rheb (Thomas et al., 2014). In fact Rab1A

KD could specifically disrupt the Rheb-MTORC1 interaction but not MTORC1 interaction with Rag C (Thomas et al., 2014). Overall the contribution of the Golgi for MTORC1 signalling still remains unclear however some crosstalk may exist.

1.6 ULK1 complex formation

It has been summarised above how amino acid availability is intricately linked to MTORC1 activation. Upon amino acid starvation, MTORC1 is inhibited, which activates autophagy, and a case has been made that this regulation occurs via direct regulation of ULK1 by MTORC1.

To introduce ULK1, it can be recognised that this kinase functions in a complex with several other essential regulatory co-factors. Understanding of the mammalian ULK1 complex is largely based on the homologous Atg1 pathway. In yeast, the Atg1 protein can interact with four other autophagy related proteins during induction of autophagy (Atg13, Atg17, Atg29 and Atg31). The Atg17-Atg31-Atg29 complex is constitutively found as a stable complex that is independent on nutritional status (Kabeya et al., 2009). However, the interaction of Atg1 with Atg13 and Atg17 is dependent on its kinase activity in addition to the target of rapamycin (TOR) signalling (Cheong et al., 2005).

In mammalian cells, ULK1 forms a homologous core complex with the mammalian homologue of Atg13, FIP200 and Atg101 (Hara et al., 2008) (Hosokawa et al., 2009b) (Mercer et al., 2009). As discussed below, the other family member, ULK2, can also substitute and enter this complex. Interestingly, this core mammalian ULK1 complex appears to adopt oligomeric organisation (or additional components) and has been observed to fractionate as a large supercomplex (~3 MDa). Both Atg13 and FIP200

have shown to be critical for the complex with roles in maintaining ULK1 stability/kinase activity and for the proper localisation of ULK1 to the site of autophagosome formation. Despite having poor sequence similarity, FIP200 has been proposed as the functional homolog for yeast Atg17 (Hara et al., 2008). Atg101 is exclusive to mammalian cells, while Atg29-Atg31 are exclusive to budding yeast, suggesting they may also represent functional counterparts (Mizushima, 2010). Interestingly, the binding of Atg101 occurs via a direct interaction with Atg13, and not FIP200 (Hosokawa et al., 2009b) (Mercer et al., 2009). On the other hand Atg31-Atg29 bind directly to Atg17 but not to Atg13 (Ragusa et al., 2012). Atg101 is now better understood to be essential and particularly important for the stability and basal phosphorylation of Atg13 and ULK1 (Hosokawa et al., 2009b) (Suzuki et al., 2015). Atg101 has been shown to be essential for the recruitment of downstream autophagic proteins, including WIPI-1, DFCP-1 and LC3 in a manner that is dependent on the Atg101 WF finger region (Suzuki et al., 2015).

The formation of the ULK1-Atg13-FIP200-Atg101 complex is independent of nutritional status and phosphorylation state, unlike the yeast system. However, upon autophagy activation signals, the ULK1/2 complex translocates to the ER-associated site of IM formation as discussed above. During nutrient sensitive autophagy, the ULK1 complex interacts with and is tightly regulated by MTORC1 (Ganley et al., 2009) (Hosokawa et al., 2009a) (Jung et al., 2009) and also by AMPK (Kim et al., 2011) (Egan et al., 2011). Moreover, several studies in recent years have highlighted how MTORC1 and AMPK control ULK1 activity via direct phosphorylation of specific sites that have begun to be mapped on ULK1. This triad of central nutrient regulatory modules

bringing together amino acids, energy-sensing and autophagy is the focal point of this thesis.

1.6.1 Regulation of ULK1 by MTORC1

The regulation of the ULK1 complex by MTOR was first demonstrated through pioneering yeast studies. Key work by Yoshinori Ohsumi group first identified, in yeast, that the protein kinase activity of Apg1 (Atg1) was enhanced by treatment with the TOR inhibitor rapamycin (Kamada et al., 2000). Furthermore TOR signalling was demonstrated to negatively regulate the association between apg1 and apg13 via hyper-phosphorylation of apg13 (Kamada et al., 2000).

Several reports have established that the functional link between atg1 and TOR is also conserved within mammalian cells (Ganley et al., 2009) (Hosokawa et al., 2009a). During amino acid-rich conditions, MTORC1 is activated leading to the association with the ULK1 complex via direct interaction with Raptor (Figure 3) (Hosokawa et al., 2009b). Based on this association, MTORC1 phosphorylates several targets in the ULK1 complex, including mAtg13, leading to inhibition of ULK1 activity and autophagy (Ganley et al., 2009) (Hosokawa et al., 2009a) (Jung et al., 2009). More recently, MTORC1 nutrient-sensitive phosphorylation sites of Atg13 have been reported (Puente et al., 2016). These studies found that MTORC1 can directly phosphorylate Atg13 on Ser^{258}, whilst Ser^{224} was modulated by the AMPK pathway (Puente et al., 2016). Perhaps more importantly, MTORC1 also phosphorylates ULK1. To date, it has been most widely reported that MTORC1 phosphorylates ULK1 on Ser^{757} (Kim et al., 2011) (Shang et al., 2011). In addition, ULK1 Ser^{637} is another phosphorylation site for MTORC1 (Shang et al., 2011). Interestingly, the phosphorylation of the ULK1 Ser^{757} by

MTORC1 has been proposed to form a critical dynamic negative regulatory event by preventing a ULK1-AMPK positive regulatory interaction (Kim et al., 2011).

Following amino acid starvation, MTORC1 becomes inactive and disassociates from the ULK1 complex, leading to less phosphorylation / dephosphorylation on mAtg13 and ULK1/2. This change forms the active conformation of the ULK1 complex, which has been proposed to involve AMPK. In addition, ULK1/2 is understood to autophosphorylate and subsequently phosphorylate mAtg13 and FIP200 to generate a fully active complex and promote autophagy (Ganley et al., 2009) (Chan et al., 2009). Several sites on Atg13 and FIP200 for phosphorylation have been elucidated recently and are discussed in more detail later (section 1.9) (Egan et al., 2015).

Recently, a starvation-induced phosphatase activity was observed to be important for ULK1 activation (Wong et al., 2015). Furthermore, protein phosphatase 2A (PP2A) has been shown to dephosphorylate the ULK1 Ser^{637} MTORC1 phosphorylation site to initiate rapid induction of autophagy. The authors were able to identify that B55-α is the key regulatory subunit that directs activity onto ULK1. Furthermore, the activity and stability of PP2A is mediated, in part, via an interaction with alpha 4 protein (Tap42 in yeast) that prevents the ubiquitination of the catalytic subunit (Jiang et al., 2013). Interestingly nutrient starvation but not Torin1 (MTOR inhibitor) treatment could disrupt the interaction between alpha 4 and PP2A. This link therefore suggests why acute nutrient starvation elicits a rapid autophagy response compared to MTOR inhibitors alone (Wong et al., 2015).

1.7 AMP-activated protein kinase (AMPK)

As highlighted above, another main proposed regulator of ULK1-dependent autophagy is the serine/threonine protein kinase AMPK. AMPK (composed of α,β and γ-subunits) is ubiquitously expressed and highly conserved throughout eukaryotes and helps maintain cellular homeostasis by monitoring intracellular energy levels. The AMPK γ-subunit detects the AMP:ATP cellular energy charge level by binding to AMP as an allosteric regulator. Binding to AMP then promotes the upstream kinase complex including the tumour suppressor LKB1, STRAD and MO25 to phosphorylate AMPK α-subunit on Thr^{172} in the activation loop leading to maximal activation (Hong et al., 2003).

It is relatively better characterised that AMPK can activate autophagy through its ability to inhibit MTORC1 via at least two separate mechanisms (Figure 3). Firstly, AMPK can phosphorylate and activate TSC2 (as described above), which promotes TSC1/2 GAP activity and GTP hydrolysis on Rheb (Inoki et al., 2003). Via this pathway AMPK can indirectly inhibit MTORC1. The second mechanism involves a more direct interaction with the Raptor MTORC1 subunit. AMPK can phosphorylate Raptor at two sites (Ser^{722} and Ser^{792}) which is subsequently followed by recruitment of 14-3-3 proteins, resulting in overall inhibition of MTORC1 (Gwinn et al., 2008). These effects linking AMPK to MTORC1 inhibition would be expected to contribute towards autophagy activation.

1.7.1 Direct Regulation of ULK1 by AMPK

Interestingly, AMPK has been linked to a more direct mechanism for activating autophagy via phosphorylation of ULK1 on a number of sites. Multiple groups have collected a range of evidence showing that AMPK directly binds and phosphorylates

multiple sites within the internal Proline/Serine (P/S)-rich spacer region (further described in a later section of this Introduction) in ULK1 (Bach et al., 2011) (Egan et al., 2011, Kim et al., 2011, Shang et al., 2011). Co-immunoprecipitation analysis also indicates that the AMPK binding motif is located within regions 654-828 within the ULK1 P/S domain (Lee et al., 2010a) (Shang et al., 2011).

One set of AMPK sites in ULK1 was identified using combined bioinformatics and biochemistry approaches, searching for novel AMPK recognition consensus sites in combination with 14-3-3 protein interaction behaviour (Egan et al., 2011). Combining these searches led to ULK1 as a AMPK target candidate and further analysis by mass spectrometry identified four phosphorylation sites in ULK1 (Ser^{467}, Ser^{555}, Ser^{574} and Ser^{637} (all mouse residue numbering system). Simultaneous mutation of these four sites (quad-mutant), markedly impaired p62/SQSTM1 degradation and mitophagy response during extended amino acid starvation. Independent studies have also corroborated the Ser^{555} site as a key AMPK-dependent phosphorylation and 14-3-3 binding site (Bach et al., 2011). In contrast, another independent approach identified further AMPK phosphorylation sites on ULK1 utilising systematic mutagenesis strategies (Kim et al., 2011). These authors identified that glucose starvation induces AMPK directed phosphorylation of Ser^{317} and Ser^{777} of ULK1 which was required for autophagy activation. This AMPK-dependent activation mechanism was inhibited when MTORC1 phosphorylated ULK1 on the Ser^{757} site. More recent work has shown that hypoxic stress also induces ULK1 Ser^{555} phosphorylation which was critical to regulate translocation of ULK1 to damaged mitochondria for the activation of the mitophagy response (Tian et al., 2015). Depletion of AMPK prevented ULK1 translocation during mitophagy, which could be rescued using a phosphomimetic

ULK1 Ser^{555D} mutant. Thus, regulation of the Ser^{555} appears to be sufficient to promote ULK1 activation in certain contexts.

Together, these data indicate that MTORC1-mediated phosphorylation of ULK1 generally inhibits the activity of the complex and autophagy. Conversely, AMPK phosphorylation of ULK1 can activate ULK1 and autophagy. The experiments in the following chapters will feature some investigation of the roles and regulation of several ULK1 sites including Ser^{317}, Ser^{555}, Ser^{757} and Ser^{777}. While other mechanisms are not looked at, it is useful to note that ULK1 has been reported to be subject to other post-translational modifications. Currently, over 70 phosphorylation sites are listed for the mammalian ULK1 in databases (e.g. phophosite.org). These modifications are detected across all three domains of ULK1 (Kinase domain, spacer domain and the EAT domain) and represent the action of a number of kinases in addition to autophosphorylation.

With this vast set of modifications, understanding of the functional roles of specific sites is still lacking and it is unclear how all the modifications are coordinated, as summarised elsewhere (Chan, 2012). Alternatively, several reports have now established that ULK1 can be modified by ubiquitin. In one system, during autophagy induction, ULK1 can undergo Lys^{63}-chain mediated poly-ubiquitination, which is controlled by the Vps34 complex partner AMBRA1 and the tumour necrosis receptor-associated factor 6 (TRAF6) ubiquitin ligase (Nazio et al., 2013). This AMBRA1-mediated ubiquitination led to further ULK1 stability and kinase activity. Furthermore, this pathway was negatively regulated by MTORC1 dependent phosphorylation of AMBRA1-Ser^{52} abrogating its positive action on ULK1 activity/stability (Nazio et al., 2013).

A recent paper has also linked ULK1 to be a substrate of the ubiquitin ligase Cul3-KLHL20 (Liu et al., 2016). It was shown that following prolonged starvation, KLHL20 leads to a feedback mechanism of autophagy termination through degradation of components of the ULK1 and Vps34 complexes (Liu et al., 2016). In agreement with this, inhibition of deubiquitinases, via WP1130, results in elevated levels of ULK1 ubiquitination (Driessen et al., 2015). This ubiquitination leads to the inactivation of ULK1 activity and transfer to aggresomes (Driessen et al., 2015).

In addition, another interesting observation was that ULK1 could be modified by acetylation via a glycogen-synthase 3 GSK3/TIP60 signalling pathway (Lin et al., 2012). In this system, starvation of growth factors led to GSK3 activation and phosphorylation of the TIP60 acetyltransferase specifically on residue Ser^{86}. TIP60 then directly acetylates ULK1 on sites which have been suggested to be Lys^{162} and Lys^{606} (in the kinase and P/S spacer domains, respectively) (Lin et al., 2012). Moreover, acetylation increased ULK1 in vitro kinase activity suggesting a potent regulatory role for this modification. Thus, the picture has emerged where ULK1 funnels in multiple upstream inputs from several different key nutrient or stress kinases (MTORC1, AMPK, Akt) in addition to ubiquitination and acetylation pathways. It remains still unclear how this wide range of signalling information is integrated to regulate autophagy downstream. I have been able to investigate only a small subset of the ULK1 phosphorylation sites and these experiments already uncovered unexpected effects that contrast with models proposed in literature, which are too reductionist, simplistic, or context dependent.

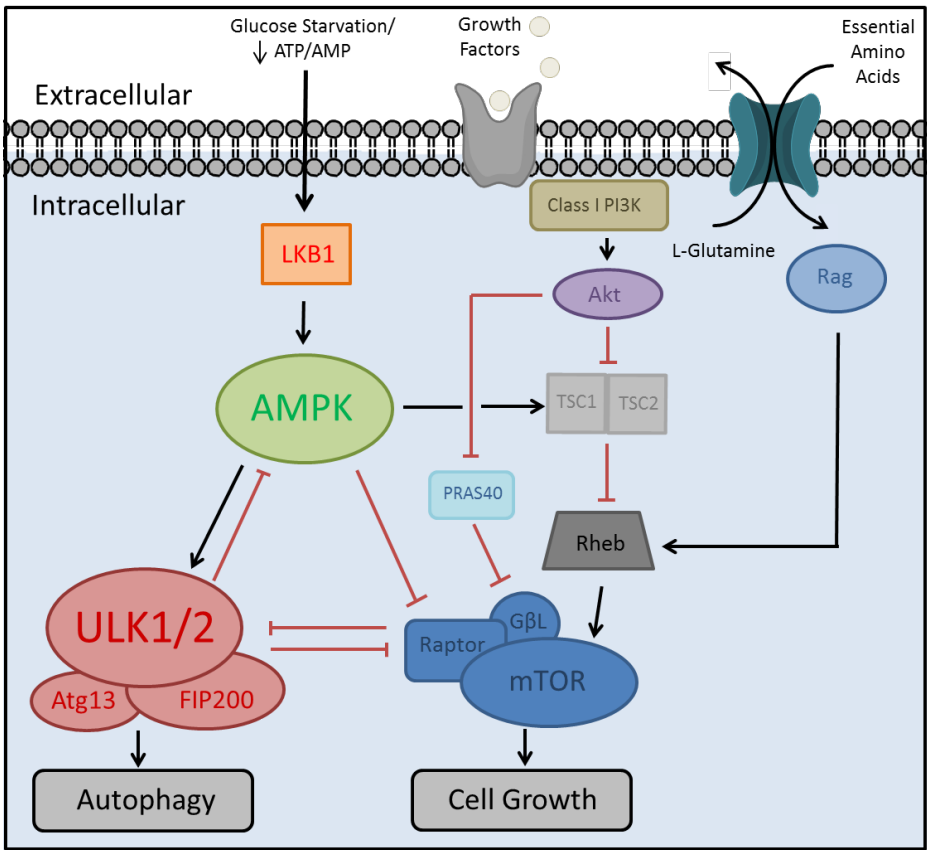

Figure 3: **Signal Regulation of ULK1/2 by AMPK and mTORC1.** Following glucose deprivation or energy stress, AMPK is activated leading to an induction of auotphagy by three seperate mechanisms including; TSC2, the Raptor subunit of mTORC1 and ULK1/2. IN contrast autophagy is inhibited by mTORC1 which is activated by release of insulin. When insulin binds to its receptor this triggers asignalling cascade invovling Class I PI3K, Akt, TSC's and also Rheb finally leading to mTORC1 activation.

1.8 Atg1/ULK1 functional mapping

Since my experiments look into how ULK1 carries out its biochemical functions, it is worthwhile to further introduce details concerning this kinase. Atg1 was initially identified through yeast genetic screens carried out by Ohsumi and colleagues (Tsukada and Ohsumi, 1993), which were also supported by other groups (Thumm et al., 1994) (Harding et al., 1995). Atg1 acts as a serine-threonine kinase (Matsuura et al., 1997) and, to date, remains the best appreciated protein kinase amongst the Atg proteins. Yeast Atg1 defines a protein kinase family highly conserved throughout eukaryotes, for example, with strong homology towards *C elegans* uncoordinated-51 (Unc-51) and *Drosophila melanogaster* Atg1 (Matsuura et al., 1997) (Yan et al., 1998) (Scott et al., 2004). In terms of physiologic function, interestingly, Unc-51 is critical to axon elongation and connectivity in *C elegans,* and roles for neuronal development are conserved in *Drosophila* and mice also (Ogura et al., 1994) (Tomoda et al., 1999) (Toda et al., 2008). Further studies in this system have shown that axon formation is mediated by an endocytic membrane traffic pathway involving ULK1/SynGAP/Rab5/Syntenin (Tomoda et al., 2004). Currently, it remains unknown how the endocytic trafficking and autophagy regulatory roles of ULK1 are coordinated. On this note, ULK1 has been proposed to also regulate MTORC1 and cell growth independent of autophagy (Jung et al., 2011).

Our research group identified ULK1 in an autophagy siRNA kinome screen performed in human HEK293 cells (Chan et al., 2007). Sequence analysis indicates that mammalian ULK1 has 41% overall amino acid similarity in comparison to Unc-51 and 29% overall similarity to Atg1 in *Saccharomyces cerevisiae* (Kuroyanagi et al., 1998), thus reflecting certain high levels of conservation. Closer inspection of degrees of

sequence conservation amongst ULK1 domains further suggests functional importance and this is explored in greater detail in Chapter 4 of this thesis. Genome database searching shows mammalian ULK1 to have several relatives which include ULK2, ULK3, ULK4 and serine/threonine kinase 36 (STK36). Despite this, only ULK1 and ULK2 show extensive sequence homology across all domains (Chan and Tooze., 2009). *ULK1* and *ULK2* mRNA have been found to be ubiquitously expressed (at varying but detectable levels) throughout murine tissues (Yan et al., 1998) (Yan et al., 1999) suggesting these proteins play important functions universal to most (if not all) mammalian cells.

Insights on the essential roles of ULK1/2 have been garnered via mouse KO studies. Full KO of key autophagy genes *Atg5* and *Atg7* in mice results in neonatal lethality (Kuma et al., 2004) (Komatsu et al., 2005). However, *ULK1* KO mice were viable, displaying normal general autophagy, with only a more tissue specific delayed erythrocyte mitophagy and maturation phenotype (Kundu et al., 2008). Similarly, *ULK2* KO mice display no aberrant autophagy or viability phenotype (Lee and Tournier., 2011). These observations in contrast with Atg5 and Atg7 models clearly reflected functional *in vivo* redundancy between ULK1 and ULK2 proteins for autophagy and viability (Kundu et al., 2008). Part of the work in my thesis studies functional roles of the ULK1/2 members in starvation induced autophagy, which has now been published (McAlpine et al., 2013).

The function of other ULK isoforms are relatively unclear. One study has established a role for ULK3 specifically during cellular senescence-associated autophagy (Young et al., 2009). Overexpression of ULK3 was sufficient to activate this specialised form of autophagy and induce premature senescence. However, ULK3 lacks significant

portions of the C-terminal regulatory regions (discussed further in Chapter 4) and is thus expected to engage a distinct set of signalling. ULK4 is also distant from ULK1/2 and has been recently shown to play a key modulatory role in corticogenesis (Lang et al., 2016). Genetic knockdown of ULK4 leads to deficiencies in neuronal migration and arborisation and in addition, also correlated with a decrease in cellular proliferation within the germinal zones (Lang et al., 2016). Mechanistically ULK4 was found to regulate the acetylation of α-tubulin, which is a key modification in microtubules (Lang et al., 2016). Overall these findings point to ULK4 playing an important role in brain development. Finally the STK36 (mammalian homolog of protein kinase Fused) isoform is yet to be linked to autophagy and limited studies have linked the STK36 protein to Hedgehog signalling (Maloveryan et al., 2007).

1.9 ULK1 Domain Structure

Full-length mouse ULK1 is 1051 amino acids with a predicted molecular weight of 113kDa (apparent molecular weight on conventional SDS-PAGE is at 150kDa). ULK1/2, like all Atg1 autophagy proteins, is comprised of three distinct domains: conserved N-terminal kinase domain, an internal PS-rich spacer domain and the conserved C-terminal domain (CTD), which has recently adopted new terminology the early autophagy targeting/tethering (EAT) domain (Chan et al., 2007) (Ragusa et al., 2012). ULK1 kinase domain (residues 1-278) contains the typical 12 conserved subdomains of the serine/threonine family of kinases which fold into the canonical common catalytic core (Hanks and Hunter, 1995). The kinase domain activation loop lies between residues 164-186, the polypeptide substrate binding region is proposed to be between residues 26-186 and the ATP binding site is localised to residues 22-165 (sites based on NCBI entry NP_033495).

The key role for kinase function in ULK1 was first revealed through mutagenesis approaches. Substitution of the conserved ATP binding lysine residue (K46R) resulted in a disruption in catalytic activity of the kinase and loss of function for ULK1 in neurogenesis regulation (Hanks et al., 1988) (Tomoda et al., 1999). Since then, it has been necessary to further describe how the K46R substitution (both positive residues) only produces a mild decrease in ULK1 kinase activity, partial loss in autophosphorylation and a mild dominant-inhibitory effect in mammalian cell autophagy assays (Chan et al., 2009). By contrast, it was found that a more disruptive K46I substitution strongly inhibited kinase activity and produced a protein that almost fully blocked starvation induced autophagy when over expressed in cells. Another charge disruptive substitution of the same residue (K46N) was reported to have similar strong properties in autophagy (Hara et al., 2008).

Recently, some further advancement has been made whereby the x-ray structure of the human ULK1 kinase domain was crystallised bound in complex with an ATP-binding site inhibitor (Lazarus et al., 2015). The use of the small molecule inhibitor appeared to help stabilise the protein to facilitate crystal formation. Analysis of this structure also revealed that ULK family members generally have a large loop between N- and C-terminal lobes of the kinase, which is not widely observed amongst other serine/threonine kinases. In addition, the structure showed the presence of an auto-phosphorylated threonine in the activation loop of ULK1 at (Thr180) that interacts with neighbouring Arg137 and Arg170, in agreement with earlier biochemical data (Yeh et al., 2010) (Bach et al., 2011) (Lazarus et al., 2015). Interestingly, mutation of Thr^{180} to alanine led to dramatic reduction in kinase activity, suggesting that autophosphorylation on the activation loop plays an important role in the activation

of ULK1 (Lazarus et al., 2015). Also, the kinase structure shed some light on the acetylation post-translational modification during growth factor deprivation (described above) (Lin et al., 2012). One of the putative acetylation sites was Lys162, which maps near to a positively charged patch that lies just opposite of the ATP binding pocket. Moreover, this site is predicted to form several key contacts with other residues, providing a mechanism on how the glycogen-synthase 3 (GSK3)/TIP60 pathway might directly regulate ULK1 activity. The kinase crystal structure also identified, for the first time that a small molecule could target ULK1. Since then, several other independently isolated ATP-binding pocket targeting small molecules have been reported with relatively strong selectivity and potency for ULK1 (Petherick et al., 2015) (Egan et al., 2015).

The internal PS-rich domain of ULK1 spans from residues 279-828 and is defined by its relatively high abundance of proline and serine residues (Ser =16%, Pro =15%). It has been proposed that a range of ULK1 autophosphorylation sites lie within the PS domain between the region 287 and 351, which contains the densest stretch of serine resides (Yan et al., 1998). In Chapter 4 it will be further discussed how the PS-region is less conserved than the kinase domain and C-terminal domains and how the PS-region is predicted to be structurally disordered. In contrast with the lower relative sequence conservation of the PS-region, this domain appears to be critical for regulation of ULK1. Numerous regulatory phosphorylation sites have been reported within this PS-region, with over 19 unique sites identified from unbiased mass spectrometry and a portion further studied functionally (Egan et al., 2011) (Shang et al., 2011) (Kim et al., 2011) and (Dorsey et al., 2009). As outlined in the section above dedicated on signalling, many of these key sites within the PS-domain are modified

by the nutrient sensors MTORC1 or AMPK. However, there is functional understanding only for a small fraction of the phosphorylation candidate sites in the PS-domain so it can be speculated that further regulatory ULK1 mechanisms have yet to be described. Importantly, binding sites for GATE-16 and GABARAP have been described within PS domain via an LC3-interaction region (LIR) at residues 357-360 of ULK1 (Okazaki et al., 2000) (Kraft et al., 2012). This interaction may help stabilise ULK1 complex binding to Atg8 family members during autophagosome initiation, a model suggested by the interaction of Atg16L1 with both FIP200 and WIPI2b (Dooley et al., 2015).

The C-terminal ULK1 EAT domain (residues 829-1051) is relatively highly conserved through evolution suggesting important biological function. This domain has multiple reported functions including acting as a scaffold for the binding of complex partners Atg13 and FIP200 (Ganley et al., 2009) (Chan et al., 2009), and is thus, the focus of my experiments in Chapter 4. ULK3, ULK4 and STK36 do not contain a similar C-terminal functional domain and thus can be predicted to not function in the canonical ULK1 complex signalling mechanism.

Work from our laboratory has made several observations concerning the function of the ULK1 EAT domain. Above, I have mentioned how kinase-dead ULK1 acted as a dominant-inhibitory protein on autophagy, but it was found that this is lost if the EAT from kinase inactive ULK1 was further deleted (Chan et al., 2009). From this, our lab proposed a model by which the EAT domain is normally folded into a closed conformation but upon kinase inactivation, a conformational change is elicited resulting in the exposure of the EAT domain allowing for the binding and titration of

key regulatory factors (Chan et al., 2009). In line with this, overexpression of the EAT domain on its own also produced a similar dominant-inhibitory effect on autophagy. Binding of ULK1 complex members maps to the EAT domain. Furthermore, it was found that deletion of the ULK1 EAT almost completely abrogated the ability of ULK1 to localise to autophagic membranes (Chan et al., 2007). It was later demonstrated that the ULK1 EAT domain alone was sufficient to bind membranes in biochemical fractions and also to localise to autophagosome puncta in HEK293 GFP-LC3 cells (Chan et al., 2009). Therefore, these data suggest that the ULK1 EAT domain directly binds membranes to promote localisation of ULK1 to the IM formation sites.

Following on from this work, other data on the homologous EAT domain of yeast Atg1 also indicated roles in direct membrane binding (Ragusa et al., 2012). Using biochemical liposomal sedimentation approaches, other authors showed further that the Atg1 EAT domain displayed a strong affinity for small vesicles with high curvature, suggesting roles in specifically sensing membrane curvature. It was also established that the EAT domain could potentiate the tethering of liposomes, increasing the fused effective diameter size, leading to the proposal that the EAT could contribute to membrane tethering. Biochemical roles and further structural insights on the EAT domain will be more fully discussed in Chapter 4.

1.10 Mammalian substrates of ULK1

A fundamental question relates to how ULK1 transduces activation signals to the downstream autophagic machinery to initiate IM formation. In addition to autophosphorylation, ULK1 can also phosphorylate its binding complex partners Atg13, FIP200 and Atg101 (Jung et al., 2009) (Egan et al., 2015). One major recent advancement has been the unbiased analysis of potential ULK1 substrates and

phosphorylation recognition sequences (Egan et al., 2015). Following on from a strategy used to analyse yeast Atg1 (Papinski et al., 2014), Shaw and colleagues screened a peptide library using purified ULK1 to determine a preferential sequence flanking the optimal phosphorylation site. Using this approach, a consensus peptide substrate sequence could be derived, termed (ULKtide), of sequence: YANWLAASIYLDGKK. Several recognition positions proposed critical for optimal phosphorylation (-3, +1, +2 positions) were further confirmed experimentally. For example, the authors analysed phosphorylation patterns on Atg101 co-expressed with ULK1 by mass spectrometry and found robust phosphorylation on Atg101 on 2 sites (Ser^{11} and Ser^{203}). The flanking sequences for these Atg101 sites were observed to generally confirm the predictive power of the ULKtide sequence. Similar co-expression analysis highlighted 3 sites on FIP200 (Ser^{943}, Ser^{986} and Ser^{1323}) and one site in Atg13 (Ser^{389}) phosphorylated by ULK1. Interestingly, the Atg13 phosphorylation site identified in this approach differs from other findings that ULK1 phosphorylates Atg13 on Ser^{318} (-TVSN(pS)SEGR) in an Hsp90-Cdc37 chaperone-mediated manner (Joo et al., 2011), although the primary data indicate incomplete-coverage in the mass spectrometry of Shaw and colleagues, which might account for this discrepancy. The Atg13 Ser^{318} site has suggested a role for regulation of mitophagy. Roles for phosphorylation of Atg101 and FIP200 still remain unclear.

A major recent advancement in autophagy has been the direct link between the ULK1 and Beclin 1 signalling. Multiple lines of evidence indicate that activated ULK1 can directly phosphorylate several different components of the Beclin 1-Vps34 complex. Initially, ULK1 was found to phosphorylate the AMBRA1 subunit of the Vps34 complex regulating the release of the complex from the dynein motor complex (Bartolomeo et

al 2010). This action was essential for the translocation of the AMBRA1-Beclin1-Vps34 complex to the ER and for autophagosome formation. AMBRA1 phosphorylation was also confirmed by independent co-expression studies (Egan et al., 2015).

Interestingly, an independent approach was able to identify that ULK1 phosphorylated Beclin1 on Ser14 following amino acid starvation and this site had a role in promoting the autophagy response (Russell et al., 2013). Phosphorylation of Beclin 1-S14 (in addition to several other sites) were confirmed in the ULKtide study (Egan et al., 2015), and the recognition sequence showed some match with the consensus sequence, for example a Met at the -3 position. This Beclin1 site is conserved in other homologues such as *Drosophila* and *C elegans* (Russell et al., 2013). In the current model, phosphorylation of Beclin 1-Ser^{14} is key for the complete activation of Vps34 to produce PI3P and drive IM formation. Interestingly, Atg14 was important for ULK1 to phosphorylate Beclin1, possibly due to mediating association of Beclin1 and Vps34 at the omegasome or IM assembly site for contact with the ULK1 complex.

Atg14 has also recently been shown to be phosphorylated by ULK1 (Park et al., 2016). Phosphorylation of Atg14-Ser29 may induce conformational changes that subsequently activates Vps34. This phosphorylation is dependent on Atg13 and its function in stabilising the interaction between ULK1 and PI3K complex (Jao et al., 2013). ULK1 has been shown to phosphorylate Vps34 directly on Ser249 (although the functional relevance of this has not yet been elucidated) (Egan et al., 2015). Altogether, the evidence is for numerous direct mechanistic interconnections between ULK1 and the Beclin 1-Vps34 complexes in nutrient dependent autophagy. The functional relevance has been substantially characterised for at least one site in

Beclin 1 and roles for AMBRA1 and Atg14 phosphorylation have been demonstrated. Thus, there seems to be a network of interactions to connect the MTORC1-ULK1 nodes to Beclin 1-Vps34 and PI3P generation during early autophagy signalling.

In addition to the ULK1-Beclin 1 pathway, there have been other reported ULK1 phosphorylation substrates. These substrates are not a direct focus of this thesis and will only be briefly summarised. ULK1 can phosphorylate syntenin-1 to promote Ub-dependent trafficking of transmembrane proteins (Rajesh et al., 2011). ULK1 has been reported to control interaction between FLCN-FNIP2 and GABARAP by phosphorylating FLCN at several sites to promote autophagic flux (Dunlop et al., 2014). In a different context, ULK1 has been shown to phosphorylate and repress the activity of STING (stimulator of interferon genes), thus halting persistent transcription of innate immunity genes (Konno et al., 2013). Another wider function of ULK1 for p62/SQSTM1 phosphorylation in response to energetic stress: ULK1 was shown to form a complex and hyperphosphorylate sestrin-2 and p62 using *in vitro* kinase assays (Ro et al., 2014).

As summarised above, several lines of evidence show ULK1 as critical for the regulation of mitophagy (Tian et al., 2015) (Egan et al., 2011) (Itakura et al., 2012a). Recent studies have shown that following mitochondrial stress such as hypoxia or mitochondrial membrane uncoupler, ULK1 becomes induced and translocates to damaged/fragmented mitochondria (Wu et al., 2014). Once at the mitochondrial membrane, ULK1 directly interacts and phosphorylates FUNDC1 at Ser^{17} and this modification is proposed to drive FUNDC1 binding to LC3 (Wu et al., 2014).

Overall, the essential role for ULK1 in mediating autophagy and mitophagy signals is well established from a number of diverse studies and approaches. As such, ULK1 is

an attractive target for the development for the drugs to modulate autophagy. Since original characterisation of ULK1 in autophagy (Young et al., 2006) (Chan et al., 2007) several ULK1 kinase inhibitors have more recently been developed, including for example MRT68921, MRT67307 and SBI-0206965 (Petherick et al., 2015) (Egan et al., 2015) (Lazarus et al 2015). Further advancement in ULK1 mechanisms and chemical biology will fuel a future era of more specific autophagy manipulation in biomedicine.

1.11 Aims and Objectives

The ULK1/2 complex is critically positioned at the earliest stages of the autophagy signalling for the control of autophagosome biogenesis. ULK1 is best appreciated to regulate nutrient dependent autophagy but other roles have been described in mitophagy and immunity regulation. Due to the positioning of ULK1 as the anchor of upstream autophagy signalling, we broadly aimed at elucidating its underlying detailed mechanisms.

ULK1 has been proposed to receive and integrate information from the upstream nutrient sensors, MTORC1 and AMPK. Although the mechanisms of MTOR/amino acid signalling pathway have been quite well characterised, the glucose/AMPK link towards autophagy is less well established and its role in autophagy remains controversial. Since amino acids and glucose represent widely different forms of cellular nutrients, better understanding is needed for how MTOR and AMPK signal regulation of autophagy. To dissect this, in this thesis, I carried out the following objectives:

1. To clarify the functionally redundant roles of ULK1 and ULK2 in basal and nutrient induced autophagy.

2. To study the differential autophagy pathways that respond to amino acid and glucose deprivation.
3. To investigate the contribution of MTORC1 and AMPK-phosphorylation on ULK1 for nutrient sensitive autophagy.
4. To perform fine domain mapping ULK1 EAT domain for binding to membranes and the Atg13 co-factor.
5. To characterise the interaction between ULK1 and ER lipid raft associated-2 (Erlin-2).

Chapter 2: Materials and Methods

2.1 Materials

2.1.1 General reagents

All materials used were of the highest grade available and were purchased from Sigma (U.K.) unless otherwise stated.

2.1.2 Antibodies

The commercial antibodies used for immunoblotting and immunofluorescence in this thesis are presented below;

Table 1: **Commercial antibodies**

Company	Cat No	Species	Antibody	Dilution	Buffer
Cell Signaling Technology	3661 3662 2215 8054 12753 5869 6888 2535 2532 2775	Rabbit Rabbit Rabbit Rabbit Rabbit Rabbit Rabbit Rabbit Rabbit Rabbit	polyclonal IgG Anti-pACC (Ser79) polyclonal anti-ACC polyclonal IgG Anti-pS6 (Ser240-244) (#2215) monoclonal IgG anti-ULK1 (D8H5) monoclonal IgG anti-pULK1 S317 (D2B6Y) monoclonal IgG anti-pULK1 S555 (D1H4) polyclonal anti-pULK1 S757 monoclonal IgG anti-pAMPKα (T172) (40H9) polyclonal anti-AMPKα polyclonal anti-LC3B (for immunofluorescence) (1/200 in Gelatin block solution)	All 1:1000	All western blotting: 5%BSA/ TBS 0.1% Tween-20
nanoTools	0231-100	Mouse	monoclonal IgG Anti-LC3B (clone 5F10)	1:400 (0.25 µg/ml)	TBS
BD Transduction Laboratories	610833 612113	Mouse Mouse	monoclonal IgG Anti-p62 (clone 3/P62 LCK Ligand) monoclonal IgG anti-Beclin	both 1:1000 (0.25 µg/ml)	TBS TBS
Sigma Aldrich	A 3853 H 9658 M 5546 F 1804	Rabbit Mouse Mouse Mouse	Monoclonal anti-actin (clone AC40) Monoclonal anti-HA (HA7) Monoclonal anti-Myc (9E10) Monoclonal anti-FLAG (M2)	All 1:1000	TBS TBS TBS TBS
Santa Cruz Biotechnology	K-23	Rabbit	Polyclonal IgG anti-ERK1 (K-23)	(0.5 µg/ml)	TBS
Thermo Scientific	35571 35518	Rabbit Mouse	IgG (H&L), DyLight 800 conjugated IgG (H&L), DyLight 680 conjugated	1:10,000 1:10,000	5% Milk 5% Milk

2.2 Cell Culture

All cell culture work was carried out in a class II cell culture fume hood under sterile conditions. All plasticware for cell culture (6cm, 10cm, 6-well, 12-well, 24-well plates and T75cm^2 flasks) were obtained from Greiner Bio-One (Austria).

2.2.1 Mammalian cell lines used

Name of Cell Line	Primary Tissue	Source (Institution)/Origin
HEK293A	Human embryonic (Kidney)	Invitrogen
HEK293A GFP-LC3 (clone 2GL9)	Human (Kidney)	(Chan et al., 2009)
HEK293 GFP-ULK1	Human (Kidney)	Derived in-house 293A stably expressing pMXIP-GFP-ULK1 (Hara et al., 2008)
HEK293 GFP-DFCP-1	Human (Kidney)	Derived in-house 293A stably expressing pBabe-Hygro GFP-DFCP1 (Axe et al., 2008)
MEF ULK1wt (cell line 1SV)	Mouse (Embryo)	(McAlpine et al., 2013) SV40-T antigen immortalised (Described below)
MEF Atg5 KO and matched wildtype control MEF	Mouse (Embryo)	(Kuma et al., 2005)
MEF ULK1 KO (cell line 2SV)	Mouse (Embryo)	(McAlpine et al., 2013) SV40-T antigen immortalised (Described below)
MEF ULK2 KO (cell line 3SV)	Mouse (Embryo)	(McAlpine et al., 2013) SV40-T antigen immortalised. (Described below)
MEF ULK1/2 DKO (cell lines 4SV, 5SV, 2 independent animals)	Mouse (Embryo)	(McAlpine et al., 2013) SV40-T antigen immortalised (Described below)
HeLa	Human (Cervix)	ATCC

Table 2: **Mammalian cell lines used within this thesis**

2.2.2 Growth and Maintenance of mammalian cell lines

Mammalian cell lines used within this thesis were all cultured in Dulbecco's Modified Eagle's Medium (DMEM) supplemented with 4.5g/L glucose (Lonza, Belgium), 10% (v/v) foetal bovine serum (FBS), 4mM L-glutamine (Lonza, Belgium), 50 units/ml penicillin and 50 units/ml streptomycin. Cells were incubated at 37 ^{o}C in humidified air containing 5% carbon dioxide.

When confluent, cells were sub-cultured using standard protocol after dissociation from the culture dish using Trypsin-Versene-EDTA (Lonza, Belgium). Cells were counted using a haemocytometer (Neubauer pattern) and seeded into well plates for experimentation as indicated. All cells were maintained by replacing the medium or subculture every 2-3 days.

2.2.3 Treatment for Autophagy Induction Assays

Autophagy was induced in cells either by nutrient starvation or through inhibition of MTORC1. For nutrient starvation cells were washed in PBS (1x) before transition into starvation media. For amino acid starvation, Earle's balanced salt solution (EBSS) was utilised containing 1g/L glucose. To test glucose starvation, glucose-free DMEM media containing 4mM L-glutamine. For complete starvation (amino acid and glucose), DPBS (Lonza, Belgium) containing Calcium and Magnesium was utilised. Where indicated in the figure legends, dialysed FBS (via ultrafiltration against 0.15 M NaCl) was also supplemented during starvation.

2.2.4 Preparation of Recombinant Retrovirus

All handling, storage and waste disposal from viral work was carried out in a designated class II microbiological safety hood (Safe 2020, Thermo Fisher Scientific,

Germany) in compliance with local University Genetic Modified Microorganism Risk assessment (Chan Laboratory, GMM36).

2.2.4.1 Production of Retrovirus

For the production of recombinant retrovirus, Phoenix Eco (Gary Nolan Laboratory, Stanford, USA) cells were plated on 6cm dishes (typically from 1/20 dilution from a confluent 10cm cell stock). At the time of transfection cells were 50% confluent.

Phoenix cells were transfected using standard calcium phosphate precipitation (Randow and Sale, 2006). Briefly, a $CaCl_2$ DNA solution was prepared to contain: 1.5µg total DNA (3:2:1 ratio of construct plasmid, pMD-GAG POL, pMD-VSV-G) (Ory et al., 1996) with 250mM $CaCl_2$. This was added drop-wise to an equal volume of 2X HBS (consisting of 16g/l NaCl, 1.5mM Na_2HPO_4 and 10g/L HEPES pH7) to form DNA/precipitate over 30mins at room temperature. DNA/precipitate was added to the cells and incubated at 37^oC for 4h. Cells were changed into regular DMEM full nutrient media and returned to the incubator.

2.2.5 Harvesting and Infection using Retrovirus

Two days after virus production, cell media with virus were collected, supplemented with 4µg/ml polybrene (1,5-Dimethyl-1,5-diazaundecamethylene polymetho-bromide), and filtered using 0.22µm Millex-GP to remove cellular debris. Freshly collected virus particles were used to transduce target cells (or otherwise stored at -80^oC until usage). When transducing cells, media was aspirated from target cells T25 flask and a minimal volume of neat virus/polybrene (1ml) was applied. Cells were incubated for 1h at 37^oC with gentle rocking to allow virus internalisation, after which additional full nutrient media added to the culture and then left for 48h at 37^oC.

Finally, cells were subjected to (250 µg/ml) hygromycin antibiotic selection (Roche, U.K.)

2.2.6 Derivation of MEF ULK KO cell lines

Primary MEF were derived from ULK1/2 deficient embryos by collaborators (S. Tooze, Cancer Research UK, London Research Institute) as described (McAlpine et al., 2013). Briefly, ULK1-deficient mice were derived at Cancer Research UK embryonic stem cell line (AC0566) carrying a pGT0lxr genetrap insertion (Wellcome Trust Sanger Gene trap consortium) targeting the mouse *ULK1* locus within the 9.8kb intron 3. Location of genetrap insertion within intron 3 was mapped by PCR and a founder carrying germline transmission of ULK1 targeting was backcrossed onto the C57BL/6 mice strains for multiple generations. ULK2 knockout mice were a kind gift from Dr. C. Tournier (University of Manchester, UK). Derivation of this line has previously been described (Lee and Tournier,. 2011).

2.2.7 DNA plasmid constructs

The below table demonstrates the DNA plasmid constructs that were utilised within this thesis;

Protein	Tag	Vector	Source (Institution)/Origin
GAG POL	N/A	pMD	(Ory et al., 1996)
VSV-G	N/A	pMD	(Ory et al., 1996)
ULK1wt **ULK1 S757A** **ULK1 S317A/S777A**	CBP/SBP	pQCXIH (Hyg)	(Kim et al., 2011)
TF-LC3	mRFP-GFP	pEGFP-C1	(Kimura et al., 2007)
Atg13	FLAG	pcDNA3.1	(Chan et al., 2009)
Atg16	FLAG	pcDNA3.1	Kind gift of Fujita and Yoshimori (Fujita et al., 2008)
WIPI-1	Myc	pEGFP-C1-WIPI1α	Kind gift of S. Tooze (Polson et al., 2010)
ULK1 **ULK1 K46I** **ULK2** **ULK2 K46I**	Myc	pRK5	(Chan et al., 2009)
ULK1 (1-1001) **ULK1 (1-985)** **ULK1 (1-958)** **ULK1 (1-928)** **ULK1 (1-898)** **ULK1 (1-878)** **ULK1 (1-861)**	Myc	pRK5	Generated in this thesis
ULK1 (ΔEAT)	Myc	pRK5	(Chan et al., 2009)
ULK1 EAT (829-1051) **EAT domain alone**	Myc	pcDNA3.1	(Chan et al., 2009)
ULK1 EAT (829-985) **ULK1 EAT (829-958)** **ULK1 EAT (829-928)** **ULK1 EAT (829-898)** **ULK1 EAT (829-861)**	Myc	pcDNA3.1	Generated in this project

Table 3: **DNA constructs**

To generate ULK1/2 double knockout lines, ULK1 KO and ULK2 KO strain mice were intercrossed to generate ULK1/ULK2 double heterozygous mice. Primary fibroblasts were isolated from E13.5 embryos of ULK1 KO, ULK2KO and two independent ULK1/2 DKO animals, in addition to wildtype littermates. Frozen primary cells were transported to the University of Strathclyde and recovered. Following, MEF were

immortalised by transduction with retrovirus expressing either pBabe-Neo–SV40 Large T antigen (to generate SVN series of MEF) or pBabe-Puro–SV40 Large T antigen (to generate SV series of MEF).

2.3 Molecular biology

2.3.1 PCR primers

Primer Name	Primer (Forward/Reverse)	Nucleotide Sequence
ULK1 EAT **ULK1 1001 EAT**	Not generated in this thesis	For further Reference see (Chan et al., 2009)
	Forward (same for all below mutants: start of EAT domain: PDL-)	CAP ECOR1 P D L P E E T GGAA GGA ATT CCT GAC CTC CCA GAG GAG ACC
ULK1 985 EAT	Reverse	L I L S H A STOPS XBA CAP CTC ATC CTC AGC CAT GCT TAGTAG TCTAGA GGCC
ULK1 958 EAT	Reverse	G L S L R L STOPS XBA CAP GGC CTC AGC TTG CGA CTT TAGTAG TCTAGA GGCC
ULK1 928 EAT	Reverse	I D Q I R A STOPS XBA CAP ATT GAC CAG ATT CGA GCT TAGTAG TCTAGA GGCC
ULK1 898 EAT	Reverse	R E W G F A STOPS XBA CAP CGA GAG TGG GGC TTT GCA TAGTAG TCTAGA GGCC
ULK1 878 EAT	Reverse	G G P E Y Q STOPS XBA CAP GGT GGC CCT GAG TAC CAG TAGTAG TCTAGA GGCC
ULK1 861 EAT	Reverse	Q Q V L E I STOPS XBA CAP CAG CAA GTT CTG GAG ATT TAGTAG TCTAGA GGC

Table 4: **Oligonucleotide primers used for deletion mutational analysis**

2.3.2 Polymerase chain reaction (PCR)

PCR was employed to introduce various ULK1 EAT domain truncation mutants into DNA. For amplification of the specific required DNA sequence, sense and antisense oligonucleotide primers were designed and synthesised by Life Technologies. The PCR reaction mix contained typically 20ng template plasmid DNA, 200nM of each primer (forward and reverse) (Table 4), 10µl of (10X) PCR Buffer Accuzyme (Bioline) for 2.5-

5.0 units DNA Accuzyme polymerase, 2.5mM dNTPs (consisting of dATP,dCTP, dGTP and dTTP) and 50mM MgCl. PCR reactions were carried out on a BioRad PTC-200 Peltier thermal cycler DNA engine with a Chromo4™ Real-Time PCR detector (BioRad, U.K.). The cycling conditions consisted of an initial denaturation step at 95^{o}C for 2mins. This was then followed by 25 cycles of denaturation at 95^{o}C for 30secs and annealing 55^{o}C for 30secs and extension step at 72^{o}C for typically 30-90secs (calculated at 1min per kb).

2.3.3 Agarose gel electrophoresis

PCR products, DNA plasmids fragments were separated on 0.8% - 1.0% (w/v) agarose gels (in 1x TAE (40mM Tris-Acetate and 1mM EDTA) stained with ethidium bromide. Prior to loading, samples were mixed with (6X) loading dye (0.5M EDTA pH 8, 1M Tris pH 7.5, 100% (v/v) glycerol, bromophenol blue, xylene cyanol). Bands were visualised under a UV transilluminator (GeneFlash, Syngene) and a PULNIX TM-300 CCD camera. The molecular sizes were estimated by comparison with 2-Log DNA ladder (New England BioLabs (#N3200S). PCR products were purified using standard QiaQUICK microcentrifuge spin column kits (standard manufacturers protocol) (Qiagen) and eluted in sterile Milli-Q purified water.

2.3.4 Purification from Agarose Gels

Following restriction enzyme digestion of PCR products, fragments were re-purified from agarose gels. Samples were resolved on by electrophoresis on 1.0% (w/v) agarose gels, the appropriately sized product was extracted using a sterile scalpel and purified using QIAquick gel extraction kit (QIAGEN) following standard manufacturer's

protocol. Products were eluted in Milli-Q water and concentrations of final eluted products were confirmed by further agarose gel electrophoresis.

2.4 Molecular Cloning

2.4.1 Restriction enzyme digestion of plasmid DNA

pRK5 and pcDNA3.1 plasmid vectors (Table 3) were digested using restriction endonucleases (New England Biolabs) in 1x of appropriate NEBuffer using standard manufacturers protocol. Digested vector fragments were resolved on by electrophoresis on 0.8% (w/v) agarose gels and purified using QIAquick gel extraction kit as described above. Products were confirmed by further agarose gel electrophoresis.

DNA/PCR fragment inserts were subsequently ligated into plasmid vectors in 10µl reactions containing using 0.5µl (200 Units) T4 DNA ligase (New England Biolabs). Ligation reactions were incubated at 16^{o}C overnight, alongside appropriate vector-only and other controls.

2.4.2 E. coli Transformation and Plasmid isolation

Ligation products were transformed into subcloning efficiency calcium chloride chemically competent DH5α *E. coli* strain (Invitrogen Life technologies). Transformed cells were selected on LB media (1% (w/v) tryptone, 0.5% (w/v) yeast extract and 200mM NaCl)/ agar plates containing 100µg/ml ampicillin. 2ml cultures from multiple *E. coli* clones were grown overnight in LB/ampicillin broth. Plasmid DNA was isolated using standard microcentrifuge QIAprep columns. Isolated DNA was checked via restriction enzyme digestion for insertion of correctly sized product. Select clones were further confirmed by standard sequencing (GATC Biotech AG, Germany). Sequence data was handled using 4Peaks software (version 1.7.1).

Confirmed clones were re-transformed back into DH5α *E. coli* and expanded in 200ml LB/ampicillin culture for plasmid purification using QIA Maxiprep kits according to standard protocol. DNA concentration and purified were confirmed on an Ultrospec 2100 Pro spectrophotometer (Amersham Biosciences) for 260/280 absorbance. DNA yield was then determined and diluted to 1.0 µg/ µl stocks and stored at -20^{o}C until usage.

2.4.3 Spectrophotometric quantification of DNA/RNA Concentration

To precisely determine the concentration of DNA/RNA an Ultrospec 2100 pro spectrophotometer (Amersham Biosciences) was utilised. Concentrations were calculated by measuring absorbance at a wavelength of 260nM. A sample with an OD value of 1 represents 50µg/ml of double stranded DNA or 40µg/ml of single stranded RNA at this wavelength (Sambrook, 2001)

In addition the absorbance at a wavelength of 280nm was measured and subsequently the 260/280 ratio calculated to assess sample purity. Samples with the ratio ~1.8 are generally considered pure for DNA and a ratio ~2 is considered pure for RNA. DNA was diluted accordingly and stored at -20^{o}C until usage.

2.5 Transient Transfections

HEK cells (parental or expressing GFP-LC3) lines were seeded in 24-well plates containing single glass coverslips. Before plating, coverslips were sterilised using 70% ethanol followed by two washes with sterile H_2O. For HEK cells, to improve adherence, coverslips were coated in 0.1mg/ml poly-D-lysine for 5mins and subsequently washed twice with sterile H_2O. HEK cells were plated and left for 24h before transfection.

Transient transfections into HEK cells were carried out using Lipofectamine 2000 (Invitrogen Life Technologies) essentially following the manufacturers standard protocol. The transfection complex was prepared using Opti-MEM (Invitrogen Life Technologies). Final concentrations were 0.8µg/ml plasmid DNA and 3.2µl/ml Lipofectamine 2000 final in Opti-MEM. Cells were incubated in the Opti-MEM transfection mix for 2 hours at 37^{o}C, after which transfection mix was aspirated and cells were replaced with full nutrient DMEM media. Cells were used for imaging experiments the following day.

2.6 Preparation of Cytosolic Cell Lysates

2.6.1 Preparation of cell lysates

Cells were grown to confluency in 6, 12 or 24 well plates and were stimulated with the appropriate treatment for an exact time, as indicated in the figure legends. After treatments, plates were put on ice, media was aspirated and wells were washed with PBS. Proteins were extracted in an appropriate volume of TNTE lysis buffer (30-40 µl/well) (20mM Tris pH7.5, 150mM NaCl, 0.3% TX-100 and 5mM EDTA) supplemented with a freshly prepared cocktail of protease inhibitors (Roche, U.K.). In phosphorylation signalling experiments, TNTE also contained phosphatase inhibitors

(sodium fluoride and β-glycerophosphate). Wells were scraped, transferred into 1.5ml centrifuged tubes and cleared by centrifugation (12,000rpm for 3mins at 4^{o}C). Protein extract supernatant was mixed with concentrated 1.5x Laemilli sample buffer to give final concentration (0.05M tris 6.8, 20% (v/v) glycerol, 2% (w/v) sodium dodecyl sulphate (SDS) and 5% (v/v) β-mercaptoethanol). Prior to loading for SDS-PAGE, samples were heated at 95^{o}C for 5 mins.

2.6.2 Co-Immunoprecipitation

Following stimulation, cells were washed in PBS and lysed and cleared as lysate section. Protein G-Sepharose beads (20µl/binding reaction) pre-coupled to anti-Myc (9E10) antibody or anti-FLAG M2 antibody were equilibrated by washing in TNTE (3X) containing protease inhibitors at 4^{o}C. Note: In the preparation of anti-HA protein G-Sepharose beads, 20µl of beads were washed as above then incubated with 1µl of HA7-antibody (1µl / precipitation reaction) for 30mins on the shaker plate at 4^{o}C followed by a final set of washes as above. Supernatants were then incubated with beads (either myc, FLAG or HA tagged) for 2h on a rotator plate at 4^{o}C. Finally the immunoprecipitates were subjected to a final set of washes in TNTE with inhibitors. Proteins were eluted by adding 20µl of 1.5x Laemilli sample buffer (LSB) (0.075M Tris-HCl pH 6.8, 30% (v/v) glycerol, 3% (w/v) SDS and 7.5% (v/v) β-mercaptoethanol). Control binding reactions were also set up including a 'beads only' with no supernatant (to detect background due to antibody used for precipitation). Equal transfection and expression of tagged constructs was confirmed by analysing protein extracts. Prior to analysis samples were heated to 65^{o}C for 5mins and run using SDS-PAGE (section 2.6.1).

2.6.3 Crude membrane Fractionation

Following various stimulations HEK 2GL9 (GFP-LC3) cells, grown on 10cm plates, were briefly washed in PBS and immediately scraped in 1ml ice-cold homogenisation buffer (HB) consisting of (20mM HEPES, pH 7.2, 1mM EGTA, 5mM $MgCl_2$, 150mM KCl) supplemented protease inhibitors. In collection tubes, cells were homogenised, on ice, by passing through a 26-gauge needle (BD Microlance™, Spain) 20 times using a 1ml syringe (BD Plastipak™, Spain). Whole cell homogenates were cleared by centrifugation at 1,000*g* centrifugation for 3mins at 4^{o}C to remove the nuclei and any cellular debris. To obtain a crude membrane fraction the supernatant was transferred into Beckman tubes (Beckman, U.S.A) and subsequently centrifuged at 100,000*g* at 4^{o}C for 1h using a (Optima™ TLX Ultracentrifuge, Beckman, C.A.).

For lipid raft fractionation experiments, membrane fractions were given an additional wash in HB containing 1% (v/v) TX-100. The samples were then passed through a 26-gauge needle 10 times and then ultra-centrifuged at 100,000*g*. Next the supernatant was aspirated and the membrane pellet re-suspended in 200µl HB containing 1% TX-100 and once again passed through a 26-gauge needle (10x). Finally, both membrane and supernatant fractions were mixed with LSB, heated to 65°C for 5 min, and resolved by SDS-PAGE for immunoblotting.

2.7 SDS-PAGE and Immunoblotting

2.7.1 SDS-Polyacrylamide Gel Electrophoresis (SDS-PAGE)

For crude membrane fractionation and co-immunoprecipitation experiments, samples were separated on standard Laemilli recipe polyacrylamide wide-mini (20.5 x 10 cm) gels (SCIE-PLAS, Cambridge UK) consisting of a 10 or 15 well stacking gel set on top of a resolving gel. The resolving gel, employed for protein separation, was prepared with 30% (w/v) acrylamide:bis-acrylamide with 1.5M Tris-HCl pH 8.8, 0.4% (w/v) SDS, ammonium persulphate (APS) and tetramethylethylenediamine (TEMED) were added for gel polymerisation. After polymerisation the stacking gel was prepared and added in a similar fashion 30% (w/v) acrylamide: N-methylenebis-acrylamide, 0.5M Tris-HCl pH8.8, 0.4% (w/v) SDS, APS and TEMED.

For all other experiments samples were run on 4-12% gradient NuPAGE pre-cast gels with corresponding NuPAGE (20X) MES SDS Running buffer (Invitrogen Life Technologies). Gel electrophoresis for was carried out using the Xcell SureLock™ gel system (Invitrogen, U.K.) filled with electrophoresis running buffer (300mM Tris, 2M glycine and 1% (w/v) SDS). Protein samples were loaded into the wells using gel tips (Alpha laboratories, U.K.) alongside a pre-stained molecular weight marker to identify the protein(s) of interest (Methods figure 1). Samples were run at constant 180V until the bromophenol blue had reached the bottom of the gel (approx 40mins). The proteins separated by electrophoresis were then transferred onto immobilon FL membrane (Millipore, U.K) which was pre-soaked in methanol, using a transfer kit (Idea Scientific Company, Minneapolis U.S.A). All components were immersed in transfer buffer (250mM tris, 2mM glycine and 20% (v/v) methanol) and run at 24V for 30mins.

2.7.2 Immunoblotting

Following protein transfer the immobilon FL membrane was stained with red ponceau for the rapid reversible detection of the protein bands and was subsequently washed using dH_2O. The membranes were washed using TBS (150mM NaCl, 25mM Tris-Base pH 7.4) and incubated with 5% non-fat dried milk powder in TBS for 1 hour to block non-specific binding. Membranes were probed with antibodies over a range of times depending on the manufacturer's recommended instructions. In addition, primary antibodies were prepared in TBS buffer unless otherwise stated. After three washes (3 x 5mins) with TBST (150mM NaCl, 25nM tris-base pH7.4, 0.05% (v/v) Tween-20) membranes were incubated with specific horseradish peroxidise (HRP) coupled secondary IgG antibodies at 1:10,000 in 5% non-fat dried milk powder in TBST, for 1h at room temperature (RT). Membranes were washed (3 x 5mins) in TBST to remove any excess unbound antibody.

2.7.3 Quantification

The binding complexes were detected using the Odyssey, infrared imaging system (LI-COR biosciences, U.S.A.). For each densitometer measurement, identical ellipsis was drawn and the intensity quantified. The local background for each band was also analysed and subtracted from band intensity to give a more accurate and precise quantification.

2.8 Microscopy

2.8.1 Immunofluorescence Microscopy

All cells lines were seeded in 24 well plates on regular plastic coverslips pre-coated in poly-D-lysine as in section 2.3. Cells were grown to ~50% confluency before treatment or transfection. Cells were washed in PBS solution prior to fixation with 4%

paraformaldehyde for 15mins at RT. Cells were then washed again in PBS and permeabilised by addition of 0.2% TX-100/PBS for 5 minutes. Following another set of 3 washes, cells were incubated in 0.2% (v/v) Gelatine for 20mins to block non-specific binding.

Next, coverslips were inverted, without washing, onto a 50µl drop of primary antibody (concentration dependent on manufacturer's recommendation) in a humidified chamber and stored overnight at 4^{o}C. Cells were carefully washed 3 times in PBS and were placed cell side down on the corresponding secondary antibody (again following manufacturer's protocol) for 20mins at RT in the dark. Finally coverslips were then mounted on glass coverslips using MOWIOL and left to dry overnight before storage in the dark in 4^{o}C until viewing. Cells were visualised using a Nikon upright epifluorescent microscope using a 60x oil immersion objective lens. Images were taken by use of a digital CoolSnap Fx digital camera and were processed and analysed using Metamorph™ imaging series 7.0 software.

2.8.2 Confocal Microscopy

For confocal fluorescent images, cells were plated, fixed and mounted as described in 2.10.1. Images were obtained using a Leica TCS SP5 confocal laser scanning microscope to detect flurophores introduced into HEK293, HeLa and MEF cell lines. Images were taken using a 63x/1.4 oil objective lens.

Sequential excitation was provided by Argon and Helium-Neon (HeNe) gas lasers at 488nm and 543nm wavelengths respectively. After sequential excitation, green and red fluorescent images of the same cell were collected by emission filters. All images were subsequently analysed using Leica LAS AF software. For 3 dimensional (3D)

modelling multiple Z-stacks were collected (pinhole setting 1 Airy). 3D image stacks were modelled using Volocity software (PerkinElmer).

2.8.3 Live Cell imaging using Inverted Epifluorescence microscopy.

For live-cell analysis, cells were seeded onto specialised glass bottomed 35mm^3 dishes with 14mm micro-well (In Vitro Scientific). Before analysis cells were washed and replaced into HBSS containing 0.1% FBS and 75mM HEPES to prevent any autofluorescence observed regular DMEM media. Time-lapse imaging was performed in a pre-heated environmental chamber (37^{o}C) built around an inverted epifluorescent microscope (Axioplan) using a 63 x/1.4 oil immersion lens. Time-lapse movies were initiated 15 mins after amino acid withdrawal and images were taken every 20 seconds using the Metamorph® software.

2.9 Statistical Analysis

Western blots were scanned on the Odyssey® infrared imaging system and quantified using the Image Studio™ Lite V3.1 software (LI-COR Biosciences). For final preparation images were adjusted for brightness/contrast in ImageJ software.

All data shown were expressed as the mean ± SEM experiments and are representative of three separate experiments unless otherwise stated in the figure legend. Wherever applicable statistical analysis was performed using Minitab V16 and GraphPad Prism® software. Statistically significant results are denoted by asterisks (*) where $P<0.05$, ** $P<0.01$, *** $P<0.001$.

Chapter 3: Regulation of Nutrient-Sensitive Autophagy by ULK1/2

3.0 Introduction

Over two decades ago the *apg1* gene was discovered during a global screen investigating autophagy defective mutants in *Saccharomyces cerevisiae* (Tsukada and Ohsumi, 1993) and this gene was found to encode the first annotated autophagy related protein Atg1 (Matsuura et al., 1997). Since then, multiple mammalian homologues of yeast Atg1 have been discovered and these are named the uncoordinated-51-like kinases (ULK). To date, five ULK1 homologs have been discovered ULK1, ULK2, ULK3, ULK4 and STK36 but only ULK1 and ULK2 are known to regulate nutrient sensitive autophagy (Chan et al., 2007, Lee and Tournier, 2011).

Recent evidence from hierarchal analysis has proposed the ULK1 (Atg1) complex as the most upstream component of all the Atg proteins (Itakura and Mizushima, 2010). Both ULK1 and ULK2 are found within multimeric complexes containing mAtg13 (mammalian homologue of yeast Atg13) and the scaffold protein FIP200 (orthologue of yeast Atg17) (Ganley et al., 2009). A further Atg13 binding protein, Atg101, has been identified, which is believed to be essential for the stability and basal phosphorylation of Atg13 and ULK1 by averting proteasomal degradation (Hosokawa et al., 2009b) (Mercer et al., 2009).

The ULK1/2 complex plays an important role in the initiation of autophagy and various studies have indicated a certain degree of ULK1/2 functional redundancy between these isoforms. Mammalian ULK1 and 2 contain an overall 52% sequence identity and share the same domain structure unlike other ULK isoforms with an N-terminal kinase domain, proline/serine spacer domain and a C-terminal domain (Yan et al., 1999).

Interestingly, the kinase domain shows good homology with 76% identity suggesting a conserved function. Both of these isoforms are ubiquitously expressed throughout most adult tissues (Yan et al., 1998, Yan et al., 1999). Despite the similarities between the amino acid and domain structures, the best evidence for functional redundancy is derived through knockout studies.

In vivo studies confirm that ULK1$^{-/-}$ mice are in fact viable and show no obvious adverse phenotype (Kundu et al., 2008). However knockout of this kinase has been linked to an impairment of reticulocyte differentiation due to defects in the clearance of mitochondria (Kundu et al., 2008). In addition, ULK1$^{-/-}$ MEF also were reported to display a repressed LC3-lipidation response following rapamycin treatment despite a normal LC3 lipidation being observed following glucose starvation (Kundu et al., 2008). The precise role and function of ULK2 is less well understood. ULK2$^{-/-}$ MEF are also viable and exhibit no adverse autophagic phenotype (Lee and Tournier, 2011). Therefore, from these data, it became necessary to clarify the ULK1 and ULK2 functional redundant roles *in vivo* during non-selective autophagy.

This ULK1 complex integrate signals from the master nutrient sensors: mechanistic target of rapamycin complex 1 (MTORC1) and the AMP-activated protein kinase (AMPK), to regulate the activation of autophagy during nutrient deprivation. During nutrient-rich conditions, MTORC1 inhibits autophagy through inhibitory phosphorylation of a number of substrates including, but not exclusive to, the ULK complex via phosphorylation of components ULK1/2 (Ser^{757}) and Atg13 (Ganley et al., 2009) (Kim et al., 2011). Inhibition of MTORC1 results in increased ULK1 kinase activity and subsequent phosphorylation of Atg13 and FIP200 (Ganley et al., 2009).

On the other hand AMPK has been proposed to activate autophagy by several mechanisms including inhibition of MTORC1 activity via phosphorylation of TSC2 (Inoki et al., 2003) and RAPTOR (MTORC1 subunit) (Gwinn et al., 2008). In addition to this, AMPK can also directly associate and phosphorylate ULK1 on several sites (Egan et al., 2011, Kim et al., 2011, Shang et al., 2011). Therefore, it is apparent that MTORC1 plays a negative role, whilst AMPK has been characterised to positively regulate autophagy under certain starvation conditions. Despite the mechanisms of MTOR/amino acid signalling pathway being quite well characterised, the glucose/AMPK link towards autophagy is less well established and my work in this chapter uncovered unexpected differences.

To summarise, the principal aims in this Chapter are as follows:

- To investigate and evaluate the functionally redundant roles of ULK1 and ULK2 in basal and nutrient induced autophagy.
- To study the differential autophagy pathways that respond to amino acid and glucose deprivation.
- Utilise MTORC1 and AMPK-phosphorylation site ULK1 mutants to investigate the contribution of these signalling pathways to nutrient sensitive autophagy.

3.1 Results

3.2 Preliminary characterisation of nutrient-dependent autophagy in Atg5 knockout Mouse Embryonic Fibroblasts.

The main aim of this chapter was to investigate the role of the autophagy in newly derived ULK-deficient mouse embryonic fibroblasts (MEF). During the initial phase of my project, it was important to establish methodology to study rates of early and late stage autophagy markers. For assessing autophagic activity, LC3 conversion was monitored through immunoblotting. During autophagy, the LC3 protein is converted from its cytosolic LC3-I form to a membrane bound LC3-II in an ubiquitination-related conjugation reaction (Tanida et al., 2004). The end product of this reaction results in the lipid phophatidyletholamine (PE) being conjugated to LC3-I thereby allowing its association with the membrane. The lipidated LC3-II form is specifically localised to both the inner and outer membrane of various autophagic structures following activation and is therefore a commonly used biochemical marker for autophagy induction as well as for imaging of autophagosome membranes (Kabeya et al., 2000).

To establish assays for these experiments, mouse embryonic fibroblasts (MEF) derived from Atg5 knockout (KO) mice were used as a reference, which lacks the machinery at a relatively late essential downstream step, LC3 lipidation (Kuma et al., 2004). As summarised in Chapter 1, Atg5 plays an indispensable role in driving the formation and elongation of nascent autophagosomes. By forming part of the Atg12-Atg5-Atg16L multimeric complex, Atg5 function promotes lipidation and targeting of Atg8 members (such as LC3) to the isolation membrane (Mizushima et al., 2001) (Mizushima et al., 2003). Atg5 knockout (KO) MEFs, derived from E13.5 Atg5 homozygous embryos, have been a widely characterised by multiple independent

groups since their initial description (Kuma et al., 2004) (Itakura and Mizushima, 2010) (Nath et al., 2014).

In this experiment, matched wildtype (WT) and Atg5 KO MEF were treated with either full nutrient media (FM) or starved of amino acids with or without the lysosomal inhibitor bafilomycin A_1 for 2 hours (Figure 3.1). The ratio of LC3-I and II remained essentially identical in control untreated cells in comparison to cells replenished with FM, implying a high basal autophagy level within this cell system. Following amino acid starvation (-AA), there was a clear increase in the LC3-II/LC3-I ratio, reflecting the expected rapid conversion of LC3-I to LC3-II, consistent with an induction of autophagy signalling. The intensity of LC3-II was not elevated after amino acid starvation (compared with either untreated or FM controls), suggesting that LC3-II protein turnover was activated relative to basal conditions.

To better visualise LC3 turnover, it was necessary to confirm, as control, the effects of bafilomycin A_1 (Baf). Baf acts to impair autophagic flux by targeting the vacuolar ATPase and proper acidification of the lysosome. Therefore, this impairs lysosomal hydrolase activity preventing the maturation and fusion of autophagosomes with lysosomes (Klionsky et al., 2008). It was found that addition of Baf at the same time as amino acid starvation led to stronger LC3-II protein levels in comparison to starvation alone. These data indicate clear detection of starvation induced early autophagy activation and late degradative flux phases by these methods. As a further control, it was found as expected that with Atg5 KO, all LC3-II production was abolished, both in basal and starvation conditions. Surprisingly, LC3-I did not seem to be massively accumulating, but still detectable indicating potential feedback downregulation.

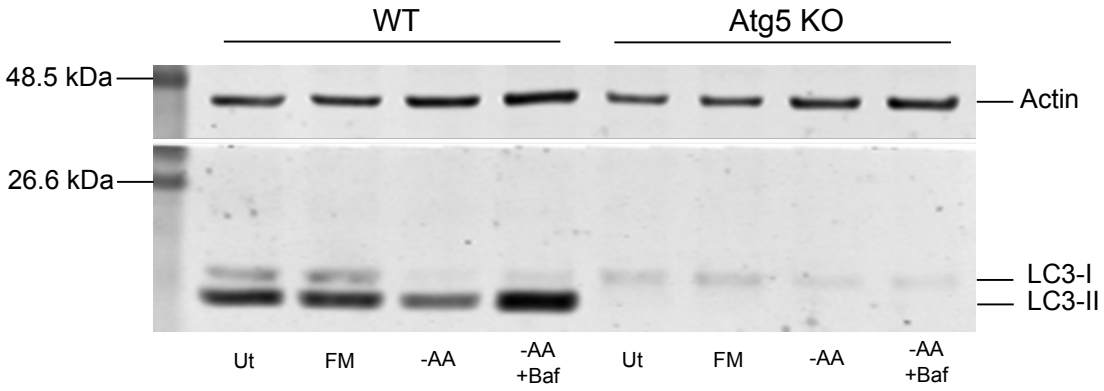

Figure 3.1: **The effects of Atg5 KO on LC3 lipidation in mouse embryonic fibroblasts.** MEF WT and Atg5 KO cells were untreated (Ut) or treated with either full nutrient media (FM), EBSS (-AA) or EBSS + Bafilomycin A_1 (50nM) for 2 hours. Cell lysates were resolved by SDS-PAGE, as previously described in methods, and then subsequently blotted for LC3 protein. LC3 was detected as two seperate bands LC3-I (18kDa) and LC3-II (16kDa). Actin (42kDa) was used as a loading control and the data shown representative of one experiment.

3.3 ULK1/2 double knockout inhibits LC3 conversion in response to amino acid deprivation

The larger goal was to gain a further insight into the role and regulation of the ULK1/2 complex. In contrast to Atg5, the relative roles and redundancies of ULK1 and 2 in the response to amino acid starvation were controversial (Alers et al., 2012). To achieve this it was necessary to generate ULK1 deficient mice using embryonic stem cells carrying a splice acceptor genetrap found within intron 3 of the mouse *ULK1* locus (McAlpine et al., 2013). These mice were largely without overt phenotype, so were thus crossed with ULK2 KO mice (Lee and Tournier, 2011). The resulting ULK1/2 double KO (DKO) progeny were undetectable in litters and were concluded to be embryonic lethal. Accordingly, MEF cell lines were generated from DKO E13.5 embryos, in parallel with single ULK1/2 KO or WT littermates.

Having these newly generated MEF lines, amino acid dependent autophagy activation (in conjunction with Baf) was analysed using an LC3 immunoblotting assay. As a control, the matched WT MEFs showed a basal LC3 ratio that increased upon starvation (in the presence of Baf) (Figure 3.2A,B), similar to WT MEF in the Atg5 experiment. In contrast, single ULK1 KO showed slightly impaired LC3 lipidation, detectable under basal and starved +Baf conditions (see Figure 3.2B,C). In contrast, ULK2 KO cells exhibited a distinct pattern, with high basal LC3-II ratios and an abnormally high level of LC3-II in starved cells further treated with Baf.

It was possible to detect a clearer effect upon ULK1/2 DKO (that was seen in two independently derived cell lines). In these cases, there was a strong block in LC3-II generation upon amino acid starvation with Baf absent or present. Therefore, these

results suggest that ULK1 may play a more pivotal role in LC3 activation but strongest targeting of the pathway occurs only when both ULK1/2 gene members are lost.

The normal expression of ULK1 was confirmed in both WT and ULK2 KO cell lines, while ULK1 loss was confirmed in ULK1KO and DKO cell lines. ULK2 was not tested by immunoblotting since we lacked a suitable antibody. However, expected targeted expression of *ULK1* and *ULK2* transcripts could be confirmed (McAlpine et al., 2013). It must be noted that even with ULK1/2 DKO, LC3-II formation is not completely abolished. In contrast, Atg5 KO completely ablated LC3-II. This suggests that there may be ULK independent (non-canonical) autophagic pathways involved in LC3 activation that can function even after combined loss of ULK1/2.

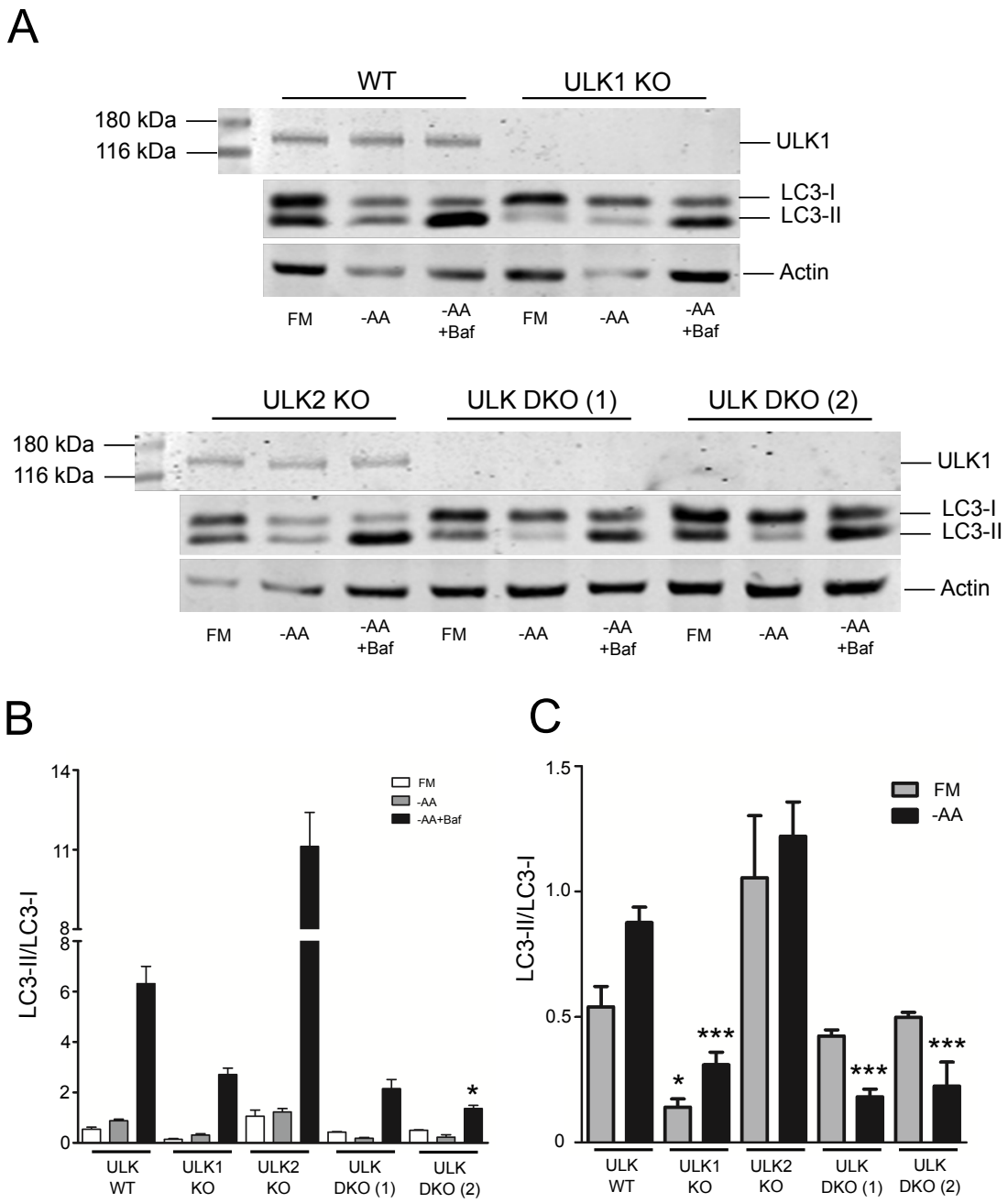

Figure 3.2: **The role of ULK1 and ULK2 in LC3 lipidation during amino acid starvation.** (A) MEF ULK WT, ULK1 KO, ULK2 KO and two ULK DKO cell lines were treated with either full media (FM), EBSS (-AA) or EBSS + Bafilomycin A1 (50nM) for 2 hours. Cell lysates were resolved by SDS-PAGE and blotted for ULK1 and LC3. ULK1 appeared as a single band with an apparent molecular weight of ~150kDa. (B-C) Quantified ratios of LC3-II/LC3-I are expressed as mean ±S.E.M. Two-tailed paired t-tests were performed relative to MEF WT under the same treatment conditions (*p<0.05, ***p<0.005). Actin was used as a loading control and the data shown representative of four independent experiments.

3.3.1 Differential effects of ULK1/2 DKO on LC3 conversion after glucose starvation

To study complementary modes of nutrient starvation, the effects of ULK DKO on autophagy were examined following glucose withdrawal. Starvation of glucose has been reported as another activator of autophagy which acts through energy sensor AMPK. Decreases in the ATP/AMP ratio signals to activate AMPK signalling in LKB1 dependent manner, which are proposed to activate autophagy (Shaw et al., 2004). As such, glucose withdrawal acts by mechanisms distinct from MTORC1-mediated amino acid sensing, so it was therefore necessary to examine ULK function within this signalling pathway.

WT and ULK1/2 DKO MEF were treated in glucose free media for 2h or 18h and then LC3 lipidation assessed by immunoblotting. Surprisingly, during 2h acute glucose starvation, no apparent increase in LC3 lipidation could be detected, either in starvation alone or in the presence of Baf (relative to basal conditions) (Figure 3.3, panel A and C). The lack of strong effect of Baf relative to glucose starvation alone was unexpected and in clear contrast to the parallel results in the same cell line following amino acid starvation (Figure 3.2). These results suggested that glucose starvation may in fact be blocking proper lysosomal engagement and autophagic flux.

In comparing WT with ULK1/2 DKO, a very similar response was observed during glucose starvation. Loss of ULK1 and 2 slightly elevated basal autophagy (but this was only in one of the DKO lines so may not be a conserved effect (Figure 3.3, panel B and D). Furthermore, addition of Baf failed to reveal a strong accumulation of LC3-II indicating that large amounts of turnover were not occurring.

The effects after an 18h time-point were also studied since glucose starvation may require longer to stimulate autophagy also required to be studies. In WT MEF, overnight glucose starvation also led to LC3-II accumulation, although the addition of Baf did not reveal high levels of degradative flux (LC3 turnover) consistent with 2h data. Mild accumulation of LC3-II also occurred in ULK1/2 DKO after overnight glucose starvation. These results contrast with the block in amino acid starvation responses following loss of ULK1/2 function. The response to glucose starvation also had a markedly differential interaction with Baf treatment. This data thus suggests that ULK1/2 are not essential to the unique autophagic responses observed after glucose deprivation. This corroborates with previous findings showing that ULK1 and/or ULK2 is not required for an autophagic response to glucose deprivation or ammonia exposure (Cheong et al., 2011).

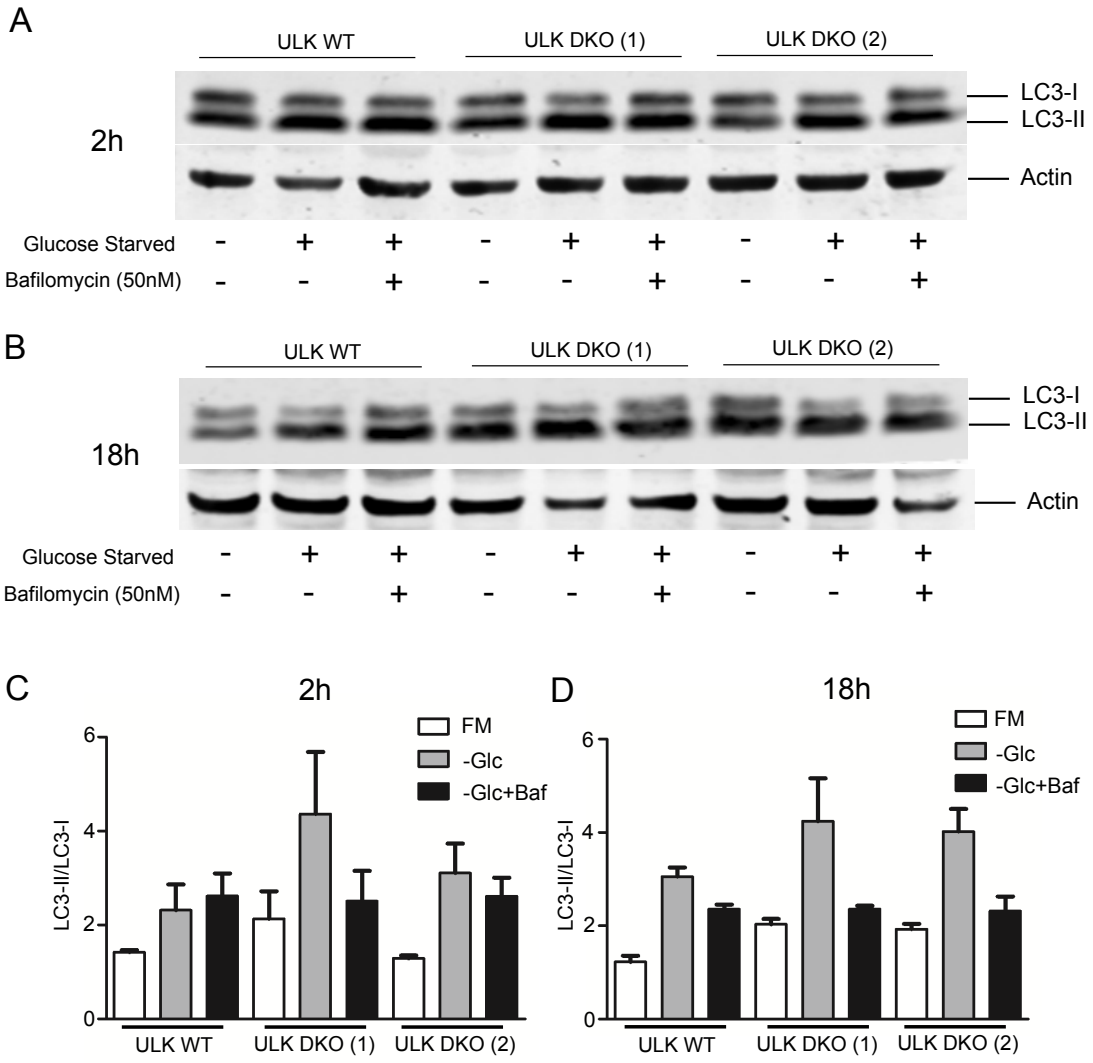

Figure 3.3. **The role of ULK1/2 in LC3 lipidation during short and long term glucose starvation**. MEF ULK WT and two ULK DKO cell lines were treated with either full media (FM), glucose free media (-Glc) or -Glc with Bafilomycin A_1 (50nM) for (A) 2 hours (B) 18 hours. Cell lysates were resolved by SDS PAGE and blotted for the LC3 protein. LC3-II/LC3-I ratios were quantified after (C) 2 hours and (D) 18 hours and are expressed as mean ±S.E.M (n=3). Actin was used as a loading control an data is representative of three separate experiments.

3.4 The effects of nutrient starvation on AMPK and MTOR activity in ULK double knockout MEFs.

To complement our analysis of nutrient sensing and LC3 lipidation, parallel experiments were set up to investigate whether knockout of both ULK1 and ULK2 isoforms affected activation of AMPK and MTORC1 following amino acid or glucose starvation. This is due to reported potential ULK1/2 signalling feedback mechanisms in the AMPK-mTOR-ULK1/2 axis (Lee et al., 2007) (Loffler et al., 2011).

3.4.1 The effect of ULK DKO on AMPK and mTOR activity following amino acid starvation.

WT and ULK DKO MEF were replenished with full nutrients (FM) or starved of amino acids for 2h or 18h. Cell lysates were blotted for phosphorylated acetyl-CoA carboxylase (p-Ser^{79}ACC) and S6 ribosomal protein (p-Ser$^{240/244}$S6). Acetyl-CoA carboxylase catalyses a crucial step in the fatty acid synthesis pathway and AMPK has the ability to inactivate this carboxylase via phosphorylation at the Ser^{79} residue (Winder and Hardie, 1996). One method for assessing MTORC1 activation is measuring the indirect phosphorylation of downstream effectors such as S6 ribosomal protein (S6). The phosphorylation of the S6 proteins occurs via p70 ribosomal protein S6 kinase (p70S6K) which is found immediately downstream of activated MTORC1 (Hara et al., 1998).

It was confirmed that WT MEF cells displayed typical basal autophagy and upon 2h amino acid starvation (induction of 2.2-fold increase in LC3 lipidation ratios) (Figure 3.4A, panels A and D). ULK1/2 DKO cells on the other hand were nutrient unresponsive as no changes in LC3 lipidation were observed.

Amino acid starvation led to a mild decrease in AMPK signalling (p-ACC levels) in WT MEF. In addition, ULK1/2 DKO led to a mild elevation of ACC phosphorylation (around 1.3-fold) in full nutrient conditions in comparison to MEF WT cells (Figure 3.4A, panel A-B). Assessing MTORC1 activation, phosphorylated S6 protein was readily detected under full nutrient media conditions in both WT and DKO MEF. Subsequently, after 2h amino acid starvation, phosphorylation of S6 was markedly reduced and this response was very similar between WT and DKO cell types (Figure 3.4A, panel A and C). Therefore, it can be concluded that loss of ULK1 and 2 had no adverse effects on MTORC1 inactivation following amino acid starvation, even though autophagy responses were impaired.

Because, our analysis of glucose starvation condition extended into longer-term (overnight treatments), the parallel timepoint was analysed following amino acid starvation. From this study, it was observed (similar to the 2h data) that 18h amino acid starvation led to mild decreases in AMPK signalling (Figure 3.4A, panel E and F). However, other trends contrasted with the 2h data. For example, LC3-I and LC3-II protein levels extremely low following 18h amino acid starvation, furthermore, this was the case in both WT and ULK DKO lines. In addition, following 18h amino acid starvation, MTORC1 inactivation is no longer apparent which agrees with previous findings that MTOR is reactivated following prolonged starvation (Yu et al., 2010). Together, these data suggest that while ULK1/2 DKO clearly blocks autophagy following acute short term amino acid starvation, after long term amino acid starvation, other ULK1/2-independent pathways lead to LC3 degradation and non-canonical autophagy responses.

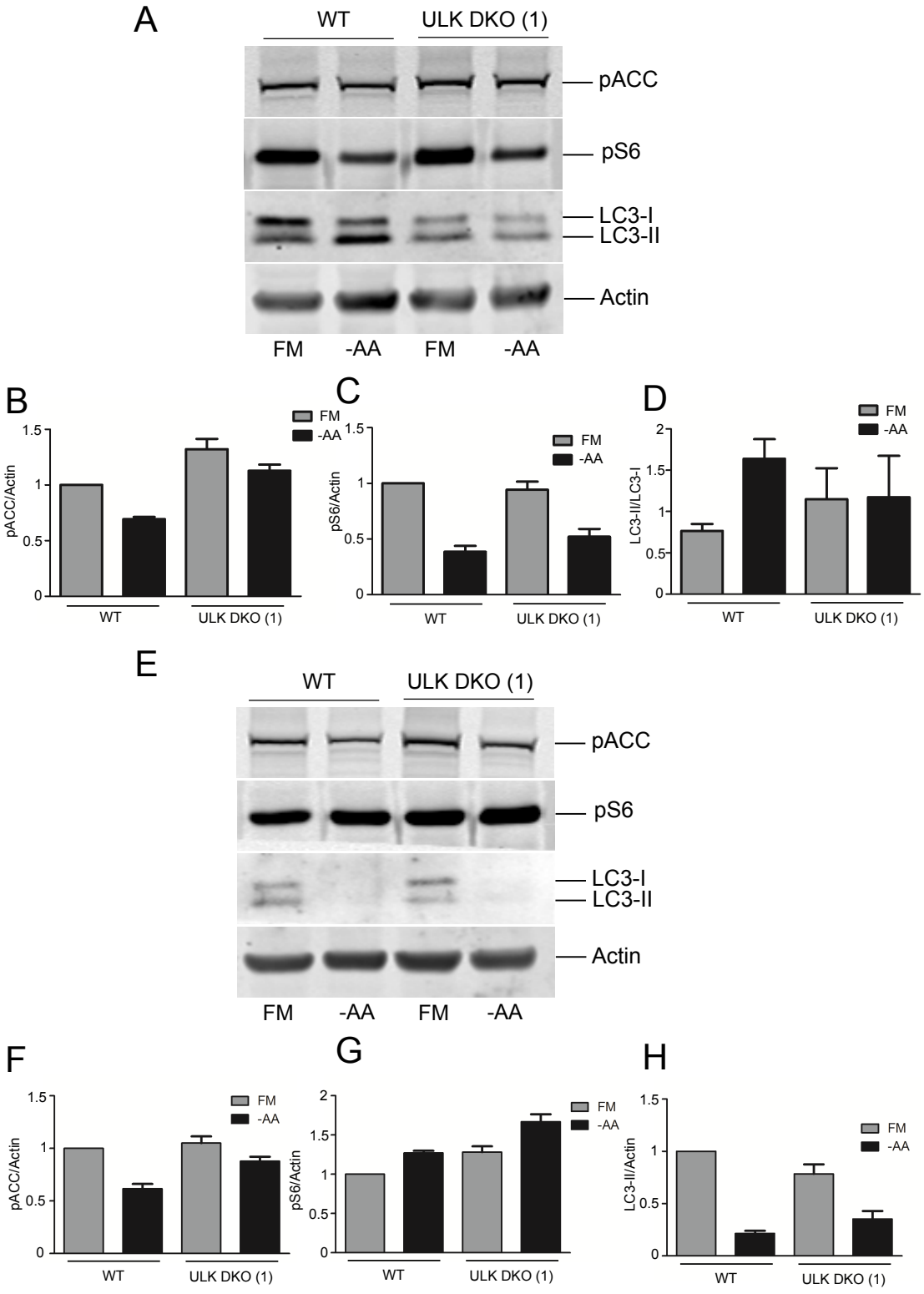

Figure 3.4A: **The effect of short and long term amino acid starvation on AMPK and mTOR signalling in ULK1 WT and DKO MEF's**. MEF ULK WT and ULK DKO cell lines were treated with full media or EBSS supplemented with 10% dFBS for (A) 2 hours (E) 18 hours. Cell lysates were resolved by SDS PAGE and blotted for pACC, pS6 and LC3 proteins. p-ACC and p-S6 were observed as single bands with apparent molecular weights of 280 kDa and 32kDa respectively. The quantified ratios of p-ACC/ actin, pS6/actin and LC3-II/LC3-I are shown for (B-D) 2 hours and (F-H) 18 hours. Actin was used as a loading control and data is representative of three separate experiments (n=3).

3.4.2 The effect of ULK DKO on AMPK and MTOR activity following glucose starvation.

In parallel to the previous experiment, WT and ULK DKO MEF were examined for AMPK and MTORC1 activity following short and long term glucose withdrawal. LC3 lipidation was monitored also for control purposes. Consistent with earlier experiments, 2h withdrawal of glucose triggered an increase in LC3-II accumulation that was overall similar between WT and ULK DKO cells (Figure 3.4B, panel A and D). As expected, 2h glucose withdrawal led to higher levels of phosphorylation of ACC in WT MEF, although this was unexpectedly dampened in ULK DKO MEF. However, 2h glucose starvation did not affect MTORC1 activation in either cell type. These results again confirm our earlier data showing ULK1/2-independent LC3 accumulation following glucose starvation, although these changes are not necessarily tightly associated with AMPK activation.

Following overnight glucose starvation, AMPK activation was more pronounced and was observed in both WT and ULK DKO MEF (Figure 3.4B, panel E and H). 18h glucose starvation also led to strong LC3-II accumulation and levels were similar between WT and DKO lines. Interestingly, overnight glucose starvation led to clear MTORC1 inactivation in both WT and ULK DKO MEF. This finding agrees with recent findings that glucose deprivation (16h) led to the increased binding of Hexokinase II to MTORC1 resulting in inhibition of mTORC1 and phosphorylation of its downstream substrates (Roberts et al., 2014).

These experiments aimed to gain insight into the AMPK and MTORC1 signalling changes following amino acid vs glucose starvation since these led to different responses in the MEF models. It can be concluded that amino acid sensing in ULK DKO

lines is generally intact although autophagy is not responsive, at least following short term starvations. In addition, AMPK and MTORC1 nutrient sensing and also changes in the autophagy pathway following glucose starvation are generally similar even after ULK DKO. However, some smaller differences in nutrient signalling can be observed, which may highlight other underlying negative feedback mechanisms that may be in place to modulate the autophagic response (Loffler et al., 2011).

3.5 The differential effects of amino acid and glucose starvation to autophagy during short term starvation.

In terms of autophagy signalling, the effects of amino acids starvation have been more thoroughly investigated in mammalian cells. The role of glucose starvation in autophagy is relatively less well understood although interest in AMPK as a promoter of autophagy has been developing in recent years (Kim et al., 2013) (Zhang and Lin, 2016). Several different signalling mechanisms for AMPK mediated autophagic activity have been reported. Firstly AMPK can inhibit MTORC1 activity through phosphorylation of the TSC2 protein and directly on the RAPTOR subunit of the MTORC1 complex (Inoki et al., 2003) (Gwinn et al., 2008). More recently AMPK has been shown to directly phosphorylate ULK1 and Beclin-1 on several residues thereby inducing autophagic activity (Kim et al., 2011, Egan et al., 2011, Shang et al., 2011, Kim et al., 2013).

Our collaborator (Sharon Tooze, Cancer Research UK, London) carried out parallel studies in WT and ULK DKO MEF investigating autophagosome formation in response to glucose starvation (McAlpine et al., 2013). From this study, it was concluded that glucose starvation may be driving non-canonical types of autophagy that were independent of ULK1/2, PI3P generation and formation of WIPI-1/2 associated

puncta. These emerging concepts led us to further explore the relationship between different nutrient starvation conditions and proper degradative autophagic flux.

To this aim, the LC3 turnover assay was utilised to further investigate differences between nutrient starvation conditions using the laboratory's other standard experimental model for dissecting autophagy signalling mechanisms, HEK293A cells. HEK293A cells were amino acid or glucose starved with/without the presence of Baf for 2h (Figure 3.5). HEK293A cells are notable for their relatively low levels of activated LC3-II under basal conditions, and this could be seen in this experiment, either in untreated cells or following replenishment with full nutrient media. Following a lysosomal block by the addition of Baf, LC3-II accumulated due to the inhibition of lysosomal protein degradation and autophagosomal maturation, which suggested that under basal conditions, LC3-II was formed and rapidly degraded. As expected, amino acid starvation alone, led to a clear accumulation of LC3-II, indicating activation of LC3 lipidation. Furthermore, addition of Baf during amino acid starvation led to further LC3-II accumulation as expected. Quantification revealed significant (average 3.5-fold) elevation of LC3-II conversion, comparing amino acid starvation in the presence of Baf with basal conditions and the Baf blockade (Figure 3.5 B). This is indicative of amino acid deprivation leading to the activation of autophagy and promotion of autophagic flux.

Amino acid starvation conditions in HEK293 experiments of the laboratory have historically been performed using EBSS, which presents amino acid and serum free conditions (but with the presence of glucose). To further probe dependency on nutrient factors, it was necessary to test the effects of serum. Interestingly, an addition of 10% dialysed foetal bovine serum (dFBS) to EBSS (Figure 3.5 A, lanes 4 and

6) did not substantially alter the activation of LC3 lipidation. On probing for MTORC1 inactivation it was noted that the levels of p-S6 were similarly reduced in all amino acid starvation lanes, irrespective of Baf or dFBS additions. In HEK293, 2h of amino acid starvation also did not activate AMPK.

When HEK293 cells were starved for 2h of glucose (also serum free) (Figure 3.5 A, lane 7), LC3-II accumulation (as in MEF) was also detected although this response was not as strong compared to amino acid starvation. Glucose starvation also led to clear MTORC1 inactivation and AMPK activation. Importantly, addition of Baf to the glucose starvation condition did not lead to any increases in LC3-II accumulation compared to basal +Baf (lanes 3 and 8). Quantification confirmed that glucose starvation did not activate LC3 flux (Figure 3.5B). Interestingly, when cells were treated with glucose free media + 10% dFBS, the mild LC3 lipidation response and effects on MTORC1 activity were reduced, whilst still maintaining elevated ACC phosphorylation. This suggests that serum starvation had some contribution in this condition.

3.6 Glucose withdrawal exhibits atypical autophagic flux.

One of the main findings was that glucose starvation does not activate autophagic flux in contrast to amino acid starvation. To further establish this unconventional idea, it was important to monitor LC3-II accumulation in a time course analysis of autophagic flux at 1, 2 and 4h following nutrient deprivation (Figure 3.6). In control unstarved cells treated with Baf, LC3-II gradually accumulates indicating some basal levels of LC3 activation. In combination with amino acid starvation, LC3-II levels are substantially elevated within 1h treatment and remained strong. Intriguingly, the time course profile following glucose deprivation (+Baf) displayed no apparent

difference compared to control cells at all time points (Figure 3.6). These data once more suggest amino acid withdrawal leads to autophagy induction whereas glucose starvation fails to produce a strong response.

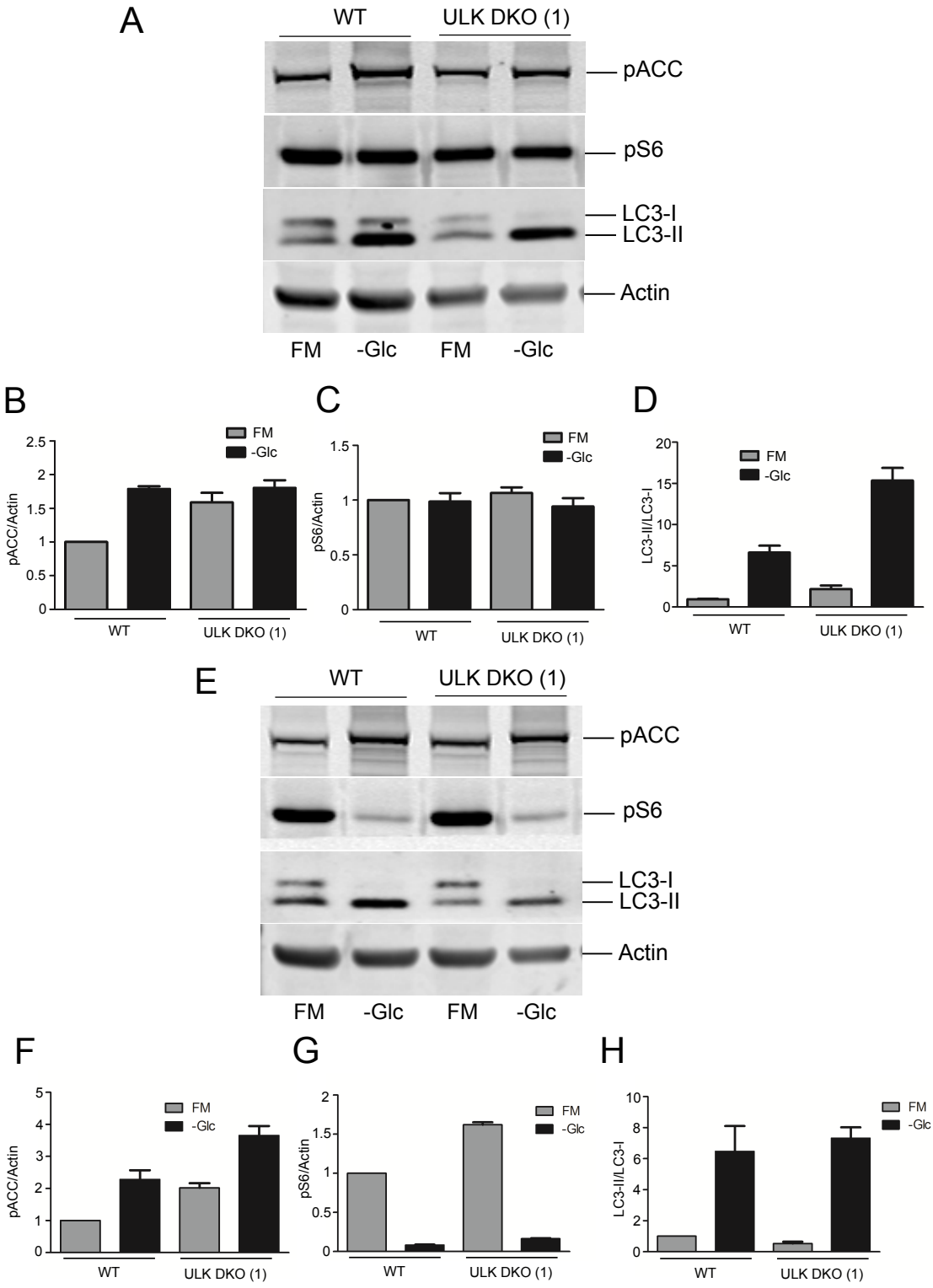

Figure 3.4B: **The effect of short and long term glucose starvation on AMPK and mTOR signalling in ULK1 WT and DKO MEF's**. MEF ULK WT and ULK DKO cell lines were treated with full media or glucose free media supplemented with 10% dFBS for (A) 2 hours (E) 18 hours. Cell lysates were resolved by SDS PAGE and blotted for pACC, pS6 and LC3 proteins. p-ACC and p-S6 were observed as single bands with apparent molecular weights of 280 kDa and 32kDa respectively. The quantified ratios of p-ACC/actin, pS6/actin and LC3-II/LC3-I are shown for (B-D) 2 hours and (F-H) 18 hours. Actin was used as a loading control and data is representative of three separate experiments (n=3).

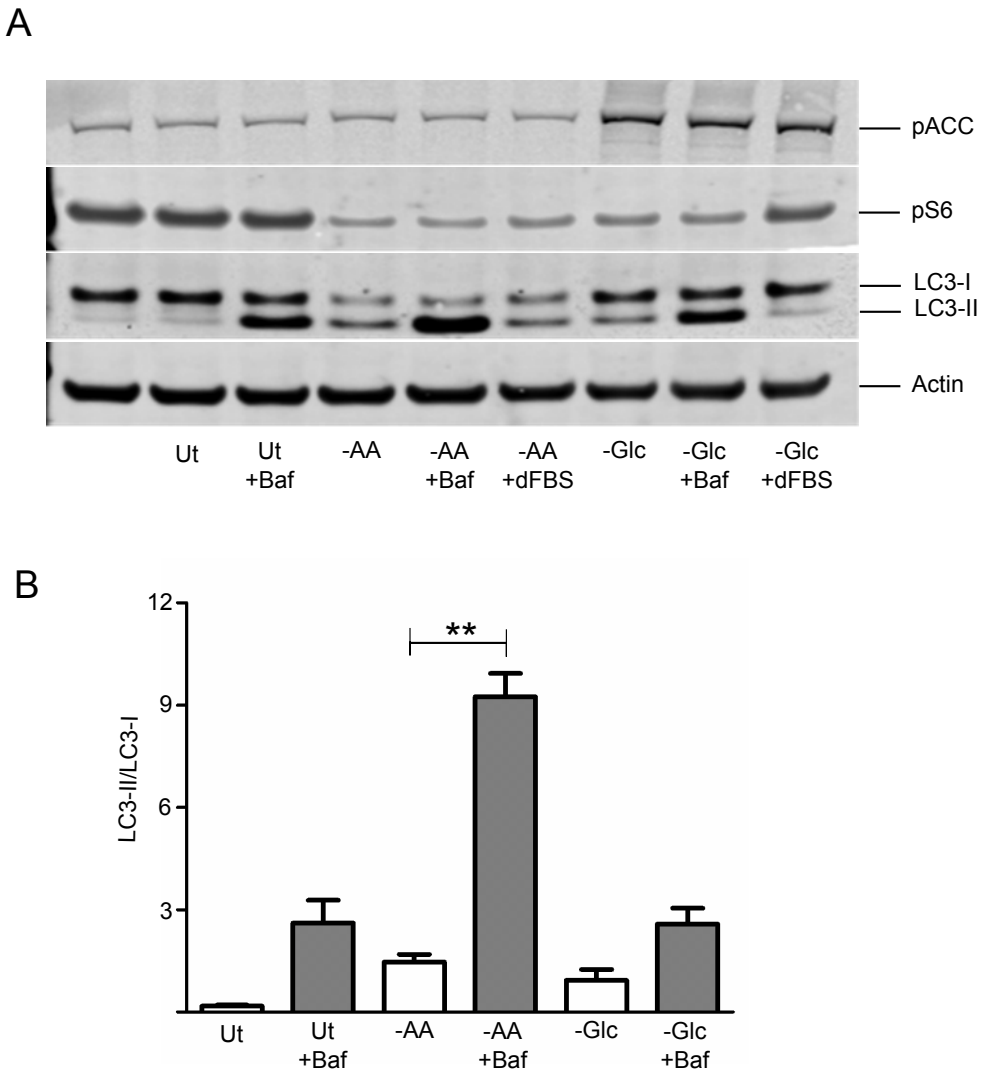

Figure 3.5: **The differential effects of amino acid and glucose withdrawal to autophagy induction during short term starvation**. (A) HEK293A cells were left untreated or were treated with either Bafilomycin A_1 (50nM), EBSS (-AA) alone, EBSS with Bafilomycin A_1 (50nM), glucose free media (-Glc) alone or Glc with Bafilomycin A_1 (50nM) for 2 hours. Cell lysates were resolved by SDS-PAGE and blotted for LC3. (B) Quantified ratios of LC3-II/LC3-I are expressed as mean ± S.E.M. Paired T-tests were performed relative to the untreated (**p<0.01). Actin was used as a loading control and data is representative of three seperate experiments (n=3).

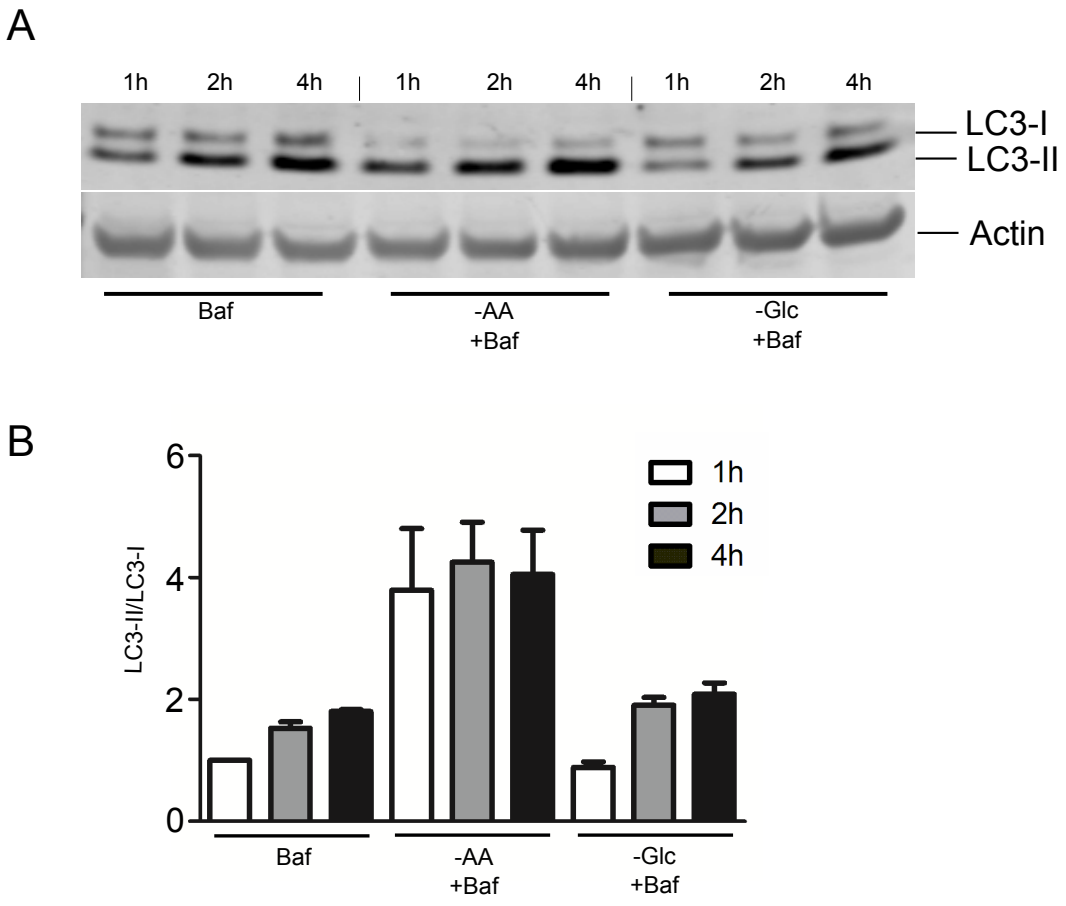

Figure 3.6: **Glucose withdrawal exhibits atypical autophagic flux during short timecourse** . (A) HEK293A cells were treated with Bafilomycin A1 (Baf) (50nM), EBSS with Baf or Glucose free media with Baf for 1h, 2h and 4h. Cell lysates were resolved by SDS-PAGE and blotted for LC3. (B) Quantified ratios of LC3-II/LC3-I are expressed as mean ± S.E.M. Actin was used as a loading control and data is representative of three seperate experiments (n=3).

3.7 HEK293A cells displayed impaired p62 degradation following glucose starvation

Although LC3 turnover is a well-accepted indicator of autophagic flux, it was also necessary to examine the localisation and protein degradation of the p62 (Sequestosome-1) autophagy adaptor protein to further understand the glucose starvation response. During certain forms of autophagy, a small group of ubiquitin binding adaptor proteins allow for the targeting of specific ubiquitin-tagged-cargo to the inner autophagosomal membrane. p62 was the first adaptor protein discovered, that also contains an LIR (LC3 interacting region) between the zinc finger and UBA domains (Ichimura et al., 2008). This 11 amino acid motif (Ser^{334}-Ser^{344}) allows p62 to directly bind to LC3 and GABARAP family proteins located on the autophagosomal membranes. Therefore, this allows p62 to act as a link between ubiquitinated cytoplasmic cargo and the autophagic machinery (Bjorkoy et al., 2005) (Pankiv et al., 2007). Once bound, p62-ubiquitinated protein complexes are then integrated into completed autophagosomes where they are eventually degraded within autolysosomes. Consequently, decreases in p62 levels can be used as a specific marker for autophagic degradation.

To examine p62 degradation, western blot analysis was utilised (Figure 3.7). HEK293A were starved of nutrients over time points of 2, 4 or 18h. These cells under nutrient rich conditions displayed relatively minor elevation in p62 levels across the time course. However, a minor activation of AMPK (probing for p-ACC) could be detected by 18h, possibly suggestive of a gradual depletion of glucose. Importantly, while amino acid starvation produced modest decreases in p62 levels at short time points (2h (~20%) and 4h (~25%)), p62 degradation was clear (~65%) following long term 18h

starvation (Figure 3.7 A,C). Glucose deprivation on the other hand, did not show similar levels of p62 reduction. Hence, these data demonstrate that p62 degradation is relatively small in glucose starved cells compared to amino acid starvation. Interestingly, another study found that glucose starvation led to accumulated levels of p62 in HeLa and Bax/Bak deficient MEF's (Ramirez-Peinado et al., 2013). It could be confirmed that glucose starvation rapidly and strongly activated AMPK as assessed by p-ACC levels (Figure 3.7A,B).

In HEK293 cells, glucose starvation to obvious AMPK activation, but unexpectedly not autophagy. ULK1 is understood to be phosphorylated by AMPK on at least 4 separate sites (Ser^{467}, Ser^{555}, Thr^{574} and Ser^{637}) and two of these sites (Ser^{467} and Ser^{555}) have been reported to be critical for the induction of autophagy (Egan et al., 2011). Other work further showed that ULK1 is a substrate of AMPK leading to binding via putative 14-3-3 motifs around Ser^{555} and Thr^{659} (Bach et al., 2011) (Mack et al., 2012). It was found after 2h of glucose starvation that there was an apparent mild 1.5-fold elevation in phosphorylated Ser^{555} in comparison to control cells (Figure 3.7D,E). Interestingly, after 18h of glucose starvation, Ser^{555} phosphorylation dropped nearer to basal levels. Furthermore, at all timepoints, ULK1 Ser^{555} never showed robust phosphorylation that matched p-ACC levels. Analysis of amino acid starvation also shed some light on ULK1 Ser^{555} phosphorylation. Clearly, amino acid starvation markedly reduced ULK1 Ser^{555} phosphorylation relative to basal levels of full nutrient conditions at all time-points. Additionally, parallel control analysis of LC3 confirmed that amino acid starvation produces strong LC3 lipidation and degradative flux over 18h, in contrast with glucose starvation (Figure 3.7D,F,G).

The results here indicate that AMPK activation and ULK1 Ser^{555} phosphorylation may not play a significant or essential role in amino acid induced autophagy. This contrasts with other data showing ULK1 Ser^{555} phosphorylation after amino acid starvation by AMPK is dependent on Ca^{2+}-CaMKK-β (Ghislat and Knecht, 2012).

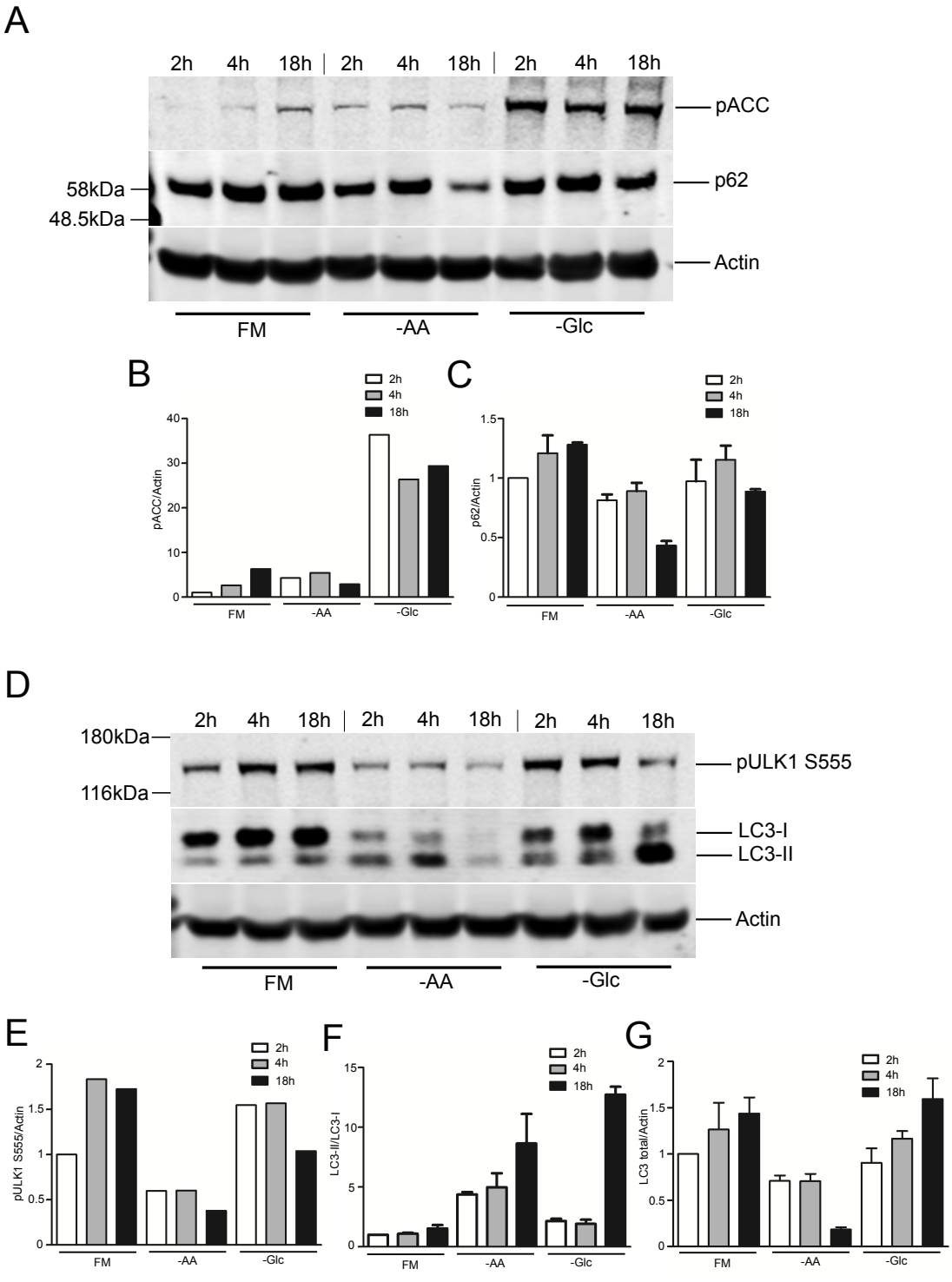

Figure 3.7: **Time course analysis displaying the effect of nutrient starvation on p62 degradation in HEK293A cells**. HEK293A cells were treated with full media or EBSS or glucose free media for 2, 4 or 18 hours. Note for EBSS and glucose free media treated cells, 10% dialysed FBS was supplemented into media. Cell lysates were resolved by SDS PAGE and blotted for pACC, p62, pULK1 S555 and LC3 proteins. pULK1 S555 and p62 were observed as single bands with apparent molecular weights of 140kDa and 58kDa respectively. The quantified ratios of p-ACC/actin, p62/actin (B-C) and pULK1 S555/actin, LC3-II/ LC3-I and LC3 total/actin (E-G) are shown and are expressed as mean ±S.E.M. Actin was used as a loading control and data is representative of three separate experiments (n=3) excluding pULK1 S555 and pACC (n=1).

3.8 Tandem flag mRFP-GFP-LC3 reporter assay investigating autophagic flux during nutrient starvation.

One alternative method to report autophagic flux is by usage of a tandem flag mRFP-GFP-LC3 (TF-LC3) reporter protein (Kimura et al., 2007). Tandem flag LC3 is now a widely used tool to probe both the formation of autophagosomes and maturation into autolysosomes on a cell-by-cell and morphological basis. The TF-LC3 reporter exploits differences in the pH-dependent properties between monomeric red fluorescent protein (mRFP) and green fluorescent protein (GFP) (Figure 3.8A). At physiological pH, GFP is a stably folded protein that is resistant to degradation by lysosomal proteases. However, within the highly acidic lysosomes, GFP fluorescence is quenched. In contrast, mRFP is more stable in acidic compartments and the signal can be detected from within the autolysosome. Therefore, it is possible to detect autolysosomes labelled red (mRFP) only vs. autophagosomes which will show both mRFP and GFP (yellow upon channel merge) during fluorescence microscopy.

HEK293 cells were transiently transfected with the mRFP-GFP-LC3 construct and treated to nutrient starvation for 2h (Figure 3.8). As expected, relatively few red puncta (autolysosomes) and no apparent green puncta (autophagosomes) were observed in the control cells in full nutrients. Amino acid deprivation resulted in an induction of green punctate structures (early non-quenched autophagosomes) and a larger number of red puncta (autolysosomes) consistent with an induction of autophagy and rapid flux. In contrast, following glucose withdrawal, only few GFP+ puncta were observed and the number of red puncta were similarly fewer. Many red puncta were GFP negative indicative of some acidification but these autophagy readouts were generally mild relative to amino acid starvation conditions.

For control purposes, it was necessary to examine the effects of the lysosomal inhibitor Baf which resulted in a clear accumulation and overlap of both green and red puncta. Thus, indicating the expected loss of lysosomal acidification. In this regard, chloroquine displayed similar results to Baf. Interestingly, both GFP and RFP puncta were larger and more aggregated after chloroquine treatment as compared to Baf. At this point, it can be noted that chloroquine, on entering the cell can cross the lysosomal membrane. Once inside the lysosome, chloroquine becomes protonated and trapped due to its weakly basic properties. This subsequently leads to an osmotic influx of water and swelling, a phenomenon previously referred to as cytoplasmic vacuolisation (Ohkuma and Poole, 1981).

3.9 Immunocytochemistry of endogenous LC3 and p62 levels following nutrient starvation.

Having established the differential effects of amino acid vs glucose deprivation on autophagosome formation and maturation using TF-LC3, it was necessary to examine autophagy membranes using immunocytochemical analysis of endogenous markers to rule out any artefacts from overexpression of proteins. HEK293 cells were starved of amino acids or glucose for 2h. Fixed cells were stained for endogenous LC3-targeted membranes (Figure 3.9). In untreated conditions, HEK293 cells have a small number of LC3 puncta reflecting low basal autophagy. Upon induction of autophagy by amino acid withdrawal, a clear increase in the number of endogenous LC3-punctate structures was detected. In contrast, 2h glucose starvation did not induce similar LC3-labelled membranes. However, due to the appearance of background staining and heterogeneity in signals, it became apparent that it was not straightforward to clearly quantify these differences.

Based on this, it became necessary to search for better staining markers of autophagy membranes and next investigated endogenous p62 patterns in HEK293 cells. It was found that p62 membranes could be very clearly visualised in HEK293 cells. p62-labelled membranes were relatively few in untreated conditions (Figure 3.9). Subsequently, following amino acid withdrawal, a significant elevation (over 2-fold) of p62 structures was observed in the cell population (Figure 3.9B). In contrast, glucose starvation failed to induce p62 puncta per cell, consistent with our earlier western blot analyses.

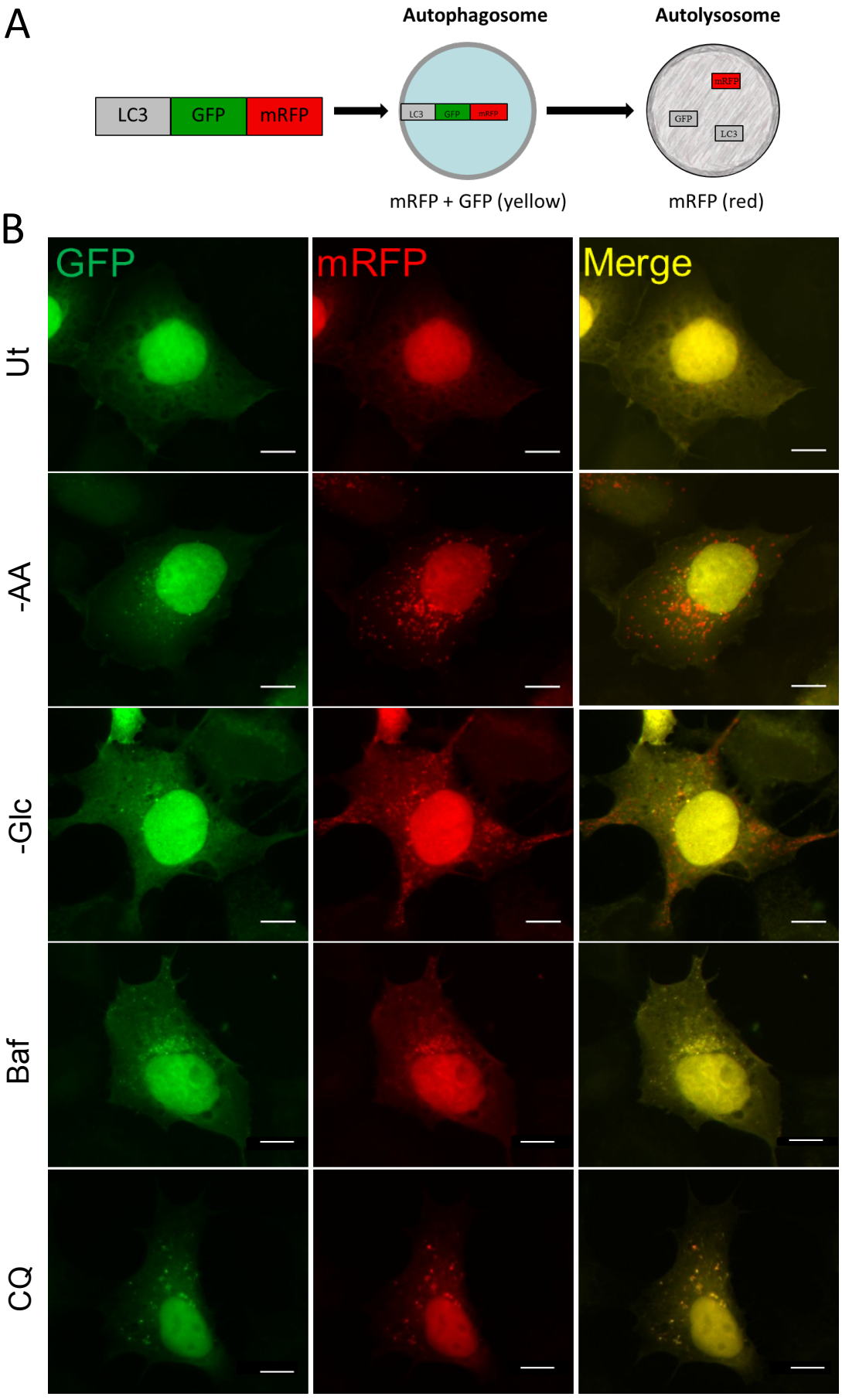
A
Autophagosome
Autolysosome
LC3
GFP
mRFP
mRFP + GFP (yellow)
mRFP (red)
B
GFP
mRFP
Merge
Ut
-AA
-Glc
Baf
CQ

Figure 3.8 **Epifluorescense micrographs showing the effects of various autophagic effectors on mRFP-GFP-LC3 puncta formation** . (A) Schematic diagram of the tandem flag mRFP-GFP-LC3 (TF-LC3) plasmid. (B) Immunocytochemistry of HEK293A cells transfected with the TF-LC3 and treated with either EBSS (0.1% dFBS) (-AA), glucose free media (0.1% dFBS) (-Glc), bafilomycin A1 (50nM) or chloroquine (25μM) for 2 hours. In merged channel; red puncta (mRFP) indicate autolysosomes and yellow puncta (mRFP + GFP) represent autophagosomes. All images were captured with an X60 oil immersion objective lens (total magnification X600). Scale Bar = 10μm

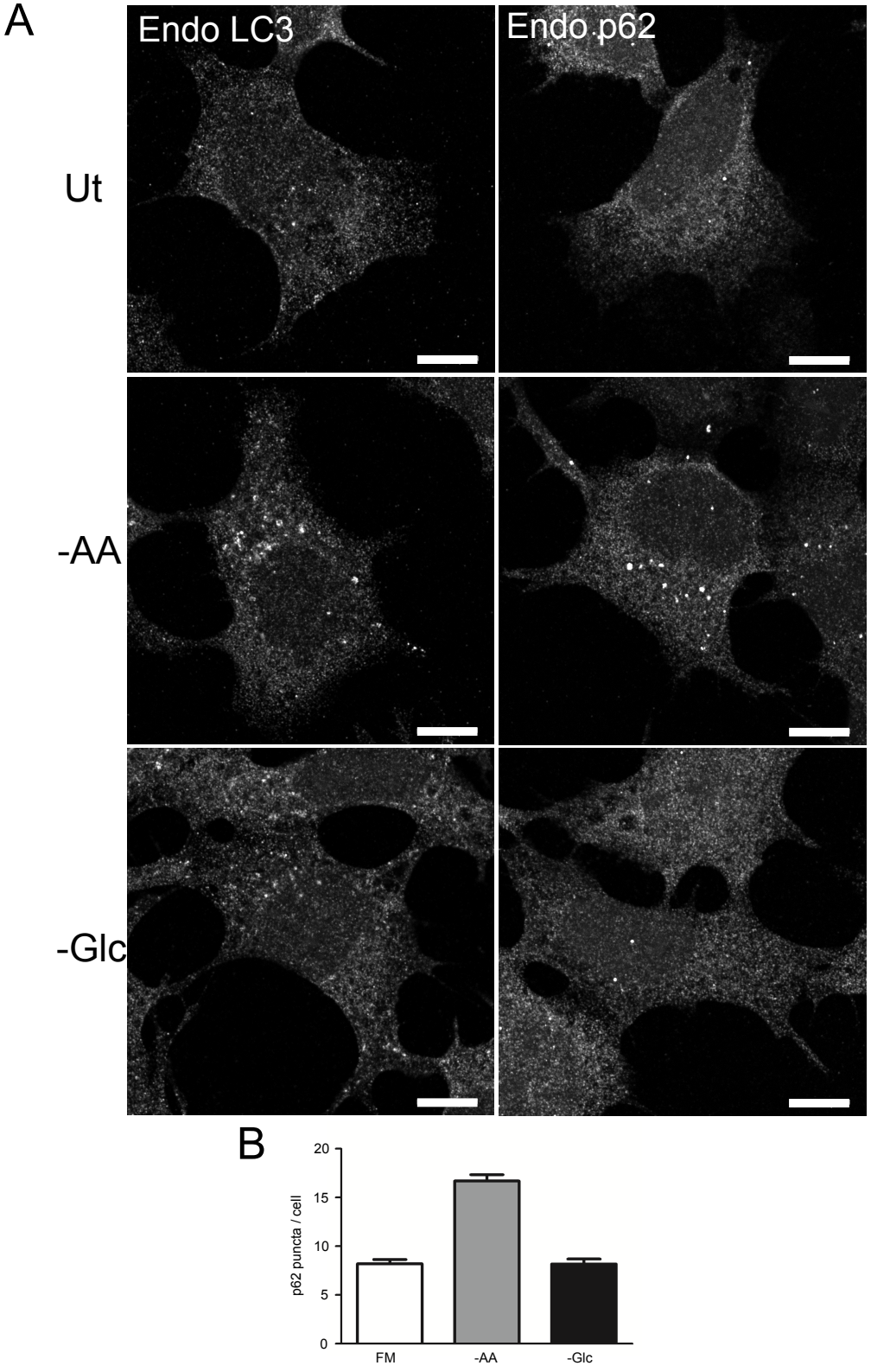

Figure 3.9: **The effect of nutrient starvation on LC3 and p62 puncta formation in HEK293A cells**. (A) HEK293A cells were plated on glass coverslips and left untreated (control) or treated with EBSS (0.1% dFBS) or glucose free media (0.1% dFBS) for 2 hours. Coverslips were immunostained for endogenous LC3 or p62 and were subjected to confocal microscopy using a Leica TCS SP5 confocal microscope. (B) Quantifation of p62 puncta per cell are expressed as mean ± S.E.M (n=40). All images were taken using an oil immersion objective lens (63X) and analysed using the Leica Microsystems LAS AF software. Scale Bar = 10μM.

3.10 LC3 and p62 co-localise in HEK 293 cells following amino acid starvation.

p62 plays a key role in acting as an adaptor between poly-ubiquitinated cargo and LC3 on the surface of the isolation membrane (Bjorkoy et al., 2005) (Pankiv et al., 2007) . Thus, it was essential to confirm this mechanistic link with the cell systems used in our laboratory. For this, HEK293 cells stably expressing GFP-LC3 (HEK 2GL9) (Chan et al., 2007) were starved of amino acids for 2 hours. Fixed cells were stained for endogenous p62 and analysed by confocal microscopy. As seen in HEK293A cells, starvation of amino acids strongly induced GFP-LC3 and p62 puncta formation in comparison with cells in full nutrients. The imaging results also showed that LC3 and p62 did not completely reside to any particular region within the cell. However, many puncta did localise to the perinuclear region. To assess co-localisation between GFP-LC3 and p62, the overlay did reveal the majority of p62 and LC3 overlap (formation of yellow puncta) although noticeably not 100% (Figure 3.10). However, this confirmatory analysis further supports the use of p62 as a suitable and reliable marker of autophagosomes.

3.11 The effects of nutrient starvation on endogenous ULK1 puncta formation.

In the survey for markers of autophagy membranes, attention was turned to further upstream autophagic machinery including the ULK1 complex which is widely accepted to be at or near the apex of earliest autophagy proteins associated with the ER, driving the formation of the isolation membrane (Itakura and Mizushima, 2010). The effects of nutrient starvation on endogenous ULK1 puncta formation in HEK293A cells were thereby examined (Figure 3.11). In untreated cells, ULK1 staining was diffuse and

rarely formed single punctate structures. Starvation of amino acids induced a sharp increase in the number of ULK1 puncta suggesting ULK1 functions during amino acid deprivation. On the other hand, glucose withdrawal clearly showed no indication of ULK1 puncta formation, consistent with the acquired growing body of data that indicates autophagy is not induced in this type of starvation.

Several attempts were made to assess ULK1 in our wild-type MEFs which proved unsuccessful possibly due to lower levels of endogenous ULK1 in these lines. On the other hand, a corresponding trend of ULK1 puncta in HeLa cells could be confirmed (Figure 3.11).

3.12 p62 puncta display a larger size in comparison to ULK1.

The membranes stained by p62 and ULK1 antibodies following amino acid starvation appeared different. As such, further analysis was required of the diameter of these puncta to study the sizes of compartments that p62 and ULK1 are localising to. Regions of interest were drawn directly through the centres from sets of puncta and the diameter calculated from line intensity profile charts. It was observed that the mean puncta diameter of p62 was 1.14μm (n=90) while the mean value of ULK1 puncta was 0.85μm (n=60). On average, p62 puncta were 34% larger in diameter in comparison to ULK1 puncta (Figure 3.12). This might suggest that the ULK1 complex is only transiently found at the earliest development stages of the isolation membrane. p62 on the other hand is reported to self-oligomerise in larger adapter-cargo-LC3 complexes and be recruited further downstream.

3.13 Short time course analysis of ULK1 and p62 puncta following nutrient starvation.

Having characterised properties of detection of ULK1 and p62 puncta, it was necessary to study how these early vs late stage autophagy proteins were dynamically recruited during autophagy induction. In order to do so, HEK293A cells were starved over a short time-course (Figure 3.13). Following amino acid withdrawal, ULK1 puncta formation was rapidly induced as early as 15 mins and demonstrated further time dependent increases. After 1h of amino acid starvation, ULK1 puncta were over 10-fold higher compared to untreated cells. In contrast, glucose starvation did not induce any ULK1 puncta formation.

The parallel analysis showed that amino acid withdrawal also stimulated p62 puncta formation but this could only be detected following 30 mins and 1h starvation. This correlative comparison suggests that ULK1 is recruited earlier (by approximately 10-15 mins) than p62 during autophagic induction and membrane formation. In consensus with the other data, glucose starvation triggered no p62 puncta formation across the entire time course.

3.14 ULK1 puncta are transiently formed following amino acid deprivation.

In the previous time course experiment, it was established that approximately 50% of maximal ULK1 puncta were induced within 15mins of amino acid starvation. This suggested very rapid dynamics at the early stages of autophagy induction. Consequently, it was required to understand the timing of ULK1 assembly events in more detail. Live-cell imaging was investigated in HEK293 cells stably expressing GFP-

ULK1 starved of amino acids. From a survey of the heterogeneous pooled cell population, it was clear that three distinct populations existed: (1) cells with high GFP-ULK1 expression and hence high general cytosolic background signal with low ULK1 puncta count (Figure 3.14A, cell on left); (2) cells with obviously abnormal high GFP-ULK1 and potential aggresome-like structures; and (3) cells with medium expression and inducible GFP-ULK1 puncta formation (Figure 3.14A,B).

Of the three heterogeneous subtypes only the medium-expression subset (3) of cells, GFP-ULK1 originates as a clear single punctum that appeared to randomly translocate around the cytoplasm with no distinct direction. A representative typical GFP-ULK1 punctum could be detected in the cytoplasm for approximately 2min 40secs. The membrane formation was continuous and highly dynamic. In several cases, ring-like structures where observed potentially representing the emerging isolation membrane transforming to a complete autophagosome (one example in Figure 3.14B). The GFP-ULK1 positive ring-like structures appeared approximately 1min subsequent to the initial detection of the punctum and was present for roughly 1min 40sec.

In summary, this analysis confirmed that ULK1 can be detected to transiently localise to the isolation membrane and remain through stages including complete autophagosome closure. GFP-ULK1 labelled membranes were motile but directionality was unclear, perhaps linked to the transient nature of the interaction. Moreover, a challenge in this assay is the heterogeneous nature of the current cell population, with different expression levels which apparently has great effects on the reliability of the GFP-ULK1 marker.

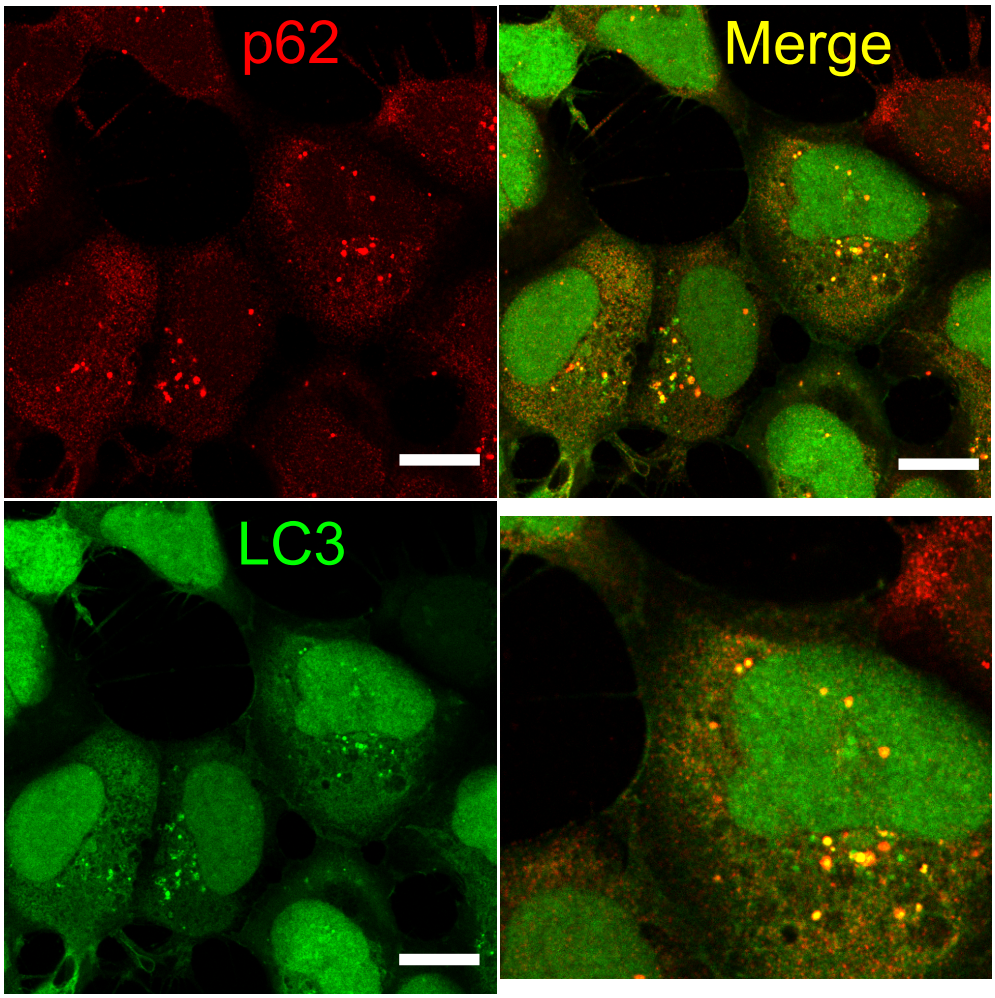

Figure 3.10: **LC3 and p62 display high colocalisation in HEK 2GL9 cells following amino acid starvation.** HEK293 cells stably expressing GFPC3 (HEK 2GL9) were plated on glass coverslips and were treated with EBSS (0.1% dFBS) for 2 hours. Cells were then immunostained for endogenous p62 and were subjected to confocal microscopy using a eica TCS SP5 confocal microscope. All images were taken using an oil immersion objective lens (63X) and analysed using the Leica Microsystems LAS AF software. Scale bar= 10µm.

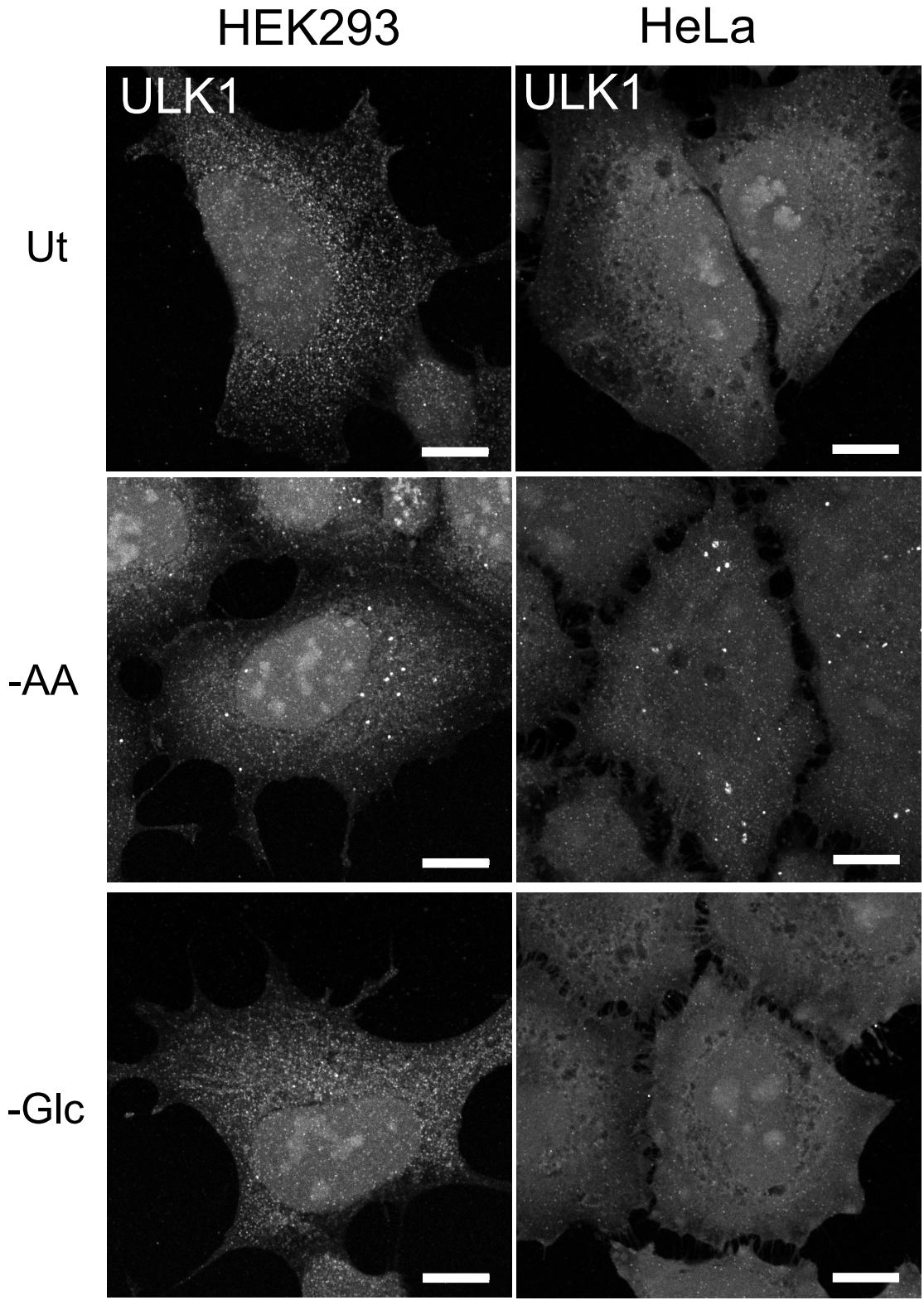

Figure 3.11: **The effect of nutrient starvation on endogenous ULK1 puncta formation in HEK293A and HeLa cells**. HEK293A cells were plated on glass coverslips and left untreated (control) or treated with EBSS (0.1% dFBS) or glucose free media (0.1% dFBS) for 2 hours. Coverslips were immunostained for endogenous ULK1 and were subjected to confocal microscopy using a Leica TCS SP5 confocal microscope. All images were taken using an oil immersion objective lens (63X) and analysed using the Leica Microsystems LAS AF software. Scale Bar = 10µM.

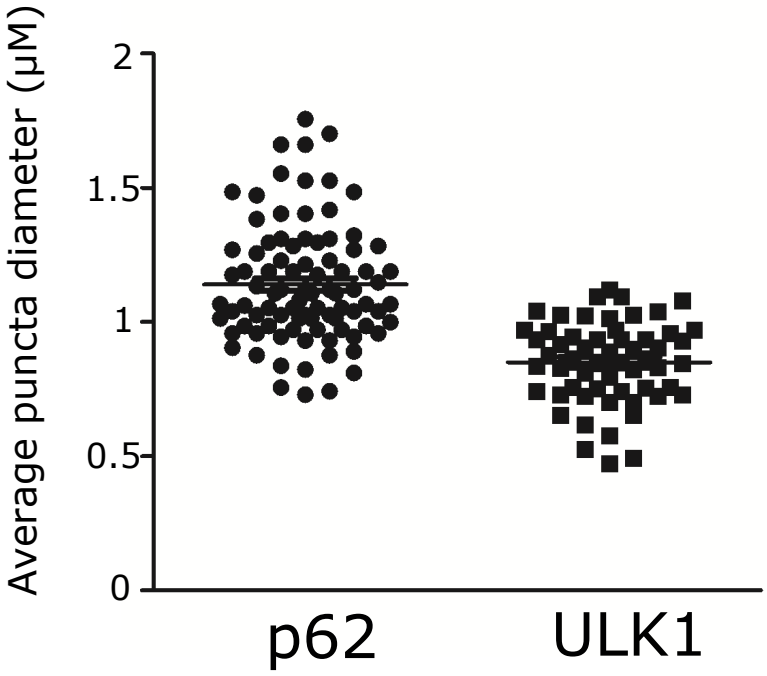

Figure 3.12: **The effect of amino acid starvation on p62 and ULK1 puncta diameter** . HEK293 cells were plated on glass coverslips and were treated with EBSS (0.1% dFBS) for 2 hours. Cells were fixed and immunostained with either p62 or ULK1 and analysed by confocal microscopy. Scatterplots were generated through measurement of average diameter of p62 and ULK1 puncta using the Leica Microsystems LAS AF software. Each point is signifies a single p62 and ULK1 punca representative cells (n=10).

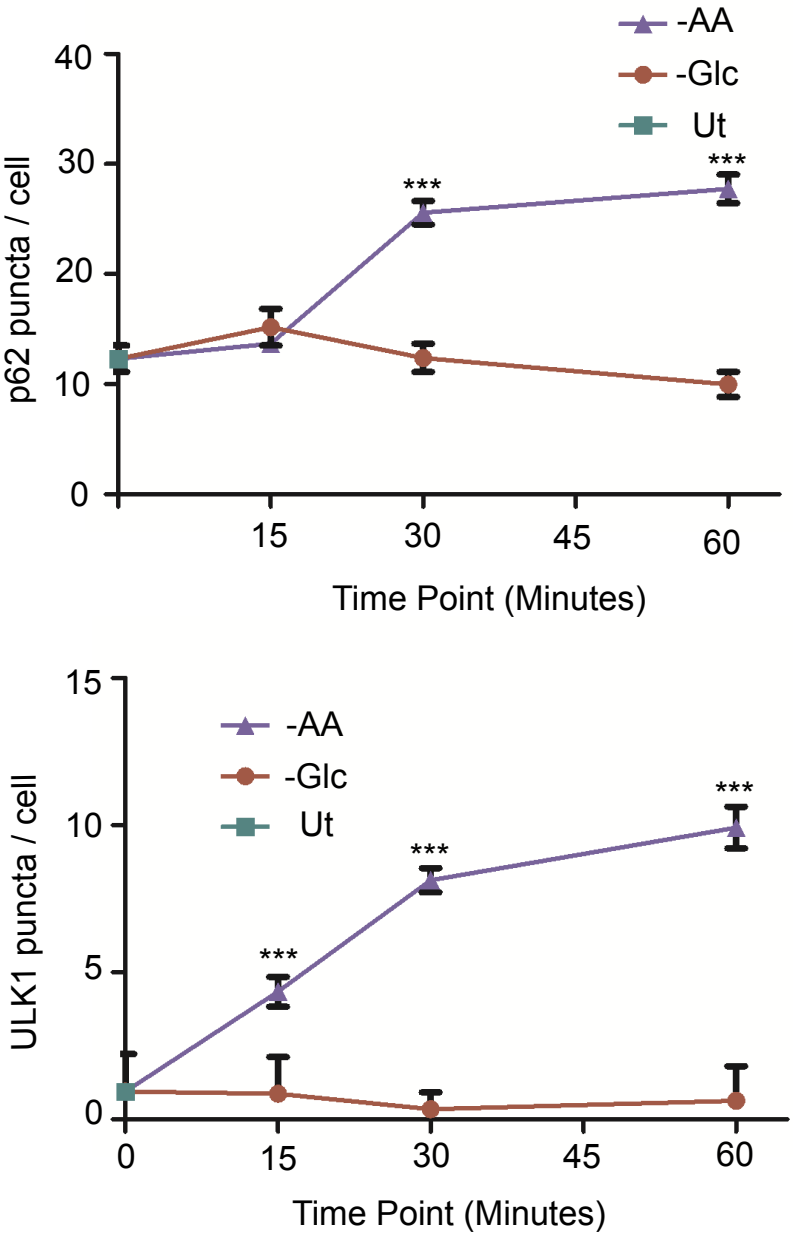

Figure 3.13: **ULK1 and p62 puncta formation is not altered following glucose starvation** . HEK293A cells were left untreated (Ut) or were treated with either EBSS (-AA) or glucose free media (-Glc) for 15, 30, 60 or 120 mins. Cells were analysed by immunofluorescence microscopy and stained using anti-p62 and anti-ULK1 antibodies. Quantifications of p62 puncta per cell (top) and ULK1 puncta per cell (bottom) are expressed as mean ±S.E.M of a minimum of 40 cells. Paired t-tests were performed (***p<0.001).

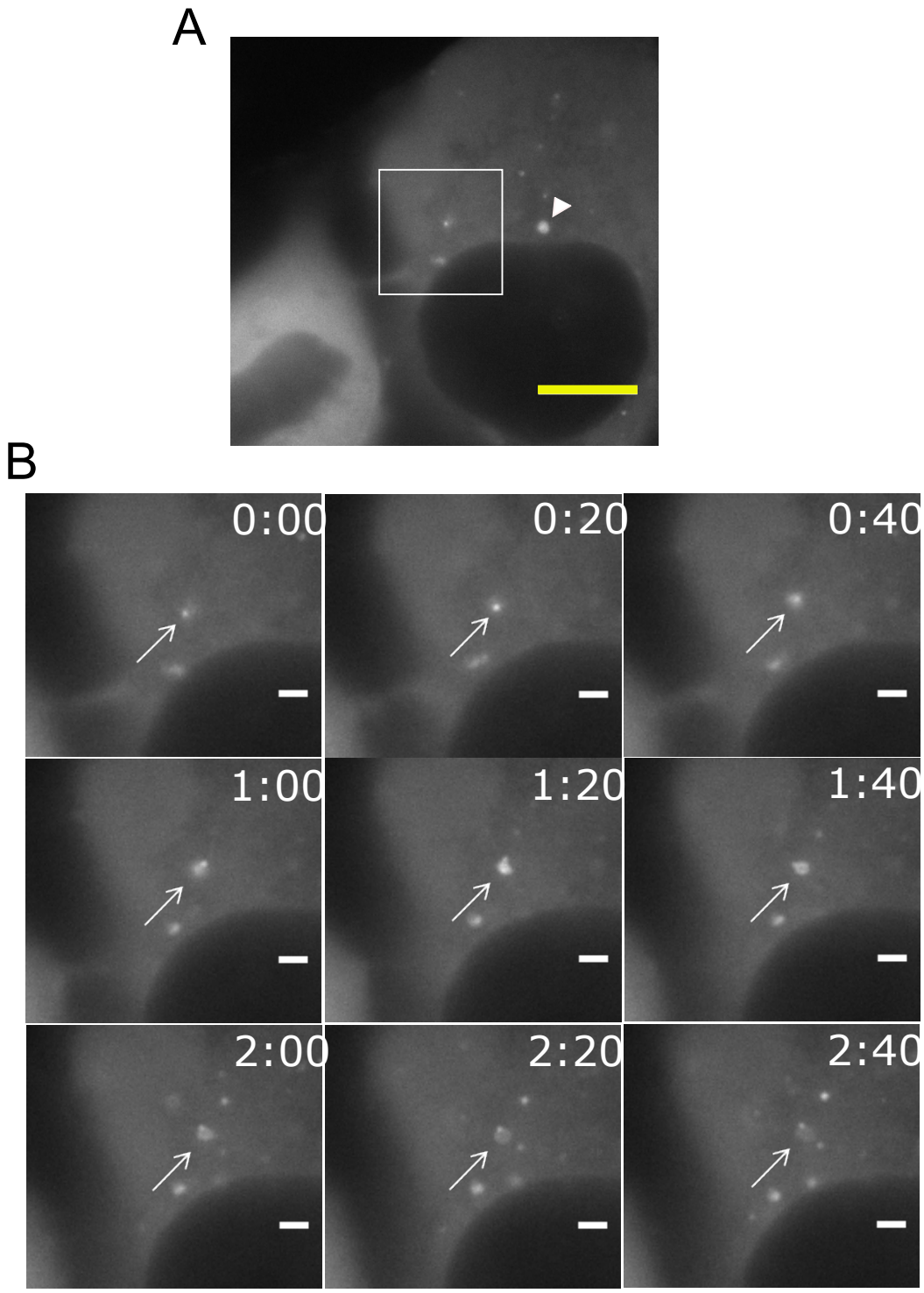

Figure 3.14: **ULK1 puncta are transiently formed and generate ring-like structures following amino acid starvation.** HEK293 cells stably expressing GFP-ULK1 were plated on glass bottomed 3.5cm^3 dishes and treated with HBSS containing 0.1% FBS and 75mM HEPES. Time-lapse movies were started 15mins after amino acid withdrawal and images were taken every 20secs for 10mins. (A) Still image taken from time-lapse movie approximately 18 mins following starvation. (B) Set of 10 images indicating the formation of a ring shaped structure possibly the isolation membrane. TIme-points are represented as min:sec and arbitrarily set to 0:00. Localisation of GFP-ULK1 puncta are indicated by white arrows and aggresome by a white arrowhead. For full movie see appendices... Scale bars= 10μm (yellow) and 2μm (white).

3.15 The effect of amino acid starvation on the generation of PI3P

The production of PI3P at the isolation membrane by the class III PI3K complex is a crucial step in the biogenesis of the isolation membrane. The ULK1 complex plays a crucial role in the induction of PI3P production by directly phosphorylating the beclin-1 subunit of class III PI3K complexes containing Atg14 (Russell et al., 2013). This phosphorylation event is proposed to increase the activity of the class III PI3K complex leading to the enrichment of PI3P in membrane subdomains, which recruits further PI3P-binding effector proteins including DFCP-1 to the omegasome (Axe et al., 2008). Given the integral role of PI3P in autophagy membrane traffic and the close interrelationship with ULK1 function, a number of approaches were undertaken to study PI3P formation relative to p62 which had become a routine and robust endogenous marker in our lab.

Firstly analysis was carried out in a HEK293 line which we derived stably expressing GFP-DFCP-1 (Figure 3.15) (Axe et al., 2008). HEK GFP-DFCP-1 cells were starved of amino acids. Fixed cells were further assessed by p62 immunocytochemistry. After amino acid starvation, GFP-DFCP-1 was found to localise within the cytosol in close proximity to the nucleus as a wide range of punctate structures. Some structures resembled typically sized autophagy puncta while GFP-DFCP-1 also localised to larger membrane compartments. Quantifications of amino acid starvation induction of GFP-DFCP-1 puncta proved problematic due to variability in the expression levels of GFP-DFCP-1 in the stable pool.

Interestingly, in the same cells, starvation induced endogenous p62 puncta remained of the expected normal size range and appearance. In addition, a fraction of the p62 puncta did show degrees of co-localisation or proximity with GFP-DFCP-1 puncta.

These data indicate PI3P enrichment only on a subpopulation of p62 membranes. It can be speculated that p62 may be longer-lived and associated with membranes even after PI3P enrichment has completed early membrane formation stages.

While stable expression of GFP-DFCP-1 in HEK293 cells was heterogeneous, transduction of the same viral vector produced lower and more homogenous levels of stable expression in MEFs. Amino acid starvation of the MEF GFP-DFCP-1 cell line exhibited a clearer induction of distinct smaller GFP-DFCP-1 puncta and ring-like membranes (Figure 3.16). Starvation also induced small numbers of distinct p62 puncta. A fraction of p62 membranes co-localised or appeared to be encircled by GFP-DFCP-1 labelled ring-shaped membranes. This type of membrane structure was particularly visible in MEF and was not as readily observed in HEK GFP-DFCP-1 cells. To gain further understanding of the 3-dimensional structure of these compartments, starved MEF GFP-DFCP-1 cells were analysed using confocal microscopy, capturing a Z-stacked image data set to reconstruct 3D models (Figure 3.16B). Rendering showed GFP-DFCP-1 puncta on the perimeter of the p62 puncta creating the appearance of a ring structure. This is consistent of p62 being located on the inner membrane of the autophagosome. In addition, in each case a single p62 puncta locates to this structure but the number of DFCP-1 spots in these ring structures varies considerably. These GFP-DFCP-1 puncta ranged from 1 to 5 distinct spots associated to p62. This could suggest different stages of isolation membrane formation or discontinuous sections of PI3P enrichment. Unfortunately, resolution in the Z-plane was somewhat limited, even though each image was captured every 0.1 micrometres (microns).

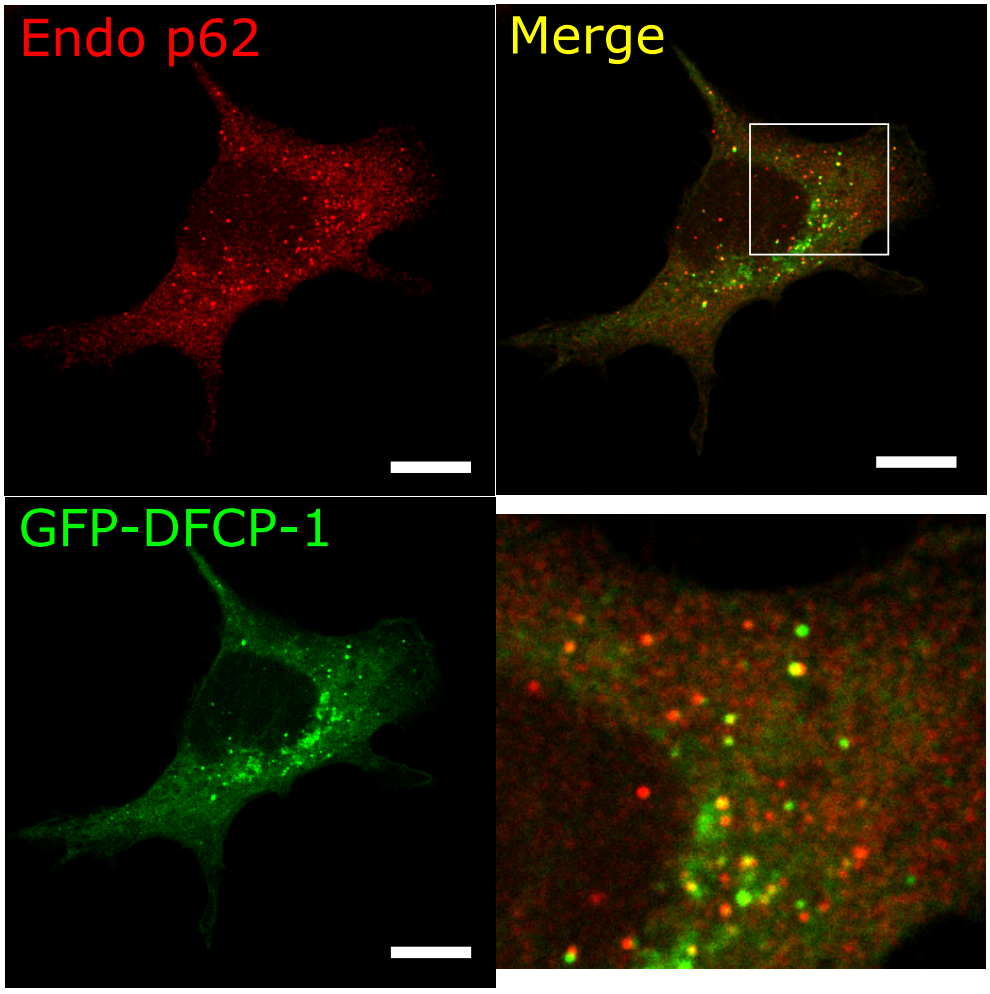

Figure 3.15: **GFP-DFCP-1 closely associates with p62 in HEK293 cells starved of amino acids.** HEK293 cells stably expressing GFP-DFCP-1 were plated on glass coverslips and were treated with EBSS (0.1% dFBS) for 2 hours. Cells were then immunostained for endogenous p62 and were subjected to confocal microscopy using a Leica TCS SP5 confocal microscope. All images were taken using an oil immersion objective lens (63X) and analysed using the Leica Microsystems LAS AF software. Scale bar = 10µm.

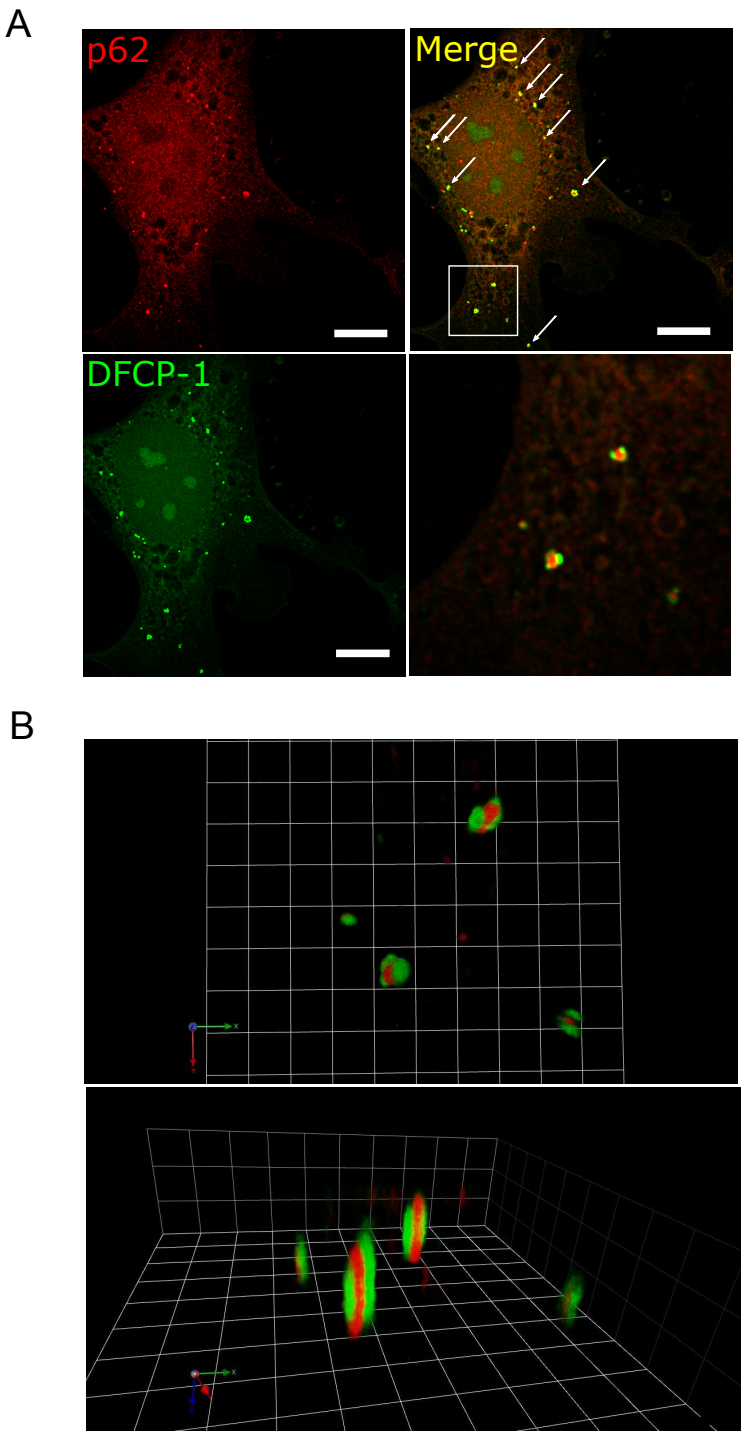

Figure 3.16: **Model of the 3D structure of the colocalisation of GFP-DFCP-1 and p62 in MEFs**. MEFs stably expressing GFP-DFCP-1 were plated on glass coverslips and were treated with EBSS (0.1% dFBS) for 2 hours. (A-B) Cells were fixed then immunostained for endogenous p62 and were subjected to confocal microscopy using a Leica TCS SP5 confocal microscope. Arrows show examples of co-localisation. Scale bar= 10µm. (B) 3D reconstitution of p62 and DFCP-1 stuctures from a Z-stack of 40 images. Scale: 1 unit=1.54µm. All images were taken using an oil immersion objective lens (63X) and analysed using the Leica Microsystems LAS AF software.

3.16 The effects of double starvation on endogenous p62 puncta formation in HEK293 and MEF cells.

Above, we have characterised the amino acid response by examining the formation of p62-labelled autophagy membranes. It has also been shown that glucose starvation does not stimulate autophagy flux and membrane formation, in contrast to amino acid starvation responses. From this it could be hypothesised that glucose starvation could potentially inhibit amino acid induced autophagy. Therefore to this aim, the effects of a complete starvation (amino acid, glucose) on p62 puncta formation in HEK GFP-DFCP-1 and MEF GFP-DFCP-1 cells were investigated.

Interestingly, HEK293 and MEFs display different numbers of p62 puncta in basal conditions (Figure 3.17, panels A and B). However, it is clear that following amino acid starvation, the expected induction in p62 puncta clearly occurs within both cell lines. In both HEK293 and MEF, glucose starvation has produced undetectable (HEK) or relatively low (MEF) induction of p62 puncta, as previously seen. Importantly, the p62 puncta induction observed by amino acid starvation is abolished in further withdrawal of glucose (DPBS condition). Overall this suggests that glucose is absolutely required for the amino acid starvation induced recruitment of p62.

3.17 The effects of complete starvation on AMPK and mTOR signalling in HEK293 cells

As a result of the above data showing interactions between starvation schemes and a block in autophagy, examination was required as to how complete starvation affects AMPK and MTORC1 signalling.

3.17.1 The effect of complete starvation on autophagic AMPK signalling

HEK293 cells were starved of various nutrients as indicated for 2h and analysed for pAMPK, pULK1 S555, and pACC; in addition to LC3 lipidation (Figure 3.18). Commencing from the AMPK energy sensor, it was again noted that amino acid starvation mildly suppressed AMPK activity (by pACC), regardless of serum levels. As expected, glucose withdrawal led to a 2-fold increase in pACC (normalising to total protein levels). Furthermore, double amino acid and glucose starvation led to a 1.92-fold increase in pACC, regardless of serum levels. Next, this pattern was compared with the phosphorylation status of ULK1 Ser^{555} which is understood to be directly phosphorylated by AMPK. Amino acid starvation reduced ULK1 Ser^{555} to 0.63-fold, while glucose starvation increased this change 1.28-fold, which generally matches pACC. When both nutrients were removed, pULK1 Ser^{555} levels unexpectedly did not increase as dramatically. This potentially may be some degree of uncoupling or different coupling between AMPK and substrates ACC vs ULK1. On this point, phosphorylation on AMPK Thr^{172} was mildly increased in all starvation conditions. When starved of both nutrients this phosphorylation rose to 2.19-fold. This suggests that depletion of both amino acid and glucose both induce the phosphorylation of the activation loop in AMPK.

LC3 lipidation was examined to assess autophagy activation under these conditions in parallel. It was clear that amino acid starvation promotes LC3 lipidation compared to basal cells and this occurred even in the presence of serum, showing effects of just amino acids. On the other hand, glucose withdrawal (in the presence of serum) could not noticeably induce LC3 conversion, consistent with work of this chapter. Strikingly, double starvation of cells showed little LC3 lipidation. This result clearly shows glucose

is required to induce a typical autophagic response at the LC3 level following, amino acid deprivation, consistent with the p62 puncta assay. However, the differences in autophagy do not closely match pAMPK, pACC or pULK S555 changes.

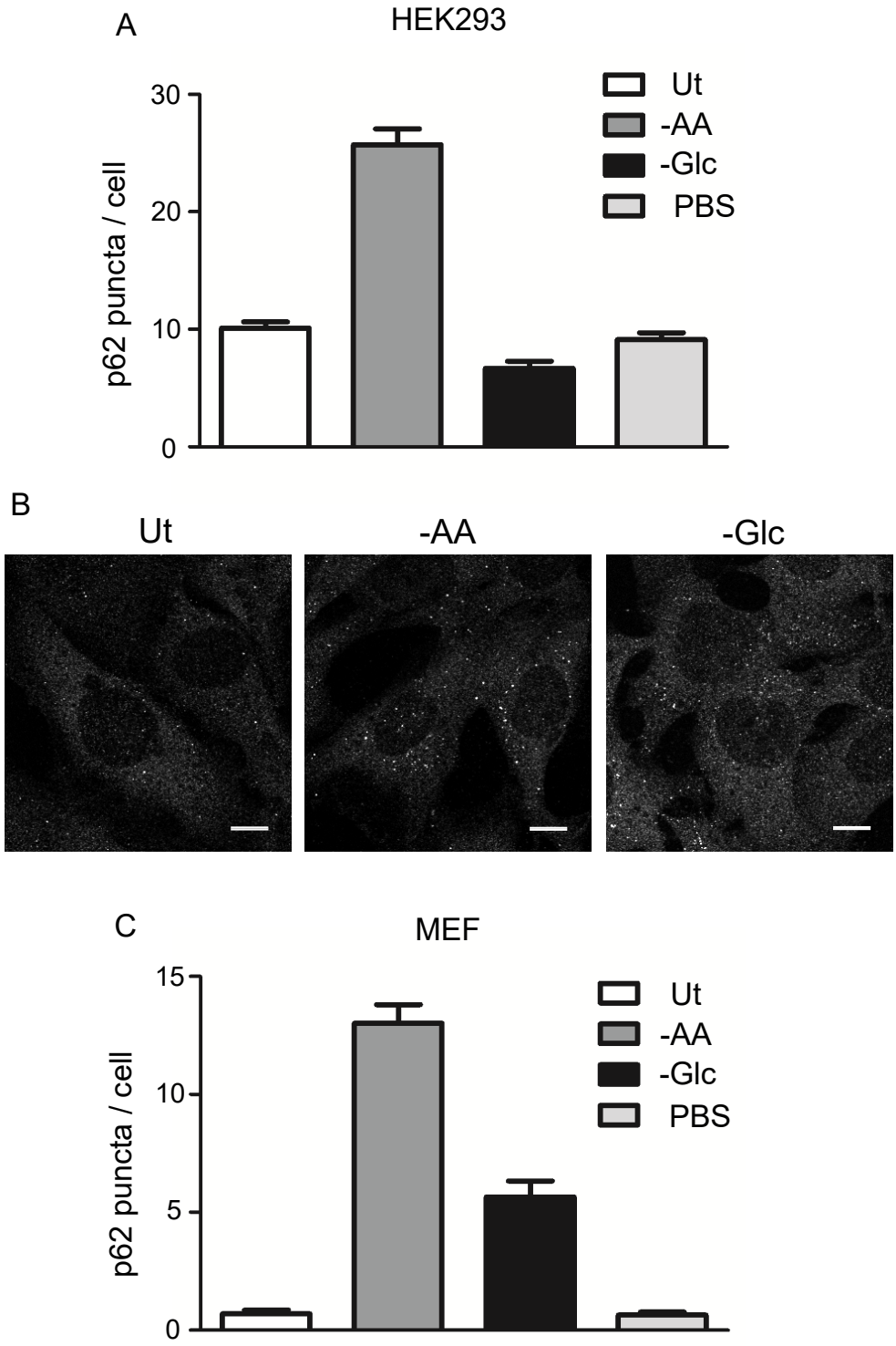

Figure 3.17: **Further starvation of glucose blocks autophagy activation from amino acid starvation in both HEK293 and MEF**. HEK293 and MEF (also expressing GFP-DFCP-1) were plated on glass coverslips and left untreated (control) or treated with either EBSS (-AA), glucose free media (-Glc) or PBS containing Ca/Mg (double starvation) (all with 0.1% dFBS) for 2 hours. Cells were then analysed by confocal microscopy and stained for endogenous p62. (A) Quantifications of p62 puncta per cell in HEK are expressed as mean ± S.E.M of 40 cells. (B-C) Representative images along with corresponding quantifications of p62 puncta per cell in MEF are also expressed as mean ± S.E.M of 40 cells. Scale Bar = 10uM.

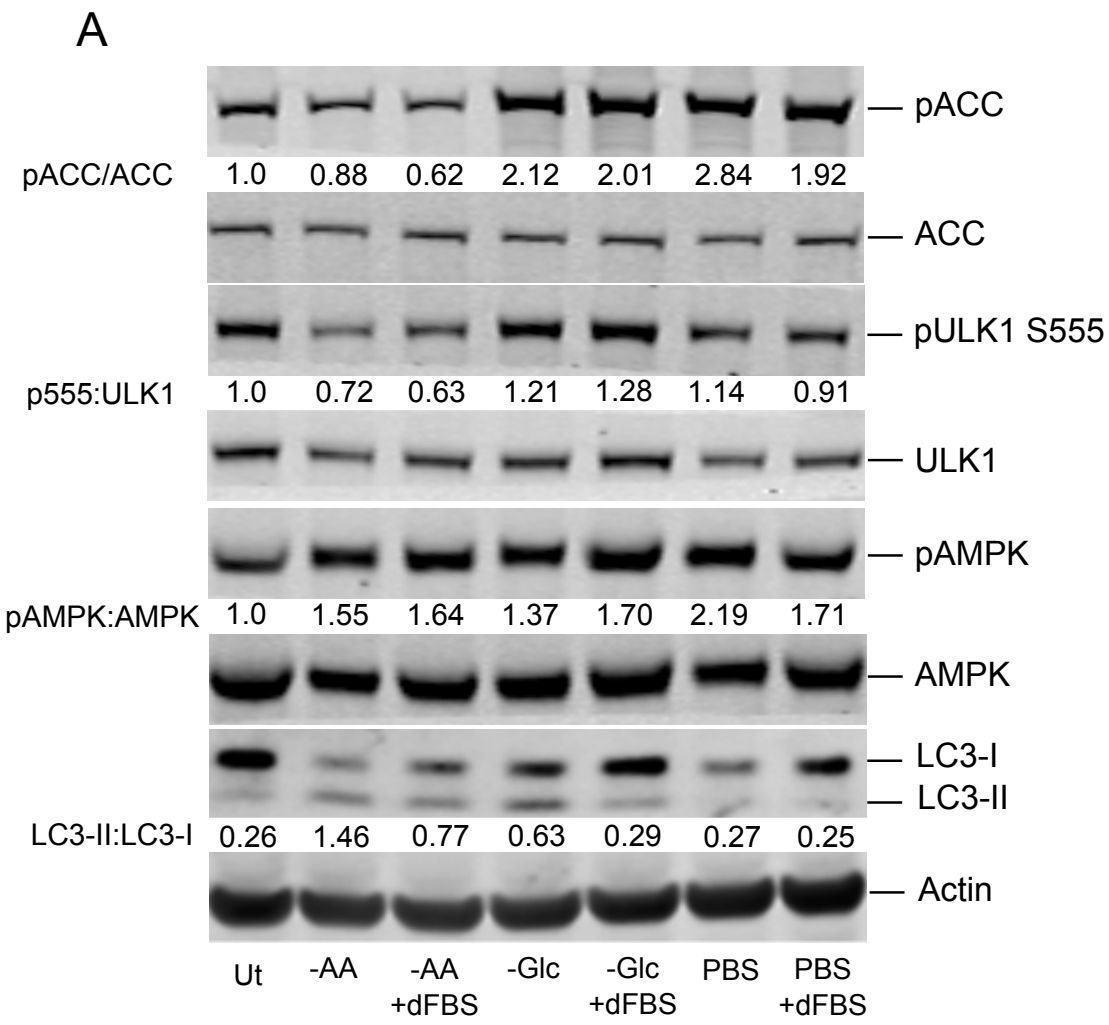

Figure 3.18: **The effect of nutrient starvation on the glucose/AMPK signalling pathway.** (A) HEK293A cells were treated with EBSS, glucose free media or PBS with/without 10% dFBS for 2 hours. Cell lysates were resolved by SDS-PAGE and blotted for ULK1, pULK1 S757, pULK1 S317 and pS6. Quantified ratios of pACC, ACC, ULK1, pULK1 S555, pAMPK, AMPK all normalised to actin and LC3-II/ LC3-I are shown. Data are representative of three seperate experiments.

3.17.2 The effect of complete starvation on autophagic MTORC1 signalling

To further explore nutrient signalling and the inhibitory effect on autophagy, experiments were performed to also assess the activity of MTORC1 signalling (Figure 3.19). It has been confirmed amino acid starvation strongly suppressed MTORC1 activity as seen by p-S6 (Figure 3.19 A). Since serum has been shown to influence nutrient sensing in our system, we also tested this condition and noted that MTORC1 activity was still strongly inhibited (p-S6) after amino acid starvation (Figure 3.19B).

Next, phosphorylation of ULK1 at Ser^{757} was examined which is the well characterised MTORC1 phosphorylation site (Shang et al., 2011) (Kim et al., 2011). MTORC1 can prevent ULK1 activation and autophagy by phosphorylation of Ser^{757} thereby disrupting interaction between ULK1 and AMPK (Kim et al., 2011). As expected, loss of amino acids clearly reduced phosphorylation of ULK1 Ser^{757} both in the absence and presence of serum (Figure 3.19A,B).

Interestingly glucose withdrawal led to different results for these markers. In fact glucose starvation inhibited MTORC1 as detected by p-S6 (as earlier demonstrated in figure 3.5). However, levels of ULK1 Ser^{757} were clearly not as strongly suppressed, both in the absence and presence of serum (Figure 3.19, A,B). Lastly, in further contrast, complete amino acid and glucose nutrient deprivation had a generally similar effect on MTORC1 as judged by p-S6. However, double starvation almost completely abolished phosphorylation of ULK1 Ser^{757}, particularly when serum was included in the starvation.

In addition, more insight was required into ULK1 regulation under these conditions so ULK1 Ser^{317} phosphorylation was examined. ULK1 Ser^{317} is a demonstrated AMPK phosphorylation site and it has been proposed that MTORC1-mediated

phosphorylation at ULK1 Ser^{757} disrupts this AMPK mechanism (Kim et al., 2011). ULK1 Ser^{317} was detected as two distinct bands that showed complex patterns in response to nutrient status suggesting multiple phosphorylation states of ULK1.

During amino acid starvation (without serum), 2-fold increases in both the hyper (upper) and hypo (lower) ULK1 Ser^{317} phosphorylated bands were observed (Figure 3.19A). Serum starvation tended to promote some forms of the hypo lower ULK1 band. With serum supplementation, the upper band of ULK1 Ser^{317} is elevated further to 2.92-fold compared to full media alone (Figure 3.19B). Glucose starvation also induced an up regulation in both bands of Ser^{317} phosphorylation. Also unexpectantly, complete starvation promoted ULK1 Ser^{317} phosphorylation.

Overall, these data highlight multiple sub-forms of AMPK-MTORC1-ULK1 signalling in response to varying levels of amino acids and glucose. Nutrient starvation generally led to suppression of MTORC1 when using p-S6 as the readout. However, this did not entirely match ULK1 Ser^{757} phosphorylation. ULK1 Ser^{317} phosphorylation also showed complex patterns following starvation, with general increases following all starvation methods, but not necessarily matching observations on the other ULK1 Ser^{555} AMPK site. More importantly, none of these ULK1 phosphorylations could explain why autophagy is strongly activated following amino acid starvation but blocked following double starvation. Also, the patterns observed on ULK1 Ser^{757} and ULK1 Ser^{317} do not fit the reported AMPK-MTORC1-ULK1 interplay mechanism (Kim et al., 2011).

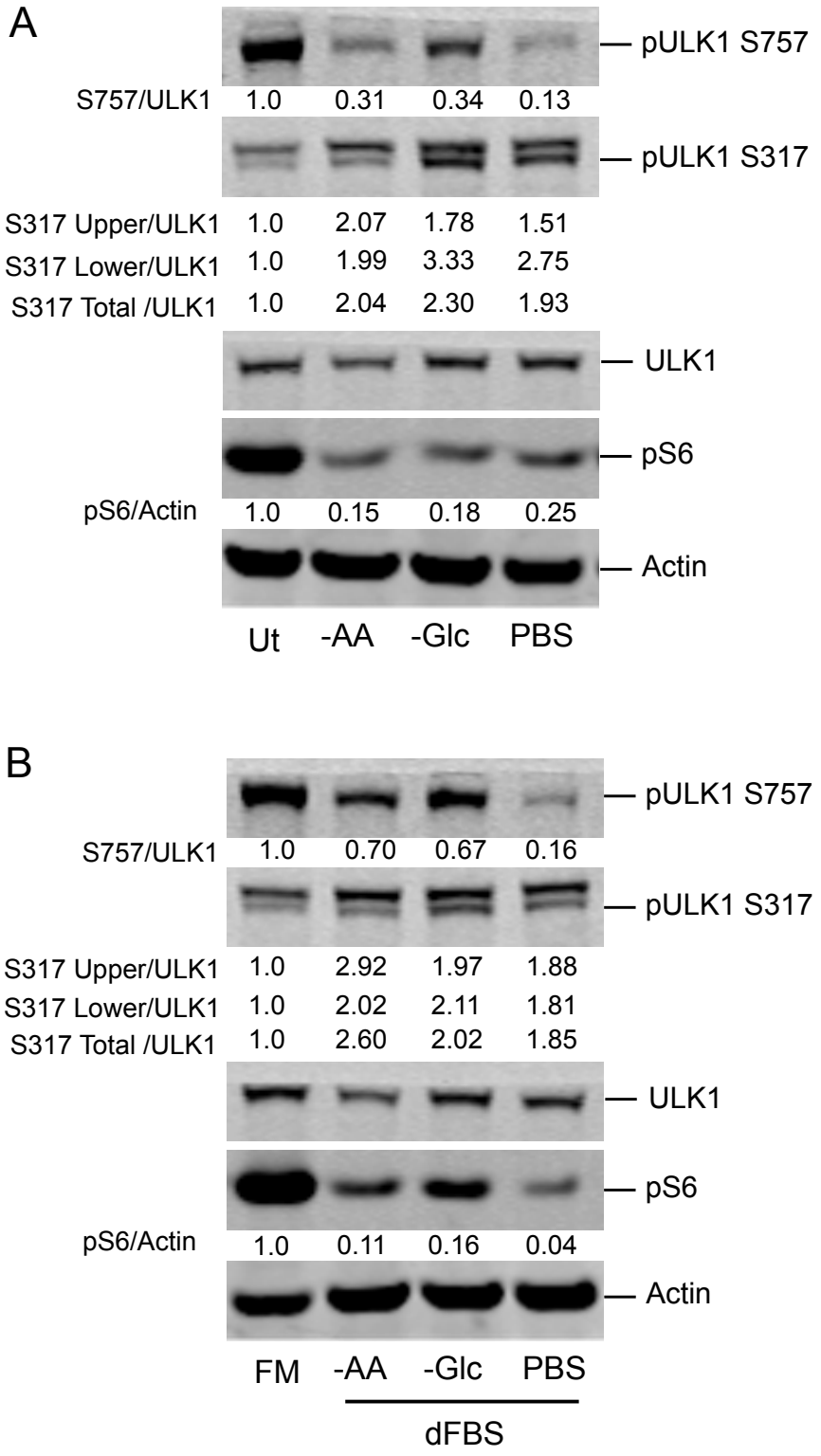

Figure 3.19: **The effect of nutrient starvation on the amino acid/MTORC1 signalling pathway.** HEK293A cells were treated with (A) EBSS, glucose free media or PBS (B) Full media, EBSS (10% dFBS), glucose free media (10% dFBS) or PBS (10% dFBS) for 2 hours. Cell lysates were resolved by SDS-PAGE and blotted for ULK1, pULK1 S757, pULK1 S317 and pS6. Quantified ratios of ULK1/actin, pULK1 S757/actin, pULK1 S317/actin and pS6/actin are shown. Data are representative of three seperate experiments.

3.18 Rescue of autophagy with reconstituted ULK1 containing specific MTOR or AMPK phosphorylation site mutations.

Having detected complex but nutrient sensitive patterns on ULK1 Ser^{317} and Ser^{757}, it was necessary to explore whether the functional contribution of these sites could be further dissected. For this, I aimed to rescue autophagic activity in the ULK1/2 DKO MEF using stable transduction of WT or ULK1 phosphorylation mutants ($ULK1^{S757A}$ (MTORC1) and $ULK1^{S317A/S777A}$ (double AMPK sites)) (Kim et al., 2011). Control immunoblotting showed that rescued ULK1 protein expression from the retroviral system to be relatively similar between WT ULK1, $ULK1^{S757}$ and $ULK1^{S317/S777}$ (in nutrient-rich full media) (Figure 3.20 panel A). It was also noted that following starvation of amino acids, reduced ULK1 protein expression was observed in all three generated lines (data not shown).

Examination of the effects of ULK1 reconstitution for autophagy in the ULK1/2 DKO MEF was then required. Similar to earlier (Figure 3.2), untreated ULK1/2 DKO MEF exhibited a basal level of LC3-II (and LC3 lipidation ratio) and that following amino acid starvation, lipidated LC3 ratios were further diminished (Figure 3.20B, C). Reconstitution of WT ULK1 into DKO MEF clearly rescued starvation induced autophagic activity. Surprisingly, rescue with the MTORC1 phosphorylation mutant $ULK1^{S757A}$ resulted in only marginal rescue of starvation-induced LC3 lipidation (Figure 3.20B, D). Unexpectedly, the double AMPK phosphorylation mutant $ULK1^{S317A/S777A}$ also displayed little rescue of induced autophagy. These together suggest that proper autophagy induced by nutrient depletion absolutely requires both sets of MTORC1 and AMPK phosphorylation sites of ULK1.

Corresponding analysis confirmed that AMPK and MTORC1 signalling were largely unaffected by the presence of ULK1 or mutations at the Ser^{317}, Ser^{757} and Ser^{777} sites. By assessing phosphorylation of ACC, amino acid starvation had no clear effect (unlike HEK) and there are no apparent differences between ULK DKO and reconstituted cell lines. In addition, MTORC1 activity was strongly inactivated following amino acid starvation, which was also consistent between DKO and all rescued cell lines. Therefore, from these data, it can be concluded that MTORC1 and AMPK nutrient sensing are not potently feedback regulated by the ULK1/2 complex.

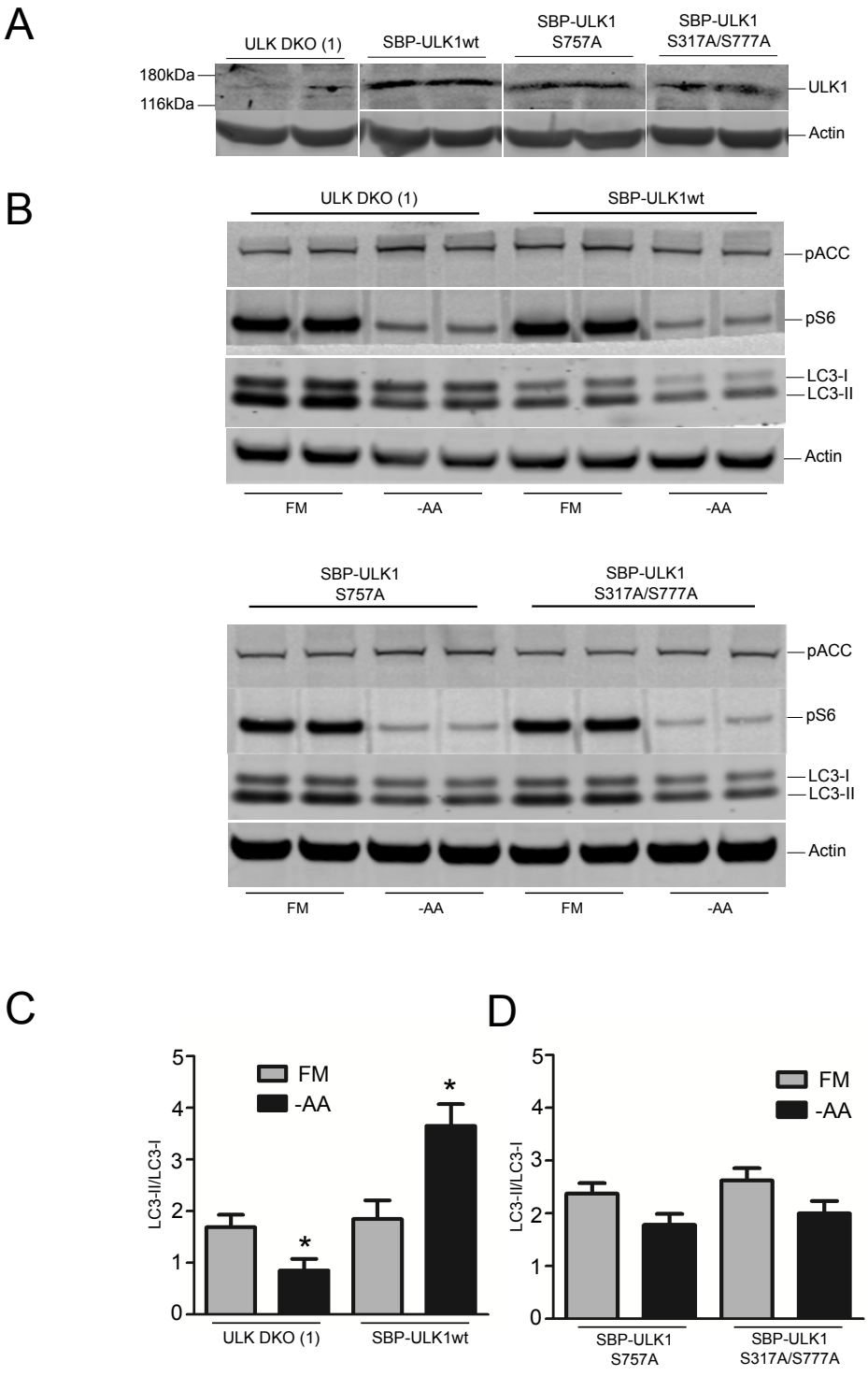

Figure 3.20: **The effect of ULK1 phosphorylation mutants in the rescue of autophagy in ULK1/2 DKO MEF**. MEF ULK DKO (1) and MEF ULK DKO (1) stably expressing pQCXIH CBP (calmodulin binding peptide)/ SBP (streptavidin binding peptide) tagged ULK1wt, ULK1^{S757A} or ULK1$^{S317A/S777A}$ were treated with full media (FM) or EBSS (-AA) for 2 hours. (A) Cell lysates were resolved by SDS PAGE and immunoblotted for expression of ULK1 protein. (B) Cell lysates were resolved by SDS PAGE and immunoblotted pACC, pS6 and LC3. (C-D) Quantified ratios of LC3-II/LC3-I are shown as mean ±S.E.M (n=4). 2 sample t tests were carried out relative to FM control of the same cell line (*p 0.05). Data are representative of two separate experiments.

3.19 Discussion

3.19.1 Regulation of nutrient sensitive autophagy by ULK1/2 in MEF

The ULK1/2 complex plays an important role in the initiation of autophagy and various studies have indicated a certain degree of ULK1/2 functional redundancy. During this thesis, a large portion of my work was aimed at clarifying the roles of ULK1/2 isoforms using a panel of ULK1$^{-/-}$, ULK2$^{-/-}$ and ULK1/2 DKO MEF cell lines. It was found that single ULK1$^{-/-}$ or ULK2$^{-/-}$ KO displayed a mild block in starvation induced LC3 lipidation supporting the concept of redundant roles for ULK1 and 2 during amino acid starvation. Consistent with this, ULK1/2 DKO very strongly blocked amino acid starvation induced LC3 lipidation. It was interesting that low levels of LC3-II were still detected in both basal and amino acid free conditions showing that LC3 lipidation can still occur independently of the ULK1/2 complex. This agrees with similar findings observed in FIP200$^{-/-}$ MEF displaying almost complete ablation of autophagic structures (Hara et al., 2008).

During the course of this study, Cheong and colleagues reported an independent ULK DKO MEF model which was characterised to have no effect on LC3 conversion following glucose starvation for 24h (Cheong et al., 2011). This ULK1/2 independent response suggested that glucose starvation may be part of non-canonical autophagy, which was an emerging concept in which formation of nascent autophagosomes proceeded without hierarchal intervention of all conventional Atg modules (Codogno et al., 2012). As such, the autophagic and AMPK energy sensing pathways in our DKO cell models were characterised. Interestingly, glucose withdrawal in the MEF lines produced a distinct type of LC3 autophagy response. Most notably, measurement in conjunction with lysosomal inhibitors showed that glucose starvation did not strongly

activate proper autophagic flux (unlike the amino acid starvation response). Also, the mild effects of glucose starvation were not blocked by ULK1/2 DKO, which was consistent with other reports (Cheong et al., 2011). It can be concluded from this data that ULK1/2 are clearly essential for amino acid induced autophagy but not for the atypical glucose starvation autophagy response. Glucose starvation and autophagy became a key focus of this chapter and this issue will be described in further detail in later sections below.

3.19.2 AMPK and mTOR activity in ULK DKO MEF

Since the ULK1/2 complex is situated directly downstream of the two major nutrient detectors, MTORC1 and AMPK, which are coupled to amino acid and glucose energy levels, it was imperative to investigate in parallel how KO of ULK1/2 might affect the MTORC1 and AMPK signalling circuitry. Following acute short term amino acid withdrawal, MTORC1 activity was greatly reduced in WT and ULK DKO cells. Therefore, loss of both ULK1 and 2 does not affect the shutdown of MTORC1 activity after amino acid withdrawal. Interestingly, during long term amino acid starvation, this loss of MTORC1 in ULK WT and DKO cell lines was not observed. This reactivation of MTORC1 after long term amino acid starvation likely reflects in our MEF system the described autophagic lysosomal reformation (ALR) pathway (Yu et al., 2010). ALR was identified as a cellular response to restore lysosome homeostasis through effectively reversing MTORC1 inactivation during prolonged starvation due to degradation of proteins and organelles within the lysosome and their subsequent recycling of nutrients back into the cytoplasm.

In terms of amino acid withdrawal, minimal AMPK activation was consistently observed in both WT and ULK DKO MEF. Therefore this confirms the dogma that

autophagy induction from amino acid starvation is sensed entirely through MTORC1. Following glucose starvation, it was generally noted that there were clear increases in ACC phosphorylation indicative of AMPK activation. Thus, glucose starvation quickly decreases cellular energy status (AMP:ATP ratio), which is directly detected by AMPK. ULK DKO MEF also showed proper activation of AMPK, confirming that the downstream ULK1/2 complex is not essential for AMPK activity.

In MEF, acute glucose withdrawal did not have any clear effects on MTORC1 activity (Figure 3.4B), indicating clear separation of AMPK and MTORC1 pathways. Conversely prolonged glucose withdrawal resulted in potent decreases on MTORC1 activity in both WT and ULK DKO MEF. This overnight effect agrees with existing studies showing that AMPK can inhibit MTORC1 activity during periods of low intracellular ATP (Inoki et al., 2003) (Gwinn et al., 2008), but here it can be confirmed that this is independent of ULK1/2. Also, this inhibitory effect from long term glucose starvation is consistent with a lack of autophagy induction and ALR, a predominant concept from my thesis.

3.19.3 MTOR and AMPK Feedback signalling in ULK DKO MEF

Although autophagy is a pro-survival mechanism helping cells to endure times of nutrient deprivation, prolonged autophagy could be detrimental and lead to cell death (Joo et al., 2011). Therefore various mechanisms are employed to maintain homeostasis and cells rely on various feedback loops to retain a fine control of signalling networks. Over recent years a number of feedback loops have been reported between AMPK, MTORC1 and ULK1. One study has proposed that ULK1/2 can induce multisite phosphorylation on the α_1, β_2 and γ_1 subunits of AMPK to negatively regulate its activity (Loffler et al., 2011). In addition, two independent groups have suggested a separate feedback mechanism involving the ULK1/2 complex

and MTORC1 (Dunlop et al., 2011) (Jung et al., 2011). Through overexpression, it was determined that ULK1 phosphorylated the MTORC1 raptor subunit and reduced substrate binding capabilities lead to inhibition of MTORC1 (Dunlop et al., 2011). Stable ULK1 knockdown by shRNA also increased MTORC1 substrate phosphorylation with a corresponding decreased phosphorylation of raptor thereby increasing cell proliferation (Jung et al., 2011).

It may have been necessary to explore feedback signalling in the ULK DKO MEF system, however, surprisingly these disturbances in feedback mechanisms were not observed. Small differences could be seen, for example, in elevated basal AMPK activity in ULK DKO, but overall, changes were minor compared to signalling patterns in response to nutrient sensing.

3.19.4 Glucose starvation fails to promote canonical autophagy activation in MEF

MTORC1-mediated autophagy regulation has been firmly established through studies of amino acid starvation and rapamycin treatment. In contrast to this, the role of glucose starvation in autophagy activation is less explored. However, a growing body of evidence indicates that glucose deprivation can activate autophagy (Gwinn et al., 2008) (Kim et al., 2011) (Shang et al., 2011) (Kim et al., 2013) and part of this is attributed to AMPK mediated phosphorylation and activation of ULK1. Some of the initial observations on the key differences between starvation methods came from our collaborator S. Tooze (Cancer Research UK, London) who detected a lack of PI3P generation and WIPI-2 puncta in MEF following glucose starvation (McAlpine et al., 2013). As mentioned above, LC3 turnover assays with Baf in MEF indicated little autophagy flux following glucose starvation as compared side-by-side with amino acid

starvation. Because this was surprising, to rule out a potential MEF-specific bias, it was necessary to conduct parallel experiments in HEK293A cells which have been a model cell type for nutrient dependent autophagy for over 10 years. Throughout that analysis, it was consistently found that no clear activation of autophagy induction or flux in glucose starved HEK293 cells was detected above the basal background. To ensure this was not due to missing a key window, further examination of the effect of glucose deprivation over a range of starvation times was conducted, but this confirmed no increases in autophagic flux.

These findings lead into a controversial area as a sizeable portion in the field proposed that glucose deprivation is a key activator of autophagy. However, in this controversy, this work did correlate with other published data and parallel findings. In one study, glucose deprivation was shown to block autophagic flux as compared with protease inhibitors pepstatin A and E64D in a number of cells including HeLa and Rh4 lines (Ramirez-Peinado et al., 2013). In case LC3 conversion measurement may be misreporting the status of the entire process, these observations were validated by investigating the p62 adaptor protein. Amino acid starvation could be seen to decrease p62 levels over short and prolonged starvation as expected to represent clear autophagy flux and degradation within the lysosome (Sahani et al., 2014). In contrast, glucose deprivation never produced any p62 loss over the same prolonged starvation period. Interestingly, an independent group found that glucose starvation actually led to accumulated (not decreased) levels of p62 protein in HeLa and Bax/Bak deficient MEF (Ramirez-Peinado et al., 2013).

Why does glucose starvation fail to activate autophagy? It can be consistently observed that glucose starvation was decreasing the cell energy status because it was

activating AMPK, demonstrated via phosphorylation of acetyl-CoA carboxylase (ACC). Since ULK1 is directly phosphorylated by AMPK at a multitude of sites including ULK1 Ser^{555} (Egan et al., 2011) (Mack et al., 2012) (Bach et al., 2011), it was considered whether this modification was involved in the observed effects. This work found that glucose starvation increased ULK1 Ser^{555} phosphorylation while in contrast, amino acid withdrawal reduced the phosphorylation status on this site. Interestingly, the Knecht research group published data contradictory with this observation. They observed that amino acids deprivation promoted ULK1 phosphorylation by AMPK at Ser^{555} and that this was dependent on a Ca^{2+}-CaMKK-β pathway in NIH3T3 cells (Ghislat et al., 2012). Therefore, the findings so far indicated that pULK Ser^{555} shows clear differential regulation correlating with the type of nutrient deprivation. Phosphorylation of this site was studied later in this chapter when double combined starvation conditions are revisited, although these data presented further unexpected patterns (see below).

3.19.5 Glucose withdrawal fails to induce expression of several late stage markers of autophagosome formation.

In light of the biochemistry data and the other insights derived from WIPI-2 membrane staining (McAlpine et al., 2013), the next section of my glucose starvation studies shifted to imaging approaches in HEK293. The first stage towards this utilised the tandem flag-LC3 construct which detected both new early autophagosomes (RFP+GFP) and autolysosomes (RFP) following starvation. Using this tool, it was confirmed that amino acid starvation stimulated the production of new autophagosomes and a resulting large population of total (maturing autolysosomes).

However, glucose starvation did not stimulate any strong response, agreeing with the body of immunoblot data. To further elucidate the membrane biology following glucose deprivation, and to avoid issues from ectopic protein expression, it was necessary to examine the recruitment of endogenous early and late stage autophagic markers. For example, clear induction of endogenous LC3 autophagosome puncta formation during amino acid starvation could be confirmed during glucose starvation. Also, during amino acid withdrawal, LC3 puncta were generally larger, and displayed greater intensity than observed with glucose withdrawal. In fact no, morphological differences in LC3 staining were apparent between basal and glucose deprived cells supporting the notion of zero autophagy response.

There was a greater complexity in quantification of the LC3 puncta, partly due to varying amounts of background staining that could not be resolved even though several commercial antibodies and staining protocols were attempted. A robust staining method turned out to be for the p62 (LC3-binding) autophagy cargo adaptor protein (Bjorkoy et al., 2005) (Itakura and Mizushima, 2011), which displayed even more pronounced differences between the two different starvations. Amino acid starvation clearly induced p62 punctate structures signifying increased incorporation of autophagic cargo into autophagosomes (Komatsu et al., 2007). It could be confirmed that there is a strong extent of co-localisation between p62 and LC3 puncta (using HEK293 stably expressing GFP-LC3). Importantly, the dramatic induction of p62 puncta was not observed with glucose deprivation, again internally consistent with the other data.

3.19.6 Glucose withdrawal fails to induce expression of several early stage markers of autophagy initiation/nucleation.

Having concluded that glucose withdrawal does not induce the recruitment of the late stage autophagy adaptor p62, attention was turned to upstream events more at the isolation membrane. Endogenous ULK1 puncta were examined building on other data showing recruitment of the ULK1/2 complex to initiation sites using tagged proteins (Chan et al., 2007) (Chan et al., 2009) (Ganley et al., 2009). An effective staining protocol was developed using a newly available commercial antibody for ULK1. Thereafter, it was noted that amino acid starvation induced ULK1 puncta formation within 15mins of starvation. This induction could be detected and confirmed in HeLa cells. However, glucose starvation could never be observed to induce ULK1 membrane recruitment, which along with LC3 and p62 staining data together indicate no autophagy induction. Near the end of this chapter, the role of nutrients with combined starvation protocols was further studied and surprisingly found that glucose starvation blocked the activating effects from amino acid starvation.

Time-course analysis indicated that ULK1 puncta could be detected earlier than the formation of p62 puncta (around 15min difference). A number of studies have established that it is critical for ULK1 to translocate to the isolation membrane (Ganley et al., 2009). At the membrane assembly site, ULK1 might provide a structural scaffolding role, which has been suggested initially from structural studies of Atg1 in yeast (Ragusa et al., 2012). ULK1 may drive steps forward by phosphorylating key substrates such as Beclin 1 (Russell et al., 2013) and influence localisation of the VPS34-Beclin 1 complex to the isolation membrane (Itakura and Mizushima, 2010).

ULK1 has been shown to phosphorylate AMBRA1 enhancing the activity of the VPS34 complex (Di Bartolomeo et al., 2010).

After establishing endogenous ULK1 puncta formation, the next aim was to further explore the behaviour of ULK1, so its localisation and morphology were examined through live-cell analysis. By monitoring GFP-ULK1 in HEK293 cells, it was found once again that following amino acid starvation, ULK1 puncta are rapidly induced and displayed a lifespan of around 160 seconds before dissipating. It must be noted that the lifespan of GFP-ULK1 puncta varied considerably with some visible for the entire analysis. These stable puncta might be an artefact from overexpressed GFP-ULK1. In numerous cells, ring shaped structures originating from ULK1 puncta were observed, which were interpreted to be larger, early fully-formed autophagosomes.

Since the ULK1/2 complex is proposed to phosphorylate, recruit and activate the VPS34-Beclin 1 complex, and clear ULK1 puncta were also detected, it was attempted to detect the next downstream step (i.e. generation of PI3P). Preliminary work using GFP-WIPI-1 constructs did not generate clear signals but GFP-tagged double FYVE containing protein 1 (DFCP-1) worked better in our cell systems. DFCP-1 is now widely accepted to bind PI3-P enriched membranes associated to the ER termed omegasomes (Axe et al., 2008). These omegasomes are now understood to form part of a cradle structure that physically encircles the autophagic membranes and donates lipid bilayer during elongation. Further ultrastructure details of the ER-omegasome-isolation membrane have been refined (Uemura et al., 2014). This work utilised an Atg3-deficient MEF system to capture incomplete autophagosomes consisting of omegasome and isolation membrane hybrid structures. In these structures, DFCP-1 localised to regions close to the edge of the isolation membrane on novel appearing

tubular structures. Overall, it was hypothesised that tubular membranes project from a subdomain of the ER to form the initial isolation membrane further fuse with each other for closure.

In fact, this work could indeed detect GFP-DFCP-1 puncta and ring-like membranes, particularly in amino acid starved MEF, which were experimentally more consistent in the same test than HEK293. GFP-DFCP-1 puncta were not detected following glucose starvation (data not shown) however it was not possible to clearly quantify this difference, which was attributed to the heterogeneous cell-by-cell response due to the overexpressed GFP- DFCP-1 (an issue resolved by quantitation of endogenously stained p62 and ULK1). It was initially attempted to co-localise ULK1 and DFCP-1 but this was unclear, most likely due to the small size and lower relative numbers of ULK1 puncta. However, co-localisation of GFP-DFCP-1 with p62 was readily detectable on adjacent or intermingled membrane compartments within the cytoplasm. Generally, p62 and DFCP-1 were not identically located but were found in close proximity and DFCP-1 could be seen physically encircling a p62 puncta, suggesting a compartment with PI3P patched membranes around the cargo adaptor protein. These observations are overall consistent with the current consensus model of PI3P dependent autophagosome formation, highlighting the specificity of the p62 puncta.

The class III Vps34 lipid product PI3P is universally regarded as a critical prerequisite during early stage autophagy membrane assembly. It was established early in the field that treatment of mammalian cells with the PI3K inhibitors 3-MA, wortmannin and LY294002 all inhibited autophagic activity (Blommaart et al., 1997). Moreover, addition of PI3P alone from external sources was sufficient to induce autophagy (Petiot et al., 2000). Despite this, our lab published data demonstrating that overnight

glucose starvation induced autophagy in MEF did not involve recruitment of the PI3P effector proteins WIPI-1 or WIPI-2 to forming autophagosomes (McAlpine et al., 2013). Glucose-dependent autophagy was also resistant to wortmannin consistent with a PI3P independent mechanism. At the time of hypothesis it was believed this may have simply been another case of non-canonical autophagy, as other Vps34 independent sources of PI3P have been reported elsewhere including direct synthesis by the class II PI3K (Devereaux et al., 2013). Another more recent proposed mechanism suggests non-canonical autophagy involving alternative lipids such as phosphatidylinositol 5-phosphate (PI5P) during glucose starvation (Vicinanza et al., 2015). This study showed evidence that PI5P could rescue autophagy even in cells treated with wortmannin or VPS34 silenced cells.

3.19.7 Glucose deprivation inhibits autophagy activation induced through amino acid starvation

Throughout this thesis it was found that glucose starvation could not strongly induce autophagy, based on studies of ULK1, p62 and LC3. However, further experiments indicated that glucose starvation can be detected to have an inhibitory effect on autophagy (as opposed to an activation of alternate non-canonical pathways). A series of experiments were carried out comparing single nutrient starvation versus double starvation of amino acid and glucose. In these comparisons, further glucose starvation blocked the ability of amino acid starvation to otherwise stimulate autophagy as detected by p62 puncta and LC3 lipidation. These unexpected findings raised some issues since AMPK activation has been proposed to drive ULK1 phosphorylation and autophagy (Egan et al., 2011, Kim et al., 2011); and so it was necessary to question whether differential patterns of AMPK vs MTORC1

phosphorylation of ULK1 could help interpret the effects of complete nutrient starvation. It can be confirmed that complete (double) starvation led to an activation of AMPK and strong phosphorylation of ACC. However, downstream phosphorylation of AMPK site ULK1 Ser^{555} was not activated and more similar to untreated cells. From this data, amino acid deprivation leads to decreases on the p-ULK1 Ser^{555} site. Despite these changes on ULK1 Ser^{555}, patterns did not fully explain the differences between amino acid vs. double starvation. The strong activation of the AMPK/ACC pathway under double starvation also indicates that the cells were not undergoing any severe metabolic crisis under and additionally cell death was never noted in these conditions.

Interestingly, complete starvation of glucose and amino acids almost entirely abolished MTORC1 phosphorylation of S6 ribosomal protein. Typically, inhibition of MTORC1 is potent to induce autophagy but this was not the case under double starvation. Double starvation also produced strongly inhibited phosphorylation of ULK1 Ser^{757}. However, during complete nutrient withdrawal this inhibition of phosphorylation was compounded and mTORC1 mediated ULK1 Ser^{757} phosphorylation was almost completely abrogated. As such, double starvation does not block autophagy by simply blocking ULK1 Ser^{757} hypo-phosphorylation.

In parallel, the other ULK1 phospho-state antibody that gave detectable signal was for the AMPK site pULK1 Ser^{317} (Kim et al., 2011). Unexpectedly, this phospho-antibody displayed two distinct bands but otherwise appeared specific since the bands were of expected mobility and changed with nutrient deprivation state. It was expected that these represent (at least) two different types of pULK1 Ser^{317} proteins with phosphorylation on other sites. The lower (fast mobility band) does become more apparent upon glucose and serum starvation, but no other correlation could be

seen, at least with AMPK, MTORC1 or autophagy. From these observations, it could be concluded that the Ser^{317} site is not entirely AMPK (glucose) specific and that the amino acid/MTORC1 pathway also regulates this phosphorylation. Time permitting, it would have desirable to analyse these phospho-bands further by mass spectrometry to identify the different ULK1 phosphorylation sub-forms. In summary, it has not yet been possible to define the specific ULK1 phosphorylation mechanism that drives autophagy upon amino acid starvation but with a blockade upon simultaneous amino acid and glucose withdrawal.

The controversial issue is how glucose starvation could have both positive effects on autophagy (as proposed in the literature) vs inhibitory effects (as observed in this work). It was found that glucose withdrawal does activate the AMPK starvation signals as well as downstream phosphorylation of ULK1, but with no autophagy. Therefore, activation of AMPK is not sufficient to induce autophagy alone. On this point, others have noted that transfection of a constitutively active form of AMPK did not alter the rate of autophagy (Meley et al., 2006).

The need for energy during autophagy may be playing a role. It has been shown that ATP is required for recruitment of cargo to the autophagosome (Plomp et al., 1987). Glucose-derived energy may be required for functional trafficking of membrane and autophagic vesicles. One study in yeast identified that glucose starvation reduced recycling from endosomes (Lang et al., 2014). Along this argument, several other studies show that glucose has a positive role on autophagy. The presence of glucose can induce LC3 lipidation as well as the number and volume of autophagic vesicles and protein degradation (Moruno-Manchon et al., 2013). Surprisingly, this mechanism was independent of AMPK and MTOR but relied on p38 MAPK. High

glucose has also been shown to reduce aggregation and increased the clearance of mutant huntingtin by promoting autophagy (Ravikumar et al., 2003).

Without glucose, lysosome function (and therefore autophagy flux) are thought to be suppressed. In mammalian and yeast cells, glucose is known to be a potent physiological regulator of the vaculolar H^+ ATPase (V-ATPase) proton pump (Sautin et al., 2005). Glucose therefore is recognised to be important for the acidification of intracellular compartments by inducing H^+ ATPase assembly and trafficking to the lysosome in a mechanism mediated by the class I PI3K signalling pathway (Sautin et al., 2005).

It is thus a challenge to reconcile these data with other evidence showing activation of autophagy following glucose nutrient starvation (Egan et al., 2011, Kim et al., 2011) (Cheong et al., 2011). Other groups have described ULK independent effects in which loss of ULK1/2 displayed no effects on LC3 conversion following glucose starvation (Cheong et al., 2011, Gammoh et al., 2013).

Multiple studies examined glucose deprivation but with long term (over 12h) starvation. With long term starvation, there is thus the potential of indirect activation of other signalling pathways via secondary signalling events and additional gene transcriptional mechanisms, further compounding the complexity of this response. One study identified that the mechanism behind 2-deoxyglucose activated autophagy was due to ER stress rather than ATP depletion (Xi et al., 2011).

3.19.8 The contribution of MTOR and AMPK signalling pathways to nutrient-sensitive autophagy.

As shown at several places within the chapter, the phosphorylation of several reported MTORC1 and AMPK phosphorylation sites of ULK1 varied robustly in response to different nutrient starvation conditions. One study found that AMPK promotes autophagy by phosphorylating ULK1 sites Ser^{317} and Ser^{777} (Kim et al., 2011). In this experimental system, MTORC1 phosphorylates Ser^{757} preventing binding between AMPK and ULK1 and autophagy function. Although phosphorylation patterns of ULK1 sites Ser^{317} and Ser^{757} rapidly responded in our hands, it was still unclear how their modifications correlated with autophagy in HEK293 cells. As an alternative approach to study functions of these sites, ULK1/2 DKO MEF were reconstituted with ULK1 mutants deficient in the MTORC1 Ser^{757} or in the AMPK sites Ser^{317} and Ser^{777}. It was expected that the ULK1 Ser^{757}Ala mutant might display constitutive or hyperactivity, since it could not be repressed by MTORC1. In contrast, it was expected that the ULK1 $Ser^{317/777}$Ala mutant would be inactive. In this way, it was possible to rescue amino acid starvation inducible autophagic activity in ULK1/2 DKO MEF with viral transduction of WT ULK1 demonstrating that levels of exogenous ULK1 alone were sufficient to reconstitute functional ULK1 complex. In contrast, transduction with the MTORC1 phosphorylation mutant $ULK1^{S757A}$ did not rescue autophagy. Similarly, the AMPK site double ULK1 phosphorylation mutant also failed to rescue the starvation response for LC3 lipidation. Therefore, all the data from these rescue experiments suggests that phosphorylation of ULK1 by both MTORC1 and AMPK is essential for a fully functional autophagic response, even though these signalling pathways have proposed opposite negative and positive (respectfully) regulatory roles for ULK1. As such, it has not been possible to replicate the basic

interplay mechanism proposed for the AMPK-MTORC1-ULK1 triad (Kim et al., 2011). The overall implication is that the regulation of ULK1 may be more complex than anticipated, especially in light of the wider range of phosphorylation and other post-translational modifications so far identified for this autophagy kinase (summarised in (Alers et al., 2012) (Wong et al., 2013)). Although speculation, AMPK and MTORC1 phosphorylation of ULK1 may each play distinct but equally critical roles for the dynamic regulation required for proper overall ULK1 function during autophagic induction.

In summary, the work in this chapter has led to several conclusions. These findings support functional redundancy between ULK1 and ULK2 for nutrient-dependent activation of autophagy. My data indicates that glucose starvation does not induce the autophagic machinery during canonical autophagy. Moreover, glucose starvation fails to promote autophagic flux, which is a key indicator of proper full autophagy activation and progression. Therefore, glucose withdrawal cannot be taken to be a predominant activating stimulus for autophagy in mammalian cells. Overall, this highlights the differential autophagy responses that arise following amino acid vs. glucose deprivation.

Chapter 4: Role of the ULK1 EAT Domain for Autophagic Membrane Formation

4.0 Introduction

The ULK1 complex is widely regarded as one of the earliest autophagy related components to associate with the ER driving the initiation of autophagic membrane formation. For example, the hierarchal analysis of autophagy related proteins showed that the complex containing ULK1 and FIP200 functionally precedes and is required for class III PI3K complex associated Atg14 puncta formation (Itakura and Mizushima, 2010).

As summarised in the preceding chapters, the ULK1/2 complex consists of ULK1 (or ULK2), mammalian Atg13, FIP200 and Atg101 (Ganley et al., 2009) (Mercer et al., 2009) (Hosokawa et al., 2009a) (Hara et al., 2008). Overall, the ULK1 complex is modelled to integrate signals from the master nutrient sensors MTORC1 and AMPK by serving as substrate for these kinase complexes, and to then transmit information to downstream autophagic machinery. In nutrient rich conditions, MTORC1 directly associates with the ULK1 complex via the raptor subunit (Hosokawa et al., 2009a). Associated MTORC1 then mediates phosphorylation of Atg13 (Ser^{258}) and ULK1 at the Ser^{757} site leading to a potent inhibition of ULK1 kinase activity (Ganley et al., 2009) (Kim et al., 2011) (Puente et al., 2016). In contrast, during amino acid starvation, MTORC1 dissociates from ULK1/2 leading to autophosphorylation, possibly at the Thr^{180} position in the ULK kinase activation loop (Bach et al., 2011). Subsequently ULK1 can phosphorylate Atg13 on multiple sites including Ser^{318} and potentially on FIP200 (at sites not completely understood) (Joo et al., 2011) (Jung et al., 2009). To date, over 30 phosphorylation sites have been identified on ULK1, including the sites

modified by MTORC1 and AMPK, indicating that ULK1 may receive multiple signal inputs for several different autophagy-specific or non-autophagy functions. Despite this concept, detailed roles for the majority of ULK1 phosphorylation have not yet been fully elucidated.

In yeast, the Atg1 complex (ortholog of ULK1) has been shown to have kinase independent roles during the induction of autophagy (Abeliovich., 2003). More recently, ULK1 has been proposed to provide a homologous conserved structural scaffolding role, based largely on structural studies of yeast Atg1 (Ragusa et al., 2012). These studies provided novel insight into the lipid binding activity of the yeast Atg1 complex. Utilising a multidisciplinary approach, these authors observed that the Atg1 C-terminal domain (CTD) could strongly interact with Folch liposomes, representing the various synthetic lipid compartments within the cell, including the ER, Golgi apparatus and the plasma membrane. Utilising liposomal sedimentation assays, it was observed that the Atg1 CTD displayed a strong affinity for small vesicles with a high curvature. In addition, the authors established that the Atg1 complex domain could potentiate the tethering of liposomes leading to increases in their effective diameter, hence renaming this region as the early autophagy targeting/tethering (EAT) domain. The tethering of small highly curved vesicles is a highly significant finding since the mammalian autophagosome has been demonstrated to be nucleated by vesicles of around 15-30nm radii and that contain Atg9 (Ge et al., 2014). Therefore, the mammalian EAT domain potentially could be playing a similar direct membrane remodelling roles for IM formation.

Since these interesting primary observations, multiple studies have examined further the dynamics of the Atg1 EAT domain as well as its solution structure in complex with

regions of binding partner Atg13 (Stjepanovic et al., 2014)(Fujioka et al., 2014)(Kofinger et al., 2015). The recent elucidation of the crystal structure of Atg1 EAT-Atg13 minimal binding complex has led to massive inroads into the understanding of the Atg1 complex (Fujioka et al., 2014). The EAT domain showed high structural similarity with a microtubule interacting and transport (MIT) domain that was identified in Vta1 (Hurley and Yang., 2008). Two MIT domains can further form a tandem arrangement for protein-protein interactions. The yeast EAT crystal structure indeed showed tandem MIT domains, each consisting of an asymmetric three helix bundle (MIT1 designated to contain α1-α3 and MIT2 containing α4-α6) (Fujioka et al., 2014). As a complementary method, an independent group examined the solvent accessibility of the EAT domain (Stjepanovic et al., 2014). These authors showed using hydrogen-deuterium exchange coupled to mass spectrometry (HDX-MS) that the MIT1 region was highly rigid, which was consistent with findings that this region was a Atg1 dimerisation or Atg13 interaction interface (Fujioka et al., 2014). On the other hand, MIT2 is much more highly dynamic and is significantly flexible (Stjepanovic et al., 2014), suggesting that this MIT fold may be able to alternate between two conformational states.

Interestingly, these structural models link back to previous functional findings from our laboratory. It had been determined that the mammalian ULK1 EAT domain was required for the localisation of the protein to GFP-LC3 positive structures (Chan et al., 2007). Deletion of the EAT domain completely abolished ULK1 membrane localisation. The ULK1 EAT domain alone could also be detected in cell membrane fractions (Chan et al., 2009). Therefore, the mammalian C-terminal EAT domain controls ULK1 regulatory function and is essential for its membrane binding and

correct localisation to the site of IM formation. Overall, the emerging structural data further stimulated our interest in understanding how this relatively small domain was directing several critical interactions with lipids and proteins. Therefore, the primary objectives of this chapter were to:

1) Analyse the protein sequence of the ULK1 EAT domain using various bioinformatical approaches to gain a further and more comprehensive understanding of previously reported roles of EAT domain during autophagy.
2) Study the role of the mammalian ULK1 EAT domain in membrane binding. By generating various ULK1 EAT domain truncation mutations, I analysed the ULK1 EAT domain interaction with membranes as well as complex partner Atg13.
3) Characterise the interaction between the ULK1 EAT domain and ER lipid raft associated-2 (Erlin-2), which we recently identified as a novel binding partner.

4.1 Bioinformatic analysis of the ULK1 EAT domain structure.

Knowledge of the native 3-D structure of a protein provides valuable insight into the precise biochemical mechanisms of its function. However, the revolutionary genomics era has led to a huge gap between proteins with experimentally determined structures and proteins without known structures. To cope with this overwhelming data gap, bioinformatic tools have emerged and are continually being refined to help determine the biophysical characteristics of a protein just from its amino acid sequence. Bioinformatics integrates two separate disciplines; biological with computational sciences. In this manner, protein bioinformatics can be used to determine the hydrophobicity of any sub-regions and furthermore advance toward predicting 3D structure.

One of the main aims of this thesis was to investigate the role of the mammalian ULK1 EAT domain during autophagy initiation and to ULK1 membrane binding. Therefore, one of the initial objectives was to analyse the ULK1 primary protein sequence using the protein Pfam database and conserved domain database (CDD) server. These databases robustly identified the three distinct regions known for ULK1 namely the: serine/threonine protein kinase domain, proline/serine rich domain and the EAT domain (Yan, 2008). Within these databases, the EAT was classified as a domain of unknown function 3543 (DUF3543) and this family has several characteristics including: being in all eukaryotes; typically between 217-291 amino acids in length; and found associated with a protein kinase domain. It was evident from these databases that the ULK1 EAT domain was rather poorly defined and not homologous to any wider protein families.

4.1.1 ULK1 EAT domain hydrophobicity.

To gain insight into specific domains of EAT that may mediate interactions with autophagy membranes, it was necessary to analyse the degree of hydrophobicity within stretches of the amino acid residues. To date, there have been many hydrophobicity scales published including methods by (Kyte and Doolittle, 1982) (Hopp and Woods, 1983) (Wimley and White, 1996). Each of these computational techniques are fundamentally similar with only slight variations between them. The most widely used method is the Kyte-Doolittle plot which involves delineating the hydrophobic propensity of given sized primary sequence windows. Within the Kyte-Doolittle method, each amino acid is assigned a specific hydrophobicity score ranging from -4.6 to 4.6 (positive being the most hydrophobic in solution). With a user defined window size (total number of amino acids being scored), the average hydropathy index is calculated for the segment, and then repeated for the next window segment shifted one residue down the primary sequence (Kyte and Doolittle, 1982)(Kyte and Doolittle., 1983).

Window sizes of 7-11 are recommended for identifying hydrophilic regions with strong negative peaks representing regions that are likely found on the surface of globular proteins in contact with solvent or water. Conversely a window size of 19-21 is more ideal for identifying membrane spanning or strongly hydrophobic larger regions. The mouse ULK1 EAT domain (residues 829-1051) was examined using window size 9 (Figure 4.1) to identify any hydrophilic surface regions and window size 19 to examine larger regions (data not shown). The hydropathy plot (window size 19) demonstrated that the EAT domain lacked any distinct peaks crossing the >1.6 threshold and any stretches of 20 hydrophobic amino acid residues. Therefore, this

confirms that the ULK1 EAT domain has zero propensity to traverse the phospholipid bilayer.

The ULK1 EAT domain analysed under window size of 9 showed multiple hydrophilic regions with several strongly negative peaks at window positions 13, 49, 67, 113, 170 and 193 (Figure 4.1). Conversely, there are several positive hydrophobic regions leading to the appearance of periodical cycling between hydrophobic and hydrophilic regions/peaks consistent with the idea of helical structures buried on one side and exposed on the other. This characterisation of regions within the EAT with different biochemical properties helped the design of later deletion mapping studies in this chapter.

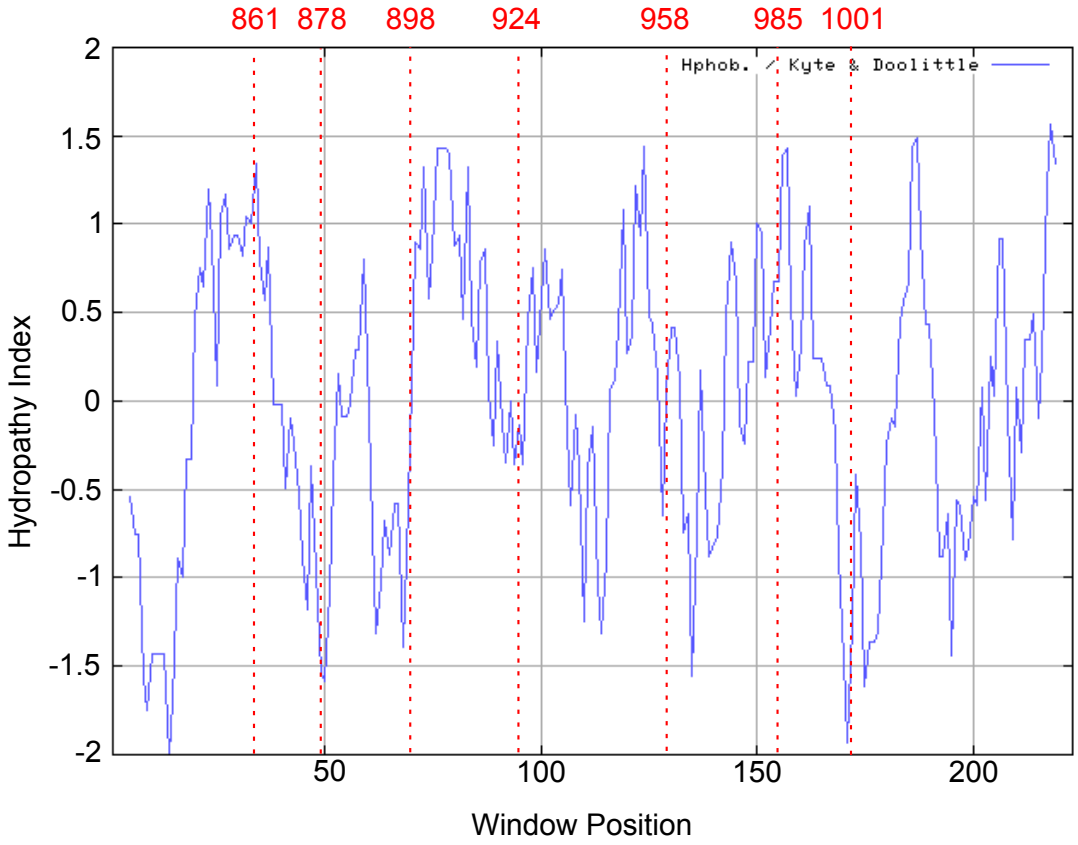

Figure 4.1: **Hydropathy plot of the mouse ULK1 EAT domain**. This plot illustrates the hydrophobic regions of the ULK1 EAT domain using the scale of Kyte and Doolittle. X-axis values represent the number of amino acid within the domain sequence analysed. Red dashed lines and numbers represent the stop codon insertion sites for truncation mutants. The Y-axis value signifies hydrophobic regions. Data generated by ExPASy ProtScale. Window size = 9 (Kyte and Doolittle.,1982).

4.1.2 Prediction of the relative solvent accessibility of the ULK1 EAT domain

In order to complement the hydrophobicity predictions, it was then necessary to assess the relative solvent accessibility (RSA), which reflects the degree to which each residue interacts with a solvent molecule. The initial concept of solvent accessibility was first introduced by Lee and Richards and has since become an important quantitative measurement to gain information on the 3D fold of a protein (Lee and Richards, 1971). Protein-protein (or protein-ligand) interactions occur on the protein surface and therefore, only residues that reside on the exposed surface area can directly interact in this fashion. In conjunction with accessibility factors, alpha-helical structure propensity was also predicted by the Psi-Pred algorithm. The ULK1 EAT domain thus predicted to contain six distinct helical regions connected by coil regions (Figure 4.2). These helical structures overall strongly correlated with predictions for having residues buried from the solvent, as observed in both the two-state and three state classifications of solvent accessibility.

In addition, the first three α-helical structures (α1-α3) (up to residue 132 from the N-terminal end) are ~30 amino acid residues in length, which classifies these regions as long α-helices. This is interesting as generally long α-helices (>25 residues) in globular proteins are not commonly found (O'Shea et al., 1991, Lovejoy et al., 1993). Long α-helices can be associated with the formation of super-secondary structures such as coiled-coils and helix bundles (Kumar and Bansal, 1996). In summary, this analysis of the EAT domain sequence identifies several key hydrophobic regions of helical secondary structure.

4.1.3 Predicted three-dimensional structures of ULK1 and ULK1 EAT domains.

Having documented potential secondary structures of the EAT domain, it was necessary to understand the 3D fold of this region. In order to do so the potential of computational protein structure prediction programmes for ULK1 full length and EAT domain were explored. In general, there are two main methods for generating 3D structural prediction: *ab-initio/de novo* which predicts the structure without relying on knowledge of any similar structures; and threading/comparative modelling which bases its prediction on similar sequences of known structure. Here, the comparative modelling tool Iterative Threading ASSEmbly Refinement (I-TASSER) was utilised (Yang et al., 2015). This method generates five full length atomic models which are ranked in order of their confidence C-score values and cluster density.

Firstly, it was necessary to attempt to generate a predicted structure for full-length ULK1 (Figure 4.3A). This model showed an overall C-score value of -2.50 which signifies a relatively poor reliability of the given predicted model. For example, values below -1.5 are generally considered to be low confidence (Roy et al., 2010). The kinase domain could be predicted with strong accuracy ratings. It is apparent that the adjoining S/P spacer domain (residues 278-829) prediction is very unreliable with the estimated predicted accuracy >10Å for significant sections. This suggests this domain has a bias towards flexibility, which correlates with a previous report suggesting this is an intrinsically disordered domain (Mei et al., 2014). Nevertheless, many portions of the EAT domain showed better accuracy scores. This small region was predicted to span a large area intermingled with the spacer domain. Unexpectedly, the EAT domain was not predicted to form extensive contacts with the kinase domain. It remains to be seen if this predicted structure resembles the native structure obtained

by X-ray crystallography (Fujioka et al., 2014) or cryo-electron microscopy (Rao et al., 2016).

Recently, the crystal structure of the Atg1 EAT domain, in complex with a fragment of Atg13, has been elucidated using proteins from the yeast *K. marxianus* (Fujioka et al., 2014) (Figure 4.4A). Based on this structure, predicted structures were obtained from the homologous Atg1 EAT sequences of yeast *S. cerevisiae*, *D. melanogaster,* as well as the ULK1 EAT domain from *M. musculus* using I-TASSER (Figure 4.4B-D). The predicted EAT domain structure from the *S. cerevisiae* showed high degree of α-helical protein structure, essentially mirroring the yeast *K. marxianus* structure, which was used in the threading algorithm (Fujioka et al., 2014). The α-helical model features two asymmetric three helix bundles, and although this is readily apparent in the *S. cerevisiae* EAT, the confidence score was unexpectedly low. This same helical arrangement was predicted from both the *D. melanogaster* and *M. musculus* EAT sequences, but with greater confidence ratings. The α-helices 1 and 2 are joined by a short spacer region with low prediction score, suggesting flexibility or disorder. The α-helices were predicted to be hydrophobic and buried from our other sequence analyses. As noted in the *K marxianus* structure co-crystal, multiple surfaces of the helical bundles form contacts with helical regions of Atg13.

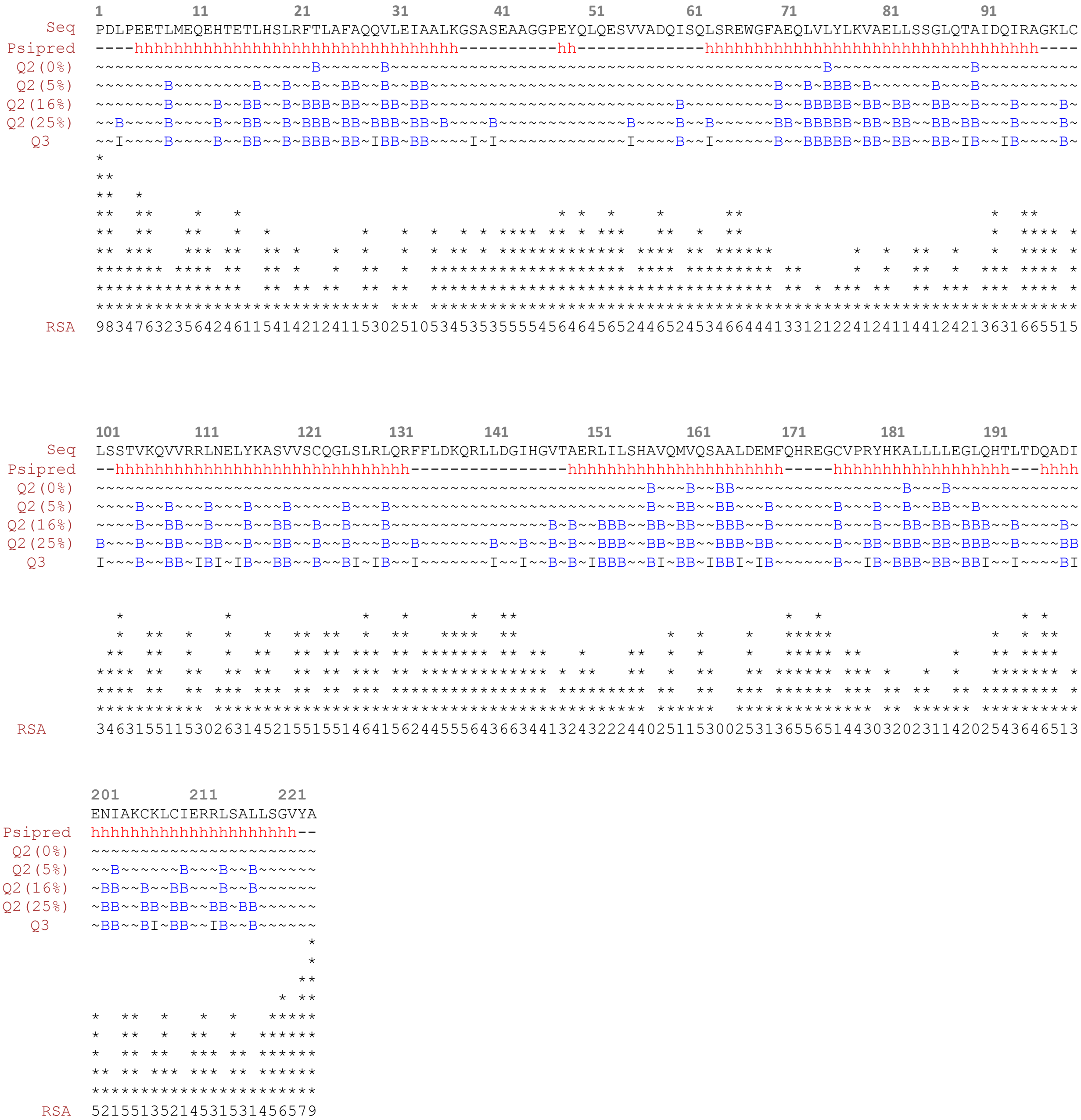

Figure 4.2 **Solvent accessibility prediction of ULK1 EAT domain**. Plot created using the solvent accessibility prediction of proteins by nearest neighbour (SANN) method (Joo et al., 2012). The predicted secondary structure elements are also shown: (-) coiled regions and (h) helical (generated using PSI-PRED) (Jones et al., 1999) (Buchan et al., 2013). The SANN prediction is displayed as two-state classification (Q2) ((~): exposed, (B): buried); or alternatively as three-state classification (Q3) ((~):exposed, (I): intermediate and (B): buried) of solvent accessibility from DSSP (Kabsch and Sander., 1983). The Q2 was carried out at four thresholds (0, 5, 16 and 25%). The predicted relative solvent accessibility (RSA) is also shown (range 0-9).

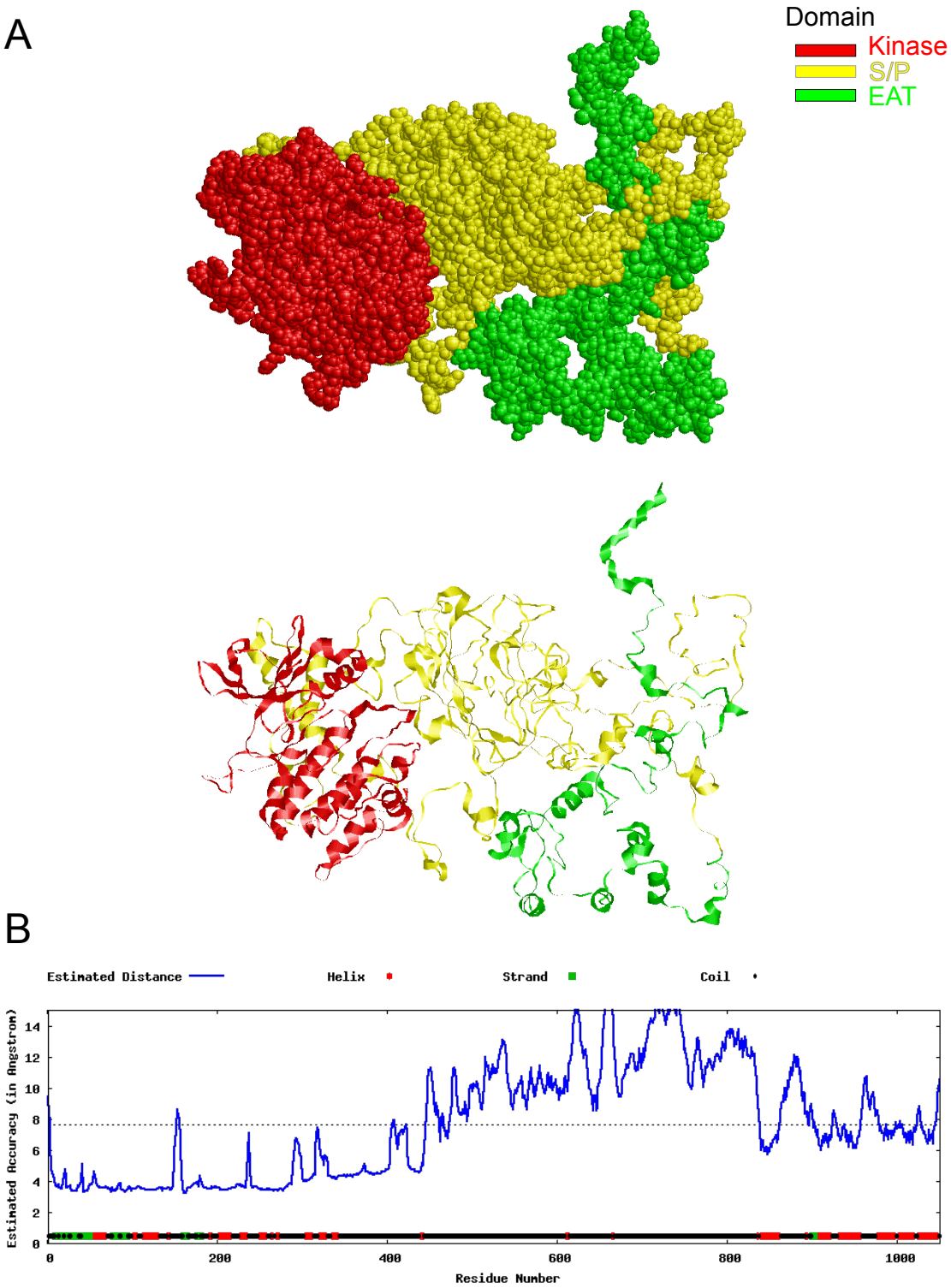

Figure 4.3: **Predicted structure of full length ULK1 using Iterative Threading ASSEmbly Refinement (I-TASSER)**. The 3D predicted structure of Mus musculus ULK1 (NP_033495.2) was generated using I-TASSER prediction (Yang et al., 2015). The top predicted model with the highest confidence score (C-Score) was utilised for further analysis. (A) Raw data from I-TASSER is shown in Spacefill (top) and Ribbon (bottom) format. The kinase domain (Residues: 1-278) shown as red; P/S spacer domain (279-828) yellow; and EAT domain (829-1051) green. (B) Distance error estimations along ULK1 generated by I-TASSER (Angstroms). Secondary structure highlighted in red (α-helices) and green (β-strands).

A

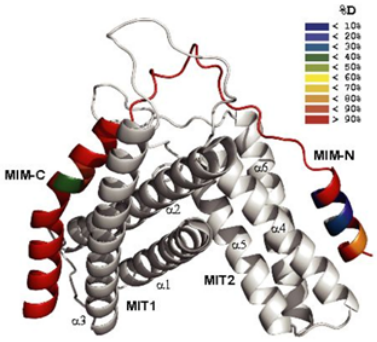

B

Saccharomyces cerevisiae

C-Score = -2.16

C

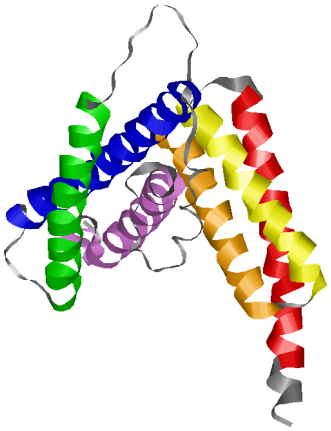

Drosophila melanogaster

C-Score = 0.09

D

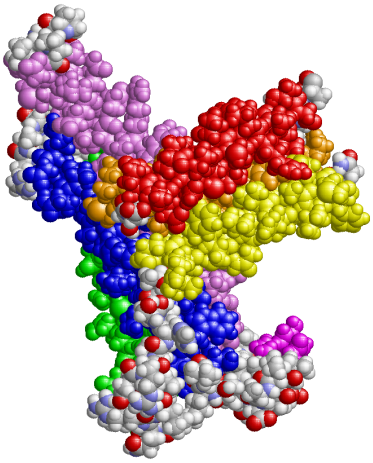

Mus musculus

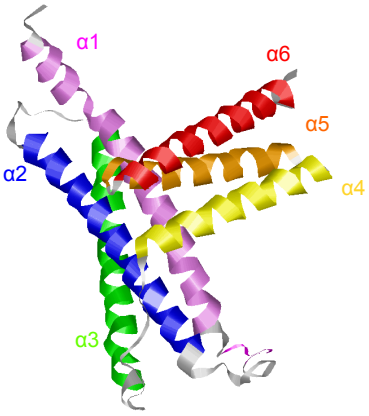

C-Score = 0.08

E

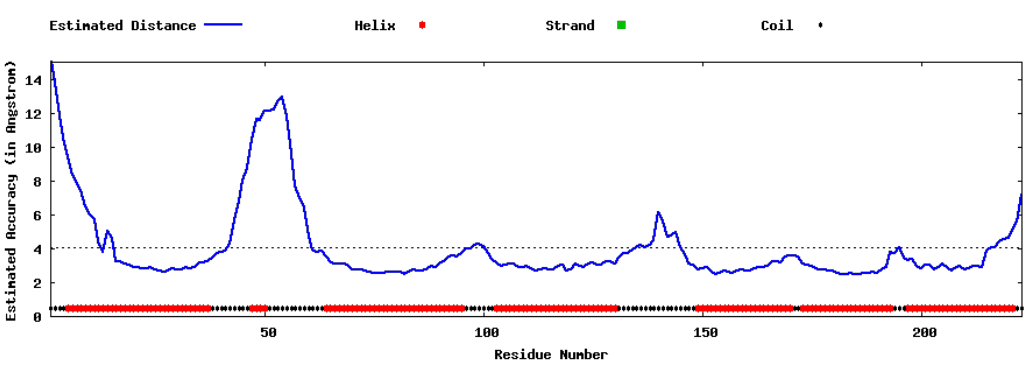

Figure 4.4: **Predicted structures of Atg1/ULK1 EAT domains from various species**. The 3D predicted structures of S. cerevisiae Atg1 EAT (KZV11049.1), D. melanogaster Atg1 (isoform B) EAT domain (NP_001163433.1) and M. musculus ULK1 EAT domain (NP_033495.2) were generated using the I-TASSER as in Figure 4.3. (A) Empirically determined crystal structure of K.marxianus Atg1EAT interacting with minimal Atg13 binding (MIM-C and MIM-N)(PDB ID: 4P1N) was used as one of the threading templates (panel extracted from Stjepanovic et al., 2014). (B-D) Data from I-TASSER was shown as Ribbon models of the Atg1/ULK1 EAT protein with α-helices (α1-α6) shown for the indicate species (multiple views as shown). Predicted confidence scores (C-Score) are displayed below each structure. (E) Residue level distance error estimations of mouse ULK1 EAT domain generated by I-TASSER (in Angstroms). Secondary structure in the model also highlighted in red (α-helices).

4.1.4 Phylogenetic analysis of ATG1/ULK1 sequences

Having observed highly consistent and conserved predicted 3D structures of the EAT domains from different species, it was necessary to confirm degrees of similarity in the primary sequences. To understand evolutionary relationships of the mammalian ULK1 EAT domain, the basic local alignment search tool (BLAST) was utilised, which is based on the Needleman-Wunsch algorithm for global sequence alignment (Figure 4.5) (Needleman and Wunsch, 1970). This tool quantified overall percentage identity between the human ULK1 protein with other vertebrate ULK1 homologs and more distant evolutionary organisms including Unc-51 (*C.elegans*) and yeast Atg1 (*K.lactis*). It was noted that the vertebrate ULK1 homologs from *M. musculus, G. gallus* and *D. rerio* displayed excellent overall global alignment and sequence conservation across the entire length of the sequence (with aid of only minor gaps to align the entire domain). Surprisingly, the homology between ULK1 homologs was closer than homology to related gene family member ULK2 (even when comparing within the *M. musculus* species). By comparison, orthologs of ULK1 from lower organisms (eg. Unc-51 of *C. elegans* and Atg1 from *K. lactis)* displayed looser homology and only sub-regions of local alignment.

Upon closer analysis of each domain, it was seen that the ULK1 kinase domain is the most highly conserved, as anticipated. The highly disordered S/T rich internal spacer domain shows more diversity through evolution (and with ULK2) suggesting that specific residues or patches of sequences may play lesser essential role. However, for the interest of this chapter, the ULK1 EAT domain was relatively well conserved within vertebrates with the protein sequences of *M. musculus* sharing 90% overall protein sequence identity and *G. gallus* 75% identity in comparison to the *H. sapiens*

sequence. As expected, as you migrate further away in the phylogenetic tree sequence conservation is lost in the EAT and in yeast, there is virtually no sequence identity, despite maintaining a conserved regulatory function within the Atg1/Atg13 complex.

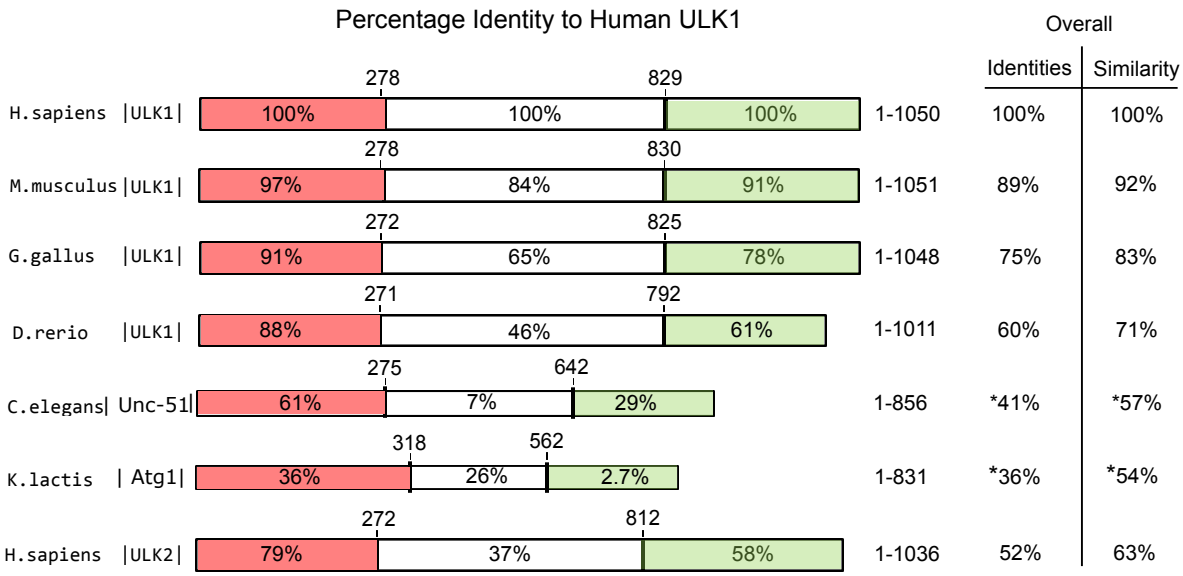

Figure 4.5: **Schematic depicting the overall sequence identity of the human ULK1 with homologous proteins**. All organisms displayed 3 distinct domain regions; Kinase (red), S/T (white) and EAT (green) domains which vary in length. The mammalian homologs of ULK1 (M.Musculus and G.Gallus) as well as the zebrafish (D.Rerio) ULK1 all displayed a relatively high sequence conservation in the kinase domain but overall lower homology in their EAT domains. The yeast Atg1 (K. Lactis) and Unc-51 (C.elegans) only displayed partial sequence alignment (represented by *) and overall identity was calculated on this region only. Overall percentage identity and similarity to the human ULK1 were generated using the protein Basic Local Alignment Search Tool (BLASTp).

4.1.5 Alignment of the ULK1 EAT domain

To select regions for truncation mutation, it was necessary to generate a multiple sequence alignment (MSA) of the mammalian ULK1 EAT domain, which highlights residues of functional importance through the visualisation of regions of strong conservation. Clustal Omega was used to create a MSA (Sievers et al., 2011) for a range of diverse species relative to human ULK1. One MSA shows *H. sapiens* ULK1 EAT domain against *M. musculus, G. gallus* and *D. rerio* (Figure 4.6). The *H. sapiens* ULK2 EAT domain was also included. All these species displayed high sequence conservation across the entire EAT domain. Different regions of completely identical, conserved and also semi-conserved regions could be identified. In addition, the predicted 6 α-helical structures are also shown. Interestingly, regions with complete sequence identity also appear to generally correspond with different regions of α-helical secondary structure. For example, the start of α-helix #1 started with –PEET- in all EAT domains analysed. The 4^{th} and 5^{th} α-helices also show strong levels of identity. This analysis gives further rationale for our deletion analysis.

4.2 Full length ULK1 and EAT truncation mutant design and expression levels.

Various truncation mutants were then designed to delete sub-regions of the ULK1 EAT domain. The aim was to dissect roles of hydrophobic/hydrophilic regions and secondary α-helical structures. In total, eight full length Myc-tagged mouse ULK1 EAT mutants were utilised within this thesis ending in residues: ULK1-1001, 985, 958, 924, 898, 878, 861 and ΔEAT as described in methods (Figure 4.7A). ULK1-1001 and ULK1 ΔEAT plasmids were previously generated from our laboratory (Chan et al., 2009). An initial control experiment was carried out in HEK-293 GFP-LC3 cells to examine

expression of each mutant (Figure 4.7B). It could be observed that all mutants were expressed evenly and comparable to overexpressed WT ULK1 suggesting that all constructs are stable within this mammalian cell system. Also, the deletion constructs showed expected mobilities.

In this same test, the mutations were examined for overt effects on LC3 lipidation during amino acid withdrawal (Figure 4.7B). Previous results from our group have shown that ULK1 overexpression can have a dominant inhibitory effect on autophagy that was dependent on the function of the EAT (Chan et al., 2009). Untransfected HEK293 GFP-LC3 cells exhibited extremely low levels of lipidated GFP-LC3-II when left untreated under full nutrients. Following deprivation of amino acids for 2h, a clear increase in GFP-LC3-II levels was observed. Transfection with full length ULK1wt led to mild a drop in LC3 lipidation in comparison to untransfected cells, whilst further full deletion of the EAT domain (ULK1 ΔEAT) let to a stronger block in LC3 lipidation, as expected based on our previous study (Chan et al., 2009). Intermediate sized deletions led to intermediate LC3 effects but overall the differences were not dramatic.

In parallel, deletion mutants were generated within just the isolated EAT domain sequence (Figure 4.8), since the previous experiments have found strong inhibitory effects when just the EAT region was expressed on its own (Chan et al., 2009). Note that the EAT mutant ending at residue 924 could not be cloned. Other truncation mutants were transfected into HEK293 GFP-LC3 cells. The full-length EAT, EAT 985 and EAT 958 all displayed detectable levels of protein expression, but EAT 898 and smaller mutants were not stable or were not properly expressed. To test ability of these EAT deletion mutants to block autophagy, transfected HEK293 GFP-LC3 cells

were starved of amino acids for 2h (Figure 4.8B). Following amino acid withdrawal, there is a clear increase in GFP-LC3-I to GFP-LC3-II conversion and as expected, overexpression of the full-length EAT domain inhibited starvation induced LC3 lipidation. Deletion of the last 66 residues of the C-terminal (EAT 985), which removes both the 5^{th} and 6^{th} α-helices, rendered a EAT fragment that was no longer dominant-inhibitory. Similar results were obtained with the EAT 1001 mutant consistent with our previous publication (Chan et al., 2009).

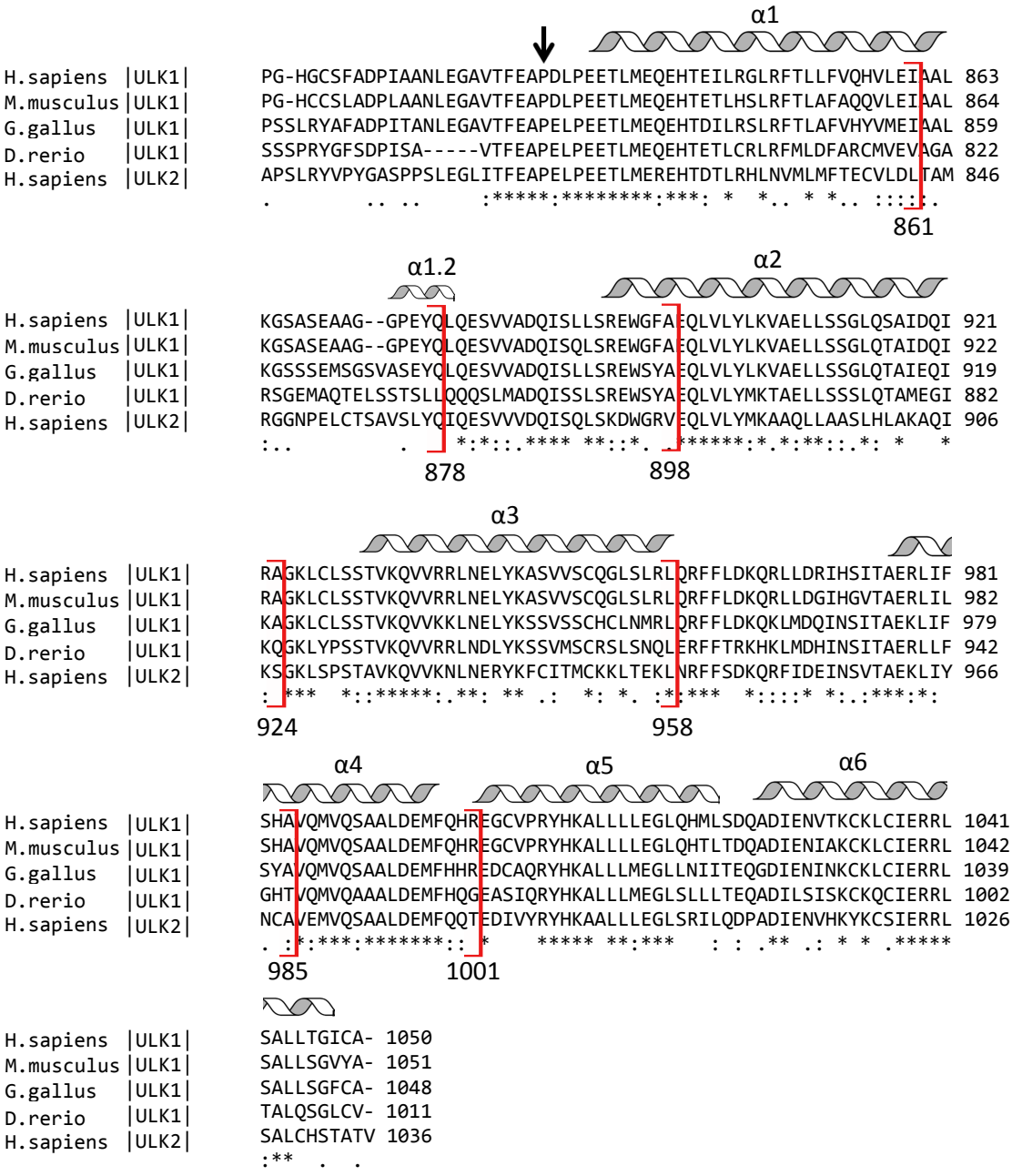

Figure 4.6: **Multiple amino acid sequence alignment of the ULK1 EAT domain**. The ULK1 EAT domain sequence (H sapiens) was aligned using the Clustal Omega (EBI web server) (Sievers et al., 2011). The predicted secondary structure was generated using I-TASSER (Zhang, 2008). Regions that correspond to a predicted alpha helix structure are shown above the sequence. The Entrez sequence database accession number are: H.Sapiens NP_003556.1, GI: 4507831. M.musculus ULK1: NP_033495.2, GI:40254402. G.gallus ULK1 XP_415091.2, GI:118098424. D.rerio ULK1 (Isoform 1): XP_002665971.2, GI:326677670. H.sapiens ULK2: NP_001136082.1, GI: 217330559. (*) Identical residues, (:) Conserved residues and (.) Semi Conserved. Red brackets represent site of stop codon used to generate truncation mutations (1001, 985, 958, 924, 898, 878 and 861 using Mus ULK1 numbering). Dashes represent gaps in the sequence during alignment. Black arrow represents start of the EAT domain sequence.

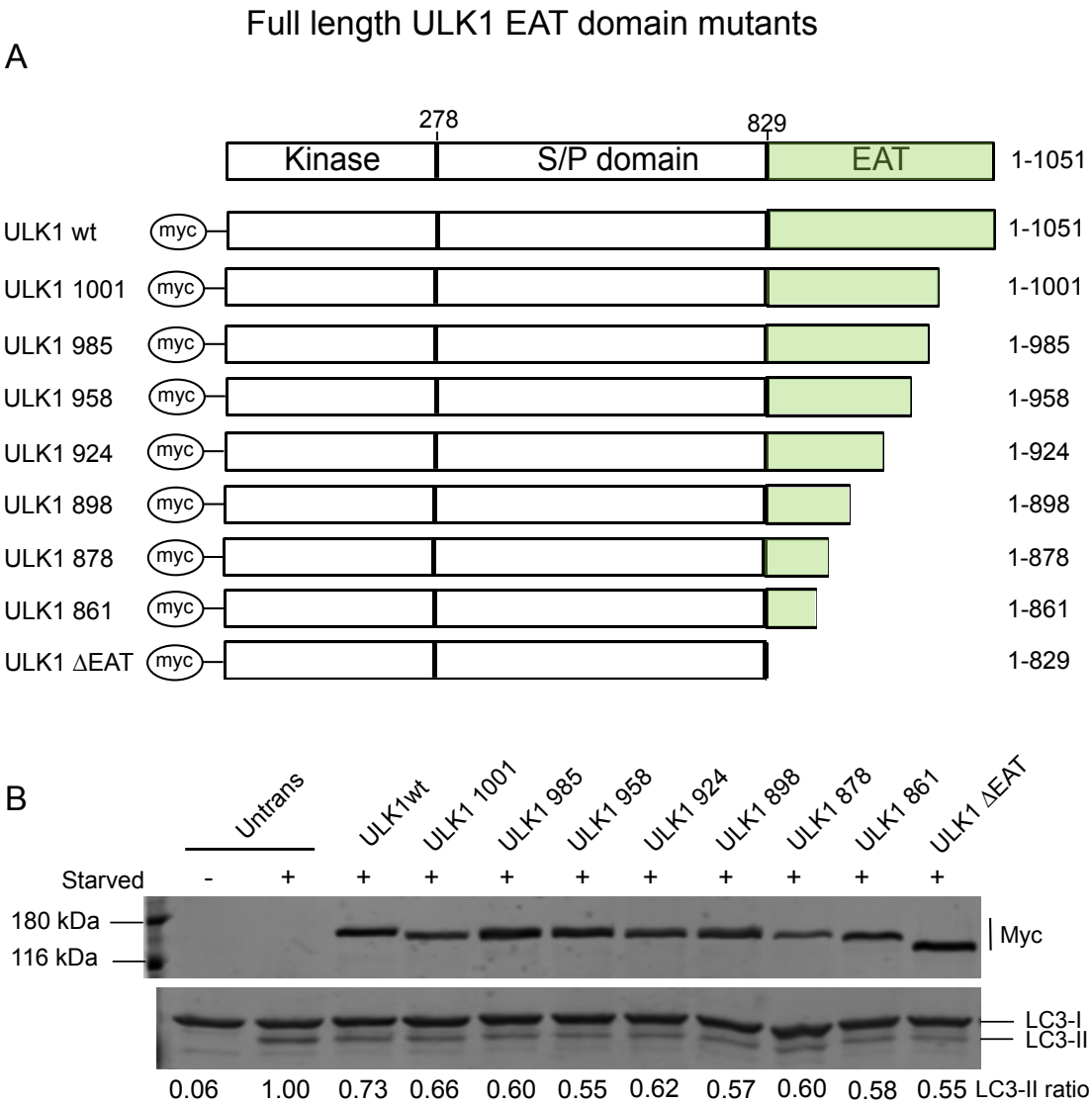

Figure 4.7: **Full length ULK1 EAT domain truncation mutant design and protein expression.** (A) Schematic diagram representing the domain architecture of full length mouse ULK1 and the various myc-tagged Full ULK1 EAT domain C-terminal mutants. Numbers denote amino acid residue position ranging from 1-1051. (B) Protein expression of the ULK1wt and each EAT truncation mutant. HEK293 cells (also stably expressing GFP-LC3) were left untransfected or transfected with each myc-tagged ULK1 EAT domain mutant as indicated. Twenty-four hours following transfection, cells were left untreated or starved with EBSS for 2h. Cell lysates were resolved by SDS-PAGE and blotted for Myc and LC3 antibodies. Quantified ratios of LC3-II/(LC3-I+LC3-II) are expressed below blot. Data representative of one experiment.

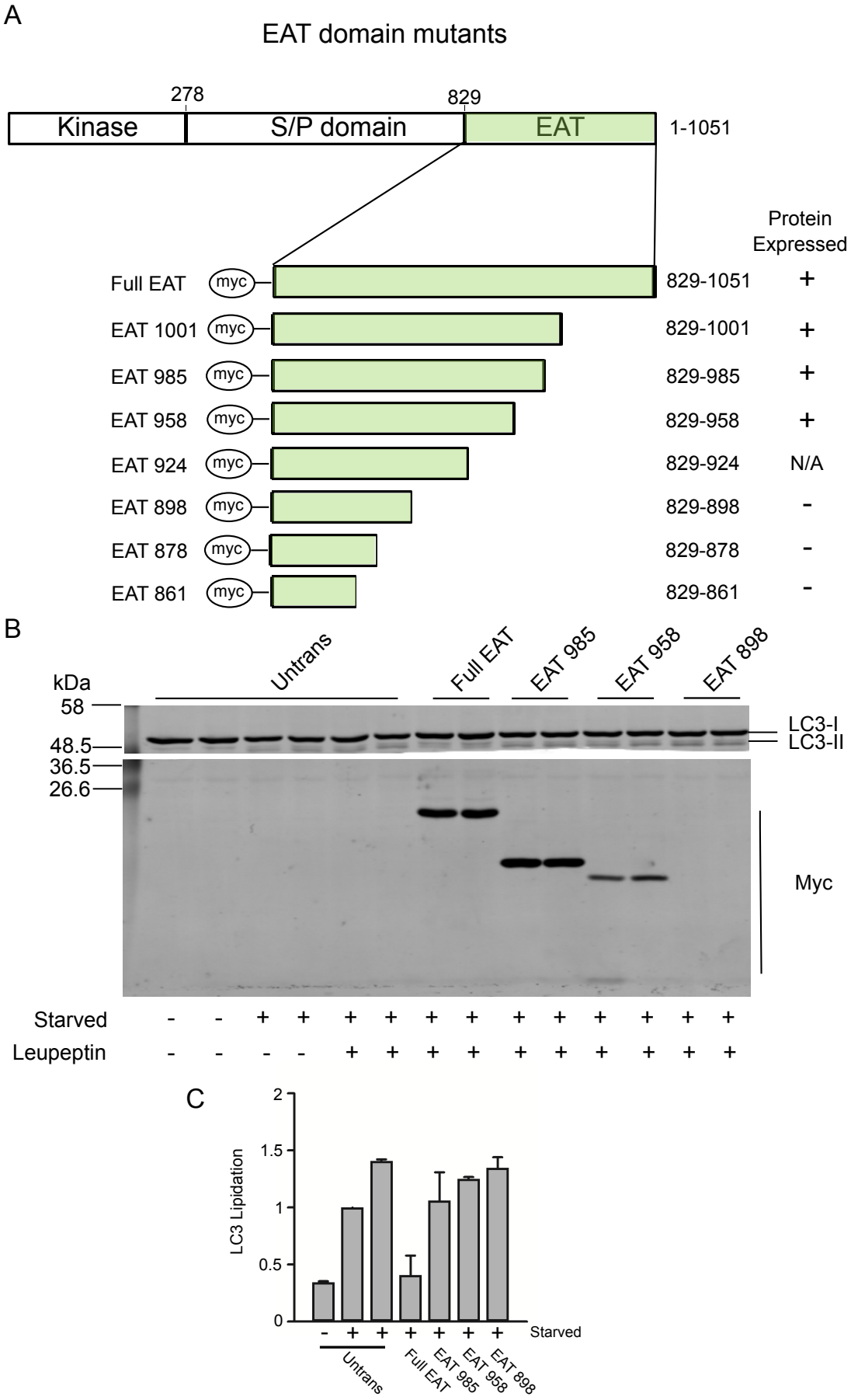
A
EAT domain mutants
278
829
Kinase
S/P domain
EAT
1-1051
Protein Expressed
Full EAT
myc
829-1051
+
EAT 1001
829-1001
+
EAT 985
829-985
+
EAT 958
829-958
+
EAT 924
829-924
N/A
EAT 898
829-898
-
EAT 878
829-878
-
EAT 861
829-861
-
B
kDa
58
48.5
36.5
26.6
Untrans
Full EAT
EAT 985
EAT 958
EAT 898
LC3-I
LC3-II
Myc
Starved
Leupeptin
C
LC3 Lipidation
2
1.5
1
0.5
0
Starved
Untrans
Full EAT
EAT 985
EAT 958
EAT 898

Figure 4.8: **ULK1 EAT domain truncation mutant design and protein expression levels.** (A) Schematic diagram representing the domain architecture of full length mouse ULK1 and the various myc-tagged EAT domain C-terminal mutants utilised within this thesis. Numbers denote amino acid residue position ranging from 829-1051. (B) Protein expression of the full EAT domain and each EAT truncation mutant. HEK293 cells were left untransfected or transfected with each myc-tagged EAT domain mutant as indicated. Twenty- four hours following transfection, cells were left untreated or starved with EBSS (supplemented with leupeptin) for 2h. Cell lysates were resolved by SDS-PAGE and blotted for Myc and LC3 antibodies. (C) Quantified ratios of LC3-II/(LC3-I+LC3-II) are expressed as mean ± Range. Data representative of two experiments.

4.3 Atg13 binds to residues between Ile878 and Glu898 ULK1 EAT domain

The mechanism (cellular target) underlying the dominant-negative effect from the ULK1 EAT domain remains unclear. However, the EAT domain is understood to be vital for the binding of its co-factors Atg13 and FIP200 (Chan et al., 2009) (Hara et al., 2008). Some mutational mapping of the yeast EAT region for Atg13 binding has been documented (Cheong et al., 2008). More recently, a crystallised structure of a *K. marxianus* Atg1 EAT-Atg13 complex was elucidated to show a network of interactions involving grooves formed between α2 and α3; in addition to between α5 and α6 of the Atg1 EAT (Fujioka et al., 2014). Within mammalian cells, our lab has already determined that Atg13 binds to the ULK1 EAT domain independently of the extreme C-terminal IERRLSA motif (Chan et al., 2009). To more precisely understand mammalian ULK1-Atg13 binding, I explored this biochemically using my panel of truncation mutants.

Firstly, a confirmatory control experiment was setup to establish the methodology to detect interactions, initially using the ULK1 EAT domain and mammalian Atg13 (Figure 4.9). Using cells co-transfected with myc-EAT and mAtg13-FLAG, mAtg13-FLAG immunoprecipitated by anti-FLAG beads successfully pulled-down myc-EAT. The reciprocal CO-IP also was effective, with myc-EAT precipitating detectable mAtg13-FLAG. As controls, mock transfected cells as well as beads alone gave minimal background.

It was then necessary to examine which ULK1 residues are essential for Atg13 binding. For this, various full length ULK1 EAT domain mutants were utilised (since transfection of just EAT domain mutants with some of the larger deletions failed to generate

protein expression). HEK293 cells were co-transfected with Atg13-FLAG and ULK1 EAT deletion constructs and lysates were bound to anti-FLAG beads. As expected, myc-ULK1 ΔEAT failed to be precipitated with the Atg13-FLAG (Figure 4.10). Conversely, full-length ULK1 and mutants larger than the ULK1 924 truncation mutant displayed typical binding. The ULK1 mutant ending at 898 displayed mild loss of binding and with further truncation of the next 20 residues (1-878), binding is almost completely abrogated. Unbound myc-ULK1 proteins could be detected in supernatants indicating relatively equal expression. In summary, this suggests that Atg13 binding to ULK1 does not require C-terminal regions but depends on residues between Ile 878 and Glu 898.

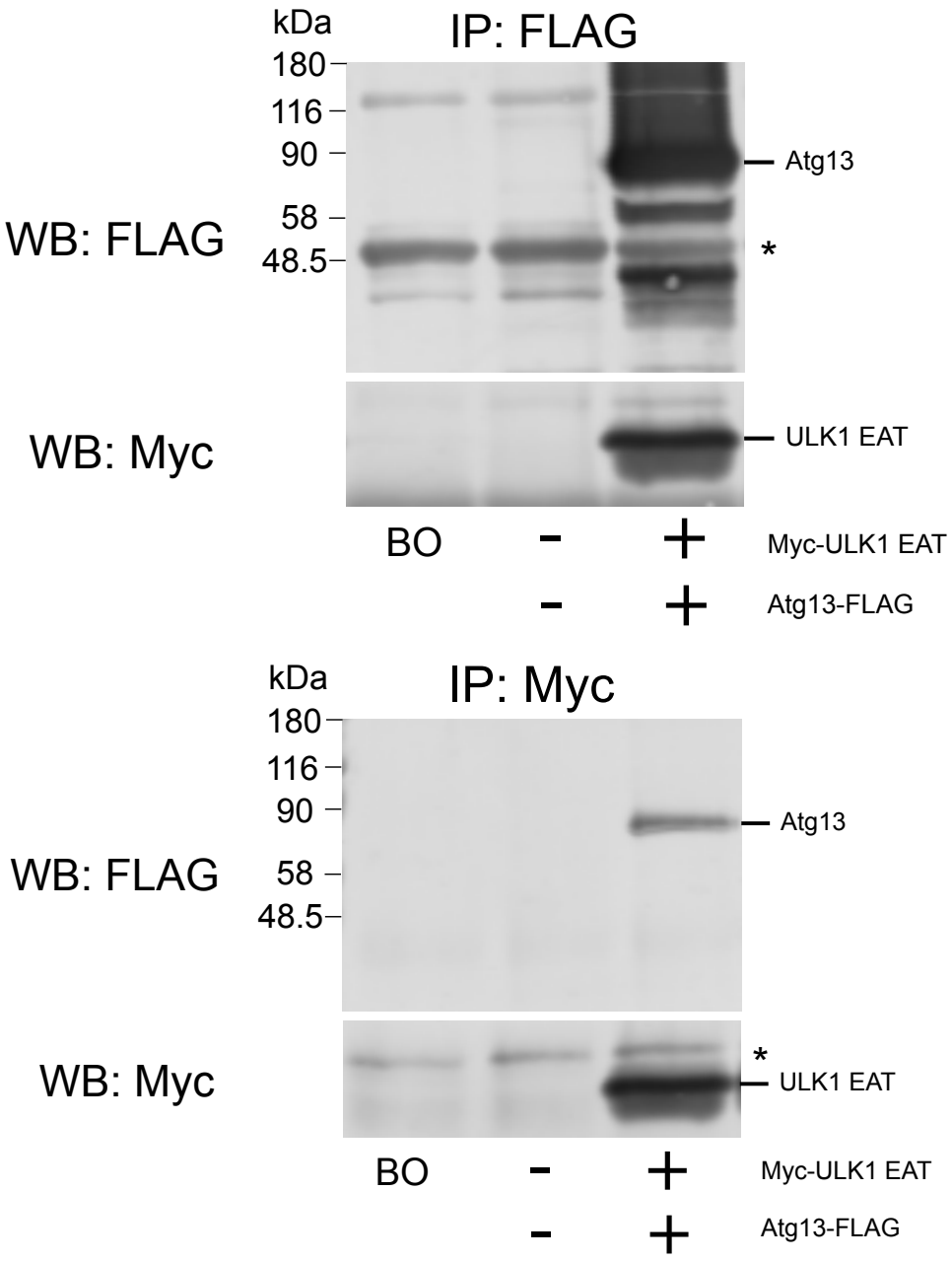

Figure 4.9: **Co-immunoprecipitation confirms interaction between ULK1 EAT domain and Atg13**. Reciprocal co-immunoprecipitation of HEK23A cells transiently transfected with myc-Full-length EAT and Atg13-FLAG as indicated. Cells were lysed 24h subsequent to transfection and half the cell lysate immunoprecipitated with anti-Myc beads and the other half with anti-FLAG beads. Immunoprecipitated proteins were then resolved using immunoblotting and detected with anti-Myc or anti-FLAG antibodies. As negative controls myc and FLAG tagged beads only (BO) or with untransfected whole cell extract were utilised. Representative of one experiment.

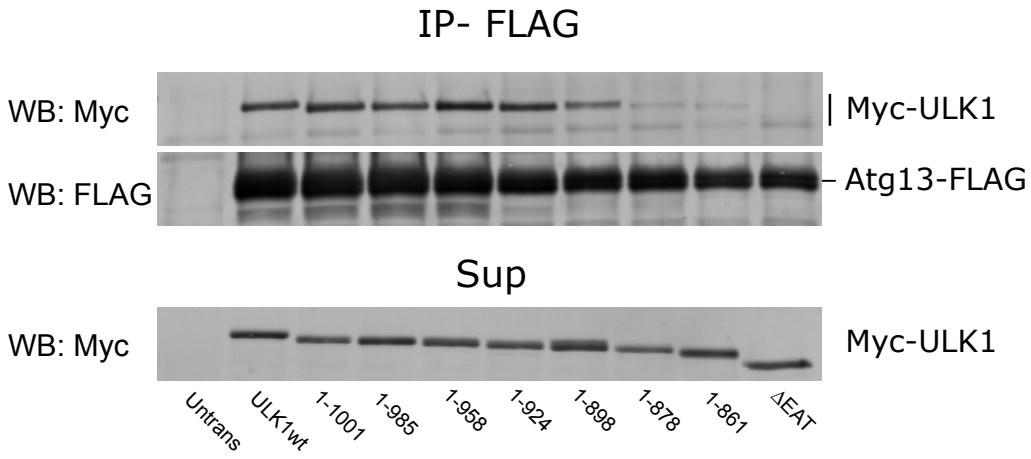

Figure 4.10: **ULK1 EAT binds to Atg13 between residues Ile878 and Glu898 of ULK1**. Co-immunoprecipitation of HEK23A cells transiently transfected with Atg13-FLAG and various full length ULK1 EAT domain mutants as indicated. Cells were lysed 24h subsequent to transfection and the total cell lysate immunoprecipitated with anti-FLAG beads. Immunoprecipitated proteins were then resolved using immunoblotting and detected with anti-Myc or anti-FLAG antibodies. As negative controls FLAG-tagged beads immunoprecipitated with untransfected whole cell extract were utilised. Supernatants were also resolved to detect unbound myc-ULK**1.**

4.4 Membrane association of autophagy related proteins during nutrient dependent autophagy.

In addition to the ULK1 EAT domain being key for protein binding and ULK1 complex formation, another fundamental proposed role is for direct binding to early autophagic membranes. For example, previous work from our lab demonstrated that EAT domain is required for the localisation of ULK1 to LC3-positive membranes (Chan et al., 2007) and that the EAT can biochemically be detected in membrane precipitation methods (Chan et al., 2009). More recent work has displayed a role of the Atg1 EAT domain (ULK1 ortholog) to be a potent membrane curvature sensor that also has a specialised ability to tether small lipid vesicles in vitro (Ragusa et al., 2012).

Therefore, the next stage was to examine the membrane association of ULK1 EAT deletion mutants. Firstly, the aim was to establish the methods using another member of the ULK1 complex (namely mAtg13) and also Atg16L1, which interacts with early isolation membranes and also forms interaction with the ULK1 complex via FIP200 binding (Gammoh et al., 2013, Nishimura et al., 2013).

HEK293/GFP-LC3 cells were transiently transfected with Atg13-FLAG or FLAG-Atg16L1 and these cells were either left untreated or were starved of amino acids for 2h (Figure 4.11). Cells were lysed, homogenised and then assessed by crude membrane fractionation using the protocol previously reported (Chan et al., 2009). From these results, both Atg13-FLAG and FLAG-Atg16L1 could be detected in association with crude membrane fractions. In unstarved cells, only 1%-2% of the Atg13 and Atg16L1 proteins were membrane bound indicating only a small fraction was bound during basal conditions. It was expected that amino acid starvation would drive membrane association. However, deprivation of amino acids did not change the ratio of

membrane binding for both Atg13-FLAG and FLAG-Atg16L1. Within this experiment, membrane binding of (lipidated) GFP-LC3-II was used as control. As expected, GFP-LC3-II was only detected on membrane fractions (for example in the Atg13 samples) and this was increased following starvation. Interestingly, transfection of FLAG-Atg16L1 noticeably blocked GFP-LC3-II formation.

Next, membrane association of ULK1 was examined and the related family member ULK2. Once again, HEK293/GFP-LC3 cells were transfected with either myc-ULK1wt or myc-ULK2wt and amino acid starved (Figure 4.12). As expected, both ULK1 and ULK2 were detected in the membrane (and also cytoplasmic) compartments. In contrast to Atg13 and Atg16, the ratios of membrane/cytoplasmic association were considerably higher for ULK1 and ULK2 (10-12% within crude membrane fraction). However, an unexpected result was that ULK1/2 membrane binding did not increase following nutrient starvation.

To further search for Atg factors with starvation induced membrane binding, the mammalian Atg18 homolog, WIPI-1, was examined. In agreement with all other autophagy related proteins examined, WIPI-1 also associates with the crude membrane fraction and binding was not affected by nutrient deprivation (Figure 4.13). In this pilot experiment, examination was necessary to establish whether WIPI-1 was enriched on detergent resistant membranes (DRM) which have been described to be enriched in the lipid raft fraction (Garofalo et al., 2016). Previous work from our group has suggested that ULK1 can be found on TX-100 DRM (Chan et al., 2009). To test if other membrane binding factors such as WIPI-1 could be experimentally detectable in DRM, an additional wash on the crude membrane fraction with homogenisation buffer supplemented with 1% TX-100 was carried out. As expected,

starvation increased amounts of GFP-LC3-II binding to crude membranes but binding of both GFP-LC3-I and –II was completely abolished following detergent washing. Interestingly, WIPI-1 was also detected in crude membranes and a fraction remained associated in DRM, suggesting that this Atg protein might be present in lipid rafts. Importantly, endogenous Caveolin-1, an abundant constituent of lipid rafts and widely used marker, was stably membrane bound after washing, validating this method. Surprisingly however, binding of WIPI-1 to membranes was generally not induced following starvation.

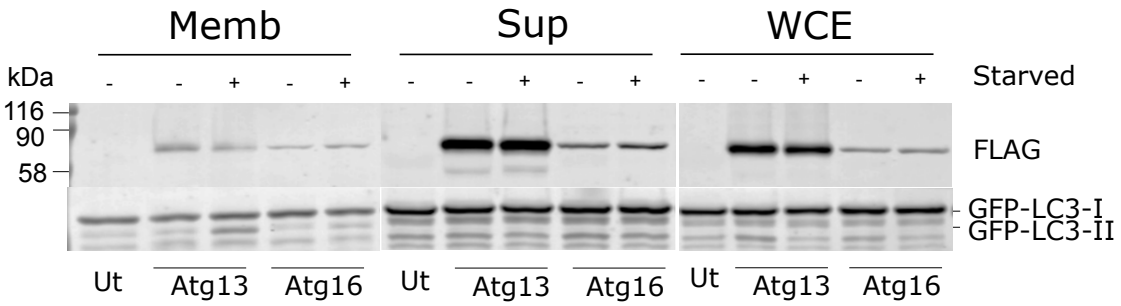

Figure 4.11: **Atg13 and Atg16L1 are present in both membrane and cytosolic fractions independent of nutritional status**. HEK293 cells stably expressing GFP-LC3 were transiently transfected with Atg13-FLAG or FLAG-Atg16L1 as indicated. Twenty four hours after transfection, cells were left untreated or were treated with EBSS (Starved) for 2 hours. Cell homogenates were subject to ultracentrifugation to isolate crude membrane (Memb) and cytosolic (Sup) fractions as described in methods. Samples of supernatant fraction representing 2% of total, membrane fraction (10% of total) and whole cell extract (1%) were resolved by SDS-PAGE and subsequently blotted for FLAG and LC3 proteins. Data shown is representative of two independent experiments.

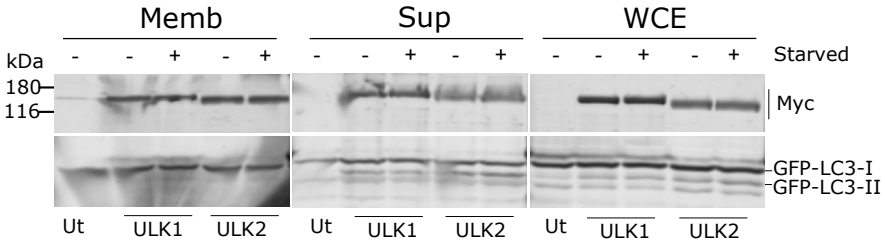

Figure 4.12: **ULK1 and ULK2 are found in membrane and cytosolic fractions independent of nutritional status.** HEK293/GFP-LC3 cells were transiently transfected with Myc-ULK1 or Myc-ULK2 as indicated. Twenty four hours after transfection cells were left untreated or were treated with EBSS (Starved) for 2 hours. Cell homogenates were analysed as in Figure 4.11. Samples of supernatant fraction representing 2% of total, membrane fraction (10% of total) and whole cell extract (1%) were resolved by SDS-PAGE and subsequently blotted for Myc and LC3 proteins. Data shown are representative of two experiments**.**

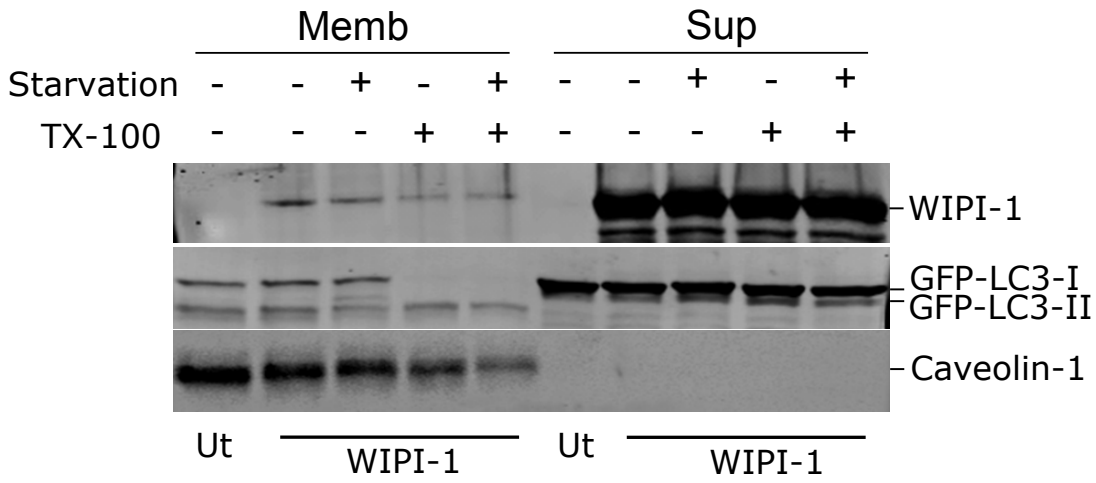

Figure 4.13. **PI3P effector protein WIPI-1 binds to detergent resistant membranes (DRM)**. HEK293/ GFP-LC3 cells were transiently transfected with Myc-WIPI-1 as indicated. Twenty four hours after transfection cells were left untreated or were treated with EBSS (Starved) for 2 hours. Cell homogenates were ultracentrifuged to isolate membrane (Memb) and cytosolic (Sup) fractions. Membrane pellets were also washed in buffer supplemented with 1% TX-100 where indicated. Samples of supernatant fraction representing 2% of total, membrane fraction (10% of total) were resolved by SDS-PAGE and subsequently blotted for Myc and LC3 proteins. Caveolin-1 was used as DRM control protein. Data shown are representative of one experiment.

4.5 Membrane binding of the ULK1 EAT domain

Our group previously found that the mammalian ULK1 EAT can be shown to bind to membranes through imaging and in crude fractionation experimentation (Chan et al., 2009). Following on, it was reported that the yeast Atg1 EAT domain alone can bind liposomes and therefore sense membrane curvature with an additional potential role to tether lipid vesicles (Ragusa et al., 2012). Therefore, the membrane fractionation protocol and set of deletion mutants was used to better identify EAT regions important for lipid binding. HEK293/GFP-LC3 cells were transfected with either full-length ULK1 EAT, EAT 985 or EAT 958 mutants and subsequently analysed for membrane and cytoplasmic fractions (Figure 4.14). As expected, the full-length EAT domain could be strongly detected within the crude membrane pellets. Interestingly, membrane binding was retained, even with deletion of the last 93 residues (EAT 985 and EAT 958). The shorter EAT 958 showed lower expression but proportionate membrane binding could be seen. GFP-LC3-II was also clearly detected in the membranes as control. This suggests that key membrane binding regions are not located at the C-terminal region of the EAT domain and do not depend on the 4^{th}-6^{th} α-helices.

Next, it was examined whether the EAT domain could associate with DRM (Figure 4.15), as this issue had never been previously studied. It could be shown that the EAT domain was detected in DRMs, similar in extent to the Caveolin lipid raft marker. In addition, the results also highlighted that this raft association is still strong after truncation of the last 50 amino acids (5^{th} and 6^{th} α-helices) (EAT 1001). Truncation of 66 residues from the C-terminus (EAT 985) created an unstable EAT fragment, but even this construct remained somewhat in DRM.

Since the ULK1 deletion mutants in the context of the whole protein increased stability as compared to just the EAT domain mutants, it became necessary to examine the membrane binding of these ULK1 constructs. The reasoning for this approach was that it might provide information into the role of other regions not expressed in the small EAT fragments. As expected, full length ULK1 localised to the crude membrane fraction (Figure 4.16). Interestingly, it was also observed that C-terminal truncation led to an enhancement of membrane binding. In fact, ULK1 958 and ULK1 924 show approximately 5-fold increases in membrane association. This was unexpected since the ULK1 924 mutant lacks the 3rd- 6th α-helices and would have both 3 helical bundles disrupted (Fujioka et al., 2014). Deletion of the EAT from ULK1 then strongly abolished membrane binding. These data together suggest that the 1st and 2nd α-helices of the EAT have strong membrane binding residues but that further helical arrangements in the fully folded EAT partially mask these hydrophobic patches.

The deletion data highlighted that regions of the EAT with just the α-helices 1 and 2 could have membrane binding potential but such deletions would lack full Atg13 binding functionality. As such, the next aim was to further examine the role of EAT subdomains using other assays that might give information more closely linked to overall function within the ULK1 complex. Our lab and others have detected starvation dependent ULK1 translocation to membranes (i.e. puncta formation) during autophagy induction. Therefore, immunofluorescence microscopy was utilised to visualise the localisation and number of ULK1 puncta. HEK293/ GFP-LC3 cells were transfected with full length ULK1wt or deletion mutants, and then starved of amino acids for 2h before fixation (Figure 4.17). Untransfected starved cells displayed a

notable induction of GFP-LC3 puncta. As expected, transfected myc-ULK1wt formed multiple myc-ULK1 puncta (which was quantified as average 20 per cell). Myc-ULK1 puncta were localised within cytoplasmic membranes near the perinuclear region with strong co-localisation to GFP-LC3 puncta. Unexpectedly, ULK1 puncta formation was severely inhibited in the myc-ULK1 985 truncation mutant, even though this construct showed strong association to biochemical membrane fractions. Myc-ULK1 924, 861 and ΔEAT similarly all failed to form ULK1 puncta. Therefore, these data demonstrates that C-terminal residues are critically essential for the formation of ULK1 puncta during starvation induced autophagy in cells.

The above data highlighted key differences between biochemical and image-based membrane properties of ULK1 mutants. One of the limitations was that transiently overexpressed ULK1 proteins vs. endogenous proteins were being examined. As such, it was possible to confirm membrane binding by probing for endogenous ULK1 (and also Beclin 1, which is particularly well detected in endogenous levels) (Figure 4.18). In this way, it could be confirmed that endogenous ULK1 was associated to crude membranes and also that this does not increase upon starvation. Unexpectedly, endogenous ULK1 association to DRM could not be observed. However, in this pilot experiment, endogenous Beclin 1 could be detected on crude membranes and also clearly in DRM, although this was not starvation dependent. These data suggest potential lipid raft association of ULK1 that will need confirmation with other methods to minimise artefactual findings due to the overexpression.

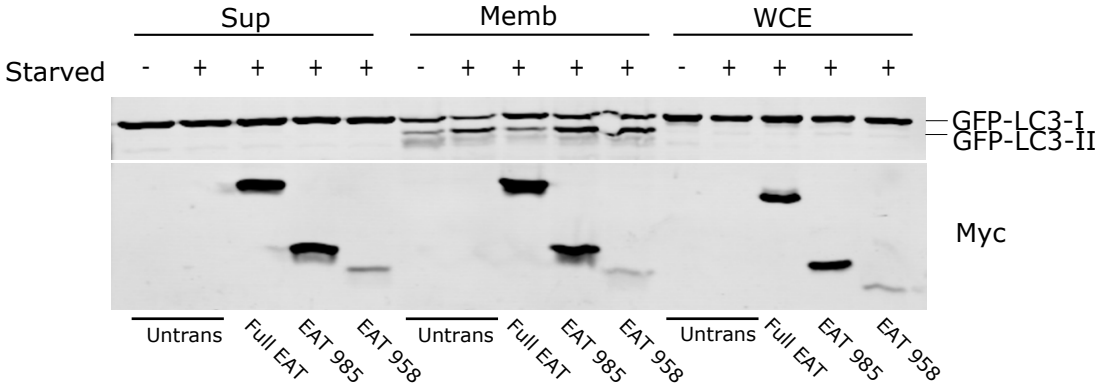

Figure 4.14: **The ULK1 EAT domain and the EAT 985 and EAT 958 truncation mutants are present in the membrane fraction**. HEK293/GFP-LC3 cells were transiently transfected with Myc-Full EAT, Myc-EAT 985 or Myc-EAT 958 as indicated. Twenty four hours after transfection cells were left untreated or were treated with EBSS (Starved) for 2 hours. Cell homogenates were ultracentrifuged to isolate membrane (Memb) and cytosolic (Sup) fractions. Samples of supernatant fraction representing 2% of total, membrane fraction (10% of total) and whole cell extract (1%) were resolved by SDS-PAGE and subsequently blotted for Myc and LC3 proteins. Data shown are representative of three experiments .

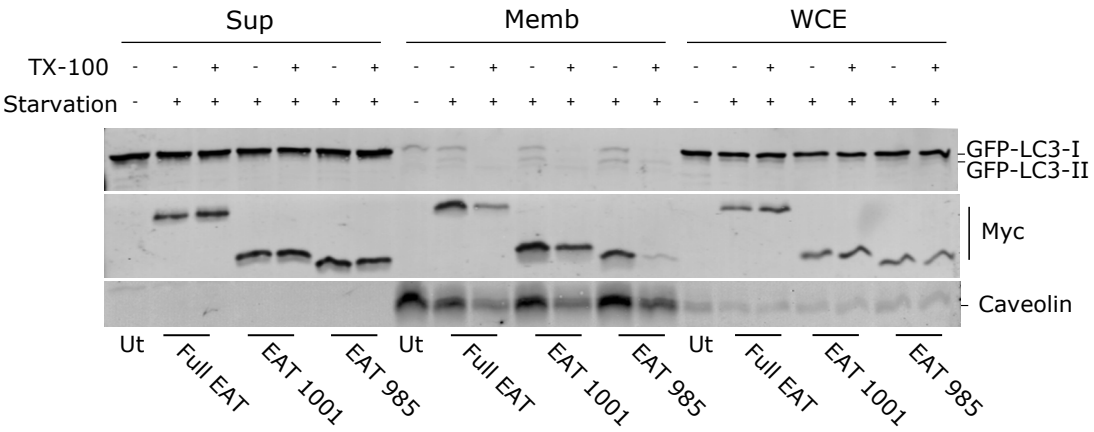

Figure 4.15: **Full-length ULK1 EAT and EAT 1001 bind to DRMs**. HEK293/GFP-LC3 cells were transiently transfected with Myc-Full EAT, Myc-EAT 1001 or Myc-EAT 985 as indicated. Twenty four hours after transfection cells were left untreated or were treated with EBSS (Starved) for 2 hours. Cell homogenates were ultracentrifuged to isolate membrane (Memb) and cytosolic (Sup) fractions. Membrane pellets were also washed in HB supplemented with 1% TX-100 where indicated. Samples of supernatant fraction representing 2% of total, membrane fraction (10% of total) and whole cell extract (1%) were resolved by SDS-PAGE and subsequently blotted for Myc and LC3 proteins. Caveolin was used as DRM control protein. Data shown are representative of two independent experiments.

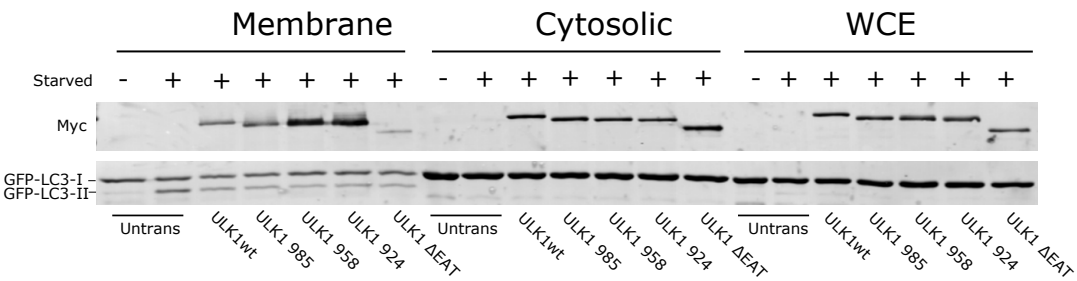

Figure 4.16: **Deletion mutants ULK1 958 and 924 displayed enhanced membrane binding whilst deletion of the ULKI EAT domain almost completely abrogates membrane binding**. HEK293/GFP-LC3 cells were transiently transfected with Myc-ULK1wt, Myc-ULK1 985, Myc-ULK1 958, Myc-ULK1 924 or Myc-ULK1 ΔEAT as indicated. Twenty four hours after transfection cells were left untreated or were treated with EBSS (Starved) for 2 hours. Cell homogenates were ultracentrifuged to isolate membrane (Memb) and cytosolic (Sup) fractions. Samples of supernatant fraction representing 2% of total, membrane fraction (10% of total) and whole cell extract (1%) were resolved by SDS-PAGE and subsequently blotted for Myc and LC3 proteins. Data shown is representative of a single experiment**.**

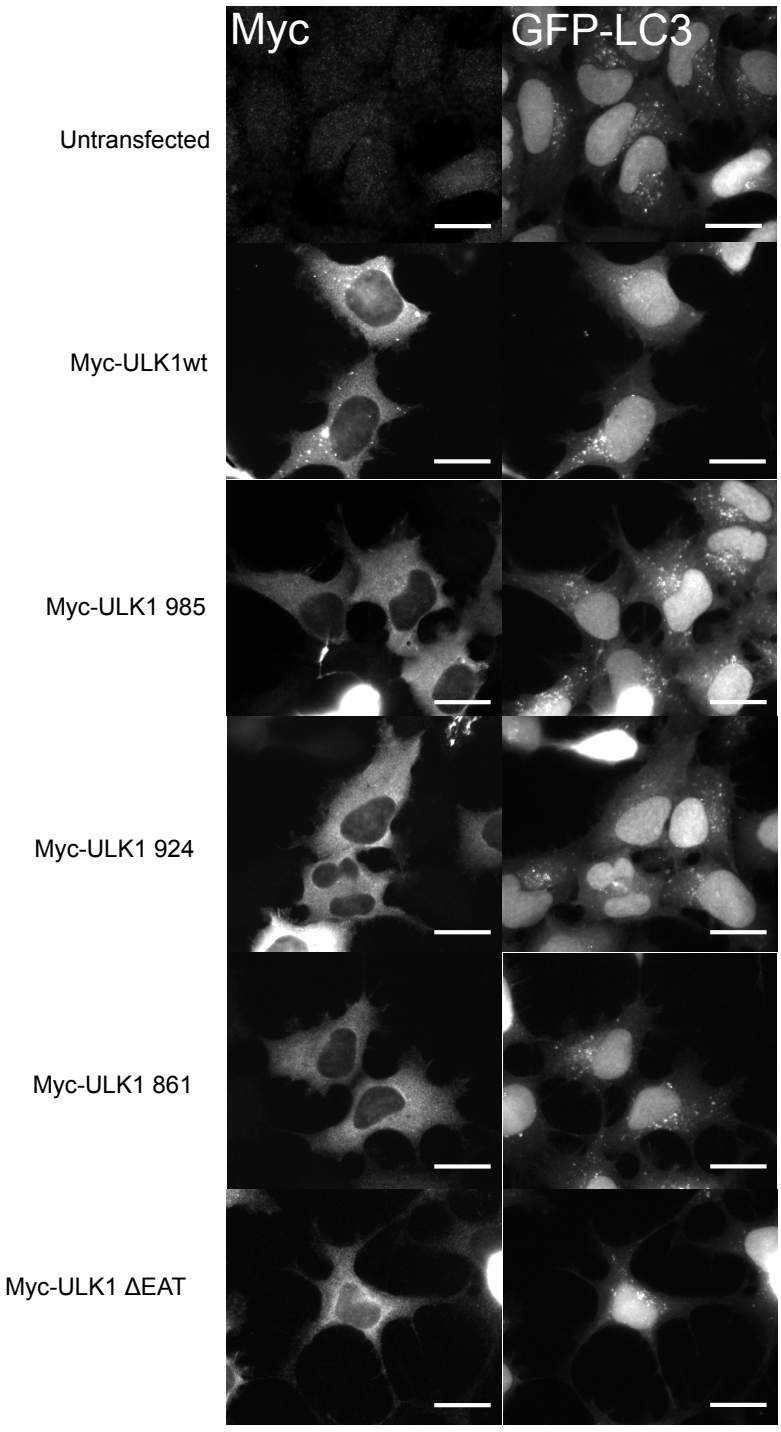
Myc
GFP-LC3
Untransfected
Myc-ULK1wt
Myc-ULK1 985
Myc-ULK1 924
Myc-ULK1 861
Myc-ULK1 ΔEAT

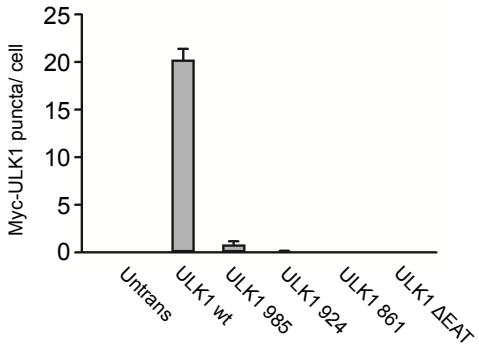
Myc-ULK1 puncta/ cell
25
20
15
10
5
0
Untrans
ULK1 wt
ULK1 985
ULK1 924
ULK1 861
ULK1 ΔEAT

Figure 4.17: **Roles of EAT sequences for ULK1 puncta formation.** (A) Immunocytochemistry of HEK293/GFP-LC3 cells left untransfected or transfected with myc-ULK1wt, myc-ULK1 985, myc-ULK1 924, myc-ULK1 861 or myc-ULK1 ΔEAT. Twenty-four hours post transfection, cells were treated with EBSS (0.1% dFBS) for 2 hours. Coverslips were immunostained for myc and were subjected to epifluorescent microscopy using a Nikon Eclipse E600 and captured on a photometrics coolSNAP f/x CCD camera (X60 oil NA1.40. Scale Bar = 10µm (B) Quantifications of ULK1 puncta/ cell are expressed as mean ±S.E.M of 20 cells. Two tailed paired t-tests were performed (*p<0.05, **p<0.01, ***p<0.001).

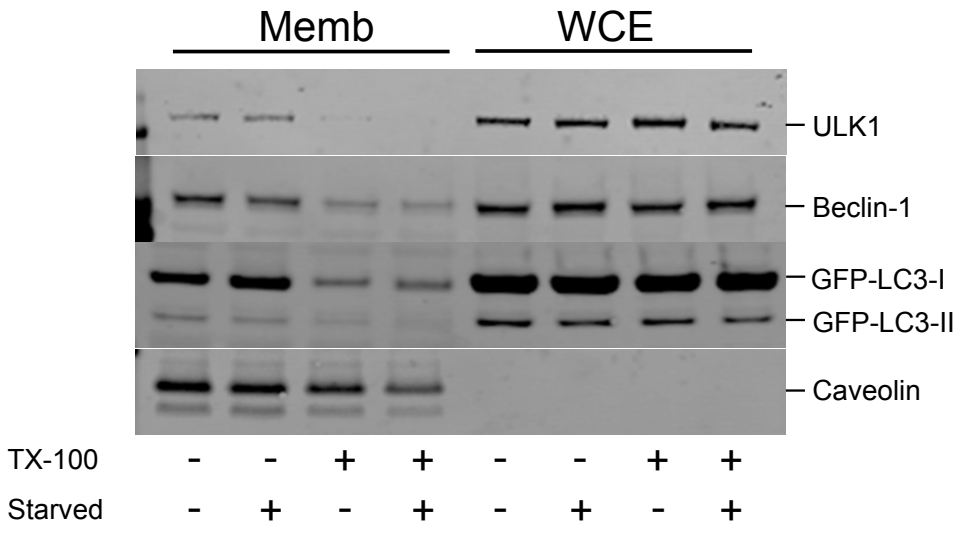

Figure 4.18: **Endogenous ULK1 and Beclin 1 are found in membrane fractions.** HEK293/GFP-LC3 cells were left untreated or were treated with EBSS (Starved) for 2h. Cell homogenates were ultracentrifuged to isolate the membrane (Memb) fraction. Membrane pellets were also washed in HB supplemented with 1% TX-100 where indicated. Samples of membrane fraction representing 10% of total and whole cell extract (1% of total) were resolved (by NuPAGE pre-cast gradient gels) and subsequently blotted for ULK1, Beclin 1 and LC3 proteins. Caveolin-1 was used as DRM control protein. Data shown are representative of one experiment.

4.6 Characterisation of a novel ULK1 EAT domain interacting protein, Erlin-2.

As an alternative approach to explore function of the ULK1 EAT domain, an experiment was carried out in collaboration with S. Tooze (Cancer research UK, London) aimed at identifying novel binding partners. This strategy used a GFP-ULK1 EAT construct stably expressed in HEK293 cells. Co-precipitating proteins captured on GFP-trap beads were assessed by mass-spectrometry (MS). The MS analysis indicated that GFP-ULK1 EAT domain interacted with a number of membrane bound proteins and that a significant proportion of these proteins were ER associated. Endoplasmic Reticulum lipid raft associated-2 (Erlin-2) was one of these candidates and was of particular interest since it had been observed previously that ULK1 proteins potentially associated with lipid rafts (Browman et al., 2006).

A tagged Erlin-2 expression vector was obtained. Erlin-2 is single pass class II transmembrane proteins. This corresponds with a single transmembrane region (residues 4-24), a short cytoplasmic N-terminal region (1-3) and a large luminal C-terminal region (25-339). Previous work has highlighted that the extreme N-terminal region of Erlin-2 is vital for the correct membrane insertion into the Endoplasmic Reticulum (Browman et al., 2006).

Firstly to confirm expression of Erlin-2, HEK293/GFP-LC3 cells were co-transfected with HA-Erlin-2 with or without myc-ULK1 EAT and the association to membrane fractions tested. HA-Erlin-2 migrated in total cell lysates and as a doublet of approximately 42kDa (Figure 4.19), potentially representing glycosylated or phosphorylated forms of the protein. Erlin-2 was particularly overexpressed and a fraction of the faster migrating HA-Erlin-2 species was found in crude membranes,

similar to the ULK1 EAT domain. Treatment of the membrane with TX-100 did not show any detectable change on Erlin-2 association to DRM consistent with strong binding to lipid rafts.

With confirmation of good co-expression of Erlin-2 and ULK1 EAT and association to membranes, reciprocal co-immunoprecipitations were performed to confirm the initial MS findings. HEK293A cells were transfected with both plasmids and then subjected to co- immunoprecipitation. It could be observed that HA-Erlin-2 (which was strongly precipitated using HA-beads) successfully pull down detectable myc-ULK1 EAT (Figure 4.20 top panel). In agreement, myc-ULK1 EAT bound to myc-beads also successfully pulled down both fast and slow migrating HA-Erlin-2 bands (bottom panel). Next, it was examined whether binding to Erlin-2 could be detected with full-length ULK1 protein as compared to the EAT domain alone (Figure 4.21). It was found that full-length ULK1 does co-precipitate HA-Erlin-2, but this was most prominent for the upper band form of Erlin-2. In this experiment, the effects were also compared with related family member full-length ULK2. In a similar way, precipitated ULK2 also bound HA-Erlin-2, displaying both forms of the Erlin-2 doublet. In addition, as internal controls, the binding of Erlin-2 was compared to the isolated ULK1 or ULK2 EAT domains. Both EAT domains could be observed to clearly precipitate both forms of HA-Erlin-2. To summarise, this experiment further confirms the ability to detect ULK1 and Erlin-2 interactions and this binding appears to take place for both ULK1/2 gene members. Furthermore, expression with ULK1 leads to a predominance of upper-band slower mobility Erlin-2, suggesting a possible phosphorylation event that is ULK1 specific.

To further examine the potential phosphorylation of Erlin-2 by ULK1, the effects from co-expression of HA-Erlin-2 with normal or kinase inactive version of ULK1 were studied. Transfected cells were left in basal conditions or were starved of amino acids for 2h as indicated (Figure 4.22) and examined by immunoblotting to detect hypershifting of HA-Erlin-2. It was clearly confirmed that co-transfection with ULK1 led to enrichment of the slower mobility hypershifted HA-Erlin-2 species. Interestingly, co-transfection with the kinase inactive ULK1 K46I mutant (Chan et al., 2009) did not lead to hypershift of HA-Erlin-2, further suggesting a phosphorylation event. In addition, HA-Erlin-2 hypershift was not observed following co-expression with ULK2 or any EAT domain alone. It must also be noted that starvation of cells did not alter the HA-Erlin-2 hypershift. Although this work is still at the exploratory stage, there is some confirmation of the initial MS identification of EAT binding proteins and a potential membrane-associated ULK1-specific phosphorylation event has been detected, leading to further analyses required.

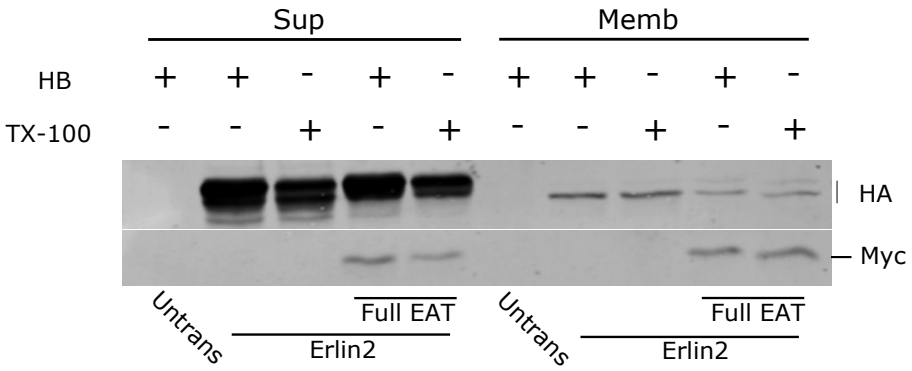

Figure 4.19: **Erlin-2 binds to DRM and similar to ULK1 EAT domain**. HEK293/GFP-LC3 cells were transiently co-transfected with Myc-ULK1 EAT and HA-Erlin-2 as indicated. Twenty four hours after transfection cells were treated with EBSS (Starved) for 2 hours. Cell homogenates were ultracentrifuged to isolate membrane (Memb) and cytosolic (Sup) fractions. Membrane pellets were also washed in homogenisation buffer (HB) or HB supplemented with 1% TX-100 where indicated. Samples of supernatant fraction representing 2% of total and membrane fraction (10% of total) were resolved by SDS-PAGE and subsequently blotted for Myc and HA proteins. Data shown are of one experiment**.**

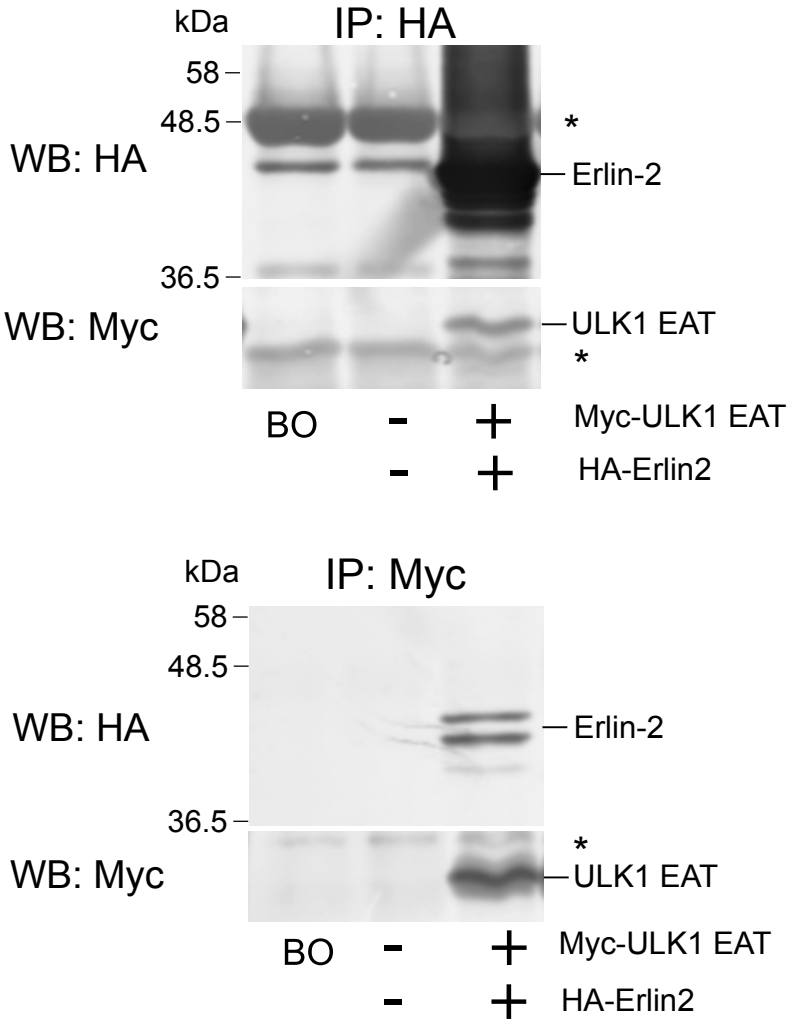

Figure 4.20: **Co-immunoprecipitation interaction between ULK1 EAT domain and Erlin-2**. Reciprocal co-Immunoprecipitation of HEK23A cells transiently transfected with Myc-Full length ULK1 EATand HA-Erlin-2 as indicated. Cells were lysed 24h after transfection and half the cell lysate immunoprecipitated with anti-Myc beads and the other half with anti-HA beads. Immuno-precipitated proteins were then resolved and detected with anti-Myc or anti-HA antibodies. As negative controls myc and HA tagged beads only (BO) or with untransfected whole cell extract were utilised. Supernatents were also resolved to represent any unbound protein in solution. A representative blot is shown from one experiment**.**

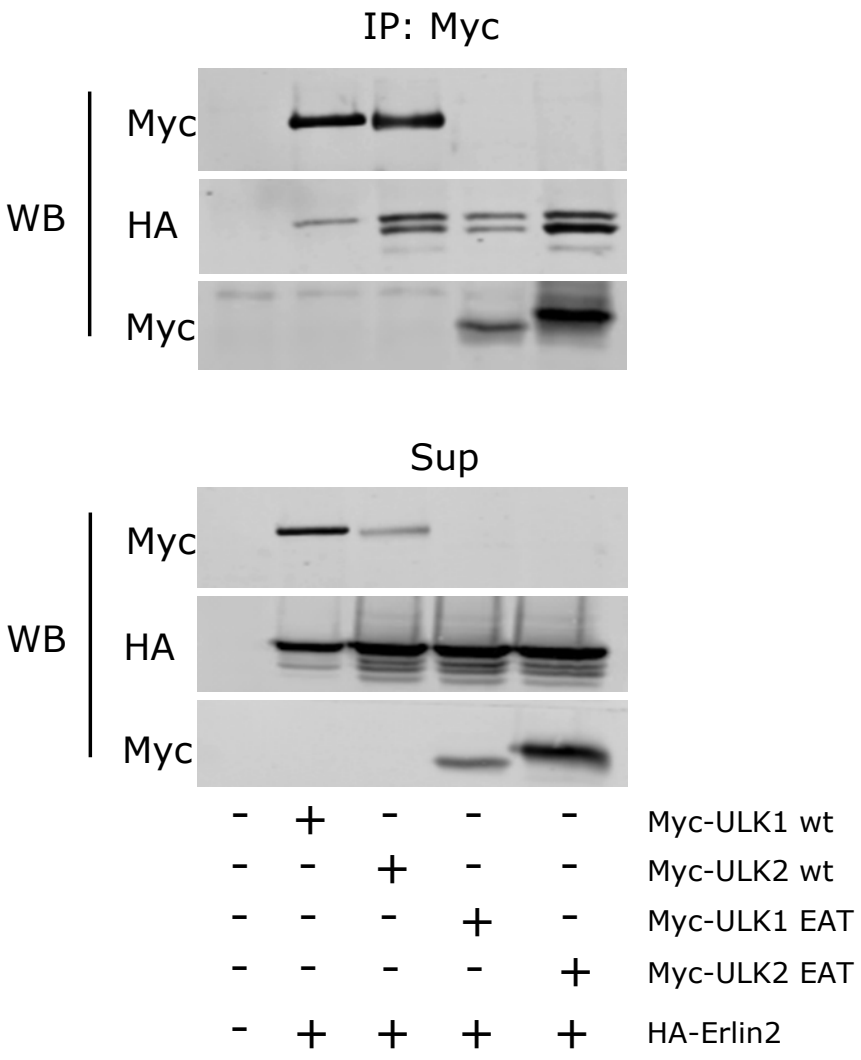

Figure 4.21: **Co-expression of ULK1wt and Erlin-2 leads to a hypershift in Erlin-2**. Co-immunoprecipitation of HEK23A cells transiently transfected with myc-ULK1wt, myc-ULK2wt, myc-full ULK1 EAT, myc-full ULK2 EAT or HA-Erlin-2 as indicated. Cells were lysed 24h subsequent to transfection and the total cell lysate immunoprecipitated with anti-myc beads. Immunoprecipitated proteins were then resolved using immunoblotting and detected with anti-myc or anti-HA antibodies. As negative controls myc-beads were incubated with untransfected whole cell extract. Supernatents were also resolved to represent any unbound protein in solution. A representative blot is shown from one independent experiment.

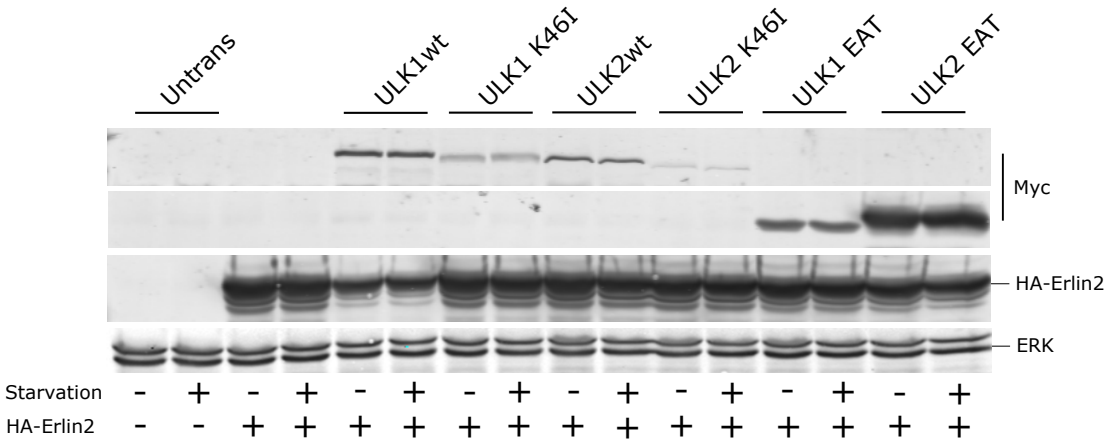

Figure 4.22: **ULK1 kinase activity is required for Erlin-2 hypershift**. HEK293/GFP-LC3 cells were left untransfected or transfected with HA-Erlin-2 and either myc-ULK1/2wt, myc ULK1/2 K46I or ULK1/2 EAT. Twenty four hours post-transfection, cells were left untreated or starved with EBSS (starvation) for 2h. Cell lysates were resolved by SDS-PAGE and blotted for Myc and HA antibodies. Total ERK (42kDa and 44kDa) was used as a loading control and the data shown representative of one experiment.

4.7 Discussion

The central focus of my thesis has been the ULK1/2 complex and its role in driving the early stages of autophagy upon starvation. Given the essential role of the ULK1/2 proteins, a long-standing interest of the laboratory has been the domain functional mapping of this kinase. This included earlier work which focused on kinase function and also on the C-terminal conserved EAT domain (Chan et al., 2007) (Chan et al., 2009). The EAT domain has been of particular interest since this region directs several key functions such as the binding of co-factors such as Atg13, interaction with forming autophagy membranes and dimerisation (Ragusa et al., 2012) (Stjepanovic et al., 2014) (Fujioka et al., 2014) (Kofinger et al., 2015). Since this relatively small domain of the protein carries out several distinct biochemical functions, it was interesting to acquire a more complete understanding of the roles of precise regions which might help design strategies for targeting ULK1 non-kinase regions to block autophagy.

4.7.1 Bioinformatic analysis of the ULK1 EAT domain.

An initial approach was to study the physical properties and structural features of the EAT domain using several basic bioinformatic tools. Bioinformatics has provided a vast range of valuable, constantly evolving and updated tools to allow scientists to investigate a biological features such as gene expression, DNA sequence comparisons and protein structural analysis. As the crystal structure of the mammalian ULK1 and EAT domains have yet to be elucidated, computational methods were explored as a first way to gain further insight into a domains structure and function. The hydrophobic/hydrophilic regions of the EAT domain were firstly identified using hydropathy plots and solvent accessibility analysis (Kyte and Doolittle, 1982). This analysis of the mammalian EAT sequence predicted a strong predominance of helical

structure correlated with highly buried hydrophobic stretches, which correlated well with the other experimental data coming out from crystallography from yeast *K. marxianus* EAT (Fujioka et al., 2014) and hydrogen-deuterium exchange/MS on *K. lactis* EAT (Stjepanovic et al., 2014). Understanding of the yeast Atg1 EAT-Atg13 complex has been further refined from small-angle x-ray scattering (SAXS) and solution structure determinations (Kofinger et al., 2015).

The EAT domain also showed strong levels of conservation at the primary sequence level amongst a number of vertebrate Atg1 proteins in model organisms such as Zebrafish. The EAT domain sequence could also be clearly distinguished based on high sequence conservation levels relative to the internal spacer region of Atg1 proteins, which can be interpreted to suggest strict levels of deviation through evolution and conversely an important critical function that is sensitive to mutational change. Many stretches of highly conserved sequences correlated with predicted helical structures. On the other hand, there was little sequence similarity when comparing mammalian and yeast Atg1 EAT, which was surprising since the domain is expected to have the same biochemical roles in terms of Atg13 binding and autophagy induction. Also, yeast and mammalian EAT domains are modelled to share similar secondary helical and 3D folding arrangements (based on robustness of threading predictions, below).

A major advance in the field was elucidation of the crystal structure of the yeast *K. marxianus* Atg1-Atg13 binding complex (Fujioka et al., 2014). This structure showed that the EAT forms two asymmetric three-α-helix bundles, each of which displays structural similarity to microtubule interacting and trafficking molecule domains (MIT domains) linked to proteins with roles for intracellular trafficking and multivesiclular body formation (Hurley and Yang, 2008). Overall, MIT domains typically drive protein-

protein interactions. Database analyses identified widespread forms with 1611 MIT domains found within 1401 proteins (Schultz et al., 1998). These include spastin, sorting nexin 15 and Vps4A. Interestingly, one study has identified that the MIT domain in Vps4A functions as a Ca^{2+}- dependent phosphoinositide-binding domain and the Ca^{2+} binding was localised to the loop between the first and second α-helices of the MIT domain (Iwaya et al., 2013).

In the EAT-Atg13 co-crystal, a helical fragment of Atg13 was shown to form extensive contacts with the EAT 1st MIT domain 3 helix bundle and an additional set of contacts with the 2nd MIT domain. Complementary information was reported by deuterium exchange experiments on the *K lactis* EAT which report general solvent accessibility on the folded structures (Stjepanovic et al., 2014). This work showed that a large fraction of the isolated native EAT domain (absence of any other interacting protein) was solvent accessible. The first three helical MIT domain was relatively less accessible (potentially more rigid) than the 2nd MIT containing the C-terminal three helical bundle, which showed much more disorder or flexibility. Comparative deuterium exchange analysis of the EAT-Atg13 complex also gave insight into regions stabilised or masked by Atg13 binding. In this way, it was found that a loop in the 1st MIT domain became more protected upon binding to a fragment of the Atg13 protein. Also, the 2nd MIT domain, which in apo-EAT was relatively exposed, showed larger amounts of protection from Atg13 binding. Together, these studies illustrate a bi-modular fold in the yeast EAT and that both MIT modules are involved in Atg13 binding.

Following from this bioformatics and published reports, the 3D protein structure prediction software (I-TASSER) was utilised (Yang et al., 2015). I-TASSER is based on

comparative predictions with threading based on similarity to known structures. Therefore, the results would be influenced by the structural data that was emerging at the time which included crystal structures of the ULK1 kinase domain (Lazarus et al., 2015)) and of the *K. marxianus* EAT-Atg13 complex (Fujioka et al 2014).

This commenced with examining the full length structure of the *Mus musculus* ULK1 protein (residues 1-1051) using I-TASSER. The predicted structure retrieved from this analysis showed the ULK1 kinase domain to have a relatively compact domain fold that is comprised of primarily α-helical structures with some β-sheets within the N-terminal regions of the kinase. In addition, the kinase was predicted within a relatively high accuracy of approximately 4Å. The P/S domain was predicted to show a high level of disordered structure. No secondary structures were predicted within this functional domain and the resulting prediction accuracy score was extremely low. On the other hand, the ULK1 EAT domain is predicted to be entirely helical. Interestingly, this predicted model in the context of full-length ULK1 shows the EAT helices do not interact and form any supersecondary structures, in contrast with the crystalised yeast Atg1 EAT domain (Fujioka et al., 2014).

Next, the predicted folding of the ULK1 EAT domain alone without the neighbouring intrinsically disordered P/S domain was examined. The mammalian ULK1 EAT was predicted by I-TASSER to display a very similar structure to the yeast Atg1 EAT domain with 2 MIT triple helix domains (Fujioka et al., 2014). Interestingly, yeast and mammalian EAT residues show relatively low conservation, in contrast with vertebrate EAT domain sequences. Could the mammalian EAT fold like the yeast EAT despite poor sequence conservation? Generally, the functions of yeast and mammalian Atg1/ULK1 EAT are understood to be quite similar in terms of essential

regulatory functions and protein interactions. It is therefore reasonable to predict similar overall 3D folding. Over evolution, sequence mutations can accumulate from an ancestral sequence leading to divergence while maintaining folding and function. The conservation of folding may be driven by requirement for hydrophobic core residues or interaction interfaces for overall protein folding and stability (Chan and Dill., 1990).

Alternatively, it is possible that mammalian EAT does not adopt the MIT domain folding of the crystallised yeast Atg1 EAT, as was predicted in the full length ULK1 I-TASSER prediction. The mammalian EAT domain predicted fold may have been overwhelmingly influenced by the yeast crystal structure data for threading. Clearly, the vertebrate EAT domains contain a high degree of helical structure and the boundaries and residues within the helical features are highly conserved. The issue is how the helices are arranged in the 3D fold of full-length ULK1. On this issue, our mutational deletion mapping below are also somewhat inconsistent with the idea of tandem MIT domain architecture for the EAT region helices.

4.7.2 Identifying the interaction sites between ULK1 EAT and Atg13

Atg13 is an essential autophagy protein from yeast to mammals. As summarised, substantial understanding on the molecular basis of the interaction between the yeast Atg1 EAT and Atg13 has been established by mutational molecular approaches, crystal structures and deuterium solvent exchange biochemistry (Jung et al., 2009, Chan et al., 2009, Stjepanovic et al., 2014). Here, it was necessary to link some understanding from the yeast to mammalian EAT using comparative bioinformatics and further domain function mapping. Experimentally, previous work from our lab has shown that kinase-inactive ULK1 displayed dominant negative properties but that

this depended on sequences at the C-terminus of the EAT (Chan et al., 2009). Since the binding of yeast Atg13 was shown to rely upon the C-terminal 20 residues of yeast Atg1 (Cheong et al., 2008), it was speculated that altered Atg13 binding was the basis of our differences in mammalian ULK1 EAT. However, previous deletion mapping and co-precipitation studies showed that Atg13 binding was still preserved in ULK1 mutants lacking C-terminal portions of the EAT. Our previous deletion studies only focussed on the extreme C-terminal portions, which is now understand to target the 5^{th} and 6^{th} helices, potentially of the putative mammalian MIT2 domain. With the recent structural insight on the EAT, further deletion mapping was carried out which was able to delete further portions including regions of the MIT1 domain.

Several further deletions were created that cut at boundaries of conserved sequences, as existing structural data were published only after the mutants were generated. Interestingly, many of the mutants correlated well with locations of predicted helices. Utilising these ULK1 EAT domain truncation mutants, it was shown that binding between ULK1 and Atg13 was robust (and potentially mildly enhanced) when the C-terminal 93 residues are deleted (1-958). This mutant corresponds to deletion of the predicted mammalian MIT2, leaving MIT1 intact. Thus, our data show that the MIT1 is sufficient to bind Atg13. More surprisingly, strong Atg13 binding was also seen in the 1-924 mutant. This deletion would be predicted to also lack α3 helix thus disrupting the 3 helix bundle of the MIT1 domain, potentially suggesting the α1-α2 helices can form a stable Atg13 binding surface, consistent with solvent accessibility data suggesting that portions of MIT1 may be robust and stably folded (Stjepanovic et al., 2014). A loss of Atg13 binding was only detected when 173 residues were deleted (1-878), representing the further α2 and portions of the joining

loop residues of MIT1. Therefore, it can be concluded that Atg13 interacts strongly with the ULK1 EAT α2 helical region.

This co-precipitation data contrasts with findings from the co-crystal structure of the *K. marxianus* Atg1-Atg13 binding complex (Fujioka et al., 2014). This group found that all six α-helices of the EAT contributed for 2 sets of Atg13 interactions and binding reactions were generally tested using both MIT in tandem. The MIT1 region within the hydrophobic groove between α2-α3 helices (Leu^{667} –Ala^{718}) formed one key set of interactions that cooperated with a second set of binding via α4 and α6 helices (Leu^{754}- Arg^{827}) of MIT2. Data so far indicates a different scenario in mammalian cells, in which sub-regions of MIT1, comprising just 2 helices, are sufficient to provide strong ULK1 EAT-Atg13 binding.

4.7.3 The role of the ULK1 EAT domain in membrane targeting

Since deletion of the EAT disrupted the ability of ULK1 to localise to autophagy puncta membranes (Chan et al., 2007), our lab previously became interested in the membrane binding potential of the EAT, initially as a possible mechanism to explain dominant negative effects. It was demonstrated that domains within the ULK1 EAT domain are sufficient to direct binding to biochemical membrane fractions of the ULK1 complex to the early autophagic membranes (Chan et al., 2009). Data from our group and others comprise a wide array of evidence illustrating that the ULK1 complex translocates to LC3 and Atg16L1 positive ER-associated to drive autophagy initiation downstream (Hara et al., 2008, Itakura and Mizushima, 2010, Karanasios et al., 2013) (Karanasios et al., 2016). Data from the previous chapter characterised the localisation dynamics of endogenous ULK1 using fixed-cell and GFP-ULK1 using live-cell approaches. The working hypothesis was that membrane localisation of the ULK1

complex is directed by the lipid binding of the EAT, although other membrane interactions have also been proposed, such as with Atg13 (Karanasios et al., 2013) (Karanasios et al., 2016). The larger question is how this interaction is specifically and rapidly induced upon amino acid starvation.

The interest on the mammalian EAT domain synergised with other key advancements in the structural and biochemical understanding of the homologous yeast Atg1 EAT domain during IM formation (Ragusa et al., 2012). This seminal study proposed a model in which an Atg17-Atg29-Atg31 oligomeric complex formed further higher order crescent-shaped dimers based around Atg17. In this initial work, some evidence suggested that the yeast Atg1 EAT formed dimers. More interestingly, evidence was presented from biochemical sedimentation assays showing that Atg1 dimers could directly bind to a range of Folch liposomes, but particularly to small sized highly curved vesicles (Ragusa et al., 2012). These data suggest that the EAT can show selective membrane sensing properties. The most striking finding of this paper was that the EAT domain alone could tether small vesicles leading to their clustering. A model has been proposed in which Atg1 physically participates in nucleation and expansion of the phagophore.

More recently, the solution structure of yeast Atg1 complex organisation has been investigated in detail (Kofinger et al., 2015). Crystallisation of the Atg1 complex was reported to be difficult due to the dynamic characteristics and flexibility of the Atg13 region between the Atg1 and Atg17 binding sites. Despite this, SAXS approaches have been developed to investigate flexible protein structures using regularisation strategies (Bernado et al., 2007) (Yang et al., 2010). Through first studying conventional puncta formation, it was proposed that the yeast PAS contains at least

7 Atg17-Atg31-Atg29 tetramers (Kofinger et al., 2015). It was also proposed that following MTOR inactivation during starvation, Atg1 and Atg13 associate with the Atg17-Atg31-Atg29 complex in an equal stoichiometric ratio. However, it must be noted that elsewhere, complete Atg1 pentamer complex have previously been reported in unstarved cells (Kraft et al., 2012). Overall, the solution structure model suggests that the Atg1-containing super complex assembly reaches a maximum of 7 cis-tetramers of a 4:4:4:4:4 stoichiometry to critically drive membrane initiation at the PAS (Kofinger et al., 2015).

This central Atg1 PAS supercomplex could contribute together with other yeast membrane binding proteins such as Ypt1 (Rab1 homologue) and TRAPPIII, which are also implicated in autophagosome initiation/elongation stages through tethering of Atg9 vesicles (Lynch-Day et al., 2010) (Tan et al., 2013). The mammalian homolog of Ypt1 (Rab1) and ER exit sites have already be implicated in autophagosome formation (Zoppino et al., 2010). Recently, it has been demonstrated that the Atg13 can associate with Atg9 in a manner that is independent on PI3P synthesis (Karanasios et al., 2016). Although ERES and ERGIC compartments have been shown to contribute to the nucleation of the autophagosome, this study showed for the first time that Atg9 co-associates with the earliest stage Atg13 compartments. A new model has been speculated in which autophagosome nucleation occurs in regions where the ULK1 complex co-localises with ER tubules, utilising the Atg9 compartment to nucleate the IM membrane. Following this, the Vps34 complex would generate PI3P enriched membrane domains to further expand the IM and recruit other autophagic machinery. Altogether, the emerging themes from yeast and mammalian systems is that Atg1/ULK1 complexes localise early to autophagosome to drive further

recruitment of Atg9-associated membranes and activation of the Beclin 1-Vps34 pathway.

Therefore, to better understand the mammalian EAT, the aim being to better map regions that bound membranes, given the opportunity to relate this with structural models. Previous experiments from our group had already determined that the C-terminal 50 residues, which corresponds to the 5th and 6th α helices of MIT2, did not contain key membrane interaction sites (Chan et al., 2009). Surprisingly, further deletion experiments here indicated that ULK1 fragments lacking a substantial portion of the EAT domain (e.g. ULK1-924, only contains MIT1 α1 and α2 helices), still associated strongly to crude membrane fractions. This data thus suggests that a similar sub-portions of the MIT1 are sufficient to bind membranes and Atg13 in cells, which raises questions on how much of the predicted three helix bundle of MIT1 is required for function.

Some other evidence from these experiments indicate that there may be caveats with the crude fractionation data. The fractionation methodology was used to probe the association of a wide range of autophagy regulatory factors understood to be membrane associated. In this way, it could detect crude membrane association of overexpressed versions of Atg13, Atg16L1 and WIPI-1. Unexpectedly, any starvation-induced membrane binding by any of these factors (or of exogenous ULK1/2) was not detected. A robust starvation-sensitive assay has been translocation of factors to membrane puncta detected by microscopy (Mizushima et al., 2010, Barth et al., 2010, Klionsky et al., 2016). In this way, it was found that deletion of MIT2 (ULK1 985) disrupted ability to localise the ULK1 complex to membrane puncta. As such, membrane puncta formation may be a more stringent test for function than

biochemical fractionation and MIT2 may be required for proper regulation and signalling from the ULK1 complex. Time permitting, these functional roles would have been explored by rescuing autophagy in ULK1/2 DKO MEF.

In light of the apparent discrepancy between imaging and fractionation data, it was attempted to resolve this by detecting membrane fractionation of endogenous proteins. From this experiment, it could be confirmed that endogenous ULK1 and Beclin 1 could be clearly detected in crude membrane fractions, providing some validation of this approach. Surprisingly, however, both endogenous ULK1 and Beclin 1 did not show starvation induced increases in membrane binding. This may suggest that these autophagy factors are associated with a cellular membrane pool in basal state but upon starvation, drive autophagy by translocating to specific ER-associated autophagosome assembly site. In any case, this modulation overall is better detected by imaging, both of endogenous or moderately overexpressed tagged versions of the autophagy factors.

4.7.4 The role of lipid rafts to formation of the isolation membrane

As mentioned above, the site of isolation membrane formation continues to be controversial. However, much evidence now suggests that the predominant source in canonical autophagy is the ER-mitochondria contact site (Hamasaki et al., 2013). ER-mitochondria contact sites (which can be biochemically isolated as the mitochondrial associated membrane (MAM) fraction) have been demonstrated to be critical for cellular processes such as calcium homeostasis, mitochondrial functions and lipid synthesis and transport (Vance, 1990, Vance, 2014, Levine, 2004). There is some evidence that detergent resistant membranes (containing lipid rafts) can determine the localisation of sigma-1 receptors to the ER-mitochondrial junction (Hayashi and

Fujimoto, 2010). In addition, previous work from our group has detected ULK1 in detergent resistant membrane fractions (Chan et al., 2009). Therefore, from the accumulating evidence, it was hypothesised that the ULK1 complex may translocate to lipid rafts which would participate in proper translocation to autophagosome assembly sites on ER-mitochondrial contacts.

The follow-on work in this thesis has shown that overexpressed ULK1 EAT can bind to these detergent-resistant cholesterol-rich membranes (lipid rafts). The findings provide further evidence that ULK1 EAT membrane binding was resistant to detergent extraction, unlike other autophagic proteins such as lipidated LC3-II. Deletion of the C-terminal 66 amino acid residues of ULK1 EAT was not sufficient to completely disrupt binding to detergent resistant membranes although interactions were dramatically weakened. However, deletion of just the C-terminal 50 residues did not largely disrupt binding to the lipid raft fraction suggesting that the 5^{th} and 6^{th} α helices of MIT2 are not involved.

Interestingly, other studies have suggested association between autophagy factors and lipid rafts. Recently, the direct molecular associated of the ganglioside GD3 (acidic glycophospholipid) with key autophagic proteins WIPI-1 and AMBRA1 has been reported (Garofalo et al., 2016). This interaction supported their model in which autophagic stimulation would generated a sphingolipid lipid raft scaffold on the ER where early autophagy related proteins are further recruited. Furthermore, Beclin1 has also been found to be recruited onto lipid rafts on the plasma membrane in response to external stress such as amyloid β_{42} leading to further activation of PI3K and generation of PI3P (Nah et al., 2013). In these experiments, it was possible to detect association of exogenous WIPI-1 and endogenous Beclin-1 in detergent

resistant membranes. However, this binding was not stimulated, at least following short term amino acid starvation, so it still has to be determined how binding to lipid rafts might be regulated in our cell systems.

4.7.5 Identification of a novel ULK1/2 interacting protein, Erlin-2

As an alternate approach to understand function of the EAT, work from a collaborating laboratory aimed at finding novel binding proteins via biochemical pull-downs followed by protein identification through mass spectrometry. One candidate that came from this work was ER lipid raft-associated protein 2 (Erlin-2) (data not shown) (Browman et al., 2006). Previous work has shown a role for Erlin-2 in mediating its physiological function in inositol 1,4,5-trisphosphate (IP3) signalling by mediating ER-associated degradation of activated IP3 receptors (Pierce et al., 2009).

Based on this biochemical work carried out on lipid raft binding, it was intriguing to further explore this novel ULK1-binding protein. In my work, Erlin-2 clearly associated exclusively with the lipid raft fraction. I could confirm clear binding between Erlin-2 and the EAT domain of either ULK1 or ULK2. Furthermore, my initial work suggests that ULK1 may phosphorylate Erlin-2 based on gel mobility shifts and this potential phosphorylation was not observed with ULK2. The next major question would be to investigate what is the functional significance of this interaction. The predicted topology of Erlin-2 raises some intriguing questions. Erlin-2 is understood to be a transmembrane protein with only three residues found on the cytoplasmic face of the ER. Although numerous studies have demonstrated that C-terminal tagging of erlin-2 results in correct subcellular localisation and insertion into the ER membrane (Browman et al., 2006), (Zhang et al., 2015), further work must be carried out to determine if N-terminal tagging of erlin-2 (as utilised within this thesis) results in the

correct membrane insertion also. Additionally, if the majority of the Erlin-2 is facing buried the ER lumen (residues 25-339), this leads to the question of how Erlin-2 can interact with ULK1. Either overexpressed ULK1 proteins are entering the ER or alternative Erlin-2 protein population with interaction domains facing the cytosol are being expressed. Further studies would be required to elucidate that ULK1 is phosphorylating Erlin-2. In addition, it remains unclear if Erlin-2 importantly is required for autophagy.

Overall, the work within this chapter has led to several main conclusions. Bioinformatic approaches have suggested that the ULK1 EAT domain shows strong conservation of helical structure, similar to other vertebrate and yeast Atg1 EAT domains. The 3D fold of the mammalian EAT might resemble that documented for yeast, but this remains to be shown experimentally. Further work through this chapter has demonstrated that the ULK1 EAT domain contains a membrane binding region that is critical for a normal autophagic nutrient-dependent response. Interestingly, evidence has been provided that the ULK1 EAT domain binds to detergent resistant membranes. These cholesterol rich regions, known as lipid rafts can play several physiological roles including signal transduction. Interestingly, I have also investigated a novel ULK1 EAT domain binding protein, Erlin-2. Although the precise function of this interaction is still unresolved, my data suggest that the lipid raft protein Erlin-2 can potentially be phosphorylated in a ULK1 specific manner. Therefore, in combination with previous studies, my data provides further evidence for a novel potential role of lipid rafts in the formation of the IM during autophagy.

Chapter 5: General Discussion

5.0 General Discussion

The overall theme of my thesis has been to understand how ULK1 functions during autophagy. The first half of my results focused on the molecular roles of the ULK1/2 complex for nutrient sensitive autophagic signalling. The second half of my work aimed to dissect roles for sub-regions of the critical ULK1 C-terminal regulatory domain. The underlying idea is that progress in the fundamental mechanisms of ULK1 will contribute towards the development of important clinical applications of autophagy targeting.

Importance of autophagy in normal physiology and disease

Autophagy is a highly conserved catabolic pathway that is present in almost all eukaryotic cells under normal physiological conditions. It is well reported that cells with an autophagy deficiency display accumulated levels of obsolete ubiquitinated proteins and damaged mitochondria leading to cell toxicity (Mizushima, 2007) (Munch et al., 2014) . Therefore, autophagy primarily acts a key regulator in cellular homeostasis by maintaining normal cellular protein housekeeping and the maintenance of a functional healthy mitochondria pool. It is fundamental to understand how normal autophagy levels are modulated (in the normal basal state), and further activated in response to normal stress conditions encountered during different physiological circumstances. Over the last decade, the link between autophagy and a range of prevalent diseases has been extensively established. To date, the most prominent biomedical areas linked with autophagy function have been cancer, neurodegenerative diseases (such as Alzheimers, Parkinsons and Huntingtons), type 2 diabetes, and microbial (bacteria and viral) infection (Ravikumar

et al., 2010) (Jiang and Mizushima, 2014). In many cases, autophagy generally promotes cell health, cytoplasmic quality control and maintains cell metabolism. Xenophagy, as a form of cell autonomous innate immunity, fights off and suppresses bacterial infection. Neuronal and cardiomyocyte longevity is maintained by autophagy. In maintaining underlying cell health, autophagy is widely accepted to contribute to organismal anti-ageing. Thus, under all these contexts, there is rationale for a means of activating beneficial autophagy.

ULK1/2 as targets for novel therapeutics

Currently, a major challenge in the autophagy field is the development of selective and potent autophagy pharmacological modulators. One set of current clinical studies have focused on the inhibitors, chloroquine and hydroxychloroquine, in combination with other anti-cancer therapies e.g MTOR inhibitors (Rangwala et al., 2014). One limitation to the targeting of the lysosome is that this degradative organelle is downstream of several membrane trafficking routes (such as endocytosis, receptor internalisation) and, as we now better appreciate, MTORC1-dependent nutrient sensing. Multiple diseases are caused by lysosomal dysfunction, which leads to symptoms such as kidney failure, mental deterioration and inability to coordinate voluntary movements. Generation of alternative therapies that selectively target the autophagic signalling machinery could improve drug efficacies and result in fewer unwanted side effects. Over the recent years, several specific Vps34 inhibitors have been isolated (Ronan et al., 2014) (Dowdle et al., 2014) (Bago et al., 2014) (Pasquier et al., 2015). These inhibitors have been reported to be more potent for autophagy inhibition, which has supported their attractiveness as good pharmacological tools. However, several of these still show unwanted secondary effects by affecting other

Vps34-dependent roles such as the endocytosis pathway and disruption of vesicle trafficking of late endosomes to lysosomal compartments (Ronan et al., 2014) (Pasquier et al., 2015).

A promising target for therapeutic intervention is the ULK1 autophagy complex. ULK1 is the best appreciated Serine/Threonine protein kinase found within the core autophagy machinery (apart from Vps15/p150). Furthermore, Atg1/ULK1 is well established to perform essential kinase-dependent signalling functions near the top of the autophagy regulatory apex in all eukaryotic cells. The ULK1 complex is also a critical dynamic signalling node integrating nutrient dependent cues from the master regulators MTORC1 and AMPK.

Essential roles for ULK1 and ULK2 in nutrient-sensitive autophagy

In yeast, *Dictyostelium*, *C. elegans* and *Drosophila*, only one Atg1 homolog in each species has been characterised. Mammalian cells have several Atg1 homologs, the ULK family of proteins, and of these ULK1 and ULK2 are the most similar by sequence. The functional roles and redundancy has been unclear. Our laboratory originally identified that RNAi knockdown of ULK1 produced strong inhibitory effects on autophagy (Chan et al., 2007). Clear inhibition of autophagy by ULK1 knockdown has been widely reported in a range of cell lines suggesting that ULK1 is the primary autophagy regulator in mammalian cells.

In contrast, from animal knockout approaches, it has been observed that ULK1 deficient mice are born with no abnormal phenotype and only display minor autophagy defects (Kundu et al., 2008). The defects that have been observed involve impaired mitochondria removal during erythropoiesis (Kundu et al., 2008). Similarly

ULK2 KO mice are also born with a normal phenotype and show typical autophagy (Lee and Tournier, 2011). These observations suggest that *in vivo*, ULK1 and ULK2 are functionally redundant, in contrast with RNAi data. Interestingly, ULK1/2 DKO mice have been subsequently reported to show embryonic lethality, consistent with strong phenotypes only with double loss of ULK1 and ULK2. Isolated MEF from these mice showed impaired autophagy as assessed during amino acid starvation (Cheong et al., 2011). Furthermore, RNAi depletion of ULK1/2 led to the accumulation of atypical mitochondria with reduced membrane potential (Egan et al., 2011). Therefore, many lines of data support the conclusion that ULK1 and ULK2 have functionally redundant roles during nutrient sensitive autophagy *in vivo*.

Before the initiation of my thesis work, previous efforts from our laboratory and collaborators were also aimed at understanding the *in vivo* functional roles of ULK1 and ULK2. This work generated a ULK1 deficient line from genetrap embryonic stem cells, which resulted in no clear phenotype. Following on, the ULK1 KO mice were interbred with a ULK2 KO mouse line that also did not show a strong phenotype (Lee and Tournier, 2011). This ULK1 x ULK2 KO cross failed to show live DKO mice at weaning age, consistent with embryonic or early post-natal lethality only when both ULK1 and ULK2 were lost. My thesis commenced with the characterisation of MEF derived from these mice.

My work demonstrated that our single ULK1 or ULK2 KO MEF lines displayed only mild block in starvation induced autophagy while ULK1/2 DKO very strongly blocked the amino acid starvation response. Thus, trends of *in vivo* survival functional redundancy were retained and reflected in the amino acid starvation autophagy responses of the MEFs. In addition, Atg13 knockdown in MEF showed a similar extent of autophagy

block compared to ULK1/2 DKO, indicating that loss of this single subunit, which has no other functional homologs in mammalian cells, was sufficient to block the complex (McAlpine et al., 2013). Further work of the single and DKO MEF systems generated here could help clarify the extent of overlapping vs. isoform-specific functions of ULK1 and ULK2, as has been suggested in certain contexts such as lipid metabolism in adipocytes (Ro et al., 2013).

Glucose starvation inhibits autophagic flux

A major issue in my work has been the regulation of autophagy by amino acid vs glucose starvation. There were several reasons for this. ULK1 was reported to be phosphorylated by MTORC1 and AMPK on distinct sites suggesting that ULK1 could integrate different signals from amino acid vs. glucose sensing pathways (Egan et al., 2011) (Kim et al., 2011). Secondly, Cheong and colleagues reported findings of a potential ULK1/2-independent pathway for regulation of autophagy following glucose starvation for 24h (using a ULK1/2 DKO MEF model generated in their group) (Cheong et al., 2011). In my work characterising the autophagic and AMPK energy sensing pathways, in both MEF and HEK293 cell models, glucose withdrawal produced a distinct atypical type of autophagy response. As a result of initial unexpected findings, I examined these differences in more detail. Interestingly, in conjunction with lysosomal inhibitors, it was observed that glucose starvation did not strongly activate proper autophagic flux (unlike the amino acid starvation response). Also, the mild effects of glucose starvation were not blocked by ULK1/2 DKO, similar to other reports (Cheong et al., 2011).

A significant conclusion from my current study is that glucose starvation fails to promote canonical autophagy activation. Through examination of autophagy during glucose starvation, it has become clear that withdrawal of glucose is not able to promote the generation of autophagosomes, for example, as detected via recruitment of ULK1 as a very early marker and p62 as a later stage marker of formed cargo-containing autophagosomes. In collaboration, we also observed that following prolonged (overnight) glucose starvation, generation of PI3P and recruitment of WIPI-2 were not observed in MEF (McAlpine et al., 2013). Our speculation is that accumulation of LC3 due to a block in autophagic flux may have led others to conclude that glucose withdrawal was a slow but positive autophagic stimulator. One possibility is that glucose starvation was inhibiting the lysosome. The v-ATPase assembly and trafficking has been documented to be dependent on glucose availability in yeast and mammalian cells (Sautin et al., 2005). As such, glucose starvation would be expected to disrupt acidification of the lysosome and lead to LC3 accumulation. This may explain why glucose starvation effects on LC3 were not further pronounced with addition of the lysosomal inhibitor bafilomycin. In summary, my data from the chapter 3 show that glucose withdrawal cannot be taken to be a predominant activating stimulus for autophagy (e.g. via the proposed AMPK-ULK1 pathway) in mammalian cells.

The ULK1 EAT domain plays a key role in autophagic membrane binding during autophagosome biogenesis

In addition to the essential kinase-dependent roles of ULK1, recent publications have also proposed additional conserved structural scaffolding roles. These findings have been based on structural studies of the homologous yeast Atg1 system (Ragusa et al.,

2012). This pioneering study delved into the lipid binding activity of the yeast Atg1 EAT domain, reporting that the domain alone is capable of not only binding to membranes, but also of tethering of the membranes. Given the prominent role of ULK1/2 proteins, a long-standing interest of the laboratory has been the domain functional mapping of this kinase. Interestingly, earlier publications within our group focused on kinase function and also of the C-terminal conserved EAT domain (Chan et al., 2007) (Chan et al., 2009). The EAT domain has been of particular interest since this region directs several key regulatory functions, such as the binding of co-factors Atg13 and FIP200, as well as interaction with forming autophagy membranes (Chan et al., 2009).

Recently there has been a series of structural elucidations of the Atg1 EAT in complex with binding partner Atg13 (Stjepanovic et al., 2014) (Fujioka et al., 2014, Kofinger et al., 2015). Since this relatively small domain of the protein carries out several distinct biochemical functions, we were interested in further understanding the roles of precise regions, which might help design alternative strategies for targeting ULK1 via non-kinase methods to block autophagy.

Initially, the work in chapter 4 of this thesis studied the physical properties and structural features of the EAT domain using several basic bioinformatic tools. As the crystal structure of the mammalian ULK1 and EAT domains have yet to be elucidated, it was important to explore computational methods as an initial way to gain further insight into the domains structure and potential function. Overall, from my predictive modelling, the mammalian ULK1 shares several structural similarities to the yeast Atg1, including the characteristic α-helical structure with two potential triple helix bundles. This suggests a potential conserved functional overlap. One limitation to

these findings is that the I-TASSER threading algorithm utilises the crystallised Atg1-Atg13 structures as the highest scoring templates and will therefore contribute overall to the predicted structure. However, the bioinformatic approach led to the identification of several conserved regions with potential functional roles which I explored further.

To more clearly understand the function of the mammalian EAT, I aimed to better map regions that bound membranes, given the opportunity to relate this with structural models. Previous experiments from our group have already determined that the C-terminal 50 residues, which corresponds to the 5^{th} and 6^{th} α helices of MIT2, did not contain key membrane interaction sites (Chan et al., 2009). Surprisingly, further deletion experiments indicated that ULK1 EAT domain lacking α3-6 helices (ULK1 924) still associated strongly to crude membrane fractions. My data thus suggests that similar sub-portions of the MIT1 are sufficient to bind membranes and Atg13 in cells, which raises questions as to how much of the predicted three helix bundle of MIT1 is required for function.

In parallel with these membrane binding studies, several reports have displayed some evidence that detergent resistant membranes (containing lipid rafts) can determine the localisation of sigma-1 receptors to the ER-mitochondrial junction (Hayashi and Fujimoto, 2010). Interestingly, previous work from our group has detected ULK1 in detergent resistant membrane fractions (Chan et al., 2009). My findings provide further evidence that ULK1 EAT membrane binding is resistant to detergent extraction, unlike other autophagic proteins such as lipidated LC3-II. Deletion of the C-terminal 66 amino acid residues of ULK1 EAT was not sufficient to completely disrupt binding to detergent resistant membranes although interactions were

dramatically weakened. My studies have also shown that deletion of the α5-6 helices of MIT2 did not disrupt raft binding. Therefore, the accumulating evidence suggests that the ULK1 complex may translocate to specialised lipid raft domains on ER-mitochondrial contacts that could acts as specialised platforms for autophagic signal transduction and proper translocation to autophagosome assembly sites.

In support of this theory, our lab, in collaboration with S. Tooze (Cancer Research, London), identified ER resident protein, Erlin-2, as a ULK1 EAT domain interacting protein and putative substrate. This thesis shows, for the first time, clear binding between Erlin-2 and the EAT domain of either ULK1 or ULK2. Furthermore, my initial work suggests that ULK1 may phosphorylate Erlin-2 based on gel mobility shifts. This potential phosphorylation was not observed with ULK2 or kinase inactive ULK1. Despite these intriguing findings, the significance of ULK1 mediated phosphorylation of Erlin-2 remains to be determined and future work could confirm this phosphorylation. Other interesting questions can also be raised- Is Erlin-2 required for autophagic activity? Do these proteins localise to the ER/mitochondria contact points, ER exit sites or even the ERGIC?

Summary

The work presented in this thesis highlights key differential autophagy responses between amino acid vs glucose deprivation. Considerable data has been put forward to warrant a reconsideration of the reported role of glucose withdrawal in autophagy activation. Furthermore, I have displayed new insights into ULK1 and EAT localisation and function during autophagosome biogenesis. As previously stated ULK1 kinase inhibition offers an exciting autophagy specific approach which may be utilised in the development of novel strategies for several disease therapies.

During the writing of this thesis, several reports on ULK1 kinase inhibitors have been published. One initial study, identified the crystal structure of the ULK1 kinase domain bound in complex to a variety of kinase inhibitors (Lazarus et al., 2015). Unfortunately the inhibitors used within this study are unsuitable for investigation in any cell based assays due to poor specificity that leads to several off target effects (Lazarus et al., 2015). Since then, two further small molecule ULK1/2 kinase inhibitors have been reported (MRT67307 and MRT68921) which can potently inhibit these kinases in vitro (Petherick et al., 2015). This study also acts as a proof of principle displaying that pharmacological ULK1 kinase inhibition can block autophagy, which highlights this as a viable target for disease therapies.

The use of ULK1 kinase inhibitors in combination with other anti-cancer therapies may also be an effective strategy. Shaw and colleagues recently reported another small molecule ULK1 kinase inhibitor SBI-0206965 which was highly selective and which, interestingly, has been shown to act in synergy with MTOR inhibitors to convert tumour cells from a cytostatic to a cytotoxic state (Egan et al., 2015).

Overall, the findings contained within this thesis further contribute to the understanding of the role and function of ULK1 during activation of nutrient sensitive autophagy pathways. However, further studies still need to be carried out to fully elucidate the finer molecular details of ULK1 regulation and signalling. This will lead to a rapid progress in the development of new potential autophagy targeted therapeutics for use in specific clinical or disease settings.

Chapter 6: Bibliography

6.0 Bibliography

ALERS, S., LOFFLER, A. S., WESSELBORG, S. & STORK, B. 2012. Role of AMPK-mTOR-Ulk1/2 in the regulation of autophagy: cross talk, shortcuts, and feedbacks. *Mol Cell Biol,* 32**,** 2-11.

AXE, E. L., WALKER, S. A., MANIFAVA, M., CHANDRA, P., RODERICK, H. L., HABERMANN, A., GRIFFITHS, G. & KTISTAKIS, N. T. 2008. Autophagosome formation from membrane compartments enriched in phosphatidylinositol 3-phosphate and dynamically connected to the endoplasmic reticulum. *J Cell Biol,* 182**,** 685-701.

BACH, M., LARANCE, M., JAMES, D. E. & RAMM, G. 2011. The serine/threonine kinase ULK1 is a target of multiple phosphorylation events. *Biochem J,* 440**,** 283-91.

BAEHRECKE, E. H. 2005. Autophagy: dual roles in life and death? *Nat Rev Mol Cell Biol,* 6**,** 505-10.

BAR-PELED, L., CHANTRANUPONG, L., CHERNIACK, A. D., CHEN, W. W., OTTINA, K. A., GRABINER, B. C., SPEAR, E. D., CARTER, S. L., MEYERSON, M. & SABATINI, D. M. 2013. A Tumor suppressor complex with GAP activity for the Rag GTPases that signal amino acid sufficiency to mTORC1. *Science,* 340**,** 1100-6.

BAR-PELED, L., SCHWEITZER, L. D., ZONCU, R. & SABATINI, D. M. 2012. Ragulator is a GEF for the rag GTPases that signal amino acid levels to mTORC1. *Cell,* 150**,** 1196-208.

BARTH, S., GLICK, D. & MACLEOD, K. F. 2010. Autophagy: assays and artifacts. *J Pathol,* 221**,** 117-24.

BARYLKO, B., MAO, Y. S., WLODARSKI, P., JUNG, G., BINNS, D. D., SUN, H. Q., YIN, H. L. & ALBANESI, J. P. 2009. Palmitoylation controls the catalytic activity and subcellular distribution of phosphatidylinositol 4-kinase II{alpha}. *J Biol Chem,* 284**,** 9994-10003.

BJORKOY, G., LAMARK, T., BRECH, A., OUTZEN, H., PERANDER, M., OVERVATN, A., STENMARK, H. & JOHANSEN, T. 2005. p62/SQSTM1 forms protein aggregates degraded by autophagy and has a protective effect on huntingtin-induced cell death. *J Cell Biol,* 171**,** 603-14.

BLOMMAART, E. F., KRAUSE, U., SCHELLENS, J. P., VREELING-SINDELAROVA, H. & MEIJER, A. J. 1997. The phosphatidylinositol 3-kinase inhibitors wortmannin and LY294002 inhibit autophagy in isolated rat hepatocytes. *Eur J Biochem,* 243**,** 240-6.

BONFILS, G., JAQUENOUD, M., BONTRON, S., OSTROWICZ, C., UNGERMANN, C. & DE VIRGILIO, C. 2012. Leucyl-tRNA synthetase controls TORC1 via the EGO complex. *Mol Cell,* 46**,** 105-10.

BRANDIZZI, F. & BARLOWE, C. 2013. Organization of the ER-Golgi interface for membrane traffic control. *Nat Rev Mol Cell Biol,* 14**,** 382-92.

BRECH, A., AHLQUIST, T., LOTHE, R. A. & STENMARK, H. 2009. Autophagy in tumour suppression and promotion. *Mol Oncol,* 3**,** 366-75.

BROWMAN, D. T., RESEK, M. E., ZAJCHOWSKI, L. D. & ROBBINS, S. M. 2006. Erlin-1 and erlin-2 are novel members of the prohibitin family of proteins that define lipid-raft-like domains of the ER. *J Cell Sci,* 119**,** 3149-60.

BRYANT, N. J. & STEVENS, T. H. 1998. Vacuole biogenesis in Saccharomyces cerevisiae: protein transport pathways to the yeast vacuole. *Microbiol Mol Biol Rev,* 62**,** 230-47.

BURMAN, C. & KTISTAKIS, N. T. 2010. Regulation of autophagy by phosphatidylinositol 3-phosphate. *FEBS Lett,* 584**,** 1302-12.

CHAN, E. Y. 2012. Regulation and function of uncoordinated-51 like kinase proteins. *Antioxid Redox Signal,* 17**,** 775-85.

CHAN, E. Y., KIR, S. & TOOZE, S. A. 2007. siRNA screening of the kinome identifies ULK1 as a multidomain modulator of autophagy. *J Biol Chem,* 282**,** 25464-74.

CHAN, E. Y., LONGATTI, A., MCKNIGHT, N. C. & TOOZE, S. A. 2009. Kinase-inactivated ULK proteins inhibit autophagy via their conserved C-terminal domains using an Atg13-independent mechanism. *Mol Cell Biol,* 29**,** 157-71.

CHANTRANUPONG, L., SCARIA, S. M., SAXTON, R. A., GYGI, M. P., SHEN, K., WYANT, G. A., WANG, T., HARPER, J. W., GYGI, S. P. & SABATINI, D. M. 2016. The CASTOR Proteins Are Arginine Sensors for the mTORC1 Pathway. *Cell,* 165**,** 153-64.

CHANTRANUPONG, L., WOLFSON, R. L., OROZCO, J. M., SAXTON, R. A., SCARIA, S. M., BAR-PELED, L., SPOONER, E., ISASA, M., GYGI, S. P. & SABATINI, D. M. 2014. The Sestrins interact with GATOR2 to negatively regulate the amino-acid-sensing pathway upstream of mTORC1. *Cell Rep,* 9**,** 1-8.

CHEN, J., ZHENG, X. F., BROWN, E. J. & SCHREIBER, S. L. 1995. Identification of an 11-kDa FKBP12-rapamycin-binding domain within the 289-kDa FKBP12-rapamycin-associated protein and characterization of a critical serine residue. *Proc Natl Acad Sci U S A,* 92**,** 4947-51.

CHEONG, H., LINDSTEN, T., WU, J., LU, C. & THOMPSON, C. B. 2011. Ammonia-induced autophagy is independent of ULK1/ULK2 kinases. *Proc Natl Acad Sci U S A,* 108**,** 11121-6.

CHEONG, H., NAIR, U., GENG, J. & KLIONSKY, D. J. 2008. The Atg1 kinase complex is involved in the regulation of protein recruitment to initiate sequestering vesicle formation for nonspecific autophagy in Saccharomyces cerevisiae. *Mol Biol Cell,* 19**,** 668-81.

CHEONG, H., YORIMITSU, T., REGGIORI, F., LEGAKIS, J. E., WANG, C. W. & KLIONSKY, D. J. 2005. Atg17 regulates the magnitude of the autophagic response. *Mol Biol Cell,* 16**,** 3438-53.

CHIANG, H. L. & DICE, J. F. 1988. Peptide sequences that target proteins for enhanced degradation during serum withdrawal. *J Biol Chem,* 263**,** 6797-805.

CHIANG, H. L., TERLECKY, S. R., PLANT, C. P. & DICE, J. F. 1989. A role for a 70-kilodalton heat shock protein in lysosomal degradation of intracellular proteins. *Science,* 246**,** 382-5.

CODOGNO, P., MEHRPOUR, M. & PROIKAS-CEZANNE, T. 2012. Canonical and non-canonical autophagy: variations on a common theme of self-eating? *Nat Rev Mol Cell Biol,* 13**,** 7-12.

CUERVO, A. M. & DICE, J. F. 2000. Regulation of lamp2a levels in the lysosomal membrane. *Traffic,* 1**,** 570-83.

DE DUVE, C. 1963. The lysosome. *Sci Am,* 208**,** 64-72.

DEGENHARDT, K., MATHEW, R., BEAUDOIN, B., BRAY, K., ANDERSON, D., CHEN, G., MUKHERJEE, C., SHI, Y., GELINAS, C., FAN, Y., NELSON, D. A., JIN, S. & WHITE, E. 2006. Autophagy promotes tumor cell survival and restricts necrosis, inflammation, and tumorigenesis. *Cancer Cell,* 10**,** 51-64.

DEVEREAUX, K., DALL'ARMI, C., ALCAZAR-ROMAN, A., OGASAWARA, Y., ZHOU, X., WANG, F., YAMAMOTO, A., DE CAMILLI, P. & DI PAOLO, G. 2013. Regulation of mammalian autophagy by class II and III PI 3-kinases through PI3P synthesis. *PLoS One,* 8**,** e76405.

DI BARTOLOMEO, S., CORAZZARI, M., NAZIO, F., OLIVERIO, S., LISI, G., ANTONIOLI, M., PAGLIARINI, V., MATTEONI, S., FUOCO, C., GIUNTA, L., D'AMELIO, M., NARDACCI, R., ROMAGNOLI, A., PIACENTINI, M., CECCONI, F. & FIMIA, G. M. 2010. The dynamic interaction of AMBRA1 with the dynein motor complex regulates mammalian autophagy. *J Cell Biol,* 191**,** 155-68.

DIBBLE, C. C. & CANTLEY, L. C. 2015. Regulation of mTORC1 by PI3K signaling. *Trends Cell Biol,* 25**,** 545-55.

DOOLEY, H. C., RAZI, M., POLSON, H. E., GIRARDIN, S. E., WILSON, M. I. & TOOZE, S. A. 2014. WIPI2 links LC3 conjugation with PI3P, autophagosome formation, and pathogen clearance by recruiting Atg12-5-16L1. *Mol Cell,* 55**,** 238-52.

DOOLEY, H. C., WILSON, M. I. & TOOZE, S. A. 2015. WIPI2B links PtdIns3P to LC3 lipidation through binding ATG16L1. *Autophagy,* 11**,** 190-1.

DRIESSEN, S., BERLETH, N., FRIESEN, O., LOFFLER, A. S., BOHLER, P., HIEKE, N., STUHLDREIER, F., PETER, C., SCHINK, K. O., SCHULTZ, S. W., STENMARK, H., HOLLAND, P., SIMONSEN, A., WESSELBORG, S. & STORK, B. 2015. Deubiquitinase inhibition by WP1130 leads to ULK1 aggregation and blockade of autophagy. *Autophagy,* 11**,** 1458-70.

DUBOULOZ, F., DELOCHE, O., WANKE, V., CAMERONI, E. & DE VIRGILIO, C. 2005. The TOR and EGO protein complexes orchestrate microautophagy in yeast. *Mol Cell,* 19**,** 15-26.

DUNLOP, E. A., HUNT, D. K., ACOSTA-JAQUEZ, H. A., FINGAR, D. C. & TEE, A. R. 2011. ULK1 inhibits mTORC1 signaling, promotes multisite Raptor phosphorylation and hinders substrate binding. *Autophagy,* 7**,** 737-47.

DUNN, W. A., JR. 1990. Studies on the mechanisms of autophagy: formation of the autophagic vacuole. *J Cell Biol,* 110**,** 1923-33.

EGAN, D. F., CHUN, M. G., VAMOS, M., ZOU, H., RONG, J., MILLER, C. J., LOU, H. J., RAVEENDRA-PANICKAR, D., YANG, C. C., SHEFFLER, D. J., TERIETE, P., ASARA, J. M., TURK, B. E., COSFORD, N. D. & SHAW, R. J. 2015. Small Molecule Inhibition of the Autophagy Kinase ULK1 and Identification of ULK1 Substrates. *Mol Cell,* 59**,** 285-97.

EGAN, D. F., SHACKELFORD, D. B., MIHAYLOVA, M. M., GELINO, S., KOHNZ, R. A., MAIR, W., VASQUEZ, D. S., JOSHI, A., GWINN, D. M., TAYLOR, R., ASARA, J. M., FITZPATRICK, J., DILLIN, A., VIOLLET, B., KUNDU, M., HANSEN, M. & SHAW, R. J. 2011. Phosphorylation of ULK1 (hATG1) by AMP-activated protein kinase connects energy sensing to mitophagy. *Science,* 331**,** 456-61.

ERLICH, S., MIZRACHY, L., SEGEV, O., LINDENBOIM, L., ZMIRA, O., ADI-HAREL, S., HIRSCH, J. A., STEIN, R. & PINKAS-KRAMARSKI, R. 2007. Differential interactions between Beclin 1 and Bcl-2 family members. *Autophagy,* 3**,** 561-8.

FADER, C. M., SANCHEZ, D. G., MESTRE, M. B. & COLOMBO, M. I. 2009. TI-VAMP/VAMP7 and VAMP3/cellubrevin: two v-SNARE proteins involved in specific steps of the autophagy/multivesicular body pathways. *Biochim Biophys Acta,* 1793**,** 1901-16.

FASS, E., SHVETS, E., DEGANI, I., HIRSCHBERG, K. & ELAZAR, Z. 2006. Microtubules support production of starvation-induced autophagosomes but not their targeting and fusion with lysosomes. *J Biol Chem,* 281**,** 36303-16.

FINGAR, D. C., RICHARDSON, C. J., TEE, A. R., CHEATHAM, L., TSOU, C. & BLENIS, J. 2004. mTOR controls cell cycle progression through its cell growth effectors S6K1 and 4E-BP1/eukaryotic translation initiation factor 4E. *Mol Cell Biol,* 24**,** 200-16.

FRAKE, R. A., RICKETTS, T., MENZIES, F. M. & RUBINSZTEIN, D. C. 2015. Autophagy and neurodegeneration. *J Clin Invest,* 125**,** 65-74.

FUJIOKA, Y., SUZUKI, S. W., YAMAMOTO, H., KONDO-KAKUTA, C., KIMURA, Y., HIRANO, H., AKADA, R., INAGAKI, F., OHSUMI, Y. & NODA, N. N. 2014. Structural basis of starvation-induced assembly of the autophagy initiation complex. *Nat Struct Mol Biol,* 21**,** 513-21.

FUJITA, N., ITOH, T., OMORI, H., FUKUDA, M., NODA, T. & YOSHIMORI, T. 2008. The Atg16L complex specifies the site of LC3 lipidation for membrane biogenesis in autophagy. *Mol Biol Cell,* 19**,** 2092-100.

FURUTA, N., FUJITA, N., NODA, T., YOSHIMORI, T. & AMANO, A. 2010. Combinational soluble N-ethylmaleimide-sensitive factor attachment protein receptor proteins VAMP8 and Vti1b mediate fusion of antimicrobial and canonical autophagosomes with lysosomes. *Mol Biol Cell,* 21**,** 1001-10.

GAMMOH, N., FLOREY, O., OVERHOLTZER, M. & JIANG, X. 2013. Interaction between FIP200 and ATG16L1 distinguishes ULK1 complex-dependent and -independent autophagy. *Nat Struct Mol Biol,* 20**,** 144-9.

GANGLOFF, Y. G., MUELLER, M., DANN, S. G., SVOBODA, P., STICKER, M., SPETZ, J. F., UM, S. H., BROWN, E. J., CEREGHINI, S., THOMAS, G. & KOZMA, S. C. 2004. Disruption of the mouse mTOR gene leads to early postimplantation lethality and prohibits embryonic stem cell development. *Mol Cell Biol,* 24**,** 9508-16.

GANLEY, I. G., LAM DU, H., WANG, J., DING, X., CHEN, S. & JIANG, X. 2009. ULK1.ATG13.FIP200 complex mediates mTOR signaling and is essential for autophagy. *J Biol Chem,* 284**,** 12297-305.

GANLEY, I. G., WONG, P. M., GAMMOH, N. & JIANG, X. 2011. Distinct autophagosomal-lysosomal fusion mechanism revealed by thapsigargin-induced autophagy arrest. *Mol Cell,* 42**,** 731-43.

GAO, X., ZACHAREK, A., SALKOWSKI, A., GRIGNON, D. J., SAKR, W., PORTER, A. T. & HONN, K. V. 1995. Loss of heterozygosity of the BRCA1 and other loci on chromosome 17q in human prostate cancer. *Cancer Res,* 55**,** 1002-5.

GAROFALO, T., MATARRESE, P., MANGANELLI, V., MARCONI, M., TINARI, A., GAMBARDELLA, L., FAGGIONI, A., MISASI, R., SORICE, M. & MALORNI, W. 2016. Evidence for the involvement of lipid rafts localized at the ER-mitochondria associated membranes in autophagosome formation. *Autophagy,* 12**,** 917-35.

GE, L., MELVILLE, D., ZHANG, M. & SCHEKMAN, R. 2013. The ER-Golgi intermediate compartment is a key membrane source for the LC3 lipidation step of autophagosome biogenesis. *Elife,* 2**,** e00947.

GHISLAT, G. & KNECHT, E. 2012. New Ca(2+)-dependent regulators of autophagosome maturation. *Commun Integr Biol,* 5**,** 308-11.

GHISLAT, G., PATRON, M., RIZZUTO, R. & KNECHT, E. 2012. Withdrawal of essential amino acids increases autophagy by a pathway involving Ca2+/calmodulin-dependent kinase kinase-beta (CaMKK-beta). *J Biol Chem,* 287**,** 38625-36.

GRAEF, M., FRIEDMAN, J. R., GRAHAM, C., BABU, M. & NUNNARI, J. 2013. ER exit sites are physical and functional core autophagosome biogenesis components. *Mol Biol Cell,* 24**,** 2918-31.

GUO, J. Y., CHEN, H. Y., MATHEW, R., FAN, J., STROHECKER, A. M., KARSLI-UZUNBAS, G., KAMPHORST, J. J., CHEN, G., LEMONS, J. M., KARANTZA, V., COLLER, H. A., DIPAOLA, R. S., GELINAS, C., RABINOWITZ, J. D. & WHITE, E. 2011. Activated Ras requires autophagy to maintain oxidative metabolism and tumorigenesis. *Genes Dev,* 25**,** 460-70.

GWINN, D. M., SHACKELFORD, D. B., EGAN, D. F., MIHAYLOVA, M. M., MERY, A., VASQUEZ, D. S., TURK, B. E. & SHAW, R. J. 2008. AMPK phosphorylation of raptor mediates a metabolic checkpoint. *Mol Cell,* 30**,** 214-26.

HAMASAKI, M., FURUTA, N., MATSUDA, A., NEZU, A., YAMAMOTO, A., FUJITA, N., OOMORI, H., NODA, T., HARAGUCHI, T., HIRAOKA, Y., AMANO, A. & YOSHIMORI, T. 2013. Autophagosomes form at ER-mitochondria contact sites. *Nature,* 495**,** 389-93.

HAN, J. M., JEONG, S. J., PARK, M. C., KIM, G., KWON, N. H., KIM, H. K., HA, S. H., RYU, S. H. & KIM, S. 2012. Leucyl-tRNA synthetase is an intracellular leucine sensor for the mTORC1-signaling pathway. *Cell,* 149**,** 410-24.

HANKS, S. K. & HUNTER, T. 1995. Protein kinases 6. The eukaryotic protein kinase superfamily: kinase (catalytic) domain structure and classification. *FASEB J,* 9**,** 576-96.

HANKS, S. K., QUINN, A. M. & HUNTER, T. 1988. The protein kinase family: conserved features and deduced phylogeny of the catalytic domains. *Science,* 241**,** 42-52.

HARA, K., YONEZAWA, K., WENG, Q. P., KOZLOWSKI, M. T., BELHAM, C. & AVRUCH, J. 1998. Amino acid sufficiency and mTOR regulate p70 S6 kinase and eIF-4E BP1 through a common effector mechanism. *J Biol Chem,* 273**,** 14484-94.

HARA, T., NAKAMURA, K., MATSUI, M., YAMAMOTO, A., NAKAHARA, Y., SUZUKI-MIGISHIMA, R., YOKOYAMA, M., MISHIMA, K., SAITO, I., OKANO, H. & MIZUSHIMA, N. 2006. Suppression of basal autophagy in neural cells causes neurodegenerative disease in mice. *Nature,* 441**,** 885-9.

HARA, T., TAKAMURA, A., KISHI, C., IEMURA, S., NATSUME, T., GUAN, J. L. & MIZUSHIMA, N. 2008. FIP200, a ULK-interacting protein, is required for autophagosome formation in mammalian cells. *J Cell Biol,* 181**,** 497-510.

HARRIS, T. E. & LAWRENCE, J. C., JR. 2003. TOR signaling. *Sci STKE,* 2003**,** re15.

HAYASHI-NISHINO, M., FUJITA, N., NODA, T., YAMAGUCHI, A., YOSHIMORI, T. & YAMAMOTO, A. 2009. A subdomain of the endoplasmic reticulum forms a cradle for autophagosome formation. *Nat Cell Biol,* 11**,** 1433-7.

HAYASHI, T. & FUJIMOTO, M. 2010. Detergent-resistant microdomains determine the localization of sigma-1 receptors to the endoplasmic reticulum-mitochondria junction. *Mol Pharmacol,* 77**,** 517-28.

HE, C. & LEVINE, B. 2010. The Beclin 1 interactome. *Curr Opin Cell Biol,* 22**,** 140-9.

HONG, S. P., LEIPER, F. C., WOODS, A., CARLING, D. & CARLSON, M. 2003. Activation of yeast Snf1 and mammalian AMP-activated protein kinase by upstream kinases. *Proc Natl Acad Sci U S A,* 100**,** 8839-43.

HOPP, T. P. & WOODS, K. R. 1983. A computer program for predicting protein antigenic determinants. *Mol Immunol,* 20**,** 483-9.

HOSOKAWA, N., HARA, T., KAIZUKA, T., KISHI, C., TAKAMURA, A., MIURA, Y., IEMURA, S., NATSUME, T., TAKEHANA, K., YAMADA, N., GUAN, J. L., OSHIRO, N. & MIZUSHIMA, N. 2009a. Nutrient-dependent mTORC1

association with the ULK1-Atg13-FIP200 complex required for autophagy. *Mol Biol Cell,* 20**,** 1981-91.
HOSOKAWA, N., SASAKI, T., IEMURA, S., NATSUME, T., HARA, T. & MIZUSHIMA, N. 2009b. Atg101, a novel mammalian autophagy protein interacting with Atg13. *Autophagy,* 5**,** 973-9.
HUANG, J. & MANNING, B. D. 2009. A complex interplay between Akt, TSC2 and the two mTOR complexes. *Biochem Soc Trans,* 37**,** 217-22.
HURLEY, J. H. & YANG, D. 2008. MIT domainia. *Dev Cell,* 14**,** 6-8.
HUTCHINS, M. U. & KLIONSKY, D. J. 2001. Vacuolar localization of oligomeric alpha-mannosidase requires the cytoplasm to vacuole targeting and autophagy pathway components in Saccharomyces cerevisiae. *J Biol Chem,* 276**,** 20491-8.
ICHIMURA, Y., KUMANOMIDOU, T., SOU, Y. S., MIZUSHIMA, T., EZAKI, J., UENO, T., KOMINAMI, E., YAMANE, T., TANAKA, K. & KOMATSU, M. 2008. Structural basis for sorting mechanism of p62 in selective autophagy. *J Biol Chem,* 283**,** 22847-57.
INOKI, K., LI, Y., XU, T. & GUAN, K. L. 2003. Rheb GTPase is a direct target of TSC2 GAP activity and regulates mTOR signaling. *Genes Dev,* 17**,** 1829-34.
INOKI, K., LI, Y., ZHU, T., WU, J. & GUAN, K. L. 2002. TSC2 is phosphorylated and inhibited by Akt and suppresses mTOR signalling. *Nat Cell Biol,* 4**,** 648-57.
ITAKURA, E., KISHI-ITAKURA, C., KOYAMA-HONDA, I. & MIZUSHIMA, N. 2012a. Structures containing Atg9A and the ULK1 complex independently target depolarized mitochondria at initial stages of Parkin-mediated mitophagy. *J Cell Sci,* 125**,** 1488-99.
ITAKURA, E., KISHI-ITAKURA, C. & MIZUSHIMA, N. 2012b. The hairpin-type tail-anchored SNARE syntaxin 17 targets to autophagosomes for fusion with endosomes/lysosomes. *Cell,* 151**,** 1256-69.
ITAKURA, E., KISHI, C., INOUE, K. & MIZUSHIMA, N. 2008. Beclin 1 forms two distinct phosphatidylinositol 3-kinase complexes with mammalian Atg14 and UVRAG. *Mol Biol Cell,* 19**,** 5360-72.
ITAKURA, E. & MIZUSHIMA, N. 2010. Characterization of autophagosome formation site by a hierarchical analysis of mammalian Atg proteins. *Autophagy,* 6**,** 764-76.
ITAKURA, E. & MIZUSHIMA, N. 2011. p62 Targeting to the autophagosome formation site requires self-oligomerization but not LC3 binding. *J Cell Biol,* 192**,** 17-27.
ITO, K., HIRAO, A., ARAI, F., TAKUBO, K., MATSUOKA, S., MIYAMOTO, K., OHMURA, M., NAKA, K., HOSOKAWA, K., IKEDA, Y. & SUDA, T. 2006. Reactive oxygen species act through p38 MAPK to limit the lifespan of hematopoietic stem cells. *Nat Med,* 12**,** 446-51.
ITOH, T. & DE CAMILLI, P. 2006. BAR, F-BAR (EFC) and ENTH/ANTH domains in the regulation of membrane-cytosol interfaces and membrane curvature. *Biochim Biophys Acta,* 1761**,** 897-912.
IWAYA, N., TAKASU, H., GODA, N., SHIRAKAWA, M., TANAKA, T., HAMADA, D. & HIROAKI, H. 2013. MIT domain of Vps4 is a Ca2+-dependent phosphoinositide-binding domain. *J Biochem,* 153**,** 473-81.
JACINTO, E., LOEWITH, R., SCHMIDT, A., LIN, S., RUEGG, M. A., HALL, A. & HALL, M. N. 2004. Mammalian TOR complex 2 controls the actin cytoskeleton and is rapamycin insensitive. *Nat Cell Biol,* 6**,** 1122-8.
JAHREISS, L., MENZIES, F. M. & RUBINSZTEIN, D. C. 2008. The itinerary of autophagosomes: from peripheral formation to kiss-and-run fusion with lysosomes. *Traffic,* 9**,** 574-87.

JEWELL, J. L., KIM, Y. C., RUSSELL, R. C., YU, F. X., PARK, H. W., PLOUFFE, S. W., TAGLIABRACCI, V. S. & GUAN, K. L. 2015. Metabolism. Differential regulation of mTORC1 by leucine and glutamine. *Science,* 347**,** 194-8.

JIANG, L., STANEVICH, V., SATYSHUR, K. A., KONG, M., WATKINS, G. R., WADZINSKI, B. E., SENGUPTA, R. & XING, Y. 2013. Structural basis of protein phosphatase 2A stable latency. *Nat Commun,* 4**,** 1699.

JIANG, P. & MIZUSHIMA, N. 2014. Autophagy and human diseases. *Cell Res,* 24**,** 69-79.

JIANG, P., NISHIMURA, T., SAKAMAKI, Y., ITAKURA, E., HATTA, T., NATSUME, T. & MIZUSHIMA, N. 2014. The HOPS complex mediates autophagosome-lysosome fusion through interaction with syntaxin 17. *Mol Biol Cell,* 25**,** 1327-37.

JOO, J. H., DORSEY, F. C., JOSHI, A., HENNESSY-WALTERS, K. M., ROSE, K. L., MCCASTLAIN, K., ZHANG, J., IYENGAR, R., JUNG, C. H., SUEN, D. F., STEEVES, M. A., YANG, C. Y., PRATER, S. M., KIM, D. H., THOMPSON, C. B., YOULE, R. J., NEY, P. A., CLEVELAND, J. L. & KUNDU, M. 2011. Hsp90-Cdc37 chaperone complex regulates Ulk1- and Atg13-mediated mitophagy. *Mol Cell,* 43**,** 572-85.

JUNG, C. H., JUN, C. B., RO, S. H., KIM, Y. M., OTTO, N. M., CAO, J., KUNDU, M. & KIM, D. H. 2009. ULK-Atg13-FIP200 complexes mediate mTOR signaling to the autophagy machinery. *Mol Biol Cell,* 20**,** 1992-2003.

JUNG, C. H., SEO, M., OTTO, N. M. & KIM, D. H. 2011. ULK1 inhibits the kinase activity of mTORC1 and cell proliferation. *Autophagy,* 7**,** 1212-21.

JUNG, J., GENAU, H. M. & BEHRENDS, C. 2015. Amino Acid-Dependent mTORC1 Regulation by the Lysosomal Membrane Protein SLC38A9. *Mol Cell Biol,* 35**,** 2479-94.

KABEYA, Y., MIZUSHIMA, N., UENO, T., YAMAMOTO, A., KIRISAKO, T., NODA, T., KOMINAMI, E., OHSUMI, Y. & YOSHIMORI, T. 2000. LC3, a mammalian homologue of yeast Apg8p, is localized in autophagosome membranes after processing. *EMBO J,* 19**,** 5720-8.

KABEYA, Y., NODA, N. N., FUJIOKA, Y., SUZUKI, K., INAGAKI, F. & OHSUMI, Y. 2009. Characterization of the Atg17-Atg29-Atg31 complex specifically required for starvation-induced autophagy in Saccharomyces cerevisiae. *Biochem Biophys Res Commun,* 389**,** 612-5.

KAIZUKA, T., HARA, T., OSHIRO, N., KIKKAWA, U., YONEZAWA, K., TAKEHANA, K., IEMURA, S., NATSUME, T. & MIZUSHIMA, N. 2010. Tti1 and Tel2 are critical factors in mammalian target of rapamycin complex assembly. *J Biol Chem,* 285**,** 20109-16.

KAMADA, Y., FUNAKOSHI, T., SHINTANI, T., NAGANO, K., OHSUMI, M. & OHSUMI, Y. 2000. Tor-mediated induction of autophagy via an Apg1 protein kinase complex. *J Cell Biol,* 150**,** 1507-13.

KARANASIOS, E., STAPLETON, E., MANIFAVA, M., KAIZUKA, T., MIZUSHIMA, N., WALKER, S. A. & KTISTAKIS, N. T. 2013. Dynamic association of the ULK1 complex with omegasomes during autophagy induction. *J Cell Sci,* 126**,** 5224-38.

KARANASIOS, E., WALKER, S. A., OKKENHAUG, H., MANIFAVA, M., HUMMEL, E., ZIMMERMANN, H., AHMED, Q., DOMART, M. C., COLLINSON, L. & KTISTAKIS, N. T. 2016. Autophagy initiation by ULK complex assembly on ER tubulovesicular regions marked by ATG9 vesicles. *Nat Commun,* 7**,** 12420.

KARSLI-UZUNBAS, G., GUO, J. Y., PRICE, S., TENG, X., LADDHA, S. V., KHOR, S., KALAANY, N. Y., JACKS, T., CHAN, C. S., RABINOWITZ, J. D. & WHITE, E. 2014. Autophagy is required for glucose homeostasis and lung tumor maintenance. *Cancer Discov,* 4**,** 914-27.

KAST, D. J. & DOMINGUEZ, R. 2015. WHAMM links actin assembly via the Arp2/3 complex to autophagy. *Autophagy,* 11**,** 1702-4.
KAUSHIK, S. & CUERVO, A. M. 2012. Chaperone-mediated autophagy: a unique way to enter the lysosome world. *Trends Cell Biol,* 22**,** 407-17.
KIM, E., GORAKSHA-HICKS, P., LI, L., NEUFELD, T. P. & GUAN, K. L. 2008. Regulation of TORC1 by Rag GTPases in nutrient response. *Nat Cell Biol,* 10**,** 935-45.
KIM, I., RODRIGUEZ-ENRIQUEZ, S. & LEMASTERS, J. J. 2007. Selective degradation of mitochondria by mitophagy. *Arch Biochem Biophys,* 462**,** 245-53.
KIM, J., KIM, Y. C., FANG, C., RUSSELL, R. C., KIM, J. H., FAN, W., LIU, R., ZHONG, Q. & GUAN, K. L. 2013. Differential regulation of distinct Vps34 complexes by AMPK in nutrient stress and autophagy. *Cell,* 152**,** 290-303.
KIM, J., KUNDU, M., VIOLLET, B. & GUAN, K. L. 2011. AMPK and mTOR regulate autophagy through direct phosphorylation of Ulk1. *Nat Cell Biol,* 13**,** 132-41.
KIM, Y. C. & GUAN, K. L. 2015. mTOR: a pharmacologic target for autophagy regulation. *J Clin Invest,* 125**,** 25-32.
KIM, Y. M., STONE, M., HWANG, T. H., KIM, Y. G., DUNLEVY, J. R., GRIFFIN, T. J. & KIM, D. H. 2012. SH3BP4 is a negative regulator of amino acid-Rag GTPase-mTORC1 signaling. *Mol Cell,* 46**,** 833-46.
KIMMELMAN, A. C. 2011. The dynamic nature of autophagy in cancer. *Genes Dev,* 25**,** 1999-2010.
KIMURA, S., NODA, T. & YOSHIMORI, T. 2007. Dissection of the autophagosome maturation process by a novel reporter protein, tandem fluorescent-tagged LC3. *Autophagy,* 3**,** 452-60.
KIMURA, S., NODA, T. & YOSHIMORI, T. 2008. Dynein-dependent movement of autophagosomes mediates efficient encounters with lysosomes. *Cell Struct Funct,* 33**,** 109-22.
KIRISAKO, T., ICHIMURA, Y., OKADA, H., KABEYA, Y., MIZUSHIMA, N., YOSHIMORI, T., OHSUMI, M., TAKAO, T., NODA, T. & OHSUMI, Y. 2000. The reversible modification regulates the membrane-binding state of Apg8/Aut7 essential for autophagy and the cytoplasm to vacuole targeting pathway. *J Cell Biol,* 151**,** 263-76.
KLIONSKY, D. J., ABDELMOHSEN, K., ABE, A., ABEDIN, M. J., ABELIOVICH, H., ACEVEDO AROZENA, A., ADACHI, H., ADAMS, C. M., ADAMS, P. D., ADELI, K., ADHIHETTY, P. J., ADLER, S. G., AGAM, G., AGARWAL, R., AGHI, M. K., AGNELLO, M., AGOSTINIS, P., AGUILAR, P. V., AGUIRRE-GHISO, J., AIROLDI, E. M., AIT-SI-ALI, S., AKEMATSU, T., AKPORIAYE, E. T., AL-RUBEAI, M., ALBAICETA, G. M., ALBANESE, C., ALBANI, D., ALBERT, M. L., ALDUDO, J., ALGUL, H., ALIREZAEI, M., ALLOZA, I., ALMASAN, A., ALMONTE-BECERIL, M., ALNEMRI, E. S., ALONSO, C., ALTAN-BONNET, N., ALTIERI, D. C., ALVAREZ, S., ALVAREZ-ERVITI, L., ALVES, S., AMADORO, G., AMANO, A., AMANTINI, C., AMBROSIO, S., AMELIO, I., AMER, A. O., AMESSOU, M., AMON, A., AN, Z., ANANIA, F. A., ANDERSEN, S. U., ANDLEY, U. P., ANDREADI, C. K., ANDRIEU-ABADIE, N., ANEL, A., ANN, D. K., ANOOPKUMAR-DUKIE, S., ANTONIOLI, M., AOKI, H., APOSTOLOVA, N., AQUILA, S., AQUILANO, K., ARAKI, K., ARAMA, E., ARANDA, A., ARAYA, J., ARCARO, A., ARIAS, E., ARIMOTO, H., ARIOSA, A. R., ARMSTRONG, J. L., ARNOULD, T., ARSOV, I., ASANUMA, K., ASKANAS, V., ASSELIN, E., ATARASHI, R., ATHERTON, S. S., ATKIN, J. D., ATTARDI, L. D., AUBERGER, P., AUBURGER, G., AURELIAN, L., AUTELLI, R., AVAGLIANO, L., AVANTAGGIATI, M. L., AVRAHAMI, L., AWALE, S., AZAD, N.,

BACHETTI, T., BACKER, J. M., BAE, D. H., BAE, J. S., BAE, O. N., BAE, S. H., BAEHRECKE, E. H., BAEK, S. H., BAGHDIGUIAN, S., BAGNIEWSKA-ZADWORNA, A., et al. 2016. Guidelines for the use and interpretation of assays for monitoring autophagy (3rd edition). *Autophagy,* 12**,** 1-222.

KLIONSKY, D. J., CUEVA, R. & YAVER, D. S. 1992. Aminopeptidase I of Saccharomyces cerevisiae is localized to the vacuole independent of the secretory pathway. *J Cell Biol,* 119**,** 287-99.

KLIONSKY, D. J., ELAZAR, Z., SEGLEN, P. O. & RUBINSZTEIN, D. C. 2008. Does bafilomycin A1 block the fusion of autophagosomes with lysosomes? *Autophagy,* 4**,** 849-950.

KOFINGER, J., RAGUSA, M. J., LEE, I. H., HUMMER, G. & HURLEY, J. H. 2015. Solution structure of the Atg1 complex: implications for the architecture of the phagophore assembly site. *Structure,* 23**,** 809-18.

KOMATSU, M., WAGURI, S., CHIBA, T., MURATA, S., IWATA, J., TANIDA, I., UENO, T., KOIKE, M., UCHIYAMA, Y., KOMINAMI, E. & TANAKA, K. 2006. Loss of autophagy in the central nervous system causes neurodegeneration in mice. *Nature,* 441**,** 880-4.

KOMATSU, M., WAGURI, S., KOIKE, M., SOU, Y. S., UENO, T., HARA, T., MIZUSHIMA, N., IWATA, J., EZAKI, J., MURATA, S., HAMAZAKI, J., NISHITO, Y., IEMURA, S., NATSUME, T., YANAGAWA, T., UWAYAMA, J., WARABI, E., YOSHIDA, H., ISHII, T., KOBAYASHI, A., YAMAMOTO, M., YUE, Z., UCHIYAMA, Y., KOMINAMI, E. & TANAKA, K. 2007. Homeostatic levels of p62 control cytoplasmic inclusion body formation in autophagy-deficient mice. *Cell,* 131**,** 1149-63.

KOSTA, A., ROISIN-BOUFFAY, C., LUCIANI, M. F., OTTO, G. P., KESSIN, R. H. & GOLSTEIN, P. 2004. Autophagy gene disruption reveals a non-vacuolar cell death pathway in Dictyostelium. *J Biol Chem,* 279**,** 48404-9.

KRICK, R., MUHE, Y., PRICK, T., BREDSCHNEIDER, M., BREMER, S., WENZEL, D., ESKELINEN, E. L. & THUMM, M. 2009. Piecemeal microautophagy of the nucleus: genetic and morphological traits. *Autophagy,* 5**,** 270-2.

KUMA, A., HATANO, M., MATSUI, M., YAMAMOTO, A., NAKAYA, H., YOSHIMORI, T., OHSUMI, Y., TOKUHISA, T. & MIZUSHIMA, N. 2004. The role of autophagy during the early neonatal starvation period. *Nature,* 432**,** 1032-6.

KUMAR, S. & BANSAL, M. 1996. Structural and sequence characteristics of long alpha helices in globular proteins. *Biophys J,* 71**,** 1574-86.

KUNDU, M., LINDSTEN, T., YANG, C. Y., WU, J., ZHAO, F., ZHANG, J., SELAK, M. A., NEY, P. A. & THOMPSON, C. B. 2008. Ulk1 plays a critical role in the autophagic clearance of mitochondria and ribosomes during reticulocyte maturation. *Blood,* 112**,** 1493-502.

KYTE, J. & DOOLITTLE, R. F. 1982. A simple method for displaying the hydropathic character of a protein. *J Mol Biol,* 157**,** 105-32.

LAMB, C. A., YOSHIMORI, T. & TOOZE, S. A. 2013. The autophagosome: origins unknown, biogenesis complex. *Nat Rev Mol Cell Biol,* 14**,** 759-74.

LANG, B., ZHANG, L., JIANG, G., HU, L., LAN, W., ZHAO, L., HUNTER, I., PRUSKI, M., SONG, N. N., HUANG, Y., ZHANG, L., ST CLAIR, D., MCCAIG, C. D. & DING, Y. Q. 2016. Control of cortex development by ULK4, a rare risk gene for mental disorders including schizophrenia. *Sci Rep,* 6**,** 31126.

LANG, M. J., MARTINEZ-MARQUEZ, J. Y., PROSSER, D. C., GANSER, L. R., BUELTO, D., WENDLAND, B. & DUNCAN, M. C. 2014. Glucose starvation

inhibits autophagy via vacuolar hydrolysis and induces plasma membrane internalization by down-regulating recycling. *J Biol Chem,* 289**,** 16736-47.
LAPLANTE, M. & SABATINI, D. M. 2012. mTOR signaling in growth control and disease. *Cell,* 149**,** 274-93.
LAZARUS, M. B., NOVOTNY, C. J. & SHOKAT, K. M. 2015. Structure of the human autophagy initiating kinase ULK1 in complex with potent inhibitors. *ACS Chem Biol,* 10**,** 257-61.
LECKER, S. H., GOLDBERG, A. L. & MITCH, W. E. 2006. Protein degradation by the ubiquitin-proteasome pathway in normal and disease states. *J Am Soc Nephrol,* 17**,** 1807-19.
LEE, B. & RICHARDS, F. M. 1971. The interpretation of protein structures: estimation of static accessibility. *J Mol Biol,* 55**,** 379-400.
LEE, E. J. & TOURNIER, C. 2011. The requirement of uncoordinated 51-like kinase 1 (ULK1) and ULK2 in the regulation of autophagy. *Autophagy,* 7**,** 689-95.
LEE, J. W., PARK, S., TAKAHASHI, Y. & WANG, H. G. 2010a. The association of AMPK with ULK1 regulates autophagy. *PLoS One,* 5**,** e15394.
LEE, J. Y., NAGANO, Y., TAYLOR, J. P., LIM, K. L. & YAO, T. P. 2010b. Disease-causing mutations in parkin impair mitochondrial ubiquitination, aggregation, and HDAC6-dependent mitophagy. *J Cell Biol,* 189**,** 671-9.
LEE, S. B., KIM, S., LEE, J., PARK, J., LEE, G., KIM, Y., KIM, J. M. & CHUNG, J. 2007. ATG1, an autophagy regulator, inhibits cell growth by negatively regulating S6 kinase. *EMBO Rep,* 8**,** 360-5.
LEVINE, B. & KROEMER, G. 2009. Autophagy in aging, disease and death: the true identity of a cell death impostor. *Cell Death Differ,* 16**,** 1-2.
LEVINE, T. 2004. Short-range intracellular trafficking of small molecules across endoplasmic reticulum junctions. *Trends Cell Biol,* 14**,** 483-90.
LIANG, C., FENG, P., KU, B., DOTAN, I., CANAANI, D., OH, B. H. & JUNG, J. U. 2006. Autophagic and tumour suppressor activity of a novel Beclin1-binding protein UVRAG. *Nat Cell Biol,* 8**,** 688-99.
LIANG, X. H., KLEEMAN, L. K., JIANG, H. H., GORDON, G., GOLDMAN, J. E., BERRY, G., HERMAN, B. & LEVINE, B. 1998. Protection against fatal Sindbis virus encephalitis by beclin, a novel Bcl-2-interacting protein. *J Virol,* 72**,** 8586-96.
LILIENBAUM, A. 2013. Relationship between the proteasomal system and autophagy. *Int J Biochem Mol Biol,* 4**,** 1-26.
LIN, S. Y., LI, T. Y., LIU, Q., ZHANG, C., LI, X., CHEN, Y., ZHANG, S. M., LIAN, G., RUAN, K., WANG, Z., ZHANG, C. S., CHIEN, K. Y., WU, J., LI, Q., HAN, J. & LIN, S. C. 2012. GSK3-TIP60-ULK1 signaling pathway links growth factor deprivation to autophagy. *Science,* 336**,** 477-81.
LIU, C. C., LIN, Y. C., CHEN, Y. H., CHEN, C. M., PANG, L. Y., CHEN, H. A., WU, P. R., LIN, M. Y., JIANG, S. T., TSAI, T. F. & CHEN, R. H. 2016. Cul3-KLHL20 Ubiquitin Ligase Governs the Turnover of ULK1 and VPS34 Complexes to Control Autophagy Termination. *Mol Cell,* 61**,** 84-97.
LIU, Y. & LEVINE, B. 2015. Autosis and autophagic cell death: the dark side of autophagy. *Cell Death Differ,* 22**,** 367-76.
LIU, Y., SHOJI-KAWATA, S., SUMPTER, R. M., JR., WEI, Y., GINET, V., ZHANG, L., POSNER, B., TRAN, K. A., GREEN, D. R., XAVIER, R. J., SHAW, S. Y., CLARKE, P. G., PUYAL, J. & LEVINE, B. 2013. Autosis is a Na+,K+-ATPase-regulated form of cell death triggered by autophagy-inducing peptides, starvation, and hypoxia-ischemia. *Proc Natl Acad Sci U S A,* 110**,** 20364-71.
LOFFLER, A. S., ALERS, S., DIETERLE, A. M., KEPPELER, H., FRANZ-WACHTEL, M., KUNDU, M., CAMPBELL, D. G., WESSELBORG, S.,

ALESSI, D. R. & STORK, B. 2011. Ulk1-mediated phosphorylation of AMPK constitutes a negative regulatory feedback loop. *Autophagy,* 7**,** 696-706.
LONG, X., LIN, Y., ORTIZ-VEGA, S., YONEZAWA, K. & AVRUCH, J. 2005. Rheb binds and regulates the mTOR kinase. *Curr Biol,* 15**,** 702-13.
LOVEJOY, B., CHOE, S., CASCIO, D., MCRORIE, D. K., DEGRADO, W. F. & EISENBERG, D. 1993. Crystal structure of a synthetic triple-stranded alpha-helical bundle. *Science,* 259**,** 1288-93.
LU, D., SUN, H. Q., WANG, H., BARYLKO, B., FUKATA, Y., FUKATA, M., ALBANESI, J. P. & YIN, H. L. 2012. Phosphatidylinositol 4-kinase IIalpha is palmitoylated by Golgi-localized palmitoyltransferases in cholesterol-dependent manner. *J Biol Chem,* 287**,** 21856-65.
LYNCH-DAY, M. A., BHANDARI, D., MENON, S., HUANG, J., CAI, H., BARTHOLOMEW, C. R., BRUMELL, J. H., FERRO-NOVICK, S. & KLIONSKY, D. J. 2010. Trs85 directs a Ypt1 GEF, TRAPPIII, to the phagophore to promote autophagy. *Proc Natl Acad Sci U S A,* 107**,** 7811-6.
MACK, H. I., ZHENG, B., ASARA, J. M. & THOMAS, S. M. 2012. AMPK-dependent phosphorylation of ULK1 regulates ATG9 localization. *Autophagy,* 8**,** 1197-214.
MAEHAMA, T. & DIXON, J. E. 1998. The tumor suppressor, PTEN/MMAC1, dephosphorylates the lipid second messenger, phosphatidylinositol 3,4,5-trisphosphate. *J Biol Chem,* 273**,** 13375-8.
MALOVERYAN, A., FINTA, C., OSTERLUND, T. & KOGERMAN, P. 2007. A possible role of mouse Fused (STK36) in Hedgehog signaling and Gli transcription factor regulation. *J Cell Commun Signal,* 1**,** 165-73.
MANNING, B. D. & CANTLEY, L. C. 2007. AKT/PKB signaling: navigating downstream. *Cell,* 129**,** 1261-74.
MARTINA, J. A., CHEN, Y., GUCEK, M. & PUERTOLLANO, R. 2012. MTORC1 functions as a transcriptional regulator of autophagy by preventing nuclear transport of TFEB. *Autophagy,* 8**,** 903-14.
MARTINEZ, J., MALIREDDI, R. K., LU, Q., CUNHA, L. D., PELLETIER, S., GINGRAS, S., ORCHARD, R., GUAN, J. L., TAN, H., PENG, J., KANNEGANTI, T. D., VIRGIN, H. W. & GREEN, D. R. 2015. Molecular characterization of LC3-associated phagocytosis reveals distinct roles for Rubicon, NOX2 and autophagy proteins. *Nat Cell Biol,* 17**,** 893-906.
MATHEW, R., KARANTZA-WADSWORTH, V. & WHITE, E. 2007. Role of autophagy in cancer. *Nat Rev Cancer,* 7**,** 961-7.
MATSUNAGA, K., SAITOH, T., TABATA, K., OMORI, H., SATOH, T., KUROTORI, N., MAEJIMA, I., SHIRAHAMA-NODA, K., ICHIMURA, T., ISOBE, T., AKIRA, S., NODA, T. & YOSHIMORI, T. 2009. Two Beclin 1-binding proteins, Atg14L and Rubicon, reciprocally regulate autophagy at different stages. *Nat Cell Biol,* 11**,** 385-96.
MATSUSHITA, M., SUZUKI, N. N., OBARA, K., FUJIOKA, Y., OHSUMI, Y. & INAGAKI, F. 2007. Structure of Atg5.Atg16, a complex essential for autophagy. *J Biol Chem,* 282**,** 6763-72.
MATSUURA, A., TSUKADA, M., WADA, Y. & OHSUMI, Y. 1997. Apg1p, a novel protein kinase required for the autophagic process in Saccharomyces cerevisiae. *Gene,* 192**,** 245-50.
MAUVEZIN, C., NAGY, P., JUHASZ, G. & NEUFELD, T. P. 2015. Autophagosome-lysosome fusion is independent of V-ATPase-mediated acidification. *Nat Commun,* 6**,** 7007.

MCALPINE, F., WILLIAMSON, L. E., TOOZE, S. A. & CHAN, E. Y. 2013. Regulation of nutrient-sensitive autophagy by uncoordinated 51-like kinases 1 and 2. *Autophagy,* 9**,** 361-73.

MCEWAN, D. G., POPOVIC, D., GUBAS, A., TERAWAKI, S., SUZUKI, H., STADEL, D., COXON, F. P., MIRANDA DE STEGMANN, D., BHOGARAJU, S., MADDI, K., KIRCHOF, A., GATTI, E., HELFRICH, M. H., WAKATSUKI, S., BEHRENDS, C., PIERRE, P. & DIKIC, I. 2015. PLEKHM1 regulates autophagosome-lysosome fusion through HOPS complex and LC3/GABARAP proteins. *Mol Cell,* 57**,** 39-54.

MEI, Y., SU, M., SONI, G., SALEM, S., COLBERT, C. L. & SINHA, S. C. 2014. Intrinsically disordered regions in autophagy proteins. *Proteins,* 82**,** 565-78.

MEIJER, A. J. & CODOGNO, P. 2004. Regulation and role of autophagy in mammalian cells. *Int J Biochem Cell Biol,* 36**,** 2445-62.

MEIJER, W. H., VAN DER KLEI, I. J., VEENHUIS, M. & KIEL, J. A. 2007. ATG genes involved in non-selective autophagy are conserved from yeast to man, but the selective Cvt and pexophagy pathways also require organism-specific genes. *Autophagy,* 3**,** 106-16.

MELEY, D., BAUVY, C., HOUBEN-WEERTS, J. H., DUBBELHUIS, P. F., HELMOND, M. T., CODOGNO, P. & MEIJER, A. J. 2006. AMP-activated protein kinase and the regulation of autophagic proteolysis. *J Biol Chem,* 281**,** 34870-9.

MENON, S., DIBBLE, C. C., TALBOTT, G., HOXHAJ, G., VALVEZAN, A. J., TAKAHASHI, H., CANTLEY, L. C. & MANNING, B. D. 2014. Spatial control of the TSC complex integrates insulin and nutrient regulation of mTORC1 at the lysosome. *Cell,* 156**,** 771-85.

MENZIES, F. M., FLEMING, A. & RUBINSZTEIN, D. C. 2015. Compromised autophagy and neurodegenerative diseases. *Nat Rev Neurosci,* 16**,** 345-57.

MERCER, C. A., KALIAPPAN, A. & DENNIS, P. B. 2009. A novel, human Atg13 binding protein, Atg101, interacts with ULK1 and is essential for macroautophagy. *Autophagy,* 5**,** 649-62.

MIJALJICA, D., PRESCOTT, M., KLIONSKY, D. J. & DEVENISH, R. J. 2007. Autophagy and vacuole homeostasis: a case for self-degradation? *Autophagy,* 3**,** 417-21.

MIZUSHIMA, N. 2007. Autophagy: process and function. *Genes Dev,* 21**,** 2861-73.

MIZUSHIMA, N. 2010. The role of the Atg1/ULK1 complex in autophagy regulation. *Curr Opin Cell Biol,* 22**,** 132-9.

MIZUSHIMA, N., KUMA, A., KOBAYASHI, Y., YAMAMOTO, A., MATSUBAE, M., TAKAO, T., NATSUME, T., OHSUMI, Y. & YOSHIMORI, T. 2003. Mouse Apg16L, a novel WD-repeat protein, targets to the autophagic isolation membrane with the Apg12-Apg5 conjugate. *J Cell Sci,* 116**,** 1679-88.

MIZUSHIMA, N., SUGITA, H., YOSHIMORI, T. & OHSUMI, Y. 1998. A new protein conjugation system in human. The counterpart of the yeast Apg12p conjugation system essential for autophagy. *J Biol Chem,* 273**,** 33889-92.

MIZUSHIMA, N., YAMAMOTO, A., HATANO, M., KOBAYASHI, Y., KABEYA, Y., SUZUKI, K., TOKUHISA, T., OHSUMI, Y. & YOSHIMORI, T. 2001. Dissection of autophagosome formation using Apg5-deficient mouse embryonic stem cells. *J Cell Biol,* 152**,** 657-68.

MIZUSHIMA, N., YOSHIMORI, T. & LEVINE, B. 2010. Methods in mammalian autophagy research. *Cell,* 140**,** 313-26.

MIZUSHIMA, N., YOSHIMORI, T. & OHSUMI, Y. 2011. The role of Atg proteins in autophagosome formation. *Annu Rev Cell Dev Biol,* 27**,** 107-32.

MORTENSEN, M., FERGUSON, D. J. & SIMON, A. K. 2010. Mitochondrial clearance by autophagy in developing erythrocytes: clearly important, but just how much so? *Cell Cycle,* 9**,** 1901-6.

MORUNO-MANCHON, J. F., PEREZ-JIMENEZ, E. & KNECHT, E. 2013. Glucose induces autophagy under starvation conditions by a p38 MAPK-dependent pathway. *Biochem J,* 449**,** 497-506.

MULLER, O., SATTLER, T., FLOTENMEYER, M., SCHWARZ, H., PLATTNER, H. & MAYER, A. 2000. Autophagic tubes: vacuolar invaginations involved in lateral membrane sorting and inverse vesicle budding. *J Cell Biol,* 151**,** 519-28.

MUNCH, D., RODRIGUEZ, E., BRESSENDORFF, S., PARK, O. K., HOFIUS, D. & PETERSEN, M. 2014. Autophagy deficiency leads to accumulation of ubiquitinated proteins, ER stress, and cell death in Arabidopsis. *Autophagy,* 10**,** 1579-87.

MYERS, M. G., JR., BACKER, J. M., SUN, X. J., SHOELSON, S., HU, P., SCHLESSINGER, J., YOAKIM, M., SCHAFFHAUSEN, B. & WHITE, M. F. 1992. IRS-1 activates phosphatidylinositol 3'-kinase by associating with src homology 2 domains of p85. *Proc Natl Acad Sci U S A,* 89**,** 10350-4.

NAH, J., PYO, J. O., JUNG, S., YOO, S. M., KAM, T. I., CHANG, J., HAN, J., SOO, A. A. S., ONODERA, T. & JUNG, Y. K. 2013. BECN1/Beclin 1 is recruited into lipid rafts by prion to activate autophagy in response to amyloid beta 42. *Autophagy,* 9**,** 2009-21.

NATH, S., DANCOURT, J., SHTEYN, V., PUENTE, G., FONG, W. M., NAG, S., BEWERSDORF, J., YAMAMOTO, A., ANTONNY, B. & MELIA, T. J. 2014. Lipidation of the LC3/GABARAP family of autophagy proteins relies on a membrane-curvature-sensing domain in Atg3. *Nat Cell Biol,* 16**,** 415-24.

NAZIO, F., STRAPPAZZON, F., ANTONIOLI, M., BIELLI, P., CIANFANELLI, V., BORDI, M., GRETZMEIER, C., DENGJEL, J., PIACENTINI, M., FIMIA, G. M. & CECCONI, F. 2013. mTOR inhibits autophagy by controlling ULK1 ubiquitylation, self-association and function through AMBRA1 and TRAF6. *Nat Cell Biol,* 15**,** 406-16.

NEEDLEMAN, S. B. & WUNSCH, C. D. 1970. A general method applicable to the search for similarities in the amino acid sequence of two proteins. *J Mol Biol,* 48**,** 443-53.

NISHIMURA, T., KAIZUKA, T., CADWELL, K., SAHANI, M. H., SAITOH, T., AKIRA, S., VIRGIN, H. W. & MIZUSHIMA, N. 2013. FIP200 regulates targeting of Atg16L1 to the isolation membrane. *EMBO Rep,* 14**,** 284-91.

NIXON, R. A. 2013. The role of autophagy in neurodegenerative disease. *Nat Med,* 19**,** 983-97.

O'SHEA, E. K., KLEMM, J. D., KIM, P. S. & ALBER, T. 1991. X-ray structure of the GCN4 leucine zipper, a two-stranded, parallel coiled coil. *Science,* 254**,** 539-44.

OBARA, K. & OHSUMI, Y. 2011. PtdIns 3-Kinase Orchestrates Autophagosome Formation in Yeast. *J Lipids,* 2011**,** 498768.

OHKUMA, S. & POOLE, B. 1981. Cytoplasmic vacuolation of mouse peritoneal macrophages and the uptake into lysosomes of weakly basic substances. *J Cell Biol,* 90**,** 656-64.

OKAZAKI, N., YAN, J., YUASA, S., UENO, T., KOMINAMI, E., MASUHO, Y., KOGA, H. & MURAMATSU, M. 2000. Interaction of the Unc-51-like kinase and microtubule-associated protein light chain 3 related proteins in the brain: possible role of vesicular transport in axonal elongation. *Brain Res Mol Brain Res,* 85**,** 1-12.

ORSI, A., RAZI, M., DOOLEY, H. C., ROBINSON, D., WESTON, A. E., COLLINSON, L. M. & TOOZE, S. A. 2012. Dynamic and transient

interactions of Atg9 with autophagosomes, but not membrane integration, are required for autophagy. *Mol Biol Cell,* 23**,** 1860-73.

ORY, D. S., NEUGEBOREN, B. A. & MULLIGAN, R. C. 1996. A stable human-derived packaging cell line for production of high titer retrovirus/vesicular stomatitis virus G pseudotypes. *Proc Natl Acad Sci U S A,* 93**,** 11400-6.

PANKIV, S., CLAUSEN, T. H., LAMARK, T., BRECH, A., BRUUN, J. A., OUTZEN, H., OVERVATN, A., BJORKOY, G. & JOHANSEN, T. 2007. p62/SQSTM1 binds directly to Atg8/LC3 to facilitate degradation of ubiquitinated protein aggregates by autophagy. *J Biol Chem,* 282**,** 24131-45.

PAPINSKI, D., SCHUSCHNIG, M., REITER, W., WILHELM, L., BARNES, C. A., MAIOLICA, A., HANSMANN, I., PFAFFENWIMMER, T., KIJANSKA, M., STOFFEL, I., LEE, S. S., BREZOVICH, A., LOU, J. H., TURK, B. E., AEBERSOLD, R., AMMERER, G., PETER, M. & KRAFT, C. 2014. Early steps in autophagy depend on direct phosphorylation of Atg9 by the Atg1 kinase. *Mol Cell,* 53**,** 471-83.

PARK, J. M., JUNG, C. H., SEO, M., OTTO, N. M., GRUNWALD, D., KIM, K. H., MORIARITY, B., KIM, Y. M., STARKER, C., NHO, R. S., VOYTAS, D. & KIM, D. H. 2016. The ULK1 complex mediates MTORC1 signaling to the autophagy initiation machinery via binding and phosphorylating ATG14. *Autophagy,* 12**,** 547-64.

PATKAR, S., TATE, R., MODO, M., PLEVIN, R. & CARSWELL, H. V. 2012. Conditionally immortalised neural stem cells promote functional recovery and brain plasticity after transient focal cerebral ischaemia in mice. *Stem Cell Res,* 8**,** 14-25.

PENA-LLOPIS, S., VEGA-RUBIN-DE-CELIS, S., SCHWARTZ, J. C., WOLFF, N. C., TRAN, T. A., ZOU, L., XIE, X. J., COREY, D. R. & BRUGAROLAS, J. 2011. Regulation of TFEB and V-ATPases by mTORC1. *EMBO J,* 30**,** 3242-58.

PETHERICK, K. J., CONWAY, O. J., MPAMHANGA, C., OSBORNE, S. A., KAMAL, A., SAXTY, B. & GANLEY, I. G. 2015. Pharmacological inhibition of ULK1 kinase blocks mammalian target of rapamycin (mTOR)-dependent autophagy. *J Biol Chem,* 290**,** 28726.

PETIOT, A., OGIER-DENIS, E., BLOMMAART, E. F., MEIJER, A. J. & CODOGNO, P. 2000. Distinct classes of phosphatidylinositol 3'-kinases are involved in signaling pathways that control macroautophagy in HT-29 cells. *J Biol Chem,* 275**,** 992-8.

PETIT, C. S., ROCZNIAK-FERGUSON, A. & FERGUSON, S. M. 2013. Recruitment of folliculin to lysosomes supports the amino acid-dependent activation of Rag GTPases. *J Cell Biol,* 202**,** 1107-22.

PLOMP, P. J., WOLVETANG, E. J., GROEN, A. K., MEIJER, A. J., GORDON, P. B. & SEGLEN, P. O. 1987. Energy dependence of autophagic protein degradation in isolated rat hepatocytes. *Eur J Biochem,* 164**,** 197-203.

POLSON, H. E., DE LARTIGUE, J., RIGDEN, D. J., REEDIJK, M., URBE, S., CLAGUE, M. J. & TOOZE, S. A. 2010. Mammalian Atg18 (WIPI2) localizes to omegasome-anchored phagophores and positively regulates LC3 lipidation. *Autophagy,* 6**,** 506-22.

PUENTE, C., HENDRICKSON, R. C. & JIANG, X. 2016. Nutrient-regulated Phosphorylation of ATG13 Inhibits Starvation-induced Autophagy. *J Biol Chem,* 291**,** 6026-35.

PURI, C., RENNA, M., BENTO, C. F., MOREAU, K. & RUBINSZTEIN, D. C. 2013. Diverse autophagosome membrane sources coalesce in recycling endosomes. *Cell,* 154**,** 1285-99.

RABINOWITZ, J. D. & WHITE, E. 2010. Autophagy and metabolism. *Science,* 330**,** 1344-8.

RAGUSA, M. J., STANLEY, R. E. & HURLEY, J. H. 2012. Architecture of the Atg17 complex as a scaffold for autophagosome biogenesis. *Cell,* 151**,** 1501-12.
RAMIREZ-PEINADO, S., LEON-ANNICCHIARICO, C. L., GALINDO-MORENO, J., IURLARO, R., CARO-MALDONADO, A., PREHN, J. H., RYAN, K. M. & MUNOZ-PINEDO, C. 2013. Glucose-starved cells do not engage in prosurvival autophagy. *J Biol Chem,* 288**,** 30387-98.
RANDOW, F. & SALE, J. E. 2006. Retroviral transduction of DT40. *Subcell Biochem,* 40**,** 383-6.
RANGWALA, R., CHANG, Y. C., HU, J., ALGAZY, K. M., EVANS, T. L., FECHER, L. A., SCHUCHTER, L. M., TORIGIAN, D. A., PANOSIAN, J. T., TROXEL, A. B., TAN, K. S., HEITJAN, D. F., DEMICHELE, A. M., VAUGHN, D. J., REDLINGER, M., ALAVI, A., KAISER, J., PONTIGGIA, L., DAVIS, L. E., O'DWYER, P. J. & AMARAVADI, R. K. 2014. Combined MTOR and autophagy inhibition: phase I trial of hydroxychloroquine and temsirolimus in patients with advanced solid tumors and melanoma. *Autophagy,* 10**,** 1391-402.
RAO, Y., PERNA, M. G., HOFMANN, B., BEIER, V. & WOLLERT, T. 2016. The Atg1-kinase complex tethers Atg9-vesicles to initiate autophagy. *Nat Commun,* 7**,** 10338.
RAVIKUMAR, B., SARKAR, S., DAVIES, J. E., FUTTER, M., GARCIA-ARENCIBIA, M., GREEN-THOMPSON, Z. W., JIMENEZ-SANCHEZ, M., KOROLCHUK, V. I., LICHTENBERG, M., LUO, S., MASSEY, D. C., MENZIES, F. M., MOREAU, K., NARAYANAN, U., RENNA, M., SIDDIQI, F. H., UNDERWOOD, B. R., WINSLOW, A. R. & RUBINSZTEIN, D. C. 2010. Regulation of mammalian autophagy in physiology and pathophysiology. *Physiol Rev,* 90**,** 1383-435.
RAVIKUMAR, B., STEWART, A., KITA, H., KATO, K., DUDEN, R. & RUBINSZTEIN, D. C. 2003. Raised intracellular glucose concentrations reduce aggregation and cell death caused by mutant huntingtin exon 1 by decreasing mTOR phosphorylation and inducing autophagy. *Hum Mol Genet,* 12**,** 985-94.
REBSAMEN, M., POCHINI, L., STASYK, T., DE ARAUJO, M. E., GALLUCCIO, M., KANDASAMY, R. K., SNIJDER, B., FAUSTER, A., RUDASHEVSKAYA, E. L., BRUCKNER, M., SCORZONI, S., FILIPEK, P. A., HUBER, K. V., BIGENZAHN, J. W., HEINZ, L. X., KRAFT, C., BENNETT, K. L., INDIVERI, C., HUBER, L. A. & SUPERTI-FURGA, G. 2015. SLC38A9 is a component of the lysosomal amino acid sensing machinery that controls mTORC1. *Nature,* 519**,** 477-81.
REGGIORI, F. & KLIONSKY, D. J. 2013. Autophagic processes in yeast: mechanism, machinery and regulation. *Genetics,* 194**,** 341-61.
RO, S. H., JUNG, C. H., HAHN, W. S., XU, X., KIM, Y. M., YUN, Y. S., PARK, J. M., KIM, K. H., SEO, M., HA, T. Y., ARRIAGA, E. A., BERNLOHR, D. A. & KIM, D. H. 2013. Distinct functions of Ulk1 and Ulk2 in the regulation of lipid metabolism in adipocytes. *Autophagy,* 9**,** 2103-14.
ROBERTS, D. J., TAN-SAH, V. P., DING, E. Y., SMITH, J. M. & MIYAMOTO, S. 2014. Hexokinase-II positively regulates glucose starvation-induced autophagy through TORC1 inhibition. *Mol Cell,* 53**,** 521-33.
RUSSELL, R. C., TIAN, Y., YUAN, H., PARK, H. W., CHANG, Y. Y., KIM, J., KIM, H., NEUFELD, T. P., DILLIN, A. & GUAN, K. L. 2013. ULK1 induces autophagy by phosphorylating Beclin-1 and activating VPS34 lipid kinase. *Nat Cell Biol,* 15**,** 741-50.
RUSSELL, S. E., HICKEY, G. I., LOWRY, W. S., WHITE, P. & ATKINSON, R. J. 1990. Allele loss from chromosome 17 in ovarian cancer. *Oncogene,* 5**,** 1581-3.

SABATINI, D. M. 2006. mTOR and cancer: insights into a complex relationship. *Nat Rev Cancer,* 6**,** 729-34.

SAHANI, M. H., ITAKURA, E. & MIZUSHIMA, N. 2014. Expression of the autophagy substrate SQSTM1/p62 is restored during prolonged starvation depending on transcriptional upregulation and autophagy-derived amino acids. *Autophagy,* 10**,** 431-41.

SAITO, H., INAZAWA, J., SAITO, S., KASUMI, F., KOI, S., SAGAE, S., KUDO, R., SAITO, J., NODA, K. & NAKAMURA, Y. 1993. Detailed deletion mapping of chromosome 17q in ovarian and breast cancers: 2-cM region on 17q21.3 often and commonly deleted in tumors. *Cancer Res,* 53**,** 3382-5.

SAMBROOK, J. R., D 2001. *Molecular Cloning: a Laboratory*

Manual, Cold Spring Harbor, NY, Cold Spring Harbor

Laboratory.

SANCAK, Y., BAR-PELED, L., ZONCU, R., MARKHARD, A. L., NADA, S. & SABATINI, D. M. 2010. Ragulator-Rag complex targets mTORC1 to the lysosomal surface and is necessary for its activation by amino acids. *Cell,* 141**,** 290-303.

SANCAK, Y., PETERSON, T. R., SHAUL, Y. D., LINDQUIST, R. A., THOREEN, C. C., BAR-PELED, L. & SABATINI, D. M. 2008. The Rag GTPases bind raptor and mediate amino acid signaling to mTORC1. *Science,* 320**,** 1496-501.

SANCAK, Y., THOREEN, C. C., PETERSON, T. R., LINDQUIST, R. A., KANG, S. A., SPOONER, E., CARR, S. A. & SABATINI, D. M. 2007. PRAS40 is an insulin-regulated inhibitor of the mTORC1 protein kinase. *Mol Cell,* 25**,** 903-15.

SANCHEZ-WANDELMER, J., KTISTAKIS, N. T. & REGGIORI, F. 2015. ERES: sites for autophagosome biogenesis and maturation? *J Cell Sci,* 128**,** 185-92.

SANJUAN, M. A., DILLON, C. P., TAIT, S. W., MOSHIACH, S., DORSEY, F., CONNELL, S., KOMATSU, M., TANAKA, K., CLEVELAND, J. L., WITHOFF, S. & GREEN, D. R. 2007. Toll-like receptor signalling in macrophages links the autophagy pathway to phagocytosis. *Nature,* 450**,** 1253-7.

SARBASSOV, D. D., GUERTIN, D. A., ALI, S. M. & SABATINI, D. M. 2005. Phosphorylation and regulation of Akt/PKB by the rictor-mTOR complex. *Science,* 307**,** 1098-101.

SAUTIN, Y. Y., LU, M., GAUGLER, A., ZHANG, L. & GLUCK, S. L. 2005. Phosphatidylinositol 3-kinase-mediated effects of glucose on vacuolar H+-ATPase assembly, translocation, and acidification of intracellular compartments in renal epithelial cells. *Mol Cell Biol,* 25**,** 575-89.

SCHULTZ, J., MILPETZ, F., BORK, P. & PONTING, C. P. 1998. SMART, a simple modular architecture research tool: identification of signaling domains. *Proc Natl Acad Sci U S A,* 95**,** 5857-64.

SCHWEICHEL, J. U. & MERKER, H. J. 1973. The morphology of various types of cell death in prenatal tissues. *Teratology,* 7**,** 253-66.

SHANG, L., CHEN, S., DU, F., LI, S., ZHAO, L. & WANG, X. 2011. Nutrient starvation elicits an acute autophagic response mediated by Ulk1 dephosphorylation and its subsequent dissociation from AMPK. *Proc Natl Acad Sci U S A,* 108**,** 4788-93.

SHAW, R. J., KOSMATKA, M., BARDEESY, N., HURLEY, R. L., WITTERS, L. A., DEPINHO, R. A. & CANTLEY, L. C. 2004. The tumor suppressor LKB1

kinase directly activates AMP-activated kinase and regulates apoptosis in response to energy stress. *Proc Natl Acad Sci U S A,* 101**,** 3329-35.
SHIMIZU, S., KANASEKI, T., MIZUSHIMA, N., MIZUTA, T., ARAKAWA-KOBAYASHI, S., THOMPSON, C. B. & TSUJIMOTO, Y. 2004. Role of Bcl-2 family proteins in a non-apoptotic programmed cell death dependent on autophagy genes. *Nat Cell Biol,* 6**,** 1221-8.
SHPILKA, T., WEIDBERG, H., PIETROKOVSKI, S. & ELAZAR, Z. 2011. Atg8: an autophagy-related ubiquitin-like protein family. *Genome Biol,* 12**,** 226.
SIEVERS, F., WILM, A., DINEEN, D., GIBSON, T. J., KARPLUS, K., LI, W., LOPEZ, R., MCWILLIAM, H., REMMERT, M., SODING, J., THOMPSON, J. D. & HIGGINS, D. G. 2011. Fast, scalable generation of high-quality protein multiple sequence alignments using Clustal Omega. *Mol Syst Biol,* 7**,** 539.
STEPHENS, L. R., JACKSON, T. R. & HAWKINS, P. T. 1993. Agonist-stimulated synthesis of phosphatidylinositol(3,4,5)-trisphosphate: a new intracellular signalling system? *Biochim Biophys Acta,* 1179**,** 27-75.
STJEPANOVIC, G., DAVIES, C. W., STANLEY, R. E., RAGUSA, M. J., KIM, D. J. & HURLEY, J. H. 2014. Assembly and dynamics of the autophagy-initiating Atg1 complex. *Proc Natl Acad Sci U S A,* 111**,** 12793-8.
STOLZ, A., ERNST, A. & DIKIC, I. 2014. Cargo recognition and trafficking in selective autophagy. *Nat Cell Biol,* 16**,** 495-501.
SU, H., LI, F., RANEK, M. J., WEI, N. & WANG, X. 2011. COP9 signalosome regulates autophagosome maturation. *Circulation,* 124**,** 2117-28.
SUZUKI, S. W., YAMAMOTO, H., OIKAWA, Y., KONDO-KAKUTA, C., KIMURA, Y., HIRANO, H. & OHSUMI, Y. 2015. Atg13 HORMA domain recruits Atg9 vesicles during autophagosome formation. *Proc Natl Acad Sci U S A,* 112**,** 3350-5.
TAKAHASHI, Y., COPPOLA, D., MATSUSHITA, N., CUALING, H. D., SUN, M., SATO, Y., LIANG, C., JUNG, J. U., CHENG, J. Q., MULE, J. J., PLEDGER, W. J. & WANG, H. G. 2007. Bif-1 interacts with Beclin 1 through UVRAG and regulates autophagy and tumorigenesis. *Nat Cell Biol,* 9**,** 1142-51.
TAKATS, S., NAGY, P., VARGA, A., PIRCS, K., KARPATI, M., VARGA, K., KOVACS, A. L., HEGEDUS, K. & JUHASZ, G. 2013. Autophagosomal Syntaxin17-dependent lysosomal degradation maintains neuronal function in Drosophila. *J Cell Biol,* 201**,** 531-9.
TAN, D., CAI, Y., WANG, J., ZHANG, J., MENON, S., CHOU, H. T., FERRO-NOVICK, S., REINISCH, K. M. & WALZ, T. 2013. The EM structure of the TRAPPIII complex leads to the identification of a requirement for COPII vesicles on the macroautophagy pathway. *Proc Natl Acad Sci U S A,* 110**,** 19432-7.
TANIDA, I., UENO, T. & KOMINAMI, E. 2004. LC3 conjugation system in mammalian autophagy. *Int J Biochem Cell Biol,* 36**,** 2503-18.
TAUNTON, J., ROWNING, B. A., COUGHLIN, M. L., WU, M., MOON, R. T., MITCHISON, T. J. & LARABELL, C. A. 2000. Actin-dependent propulsion of endosomes and lysosomes by recruitment of N-WASP. *J Cell Biol,* 148**,** 519-30.
TEE, A. R., BLENIS, J. & PROUD, C. G. 2005. Analysis of mTOR signaling by the small G-proteins, Rheb and RhebL1. *FEBS Lett,* 579**,** 4763-8.
THOMAS, J. D., ZHANG, Y. J., WEI, Y. H., CHO, J. H., MORRIS, L. E., WANG, H. Y. & ZHENG, X. F. 2014. Rab1A is an mTORC1 activator and a colorectal oncogene. *Cancer Cell,* 26**,** 754-69.
THUMM, M., EGNER, R., KOCH, B., SCHLUMPBERGER, M., STRAUB, M., VEENHUIS, M. & WOLF, D. H. 1994. Isolation of autophagocytosis mutants of Saccharomyces cerevisiae. *FEBS Lett,* 349**,** 275-80.

TIAN, S., OHTA, A., HORIUCHI, H. & FUKUDA, R. 2015. Evaluation of sterol transport from the endoplasmic reticulum to mitochondria using mitochondrially targeted bacterial sterol acyltransferase in Saccharomyces cerevisiae. *Biosci Biotechnol Biochem,* 79**,** 1608-14.

TODA, H., MOCHIZUKI, H., FLORES, R., 3RD, JOSOWITZ, R., KRASIEVA, T. B., LAMORTE, V. J., SUZUKI, E., GINDHART, J. G., FURUKUBO-TOKUNAGA, K. & TOMODA, T. 2008. UNC-51/ATG1 kinase regulates axonal transport by mediating motor-cargo assembly. *Genes Dev,* 22**,** 3292-307.

TOMODA, T., BHATT, R. S., KUROYANAGI, H., SHIRASAWA, T. & HATTEN, M. E. 1999. A mouse serine/threonine kinase homologous to C. elegans UNC51 functions in parallel fiber formation of cerebellar granule neurons. *Neuron,* 24**,** 833-46.

TOOZE, S. A. 2013. Current views on the source of the autophagosome membrane. *Essays Biochem,* 55**,** 29-38.

TSUKADA, M. & OHSUMI, Y. 1993. Isolation and characterization of autophagy-defective mutants of Saccharomyces cerevisiae. *FEBS Lett,* 333**,** 169-74.

TSUN, Z. Y., BAR-PELED, L., CHANTRANUPONG, L., ZONCU, R., WANG, T., KIM, C., SPOONER, E. & SABATINI, D. M. 2013. The folliculin tumor suppressor is a GAP for the RagC/D GTPases that signal amino acid levels to mTORC1. *Mol Cell,* 52**,** 495-505.

TUMBARELLO, D. A., WAXSE, B. J., ARDEN, S. D., BRIGHT, N. A., KENDRICK-JONES, J. & BUSS, F. 2012. Autophagy receptors link myosin VI to autophagosomes to mediate Tom1-dependent autophagosome maturation and fusion with the lysosome. *Nat Cell Biol,* 14**,** 1024-35.

UEMURA, T., YAMAMOTO, M., KAMETAKA, A., SOU, Y. S., YABASHI, A., YAMADA, A., ANNOH, H., KAMETAKA, S., KOMATSU, M. & WAGURI, S. 2014. A cluster of thin tubular structures mediates transformation of the endoplasmic reticulum to autophagic isolation membrane. *Mol Cell Biol,* 34**,** 1695-706.

UTTENWEILER, A. & MAYER, A. 2008. Microautophagy in the yeast Saccharomyces cerevisiae. *Methods Mol Biol,* 445**,** 245-59.

VANCE, J. E. 1990. Phospholipid synthesis in a membrane fraction associated with mitochondria. *J Biol Chem,* 265**,** 7248-56.

VANCE, J. E. 2014. MAM (mitochondria-associated membranes) in mammalian cells: lipids and beyond. *Biochim Biophys Acta,* 1841**,** 595-609.

VANDER HAAR, E., LEE, S. I., BANDHAKAVI, S., GRIFFIN, T. J. & KIM, D. H. 2007. Insulin signalling to mTOR mediated by the Akt/PKB substrate PRAS40. *Nat Cell Biol,* 9**,** 316-23.

VICINANZA, M., KOROLCHUK, V. I., ASHKENAZI, A., PURI, C., MENZIES, F. M., CLARKE, J. H. & RUBINSZTEIN, D. C. 2015. PI(5)P regulates autophagosome biogenesis. *Mol Cell,* 57**,** 219-34.

VIDAL, R. L., MATUS, S., BARGSTED, L. & HETZ, C. 2014. Targeting autophagy in neurodegenerative diseases. *Trends Pharmacol Sci,* 35**,** 583-91.

WANG, H., SUN, H. Q., ZHU, X., ZHANG, L., ALBANESI, J., LEVINE, B. & YIN, H. 2015a. GABARAPs regulate PI4P-dependent autophagosome:lysosome fusion. *Proc Natl Acad Sci U S A,* 112**,** 7015-20.

WANG, R. C., WEI, Y., AN, Z., ZOU, Z., XIAO, G., BHAGAT, G., WHITE, M., REICHELT, J. & LEVINE, B. 2012. Akt-mediated regulation of autophagy and tumorigenesis through Beclin 1 phosphorylation. *Science,* 338**,** 956-9.

WANG, S., TSUN, Z. Y., WOLFSON, R. L., SHEN, K., WYANT, G. A., PLOVANICH, M. E., YUAN, E. D., JONES, T. D., CHANTRANUPONG, L., COMB, W., WANG, T., BAR-PELED, L., ZONCU, R., STRAUB, C., KIM, C., PARK, J., SABATINI, B. L. & SABATINI, D. M. 2015b. Metabolism.

Lysosomal amino acid transporter SLC38A9 signals arginine sufficiency to mTORC1. *Science,* 347**,** 188-94.
WANG, X. & PROUD, C. G. 2006. The mTOR pathway in the control of protein synthesis. *Physiology (Bethesda),* 21**,** 362-9.
WEBB, J. L., RAVIKUMAR, B. & RUBINSZTEIN, D. C. 2004. Microtubule disruption inhibits autophagosome-lysosome fusion: implications for studying the roles of aggresomes in polyglutamine diseases. *Int J Biochem Cell Biol,* 36**,** 2541-50.
WEI, Y., PATTINGRE, S., SINHA, S., BASSIK, M. & LEVINE, B. 2008. JNK1-mediated phosphorylation of Bcl-2 regulates starvation-induced autophagy. *Mol Cell,* 30**,** 678-88.
WEIDBERG, H., SHVETS, E., SHPILKA, T., SHIMRON, F., SHINDER, V. & ELAZAR, Z. 2010. LC3 and GATE-16/GABARAP subfamilies are both essential yet act differently in autophagosome biogenesis. *EMBO J,* 29**,** 1792-802.
WHITE, E. 2012. Deconvoluting the context-dependent role for autophagy in cancer. *Nat Rev Cancer,* 12**,** 401-10.
WHITE, E. 2015. The role for autophagy in cancer. *J Clin Invest,* 125**,** 42-6.
WIMLEY, W. C. & WHITE, S. H. 1996. Experimentally determined hydrophobicity scale for proteins at membrane interfaces. *Nat Struct Biol,* 3**,** 842-8.
WINDER, W. W. & HARDIE, D. G. 1996. Inactivation of acetyl-CoA carboxylase and activation of AMP-activated protein kinase in muscle during exercise. *Am J Physiol,* 270**,** E299-304.
WIZA, C., NASCIMENTO, E. B. & OUWENS, D. M. 2012. Role of PRAS40 in Akt and mTOR signaling in health and disease. *Am J Physiol Endocrinol Metab,* 302**,** E1453-60.
WOLFSON, R. L., CHANTRANUPONG, L., SAXTON, R. A., SHEN, K., SCARIA, S. M., CANTOR, J. R. & SABATINI, D. M. 2016. Sestrin2 is a leucine sensor for the mTORC1 pathway. *Science,* 351**,** 43-8.
WONG, P. M., FENG, Y., WANG, J., SHI, R. & JIANG, X. 2015. Regulation of autophagy by coordinated action of mTORC1 and protein phosphatase 2A. *Nat Commun,* 6**,** 8048.
WONG, P. M., PUENTE, C., GANLEY, I. G. & JIANG, X. 2013. The ULK1 complex: sensing nutrient signals for autophagy activation. *Autophagy,* 9**,** 124-37.
WU, W., TIAN, W., HU, Z., CHEN, G., HUANG, L., LI, W., ZHANG, X., XUE, P., ZHOU, C., LIU, L., ZHU, Y., ZHANG, X., LI, L., ZHANG, L., SUI, S., ZHAO, B. & FENG, D. 2014. ULK1 translocates to mitochondria and phosphorylates FUNDC1 to regulate mitophagy. *EMBO Rep,* 15**,** 566-75.
XI, H., KURTOGLU, M., LIU, H., WANGPAICHITR, M., YOU, M., LIU, X., SAVARAJ, N. & LAMPIDIS, T. J. 2011. 2-Deoxy-D-glucose activates autophagy via endoplasmic reticulum stress rather than ATP depletion. *Cancer Chemother Pharmacol,* 67**,** 899-910.
XIE, Z. & KLIONSKY, D. J. 2007. Autophagosome formation: core machinery and adaptations. *Nat Cell Biol,* 9**,** 1102-9.
YAN, J., KUROYANAGI, H., KUROIWA, A., MATSUDA, Y., TOKUMITSU, H., TOMODA, T., SHIRASAWA, T. & MURAMATSU, M. 1998. Identification of mouse ULK1, a novel protein kinase structurally related to C. elegans UNC-51. *Biochem Biophys Res Commun,* 246**,** 222-7.
YAN, J., KUROYANAGI, H., TOMEMORI, T., OKAZAKI, N., ASATO, K., MATSUDA, Y., SUZUKI, Y., OHSHIMA, Y., MITANI, S., MASUHO, Y., SHIRASAWA, T. & MURAMATSU, M. 1999. Mouse ULK2, a novel member of the UNC-51-like protein kinases: unique features of functional domains. *Oncogene,* 18**,** 5850-9.

YAN, Q. 2008. Bioinformatics databases and tools in virology research: an overview. *In Silico Biol,* 8**,** 71-85.

YANG, J., YAN, R., ROY, A., XU, D., POISSON, J. & ZHANG, Y. 2015. The I-TASSER Suite: protein structure and function prediction. *Nat Methods,* 12**,** 7-8.

YANG, S., WANG, X., CONTINO, G., LIESA, M., SAHIN, E., YING, H., BAUSE, A., LI, Y., STOMMEL, J. M., DELL'ANTONIO, G., MAUTNER, J., TONON, G., HAIGIS, M., SHIRIHAI, O. S., DOGLIONI, C., BARDEESY, N. & KIMMELMAN, A. C. 2011. Pancreatic cancers require autophagy for tumor growth. *Genes Dev,* 25**,** 717-29.

YANG, Z. & KLIONSKY, D. J. 2010a. Eaten alive: a history of macroautophagy. *Nat Cell Biol,* 12**,** 814-22.

YANG, Z. & KLIONSKY, D. J. 2010b. Mammalian autophagy: core molecular machinery and signaling regulation. *Curr Opin Cell Biol,* 22**,** 124-31.

YLA-ANTTILA, P., VIHINEN, H., JOKITALO, E. & ESKELINEN, E. L. 2009. 3D tomography reveals connections between the phagophore and endoplasmic reticulum. *Autophagy,* 5**,** 1180-5.

YOSHII, S. R., KUMA, A., AKASHI, T., HARA, T., YAMAMOTO, A., KURIKAWA, Y., ITAKURA, E., TSUKAMOTO, S., SHITARA, H., EISHI, Y. & MIZUSHIMA, N. 2016. Systemic Analysis of Atg5-Null Mice Rescued from Neonatal Lethality by Transgenic ATG5 Expression in Neurons. *Dev Cell,* 39**,** 116-130.

YOSHIMORI, T., YAMAMOTO, A., MORIYAMA, Y., FUTAI, M. & TASHIRO, Y. 1991. Bafilomycin A1, a specific inhibitor of vacuolar-type H(+)-ATPase, inhibits acidification and protein degradation in lysosomes of cultured cells. *J Biol Chem,* 266**,** 17707-12.

YOUNG, A. R., CHAN, E. Y., HU, X. W., KOCHL, R., CRAWSHAW, S. G., HIGH, S., HAILEY, D. W., LIPPINCOTT-SCHWARTZ, J. & TOOZE, S. A. 2006. Starvation and ULK1-dependent cycling of mammalian Atg9 between the TGN and endosomes. *J Cell Sci,* 119**,** 3888-900.

YU, L., ALVA, A., SU, H., DUTT, P., FREUNDT, E., WELSH, S., BAEHRECKE, E. H. & LENARDO, M. J. 2004. Regulation of an ATG7-beclin 1 program of autophagic cell death by caspase-8. *Science,* 304**,** 1500-2.

YU, L., MCPHEE, C. K., ZHENG, L., MARDONES, G. A., RONG, Y., PENG, J., MI, N., ZHAO, Y., LIU, Z., WAN, F., HAILEY, D. W., OORSCHOT, V., KLUMPERMAN, J., BAEHRECKE, E. H. & LENARDO, M. J. 2010. Termination of autophagy and reformation of lysosomes regulated by mTOR. *Nature,* 465**,** 942-6.

ZHANG, C. S. & LIN, S. C. 2016. AMPK Promotes Autophagy by Facilitating Mitochondrial Fission. *Cell Metab,* 23**,** 399-401.

ZHANG, X., CAI, J., ZHENG, Z., POLIN, L., LIN, Z., DANDEKAR, A., LI, L., SUN, F., FINLEY, R. L., JR., FANG, D., YANG, Z. Q. & ZHANG, K. 2015. A novel ER-microtubule-binding protein, ERLIN2, stabilizes Cyclin B1 and regulates cell cycle progression. *Cell Discov,* 1**,** 15024.

ZHOU, H. & HUANG, S. 2011. Role of mTOR signaling in tumor cell motility, invasion and metastasis. *Curr Protein Pept Sci,* 12**,** 30-42.

ZONCU, R., BAR-PELED, L., EFEYAN, A., WANG, S., SANCAK, Y. & SABATINI, D. M. 2011. mTORC1 senses lysosomal amino acids through an inside-out mechanism that requires the vacuolar H(+)-ATPase. *Science,* 334**,** 678-83.

ZOPPINO, F. C., MILITELLO, R. D., SLAVIN, I., ALVAREZ, C. & COLOMBO, M. I. 2010. Autophagosome formation depends on the small GTPase Rab1 and functional ER exit sites. *Traffic,* 11**,** 1246-61.